LSHTM Research Online

https://researchonline.lshtm.ac.uk

DEVELOPMENT OF NOVEL PREDICTIVE 2D AND 3D *IN VITRO* MODELS FOR ANTI-LEISHMANIAL DRUG TESTING

Alec O'Keeffe

Thesis submitted in accordance with the requirements for the degree of

Doctor of Philosophy

University of London

September 2017

Department of Infectious and Tropical Diseases

Faculty of Immunology and Infection

LONDON SCHOOL OF HYGIENE & TROPICAL MEDICINE

Declaration

I Alec O'Keeffe, confirm that the work presented in this thesis is my own. Where information has been derived from other sources, I confirm that this has been indicated in the thesis.

Acknowledgements

First, I would like to thank Prof. Simon Croft for all the support, enthusiasm and expert guidance throughout this process. I also would like to thank Dr. Sudax Murdan for her support and ideas throughout this entire PhD.

An extra thank you to Dr. Vanessa Yardley for all of the help and organisation she provided.

A massive thank you to Dr. Katrien Van Bocxlaer, for both emotional and technical support, for guiding me through my time at the LSHTM and keeping me sane.

Many thanks to my colleagues of lab 239: Gert, Hollie, Alaa, Jon, Markella and Evangelia. For all of the good times and the bad thank you all for the support, friendship and uplifting shared experiences.

I wish to acknowledge Dr. Karin Seifert and Dr. John Raynes for the technical support and guidance. Thanks to Dr. Elizabeth McCarthy, master of the dungeon.

A special thanks to Pharmidex, in particular Dr. Martin Barrett.

A big thank you to Dr. Christine Hale and the support I received at the Wellcome Trust Sanger Institue.

I would like to thank Kapish Gupta, of Invitrocue, for his fast and efficient work on the 3D cell culture data analysis.

A huge thank you to Nadine Mogford for the support and excellent running of the course. Also for all of the good times and joy she brings.

Thanks to all of my friends and family who have supported me throughout the process, with a special mention to Xenia who suffered alongside, sharing experiences and putting the world in perspective.

My final thanks are to Rosie, a constant and unconditional source of support and confidence. Without whom my experience would have been far less enjoyable.

Abstract

The failure rates of drugs once they reach clinical trials are high, with estimates up to nearly 90%. One reason is the lack of biologically relevant models in which potential drug candidates are screened, evaluated and selected during discovery and development phases. Leishmaniasis is a disease that suffers from this problem. Current therapies are weak, toxic and there is a growing problem of drug resistance.

The aim of this thesis is to investigate different ways in which the current *in vitro* model systems could be made more predictive. Three methods of potentially improving reliability and predictability of *in vitro* models are investigated.

Firstly, the differences between the media perfusion and static cell culture systems were studied. Using macrophages and *L. major* parasites, infections within the media perfusion system were optimised. The activities of standard drugs used for the treatment of leishmaniasis, were determined. A decrease in infection rates and in the activity of standard drugs was seen when using the media perfusion.

Secondly, a 3D *in vitro* infection model was developed and used to determine the activity of standard drugs, compared with 2D cell culture. The model shows that 3D and 2D provide similar results for the activity of the standard drugs tested.

Thirdly, a variety of macrophage cell types have been used as *Leishmania* host cells for intracellular amastigote assays. The use of macrophages differentiated from induced pluripotent stem cells was investigated as a viable and more predictive alternative. The option to use a cell type that is more biologically similar to the human *in vivo* situation, but can be maintained like cell lines, is a clear benefit to in *in vitro* assays. It was concluded that macrophages differentiated from induced pluripotent stem cells would be a suitable alternative to currently used cell types.

Table of Contents

Table of Contents

Table of Contents

Table of Contents

List of Abbreviations

2D	Two dimensional
3D	Three dimensional
ADME	Absorption Distribution Metabolism Excretion
AmB	Amphotericin B
ANOVA	Analysis of variance
ATCC	American Type Culture Collection
ATP	Adenosine triphosphate
BCA	Bicinchoninic acid assay
BSA	Fatty acid free Bovine Serum Albumin
CFU	Colony forming units
CI	Confidence Interval
CL	Cutaneous Leishmaniasis
C_{MAX}	Concentration maximum
CRISPR	Clustered Regularly Interspaced Short Palindromic Repeats
Dapi	4',6-Diamidino-2-Phenylindole
DCL	Diffuse Cutaneous Leishmaniasis
DMEM	Dulbecco's Modified Eagle's medium
DMSO	Dimethyl sulfoxide
DNA	Deoxyribonucleic acid
DNDi	Drugs for Neglected Diseases initiative
DTNB	5,5-dithio- bis 2-nitrobenzoic acid
EC	Effective Concentration
ECM	Extracellular matrix
EDTA	Ethylenediaminetetraacetic acid
Edu	5-ethynyl-2'-deoxyuridine
FGF	Fibroblast Growth Factor
GFP	Green fluorescent protein
GSK	Glaxo Smith Klein
HAT	Human African trypanosomes
HBMM	Human bone marrow macrophages
HCS	High content screen
HCV	Hepatitis C virus
HeNe	Helium Neon
HEPES	4-(2-hydroxyethyl)-1-piperazineethanesulfonic acid
HiFCS	Heat inactivated Fetal Calf Serum
HIV	Human Immunodeficiency Virus
hM-CSF	Human Macrophage Colony Stimulating Factor
HPLC	High Pressure Liquid Chromatography
HTS	High throughput screen
IC	Inhibitory Concentration
iPSC	Induced pluripotent stem cells

List of Abbreviations

KO	Knock out
KSR	Knockout replacement serum
Laser	Light amplification by stimulated emission of radiation
LD	Lethal dose
LNCaP	Cell line produced from lymph node carcinoma of the prostate
LPS	Lipopolysaccharides
LSHTM	London School of Hygiene and Tropical Medicine
MA	Meglumine antimoniate
MBMM	Mouse bone marrow macrophages
MEF	Mouse embryonic feeder
MIL	Miltefosine
mRNA	Messenger RNA
MS	Mass spectrometer
MTT	3-(4,5-dimethylthiazol-2-yl)-2,5-diphenyltetrazolium bromide
NADPH	Nicotinamide adenine dinucleotide phosphate
NO	Nitric Oxide
NTD	Neglected tropical diseases
PBS	Phosphate buffered saline
PC3	Prostate cancer cell line
PD	Pharmacodynamics
PDMS	Polydimethylsiloxane
PEGDA	Poly(ethylene glycol) diacrylate
PEM	Peritoneal macrophages
PFA	Paraformaldehyde
PK	Pharmacokinetics
PKDL	Post-kala-azar dermal leishmaniasis
PM	Paromomycin
PMA	Phorbol 12-myristate 13-acetate
PMSF	Phenylmethanesulfonyl fluoride
qPCR	Quantative polymerase chain reaction
QV	Quasi Vivo
RFP	Red fluorescent protein
RFU	Relative fluorescent unit
RNA	Ribonucleic acid
RPMI-1640	Roswell Park Memorial Institute medium
RTqPCR	Reverse Transcriptase qPCR
Sb^{III}	Trivalent Antimony
Sb^{v}	Pentavalent Antimony
SCID	Severe combined immunodeficiency
SD	Standard Deviation
SSG	Sodium Stibogluconate
$T[S]^2$	Trypanothione disulphide
TH1	Type 1 T Helper cell
THP1	Human leukaemia monocyte cell line

List of Abbreviations

T_{MIC}	Time above the minimum inhibitory concentration
TNF-α	Tumour necrosis factor α
TryR	Trypanothione reductase
UK	United Kingdom
US	United States of America
VL	Visceral Leishmaniasis
V_{MAX}	Maximum Velocity (Maximum oxygen consumption rate)
WHO	World Health Organisation

List of Figures

List of Figures

List of Figures

List of Tables

Chapter 1: Introduction

The failure rates of drugs once they reach clinical trials is high, with estimates up to nearly 90%. One reason for this is the lack of biologically relevant models in which potential drug candidates are screened, evaluated and selected during both discovery and development phases. Leishmaniasis is a disease that suffers from this problem. Current therapies are weak, toxic and there is a growing problem of drug resistance. Current approaches use both 2D cell assays and *in vivo* mouse models, both of which may not accurately reflect the infection in humans.

The aim of this thesis is to investigate different ways in which the current *in vitro* model systems could be made more predictive.

1.1 Leishmaniasis

Leishmaniasis is a disease caused by protozoa of the *Leishmania* genus. *Leishmania* species are protozoan parasites with two distinct life cycle phases. One phase is the motile promastigote, which is found extracellularly in the sand-fly vector and can be grown in culture media. The other is the amastigote, an obligate intracellular stage found in the phagolysosomal compartment of macrophages, one of the most common host cells in mammals. There are over 15 species[1] of *Leishmania,* usually separated into two categories: New World (Central and South-America) and Old World (Europe, Middle East, Central Asia and Africa) species, figure 1.1.1. These two categories are based on the geographical location where the species are found. Different species of *Leishmania* can cause different forms of the disease[2]: cutaneous (CL), mucocutaneous and visceral (VL).
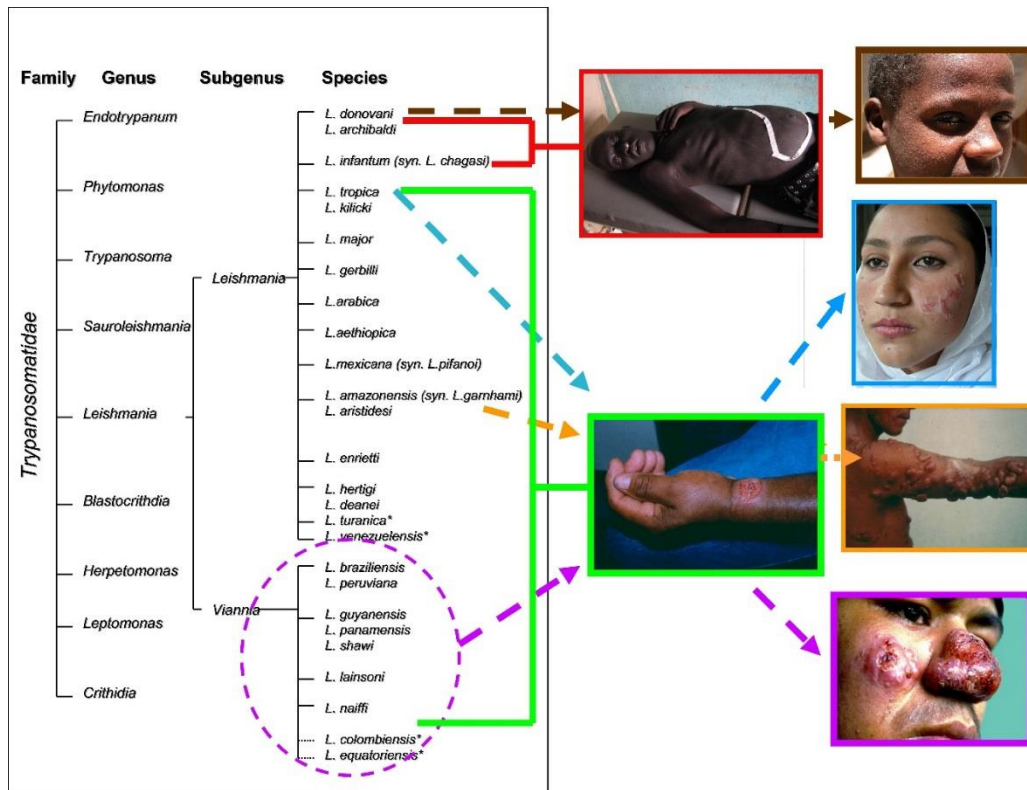
Figure 1.1-1 *Leishmania phylogeny tree and corresponding disease phenotypes[343].*

In 1901, Leishman, a colonel serving in the British Royal army medical corps, identified certain organisms in smears taken from the spleen of a patient who had died from "dum-dum fever" and proposed them to be trypanosomes; this was the first time *Leishmania* was identified in India[3]. A few months later, Captain Donovan confirmed the finding of what became known as Leishman-Donovan bodies in smears taken from people in Madras in southern India[4]. Later Ronald Ross proposed that Leishman-Donovan bodies were the intracellular stages of a new parasite, which he named *Leishmania donovani*[5].

1.1.1 Distribution and Epidemiology

Leishmaniasis is endemic in 98 countries over 5 continents and 350 million people are at risk of infection[6&7]. It is estimated to cause 0.9-1.6 million new cases every year and affect 12 million people worldwide[8]. The reported incidence of VL and CL patients is approximately 58 000 and 220 000 cases a year respectively. The overall magnitude of the problem, however, is estimated to be much higher due to underreporting. The majority (90%) of VL cases are found in six countries: India, Bangladesh, Sudan, South Sudan, Brazil and Ethiopia. In contrast, CL is more widely distributed, with 70-75% of the estimated cases occurring in

Afghanistan, Algeria, Colombia, Brazil, Iran, Syria, Ethiopia, North Sudan, Costa Rica and Peru. CL affects an estimated 10 million people and 0.7-1.2 million new cases occur every year[9].

1.1.2 Life Cycle of the *Leishmania* Parasite

The transmission of *Leishmania* species can either be zoonotic, when the parasites are transmitted from animal to man, or anthroponotic, when transmitted from man to man. *L. tropica* and *L. donovani* typically involve anthroponotic transmission[9].

The life cycle stages of the *Leishmania* parasites is summarised in figure 1.1-2. The parasites are transmitted by the bite of a female sandfly[10], of the genus *Phlebotomus* (in the Old World) or *Lutzomyia* (in the New World) [11]. Approximately 100-1000 promastigotes[12] are injected in the skin and engulfed by neutrophils, which are rapidly recruited to the site of the bite[13]. Some of the parasites survive in the neutrophils and are internalized in their phagosomes[9] that then fuse with a lysosome to become a phagolysosome. This is where they transform into amastigotes and replicate[14]. Heterogeneity in the mechanism of phagocytic uptake of the parasite into the phagolysosome, coiling versus conventional zipper phagocytosis, has been reported for different types of macrophages *in vitro*[9]. Neutrophils have been proposed to act as a transient host[15] for the amastigotes before they are taken up by either dermal macrophages or those attracted by inflammation caused by the sand-fly's bite, where they replicate. Research suggested that the presence of the amastigotes in the phagolysosome (pH 5-5.5) of the macrophage inhibits apoptosis and necrosis of the host cell and hence, contributes to the survival of the parasites[16]. Usually the low pH and enzymes in the lysosome would degrade intracellular pathogens. However, in macrophages, it is generally accepted that parasite containing phagosomes undergo 'maturation' to acquire lysosomal properties, and the *Leishmania* inhibit this process[17], potentially through the effect of a key surface lipophosphoglycan molecule. The acidic and hydrolase-rich environment of the phagolysosome is known to trigger the differentiation of the promastigote into the amastigote, and its subsequent proliferation[18]. Eventually the macrophage ruptures, releasing the pathogens which then infect other macrophages[19]. The parasites can stay in the skin or migrate to internal organs (liver, spleen and bone marrow) leading to CL or VL respectively . In CL the *Leishmania* parasites can also infect skin fibroblasts[20], it has been suggested that these cells provide a niche for survival in the face of immune attack[21].
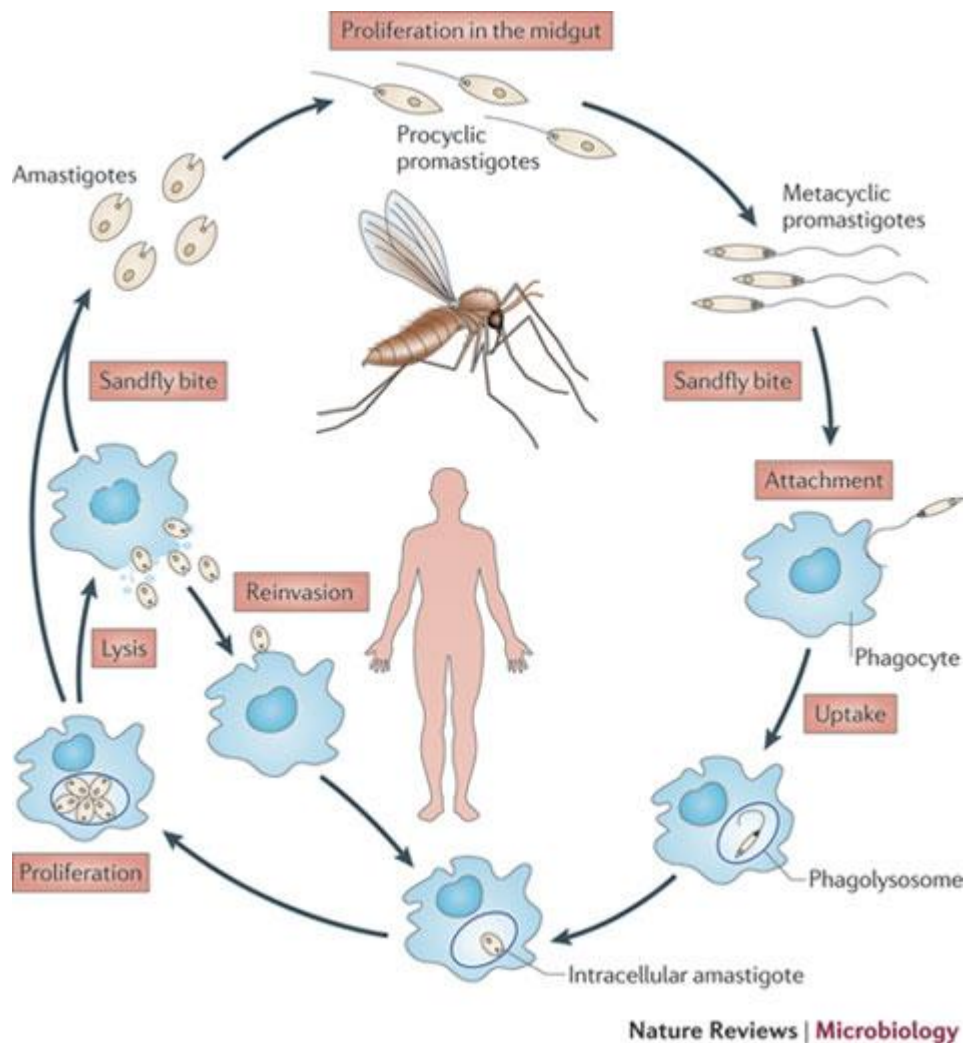
Figure 1.1-2 *The life cycle of Leishmania parasites[9].*

1.1.3   Visceral Leishmaniasis

Visceral leishmaniasis (VL) is endemic in 62 countries, with a total of 200 million people at risk, an estimated 400 000 new cases each year worldwide, and 30 thousand recorded deaths annually[6-8 &22]. Both the number of recorded cases and the geographical areas affected have grown in the past two decades. Over 90% of cases of VL occur in five countries: India, Bangladesh, Nepal, Sudan, and Brazil. It is characterized by symptoms that typically present as fever, cough, abdominal pain, diarrhoea, epistaxis, splenomegaly, hepatomegaly, cachexia, and pancytopenia, but infection with the parasites can often be asymptomatic. Infection with *Leishmania* parasites that cause VL results in systemic infection of the liver, spleen, and bone marrow. The geographical locations of reported cases of VL are shown in figure 1.1.3.

Status of endemicity of visceral leishmaniasis worldwide, 2015
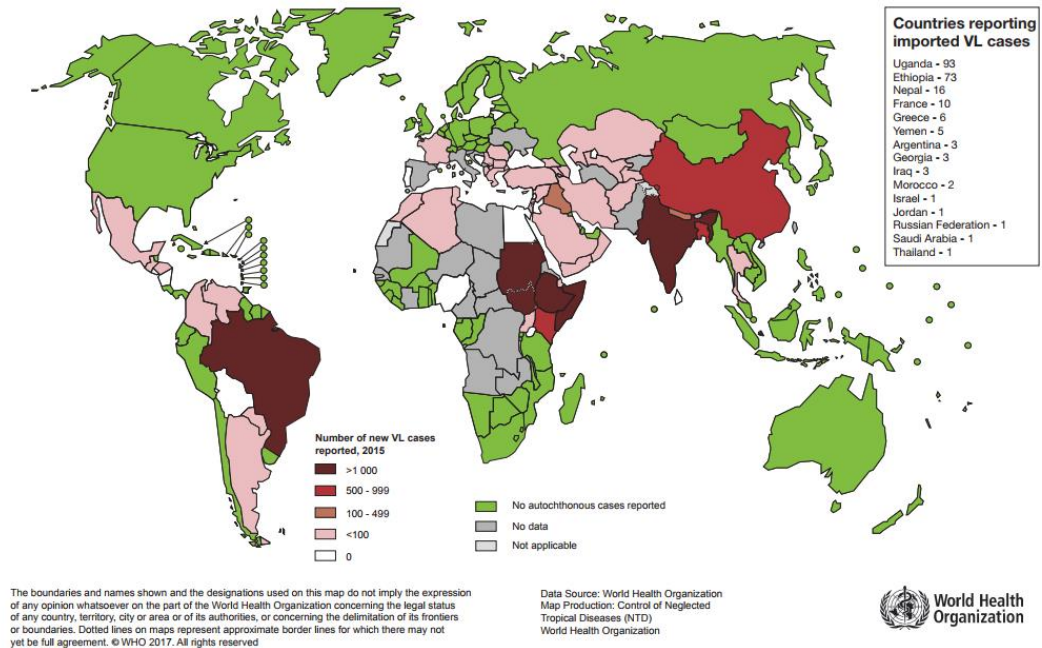
Figure 1.1-3 *World map with reported cases of visceral leishmaniasis (http://www.who.int/leishmaniasis/en/)*

1.1.4 Cutaneous Leishmaniasis

Cutaneous leishmaniasis (CL) is the most common form of leishmaniasis, its annual incidence is 1.1 to 1.5 million cases and it is endemic in 88 countries[23]. It is characterized by a variety of clinical symptoms ranging from defined nodular lesions to mucosal destruction. Most lesions tend to heal without treatment but this process can take 3 to 18 months[24] and nearly always leave a disfiguring scar, which, depending on its size and location, may cause substantial disfigurement and stigmatisation[25]. The geographical locations of reported cases of CL are shown in figure 1.1.4.

Status of endemicity of cutaneous leishmaniasis worldwide, 2015
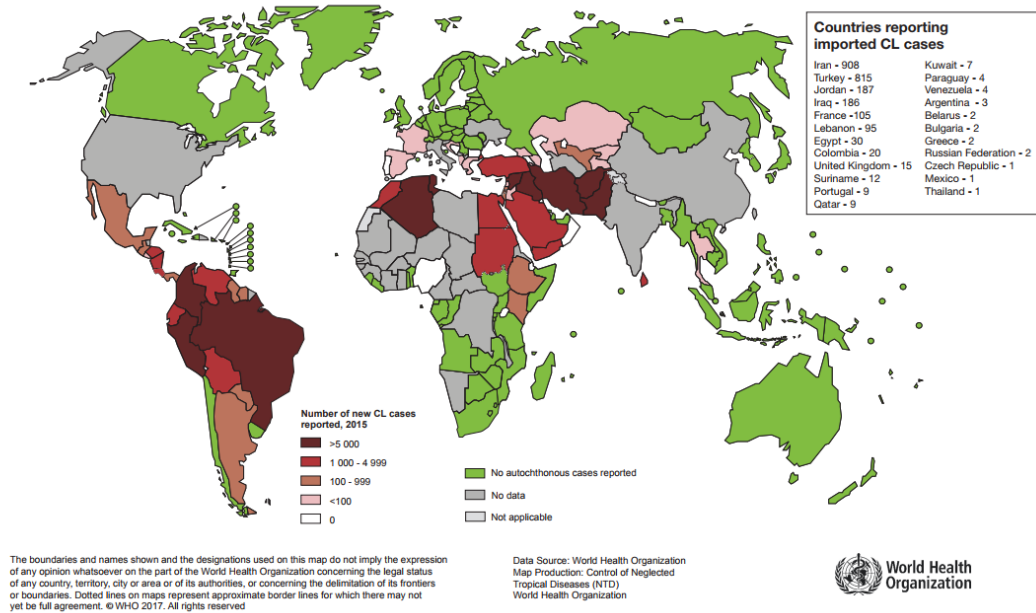
Figure 1.1-4 *World map with reported cases of cutaneous leishmaniasis (http://www.who.int/leishmaniasis/en/)*

1.1.5   Clinical Symptoms

CL has a range of symptoms, although most patients with infections probably remain asymptomatic[26]. The clinical features of CL vary in severity and depend on host, parasite and vector. Old World CL is mainly caused by *L. major*, *L. tropica* and *L. aethiopica,* whereas New World species are *L. mexicana*, *L. amazonensis*, *L. panamensis* and *L. braziliensis*.

In its simplest form, CL consists of a single localised lesion. The first sign of a localised infection is a small, itchy erythema at the site of the insect bite. Amastigotes continue to proliferate in the dermis causing the erythema to develop into a larger papule. The papule expands into a nodule that reaches its final form and size about two weeks to six months later[26]. At this point, the papule can ulcerate and a crust can form over any open wound. Sometimes the crust can fall off and an ulcer, typically with raised edges is exposed; this is particularly susceptible to further infection by bacteria[27]. Specific species might be associated with a typical clinical form but this can vary. For instance, infection with *L. tropica* can evolve to *leishmaniasis recidivans,* a chronic form of CL where satellite lesions appear in the edges of the initial healing lesion. This form is characterized by a sparsity of parasites and can last for years[28-30]. *L. aethiopica* can cause *diffuse cutaneous leishmaniasis* (DCL), a form that is characterized by widely disseminated non-ulcerated papules, nodules, plaques on the

skin. In the New World, this form is caused by *L. mexicana* and *L. amazonensis*[31]. This disease does not heal spontaneously and relapses occur frequently after treatment[32].

1.2 Treatment Challenges

It is widely accepted that all current CL treatments are unsatisfactory[34&35]. In the 1990's concern was raised about the lack of new chemical entities registered for neglected diseases. The development of a new drug is a long process that takes 9-12 years on average and costs an estimated 802 million US dollars[36&37], once the cost of all the failed attempts have been taken into account. The pharmaceutical industry is not keen to invest this amount of money in a neglected disease that only offers low return on their investment. A study published in the Lancet revealed that only 4 new chemical entities and 25 products were registered during 2000-2011 for neglected diseases[38]. Neglected tropical diseases (NTDs) are defined by the WHO as a diverse group of communicable diseases that prevail in tropical and subtropical conditions in 149 countries and affect more than one billion people, costing developing economies billions of dollars every year. They mainly affect populations living in poverty, without adequate sanitation and in close contact with infectious vectors, domestic animals and livestock.

Drug repurposing is one of the strategies to overcome the high development costs of a new drug or chemical entity[39]. This is where a known drug is tested against a different disease to its original target. This can save money and time, as the drug will already have been through toxicity testing, pharmacokinetic and pharmacodynamics studies to prove it is safe for use. Further to this, if information on the mode of action of the drug is known, then fewer studies are required. This can shorten the time it takes to get a drug to market. Another option is drug reformulation, a process that focusses on the reformulation of the active ingredient of existing drugs in order to optimise the formulation. From 2000 to 2011, all three drugs approved to treat leishmaniasis, of which one was for CL, were repurposed molecules that were initially indicated for a different disease. For example, miltefosine was first brought to the market as an anti-cancer drug[40]; amphotericin B was to treat fungal infections[41] and paromomycin was an oral treatment for intestinal amoeba infections[42].

As previously mentioned, depending on host and parasite factors, CL shows a variety of clinical manifestations. One of the main problems of treatment development is finding a treatment that is active against all *Leishmania* species. Biochemical and molecular differences between *Leishmania* species lead to differences in drug susceptibility *in vitro*[43].

This correlates with variability in clinical responses observed when the success rates of treatments are compared across different geographical regions.

There are several logistic factors that complicate the development of a treatment for CL. Firstly, CL occurs in tropical climates in regions of high temperature and high humidity where cold chains are absent. Both high temperature and humidity are known to cause instability of drug formulations[44]. Storage of some drugs can also be a problem, as they may need refrigerated conditions to maintain activity, such as liposomal amphotericin B, and reliable electricity supplies can be difficult to find in some rural areas. Furthermore, primary health centres that offer treatment for CL patients can be difficult to reach for people living in rural areas and even when reached, medication availability is not guaranteed[45].

The price per CL treatment is estimated by the WHO to range between 12-40 US$[31]. In some cases, the drug can be given freely if donated by a company or charitable organisation. This is only the direct cost of the treatment and indirect costs such as inability to work are not included. Moreover, Alvar *et al* reported that the annual income per person in areas that are greatly affected by CL range from 82 to 200 US$. This means that the price of a treatment can exceed the monthly salary for some patients[31].

Patients often seek treatment late because they will only realise they have the disease after the appearance of the first symptoms. The erythema initially could be mistaken for other diseases that may not require treatment or even considered a bad reaction to the sand-fly bite. Sometimes patients do not seek treatment because effective and safe treatments are lacking or postpone seeking help by trying herbal or homemade remedies[46]. Only after multiple herbal treatment failures, will they visit primary health care centres. Research into the treatment seeking behaviour of CL patients report variable delays between the onset of the symptoms and seeking treatment. A study in Syria reported 2.4 months on average[47], while in Paraguay this was 1-6 months[48]. By this time, the lesion might have progressed to an ulcer, which makes it more difficult to treat and increases the risk of scar formation.

Resolution happens via the action of T cells, specifically of the T helper 1(TH1) subset[33], which can stimulate host cells to kill intracellular parasites. Therefore, there is an advantage for a treatment that can kill the parasites, or encourage the immune system to clear the parasite, before extensive lesion ulceration and disfigurement can take place.

1.3 Currently Available Treatments

1.3.1 Recommended Treatments

The current first-line recommended drug treatments for CL are pentavalent antimonials. These include; 1–5 mL of 33.4 mg Sb/kg body weight per session every 3–7 days by intralesional administration, or a 15% paromomycin/12% methylbenzethonium chloride ointment applied topically twice daily for 20 days[49] . Other recommended treatments are; amphotericin B deoxycholate at 0.7 mg/kg per day by intravenous infusion for 25–30 doses, and miltefosine at 2.5 mg/kg per day orally for 28 days or in combination[33].

The available chemotherapeutics to treat CL can be divided in two groups; systemic treatments, where the drug is taken up in the blood and transported to the target tissue, or topical treatments, where the formulation is directly applied to the site of action. Systemic treatments come with a higher risk of adverse effects and is therefore typically reserved for patients with more severe or complex forms of CL.

1.3.2 Pentavalent Antimonials

The pentavalent antimonials (Sb^v): sodium stibogluconate (Pentostam®, GlaxoSmithKline and generic products)(Figure 1.3.1), often referred to as SSG, by Albert David in India and meglumine antimoniate (MA) (Glucantime™, Sanofi) (figure 1.3.1) have been first-line treatment for CL since their discovery in the 1940s[50].
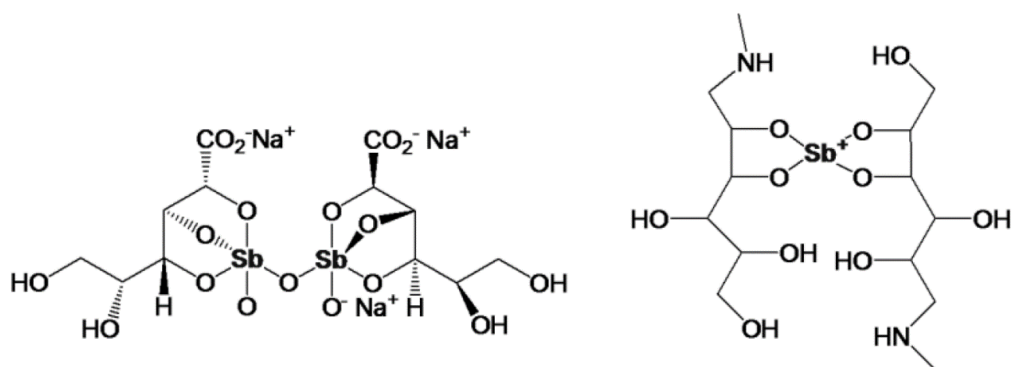
Figure 1.3-1 Chemical structure of sodium stibogluconate (Left) and Meglumine antimoniate (Right).

The mechanism of action is still not completely understood. When administered the Sb^v is converted to Sb^{III}, which is an active secondary metabolite. The data suggests that the trivalent form, Sb^{III}, disturbs the ability of the amastigotes to maintain the redox homeostasis

of the parasites, by interfering with the trypanothione reductase system that protects the parasite from oxidative damage and toxic heavy metals[51&52]. Other papers have reported DNA fragmentation and externalization of phosphatidylserine from the surface of the plasma membrane of amastigotes treated with Sb^{III}, leading to parasite apoptosis[53&54]. However, other studies indicate an intrinsic anti-leishmanial activity for Sb^V as it forms a complex with adenine ribonucleoside. This complex indirectly inhibits type I DNA topoisomerase causing a depletion of intracellular ATP possibly via inhibition of the glycolysis and fatty acid β–oxidation in the amastigotes[55]. This leads to inhibition of the biosynthesis of macromolecules in amastigotes[56-58].

Pentavalent antimonials can be administered locally or systemically depending on the severity of the disease. Local treatment consists of intralesional administration alone or in combination with cryotherapy[31]. During each session, 1-5 mL of pentavalent antimonials is injected in the edges of the lesion, followed by application of liquid nitrogen (-195 °C), if in combination. The injections can be repeated up to 5 times every 3 to 7 days. Local injections prevent or limit systemic adverse effects[59]; however, these injections are painful, causing burning, itching and inflammation at the injection site are amongst the reported adverse effects[34]. Antimonials can also be given systemically through intravenous or intramuscular administration (20 mg/kg per day for 10-20 consecutive days) when patients present with more complex CL[31]. Serious side effects such as hepatoxicity and cardiotoxicity are reported and require patient monitoring[58].

Randomised controlled trials to compare the efficacy of Sb^v treatment against placebo are sparse, and evidence-based efficacy of Sb^v against certain species is lacking[34]. *In vitro* studies confirmed species variation in drug sensitivity when tested in promastigotes[60] and intracellular amastigotes[61&62]. Moreover, an *in vivo* study testing the efficacy of Pentostam® against *L. braziliensis* and *L. mexicana* showed a statistically significant higher cure rate against *L. braziliensis*[63] compared to *L. mexicana.* It is hypothesised that this variability in drug susceptibility between different *Leishmania* species is responsible for sub-curative treatment in certain cases and consequently resistance development.

1.3.3   Amphotericin B

Amphotericin B (AmB) (figure 1.3.2) is a polyene antibiotic usually reserved for treatment of VL but is also effective against CL. It is a highly effective drug that consistently shows nanomolar EC_{50} values[64], in most anti-leishmanial *in vitro* assays.
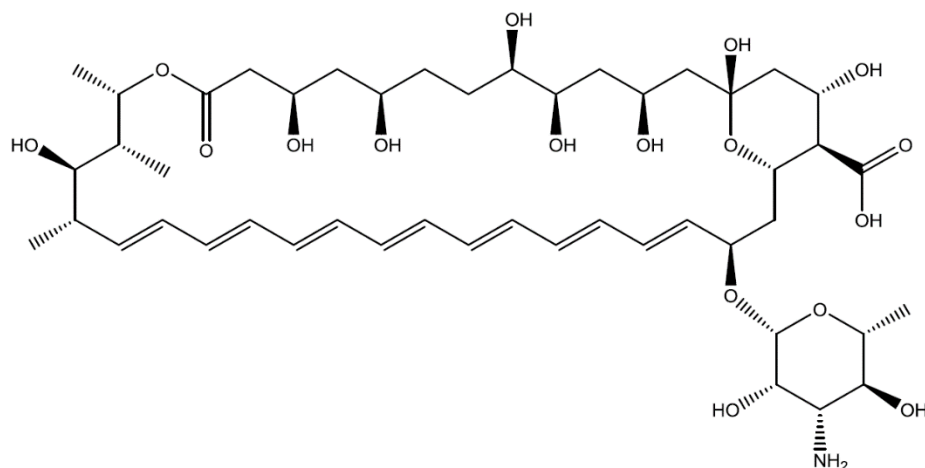
Figure 1.3-2 Chemical structure of amphotericin B.

As a treatment for CL, AmB is reserved for complex forms such as post-kala-azar dermal (PKDL) and mucocutaneous leishmaniasis, and is typically administered through slow intravenous infusion. Amphotericin B deoxycholate is given at 0.7 mg/kg/day for 25-30 doses and liposomal amphotericin B at 2-3 mg/kg/day for a total dose of 20-40 mg/kg. The conventional amphotericin B deoxycholate formulation (Fungizone®) causes acute toxic reactions including renal toxicity, for which lipid formulations were developed to reduce.

The main mechanism of action of AmB is that it alters the parasite's cell membrane permeability[65], by creating transmembrane channels, causing a collapse of ion gradients in the parasite thereby causing the parasite to die[66]. It does so by preferentially binding to sterols, within the outer cell membrane, with a high affinity for ergosterol[67]. It has been shown to act in a dose-dependent manner.

There is a lack of data from clinical trials that compare AmB treatment with placebo or Sb^v treatments even though it has successfully been used to treat patients with mucocutaneous leishmaniasis[68&69]. In a recent study, 75% of patients dropped out due to the obligatory '20 day' admission in the hospital and no cure rate was reported for the patients that completed the study[70].

1.3.4   Miltefosine

Miltefosine (MIL) (Figure 1.3.3) is recommended as a systemic treatment for both VL and CL. It is suitable for oral dosing, which makes it unique as an anti-leishmanial drug. It has been reported to show low micromolar EC_{50} values[71] in most anti-leishmanial *in vitro* assays. This

drug has been shown to have a more time dependent activity, in pharmacokinetic and pharmacodynamics studies[72]. However, it has significantly different activities against different *Leishmania* species[71].
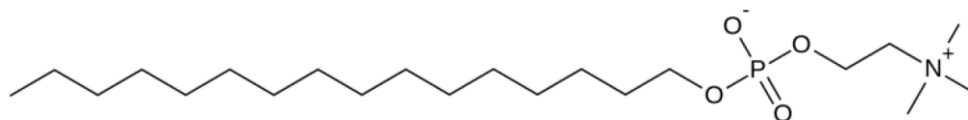
Figure 1.3-3 Chemical structure of Miltefosine.

Miltefosine or hexadecylphosphocholine, is the only oral treatment currently available against CL and VL. Initially, phospholipid derivatives were developed as anti-cancer drugs because they were found to inhibit enzymes involved in cell proliferation and growth factor signal transduction[73]. In the 1980s, a number of research groups independently showed anti-leishmanial activity of miltefosine and other phospholipid compounds[74-76].

The mechanism of action of miltefosine is not fully elucidated. Its leishmanicidal activities have been associated with perturbation of the alkyl-phospholipid metabolism and the biosynthesis of alkyl-anchored glycolipids and glycoproteins in the outer membrane of the parasite[77]. Miltefosine is a phospholipid derivative that is structurally similar to the phospholipid components of the cell membrane in both the host and parasite. Another hypothesised mechanism is the activation of the host cell mediated apoptosis of the infected macrophage via the phosphoinositide-3-kinase pathway[78].

Miltefosine is given orally at 2.5 mg/kg/day for 28 days. Gastro-intestinal problems such as vomiting and diarrhoea are the most common side effects. It is teratogenic, meaning women of childbearing age are required to take contraception whilst undergoing treatment. The long residence time of the drug in the organism (half-life:8-6 days) and the long treatment course lead to poor patient compliance and resistance development[79&80].

As with the pentavalent antimonials, a difference in intrinsic sensitivity of *Leishmania* species to miltefosine was observed *in vitro*[81&82] and might explain the variability in clinical response seen in clinical trials conducted in different regions. For example, a trial conducted in Colombia where *L. panamensis* is most common, resulted in a cure rate of 91% compared to 38% for placebo treatment. In contrast in Guatemala, where *L. mexicana* and *L. braziliensis*

were identified as CL causing species, the cure rate was only 53% compared to 32% in the placebo group[83].

1.3.5   Paromomycin Sulphate

Paromomycin (PM) (monomycin or aminosidine) (Figure 1.3.4) is an aminoglycoside antibiotic that acts by binding on the small ribosomal unit leading to misreading of the mRNA and inhibition of protein synthesis in bacteria. In the 1960's it was identified to have anti-leishmanial activity[84].
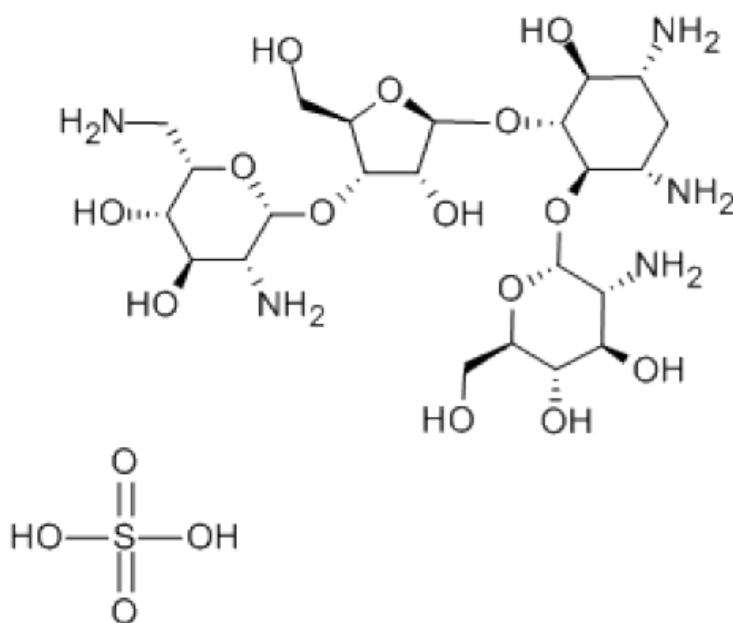
Figure 1.3-4 Chemical structure of Paromomycin sulphate.

The mechanism of action of PM against *Leishmania* parasites is not fully understood. Previous research comparing protein expression levels between PM-resistant and PM-susceptible *L. donovani* promastigotes suggested that PM reduced the protein synthesis, by inhibiting the dissociation of the ribosomal subunits[85]. Other studies in *L. mexicana* promastigotes confirmed these results and suggested that it could also lead to induction of translation errors[86] and thus altered the accuracy of protein synthesis in *Leishmania*. This increased level of misreading RNA results in defective proteins that affect parasite survival[86]. It has also been shown to change lipid metabolism, affect membrane fluidity, in the parasite, and alter uptake properties of the parasites, leading to growth arrest[87].

Paromomycin is a hydrophilic molecule with a high molecular weight (714 g/mol) resulting in poor oral availability. Therefore, a parenteral formulation was developed and is mainly used to treat VL and occasionally CL. The majority of CL patients are treated topically with Leshcutan® ointment (Teva, Israel), the only currently available topical formulation.

The topical formulation of paromomycin sulphate was first tested *in vivo* in mice by El-On et al in the early 1980's[88]. A month after the treatment (two times a day for 10 days) all lesions caused by *L. major* in BALB/C and C/C3H mice were cured.

Analyses of the subsequent clinical trials indicate a higher cure rate for paromomycin sulphate with methylbenzethonium treatment, compared to placebo, in patients infected with *L. mexicana*, *L. braziliensis* and *L. major*[34&89]. However, it is important to note that the ointment was applied after manually removing the scab of the wound and hence the drug had direct access to the affected tissues. In some studies, an occlusive dressing was used. An occlusive dressing is one that keeps water from moving either in or out of the wound but could be permeable to both water vapour and oxygen. PM has physicochemical properties that are unfavourable for skin permeation. These trial conditions do not reflect the cure rate in patients at onset of the disease where the lesions are still in the nodular stage.

1.3.6 Local Treatments

Systemic treatments for CL are often preferred for several reasons, including the fact that most new therapies for CL are derived from those used for VL. Topical or intralesional treatments are also more difficult to evaluate due to problems in standardizing the dose given during administration of a drug. Even when local treatments are known to be effective, there may be problems with crossing the skin barrier.

Intralesional injection of Sb^V drugs is the most established form of local treatment for CL[91]. Numerous studies have been performed in comparison to parenteral Sb^V treatment or other experimental therapies.

Topical paromomycin treatment for CL shows species and geographical variation. A meta-analysis conducted in 2007 concluded that in placebo-controlled trials, topical paromomycin appeared to have therapeutic activity against Old World and New World CL, with increased local reactions, when combined with methylbenzethonium chloride. However, its efficacy was not significantly different to that of intralesional Sb^V treatment for Old World CL, and it was inferior to parenteral Sb^V treatment for New World CL[91].

Many local treatments are preparations of compounds used for systemic treatment that have been formulated into topical creams/ointments. An example of this is the Amfoleish project where development of a topical formulation of amphotericin B[92] was applied locally to the CL lesion, showing high anti-parasitic effect, but without the systemic toxicity associated with amphotericin B. A Phase Ib/II open-label, randomized, non-comparative, two-arm exploratory study conducted in Colombia has recently been completed[93]. Local treatments have been used less often for New World CL due to concerns about *L. (Viannia) braziliensis* complex infections leading to mucosal leishmaniasis[91].

1.3.7   Local Physical Treatments – Cryo-and Thermotherapy

Cryotherapy and thermotherapy are the most frequently used physical therapies. Both cryotherapy and thermotherapy work by using extremes of temperature to kill the parasite, whilst only causing minimal damage to the host. The size of the host means that the body will be able to tolerate local applications of extremes of temperature, without too much damage. Once the parasites and infected cells have been killed, the body should be able to heal over any damage done to healthy skin. During cryotherapy, a cotton swab with liquid nitrogen is applied on the open wound and wound edges for about 10-25 seconds. Two studies in Iran were conducted to compare the effects of three different treatments for CL: cryotherapy alone, a combination of cryotherapy with intralesional meglumine antimoniate (MA) and intralesional MA alone[94&95]. The studies reported complete cure of patients in 52% and 67% for cryotherapy alone, 80% and 89% for a combination of cryotherapy with intralesional MA and 52% and 75% for intralesional MA alone. The researchers concluded that the combination therapy was significantly more effective than the two monotherapies. Based on these trials, it can be said that cryotherapy alone seems to be as effective as intralesional MA alone.

Thermotherapy involves the induction of heat in the superficial layers of the skin. This can be done in several ways, for instance by using a radiofrequency generator, ultrasound or infrared radiation. In Iran, a randomized controlled study compared thermotherapy and intralesional MA for 4 weeks[96]. Temperatures of 50°C was achieved and maintained on the lesions for 30 seconds. This was done once a week for four weeks. Six months after the treatment, 80% of the participants in the thermotherapy group showed complete cure, compared with 56% in the intralesional MA group. These results were in agreement with previous studies conducted in Iran.

A trial conducted in Afghanistan compared intralesional SSG for 29 days (2-5 mL every 5-7 days), daily intramuscular sodium SSG (20 mg/kg/day) for 21 days, and thermotherapy based on radiofrequency (1 session with several repeats of 1 minute of 50°C), for the treatment of CL caused by *L. tropica*[97]. Two months after the treatment, the complete cure of patients in the three groups was 47%, 18% and 54% respectively. Treatment with thermotherapy was significantly more effective than intramuscular SSG therapy, however, no significant difference with intralesional SSG was observed. Some patients that had received thermotherapy experienced superficial second-degree burn wounds.

Overall cryotherapy and thermotherapy seem to be good treatment options, as they are effective against all species. However, the main limiting factors are the requirement of expensive equipment, and availability of electricity in rural settings. The use of cyro or thermotherapy can be painful and can cause additional scars and damage to the skin. Additionally, thermotherapy requires experienced personnel to apply the treatment.

1.3.8   Immunotherapy

Research has suggested that immunotherapy can provide a useful adjuvant to chemotherapy in the treatment of CL. In contrast to chemotherapy, that aims to kill the parasite, immunotherapy stimulates the host's own immune response in order to clear the parasite from its system[7].

Imiquimod is an imidazoquinoline and acts as a potent immunomodulator. It is the active ingredient in a topical cream Aldara™ (Meda Pharma, UK). *In vitro* studies have shown that imiquimod induces a leishmanicidal activity in macrophages[98]. *In vivo* mouse studies compared the Aldara™ cream with a placebo cream and found that the group treated with Aldara™ cream showed a significant reduction in footpad swelling, when compared to the placebo group. The compound is shown to induce nitric oxide (NO) production in macrophages, which allows them to better fight off the infection. Two trials, conducted in Peru, compared the activity of standard intravenous SSG or MA combined with topical imiquimod, to treatment with antimonials alone, in patients who had not responded to previous treatment with antimonials only. Both trials indicated that treatment with imiquimod is safe and significantly increased the cure rate, compared with antimonials alone in patients. However, due to the occurrence of local irritation, a routine of application on every other day is recommended. Furthermore, the action of imiquimod reduced the residual scarring[315].

The immunomodulatory potential of simvastatin as a topical or systemic host-directed drug therapy, in controlling inflammatory responses, in an experimental mouse model of CL, caused by *L. major* has been investigated by Parihar *et al*[99]. In an ear infection model, direct topical application of simvastatin on established lesions significantly reduced severity of the disease, reflected by ear lesion size and ulceration. The host protective effect was further accompanied by decreased parasite burden in the ear, and draining lymph nodes, in both BALB/c and C57BL/6 mice. Reduced severity of disease by topical application of simvastatin in ear infection model, they found that systemic treatment with simvastatin, before *L. major* infection (prophylactic), was protective in both the resistant C57BL/6 as well as the susceptible BALB/c mice, during footpad infection[99].

Pentoxifylline is a tumour necrosis factor-α (TNF-α) inhibitor[100] that also attenuates the immune response and decreases tissue inflammation. The association of pentoxifylline with antimony improves the cure rate of mucosal and cutaneous leishmaniasis. In a randomized, double-blind pilot trial against *L. braziliensis*, cure rate was higher, although not significant, in patients who received antimony plus pentoxifylline than in those patients receiving antimony plus placebo[100].

1.3.9 New Drugs

There are currently a handful of potential new classes of drugs in the Drugs for Neglected Diseases initiative (DND*i*) drug development pipeline; amongst these are oxaboroles, nitroimidazoles and aminopyrazoles.

DND*i* and Anacor have been working together over the last few years to identify oxaborole[101] compounds, initially for the human African trypanosomes (HAT) programme. This has expanded to include both leishmaniasis and Chagas disease. DNDI-6148 has emerged as a promising lead candidate for VL and CL, and by the end of 2016, studies including exploratory toxicology necessary for possible progression to preclinical development had been successfully completed.

In June 2014, the first *in vivo* proof-of-concept for VL series 12, called the aminopyrazoles[102], from Pfizer was achieved in the hamster early curative model of VL. An initial compound gave 93% and 95% reductions in parasite number in the liver and spleen respectively after five days oral dosing at 50 mg/kg,. A subsequent compound showed even higher *in vivo* activity (>99% reduction in both the liver and spleen). The project moved into the lead optimization stage in January 2015, with further compounds being designed and tested. Profiling of

current and new leads in a panel of drug-sensitive and drug-resistant strains of *Leishmania*, exploration of the *in vivo* dose-response, rat pharmacokinetics, and initial *in vitro* safety assays are all underway.

A project based on a series of nitroimidazole compounds was started and was terminated in early 2015[103]. The decision was taken to progress with lead compounds from two sub-series previously identified from the nitroimidazooxazine backup programme (DNDI-8219 and DNDI-0690), which had good efficacy *in vivo*, higher solubility, and lower potential for cardiotoxic effects. A 14-day toxicity evaluation carried out in 2015 led to DNDI-0690 nomination as a pre-clinical candidate. In addition, with other potential lead compounds for VL, DNDI-0690 was profiled *in vitro* against CL-causing strains of *Leishmania* at the London School of Hygiene & Tropical Medicine and the Walter Reed Army Institute of Research, and showed good to excellent activity, consistent with their activity against *L. donovani* and *L. infantum*.

As previously mentioned, repurposing is a possible strategy for the development of new drugs. Some examples of repurposing being used in the treatment of leishmaniasis are imipramine[104], fexinidazole[105], tamoxifen[106] and tafenquine[107], all of which showed *in vivo* activity.

Another area in which new treatments are being explored for CL is the use of combination therapy[108]. A recent example of this is the clinical trial on the use of thermotherapy and a short course of miltefosine in combination. Local heat is applied using a localized current field radio frequency generating. The electrodes are applied to the skin heating one single lesion to 50°C. Depending on the size of the lesion, more than one application may be administered. In addition to receiving one single session of thermotherapy as described above, subjects received oral miltefosine, two or three capsules a day, which is the equivalent of 100 to 150 mg respectively for 21 days.

1.3.10 Drug Resistance

Another issue with the treatment of CL and VL, is the increasing frequency at which drug resistant strains are encountered[109-111]. Clinical resistance to amphotericin B is rare[110]. Nevertheless, with the increasing use of amphotericin B, the possibility of emerging resistance cannot be ignored.

Laboratory studies have shown that resistance to amphotericin B can be induced with minimal effort by changing their membrane chemistry[65]. One method by which the parasite

can do this is, is to alter the expression of methyl transferases in the thiol metabolic pathways[112]. Miltefosine has such a long half-life that sub-therapeutic levels are maintained over long periods in the body, which could easily lead to the emergence of resistant strains[110]. The main route of resistance against miltefosine is the reduction of uptake into the parasites[113]. Finally, there is an issue with the fact that different species are affected to different degrees by each drug. In addition to this, within each species there are different strains that also show different responses when treated[71]. There is also the host cells to consider, as drug uptake and accumulation may be different in different cell types[114]. This leads to variation in the activity of drugs even between different strains in the same host cell type, depending on the source of the cell.

1.4 Rationale for Improving the Drug Discovery Process

1.4.1 Drug Discovery

Recently there have been few advances for the treatment of simple or complex forms of CL. The main challenge for CL is to ensure that this disease is on the research and development agenda, so that new drugs are evaluated. There is a great need for the discovery and development of anti-leishmanial drugs, as those that are currently used for treatment, for either CL or VL, suffer from a wide array of side effects that can cause more discomfort than some pathologies of the disease.

In a recent high-throughput screening (HTS) of 1.8 million compounds by GSK[115] against *L. donovani*. 67,400 primary hits were identified; an overall hit rate of 4%. Confirmation of activity above the cut-off in at least one replicate was displayed for 32,200 compounds. The remaining compounds were tested in an intracellular assay of *L. donovani* infected THP1-derived macrophages, resulting in 5,500 active compounds. Compound potency (EC_{50}) as well as acute cytotoxicity of the compounds were assessed. Subsequently, 351 non-cytotoxic compounds were found. This screen shows a major problem with the development pipeline, which is the number of active compounds that are found unsafe due to high cytotoxic effects.

Another screen of note is one conducted by Novartis[116] who tested 1.5 million compounds in proliferation assays on three different parasites; *L. donovani*, *T. cruzi* and *T. brucei*. This was followed by triaging of active compounds, EC_{50} values of less than 10 µM with a clear window of selectivity with respect to growth inhibition of mammalian cells. An azabenzoxazole, GNF5343, was identified as a hit in the *L. donovani* and *T. brucei* screens.

Although GNF5343 was not identified in the *T. cruzi* screen, it has shown potent anti-*T. cruzi* activity in secondary assays.

Optimization of GNF5343 involved the design and synthesis of ~3,000 compounds, and focused on improving bioavailability and potency on inhibition of *L. donovani* growth within macrophages. A lead candidate from this cycle of chemical improvements was named GNF6702. An *in vivo* footpad infection of BALB/c mice with the dermatotropic *L. major* strain, treated with GNF6702 at $10\,\mathrm{mg\,kg^{-1}}$ twice daily caused a fivefold decrease in footpad parasite burden and a reduction in footpad swelling. Both $3\,\mathrm{mg\,kg^{-1}}$ and $10\,\mathrm{mg\,kg^{-1}}$ twice-daily regimens of GNF6702 were superior to $30\,\mathrm{mg\,kg^{-1}}$ once-daily miltefosine regimen ($P < 0.01$)[116].

1.4.2 Drug Discovery Pathway

The drug discovery pathway is a long process that takes both a lot of time and money, with estimates at $1395 million dollars[117] as an estimated average out-of-pocket cost per approved new compound. Despite the large investment, only a small number of compound will make it out of the pipeline[118]. The path to a marketed drug involves a long and exhaustive journey through basic research, discovery of the drug, preclinical development tests and formulation of the medicine and a series of complicated clinical trials with humans before regulatory approval. Usually 15 to 20 years[36&119] of research and millions of pounds later, there is a possibility that a new drug will be approved for marketing. Drug discovery and development is widely recognized as one of the most financially risky endeavours in all of science and a major challenge for the industry. Much of this cost comes from failures, which is estimated to account for 75 percent of the total research and development cost. The failure rates of drugs once they reach clinical trials is very high, and is estimated at nearly 90%[120]. One possible reason for this is the lack of biologically relevant models in which potential drug candidates are screened, evaluated and selected during both discovery and development phases. Key areas that are in particular need of better models are those that are used for pharmacodynamics and pharmacokinetic experiments as conditions that influence these factors are hard to recreate *in vitro.* Leishmaniasis is a disease that suffers from this problem, of having limited disease relevant models in many stages of its drug development pathway.

1.4.3 Need for Predictive Assays

The common and persistent failures to translate promising preclinical drug candidates into clinical success highlight the limited effectiveness of disease models currently used in drug discovery. An apparent reluctance to explore and adopt alternative cell and tissue based model systems, coupled with a detachment from clinical practice, contributes to ineffective translational research[121].

Finally, a substantial proportion of clinical trial failures for novel medicines overall are due to safety issues such as cardiotoxicity and hepatotoxicity, and serious toxicity issues are often discovered only during clinical development has been completed. Thus, more predictive toxicology models would contribute substantially towards more successful clinical translation and improved patient care[122].

1.4.4 Improving *In Vitro* Models

Despite advances in target and cell based screening technologies, the majority of drug discovery projects remain dependent on cell culture systems that were developed several decades ago, incorporating immortalized cell lines. Many researchers consider the use of such assay systems to be questionable owing to their poor disease relevance. Traditional cell culture methods typically rely on immortalized cells grown within artificial environments, and on non-physiological substrates such as functionalized plastic and glass. Although these methods have facilitated the discovery of many basic biological processes, they often fail to provide an adequate platform for drug discovery owing to their inadequate representation of key physiological characteristics[121].

Most cell-based assay screens are performed using cell lines, that have been cultured for many generations, resulting in a substantial drift in their genetic, epigenetic and physiological characteristics, which means they are not a good model of primary tissue cells[123&124]. The genetic and epigenetic abnormalities, characterized by multiple genetic rearrangements and amplified gene copy numbers, associated with long-term culture confound pharmacogenomics and functional genomic studies. Genetic adaptation resulting from long-term *in vitro* cultures also contributes to heterogeneity in cultures of the same cell line between passages, batches and laboratories. One way to improve the cells used in assays is to use either freshly isolated primary cells or cells derived from stem cells[125]. Using cells that are more closely related to human biology can reduce the problems caused by genetic drift and long-term culture. The development of induced pluripotent stem cells (iPSCs) gives the

use of these stem cells other advantages such as, easy accessibility, expandability, ability to give rise to almost any cell types desired, avoidance of ethical concerns and the potential to develop personalized medicine.

The media most commonly used for cell culture is designed for fast cell growth, incorporating large concentrations of fetal serum and nutrients, which may promote de-differentiation of primary cell types into more embryonic or fetal-like phenotypes[126]. Cells are often grown in standard incubators under high oxygen partial pressure, approximately 20%, which does not represent the steady-state conditions of human organs and tissues, fluctuating between 1% in the dermis, and 14% in arterial blood[127-130]. This has a profound impact on cell metabolism, reactive oxygen species production, mitochondrial functions and, ultimately, the differentiation and function of cells[131&132]. Additionally, conventional tissue culture systems do not readily permit the formation of short-range gradients of nutrients, hormones and oxygen that are often experienced by cells, depending on the distance to the nearest blood vessel. This can be mimicked with the adoption of microfluidic systems that can be adjusted to mimic physiological conditions and deliver nutrients, dissolved gases and remove waste products[133].

The two-dimensional (2D) planar substrates on which cells are typically grown are stiff, demonstrating high tensile strength and mechanical resistance to deformation, unlike most substrates found in the human body, with the exception of bone and cartilage[134]. Hence, the plastic or glass used in cell culture may not accurately represent the normal *in vivo* mechanical environment[135&136]. To avoid these problems a 3D environment could be used. Initially the use of collagen coating and other extracellular matrix substitutes can lead to a more natural environment for the cells. Further to this, 3D confirmations can be recreated using a scaffold for the cells, allowing complex cell behaviours to develop. Both solid scaffolds and hydrogels can be made with a variety of different tuneable properties. Stiffness, resistance to deformation and swelling behaviour can all be varied by changing either material or the concentration of polymers in hydrogels[137&138].

A further challenge in tissue modelling within current *in vitro* assays is the absence of a physiologically relevant extracellular matrix (ECM). For example, the popular use of Matrigel, a gelatinous protein mixture secreted by Engelbreth-Holm-Swarm mouse sarcoma cells with chief components of Matrigel being structural proteins such as laminin, entactin, collagen, heparan sulphate proteoglycans and growth factors, and collagen type I as an ECM substrate in hepatocyte cultures, does not represent the ECM proteins predominantly found in the

liver[139]. Many pathologies are associated with changes in ECM production. Some attempts to rectify this problem have been made; often to address this issue the solid scaffold used in cellular models is a decellularised section of tissue leaving only the ECM, which then can be seeded with new cells. In other models, the decellularised ECM is lyophilized and added to a hydrogel in order to restore the ECM proteins that would be missing from the hydrogel[140].

Cell-culture screening assays traditionally use a single cell type, whereas cells *in vivo* are in either direct contact or communicate over a long range with many different cell types. As most biological processes and pathologies involve the interaction of multiple cell types, these should ideally be incorporated into *in vitro* cellular assays whenever possible. For example, most toxicology assays use only hepatocytes, but although 80% of the liver volume consists of hepatocytes (60% of the cells); other important cell types within the liver include stellate cells, resident macrophages (Kupffer cells), sinusoidal endothelial cells and some non-parenchymal cells. Both stellate cells and Kupffer cells are known to be important for some compound toxicities and should therefore be incorporated into *in vitro* toxicology assays[141&142]. Further development of co-culture methods, which incorporate disease cells with relevant immune sub compartments, is also urgently needed to help better understand and address the role of the host immune system in the pathology and therapeutic outcomes of diseases. These considerations are of particular importance for pathogen biology and infectious diseases, which operate at multiple cellular and tissue levels[143].

1.4.5   Improving *In Vivo* Models

A model is a simple representation of a complex system. Consequently, an animal model for a human disease is by no means attempting to reproduce the human disease with all its complexities in an animal. Animals are instead used to model-specific aspects of a disease. Whenever an animal model is used, it is thus of utmost importance to define a specific question and to ensure that the chosen model is fit for purpose. Compounds fail for many reasons, but some are more avoidable than others. Poor oral bioavailability, pharmacokinetic properties or toxicity issues that are not predicted by animal pharmacology result in overlap of efficacious and toxic doses. These are often reasons for Phase I and Phase II attrition rates[144]. Indeed, animal studies seem to overestimate by about 30% the likelihood that a treatment will be effective because negative results are often unpublished[145]. Similarly, little more than a third of highly cited animal research is later tested in human trials.

First, *in vivo* studies typically use high doses of compounds, which are orders of magnitude greater than those humans are exposed to. Whilst these higher values can be scaled with

allometric scaling[146], dose-response relationships are complex, so extrapolation from these high doses to lower, human, exposure levels is difficult and results in many inaccuracies. Second, *in vivo* studies examine the response of a standard laboratory animal to a xenobiotic. This response may or may not occur in humans. Even more important is that the human population is very heterogeneous and a single strain of animal cannot accurately predict the variability in responses seen in the human population. Finally, *in vivo* exposures in toxicity testing are usually composed of a single compound. While this allows for close examination of the results of that single compound, humans are constantly exposed to mixtures of compounds daily, and the effects of these co-exposures need to be examined[147].

Many outcomes used in animal models are dependent upon subjective interpretation. While subjective evaluations are generally a very efficient way to score behavioural endpoints, it can create bias if the scorer is aware of the animals' treatment[148]. One way to avoid this is to conduct blind studies.

In animal models, treatment is frequently initiated either before or shortly after the disease pathology is initiated. This is in contrast to the clinical situation, in which treatment is normally started after onset of symptoms and clear diagnosis. Thus, a potential pharmacological effect could be overestimated in an animal model.

While most experimental set-ups are very much standardized in a particular lab, slightly different parameters in another lab may yield different results. Repetition of experimental findings in slightly different models can give different results based on the biological differences between models[148]. Each result is from a separate entity and this means that variation is inherent and unavoidable. The animals will have different responses to both the treatment and the disease; this can cause large variation in results. If this happens, it is not hard to image that a valid response to the drug could be labelled as an outlier.

The use of animal models can also be expensive. The more specific the animal strain, often allowing it to be more biologically similar, the more it can cost. Mouse strains can be inbred lines in order to maintain the specific phenotypes required by the end user. This, however, can lead to genetic issues, due to the nature of inbreeding. A well planned experiment can use many animals, as groups must be large enough to be statistically relevant despite the inherent variability in the animals. Often due to the high cost of animals, researchers will compromise on the number of groups and animals a study will consist of in order to save money.

Humanized mouse models in which immunodeficient mice are engrafted with human cells or tissues, are considered extremely useful. They allow human research studies *in vivo* and hence support clinical translation[149]. Dependent on the human disease, and question addressed, different humanized models and mouse strains are utilized. Most commonly used are the human tumour xenograft models for the study of cancer, and the humanized mouse models that mimic the human immune system.

A humanized mouse model of HIV infection generated by CD34$^+$ hematopoietic progenitor cell transplantation is used as the replication of HIV, is not supported in other murine *in vivo* models[150]. In these mice, CD34$^+$ cells generate *de novo* human immune cells capable of supporting *in vivo* HIV replication. Due to the limited tropism of HIV, *in vivo* modelling of this virus has been almost exclusively limited; use of similar lentiviruses such as SIV that reproduce many important characteristics of HIV infection have been used as a substitute. However, there are significant genetic and biological differences among lentiviruses and some HIV-specific interventions in non-human hosts. Humanized mice are systemically reconstituted with human lymphoid cells offering rapid, reliable and reproducible experimental systems for HIV research. Advantages of this humanized mouse model include: their small size, relatively low cost, making them more accessible than primate models, and multiple humanized mice can be made from different human donors, permitting control of intragenetic variables. Both primary and laboratory HIV isolates can be used for experiments; and in addition to therapeutic interventions, rectal and vaginal HIV prevention approaches can be studied[150].

Plasmodium species infecting rodents and humans are highly divergent. While some critical factors for pre-erythrocytic infection are known in rodent-infecting *P. berghei* and *P. yoelii*, it remains largely unknown how relevant they are for *P. falciparum* and *P. vivax* pre-erythrocytic infection[151]. Several humanized mouse models utilized to study human infective species at different stages of the malaria life cycle have been created. A better understanding of the receptors required for sporozoite invasion of host cells would uncover a remaining mystery about the malaria parasite and could facilitate the development of novel, immunocompetent, humanized mouse models. The first success in assessing *P. falciparum* liver stage development in liver-humanized mice used Alb-uPA on a SCID background[152]. The liver of these mice can be robustly repopulated with human hepatocytes soon after birth and these hepatocytes are susceptible to *P. falciparum* infection. More recently, it has been demonstrated that *P. falciparum* can infect fumarylacetoacetate hydrolase null mice (FRG

KO) mice. These mice lack FAH, Rag2 and IL2rγ and are efficiently transplanted with human hepatocytes (FRG KO huHep) [153]. It has been shown that this model supports robust *P. falciparum* sporozoite infection and supports complete maturation of parasites. This model is now fully established in antimalarial drug development studies. A combined humanized mouse model that can harbour liver stages, allows transitions to blood stages and continuously supports blood stage infection, would constitute a major advance.

The modelling of pharmacodynamics and pharmacokinetics is often done in animal models. Effective pharmacokinetics and pharmacodynamics (PK/PD) study design, analysis, and interpretation can help scientists elucidate the relationship between PK and PD, understand the mechanism of drug action, identify PK properties for further improvement and optimal compound design and dosing regimens. A large variety of animal models have been used to characterize the pharmacodynamics of antimicrobials[154]. Animal models have the advantage of determining antimicrobial efficacy at specific body sites such as the thigh in mice, the peritoneum in mice and rats, the lungs in mice, rats, and guinea pigs, endocarditis in rabbits and rats, and meningitis in rabbits. However, clearance of antimicrobials is more rapid in animals than in humans. Many factors, such as inoculum, media, growth-phase of the organism, site of infection, drug concentrations to measure correct drug exposure, presence of neutropenia, and measurement of outcome by colony-forming units (CFUs), survival/mortality, or another form of assessment, need to be considered to develop meaningful conclusions[154].

When adequately designed and conducted, animal models can contribute invaluable information to our knowledge of biology and medicine, including the discovery and development of new drugs. However, better design and conduct, as well as further development of animal models is warranted.

1.5 Assays to Test the Activity of Drugs

1.5.1 *In Vitro* Assays

In vitro screening has many advantages over *in vivo* screening methods, such as a vast reduction in both time taken and cost. It also avoids ethical issues related to the use of animals. Today many cell lines are widely available, and it is possible to culture many different cell types. Immortalised cell lines are relatively easy to maintain in comparison with mice and can be maintained almost indefinitely. Large screens can be conducted using cultured cells rather than hundreds of mice, over a much shorter period. *In vitro* drug assays

can be completed within a week whereas, an *in vivo* experiment may take several weeks before the infection is seen and before a drug can be applied and evaluated. The amount of drug used in *in vitro* assays is also much less than in a standard *in vivo* experiment. When conducting an *in vitro* assay, more precise control over the conditions of the assay can be achieved and because of this, reproducibility is greater than in *in vivo* assays. In order to be relevant, *in vitro* screens must provide a good prediction of activity *in vivo* and be able to reflect cellular level changes that can be viewed with ease. However, this is often not the case as *in vitro* assays are usually lacking in biological complexity.

1.5.2   *In Vitro* Assays for Testing Compounds against *Leishmania*

In vitro assays for the testing of compounds against *Leishmania* parasites can be performed in a variety of ways. A number of aspects can be studied such as rate of kill, percentage infection, total burden or burden per cell after differing number of days. When choosing an assay there are a number of things to consider. *In vitro* assays have been conducted using a variety of cell types; these include a Sticker dog sarcoma fibroblasts cell line[155], transformed rodent macrophage cell lines[156], human monocytic cell line derived from an acute monocytic leukaemia patient, primary isolated mouse peritoneal or bone marrow macrophages and human monocyte-derived macrophages[157]. Another consideration is the stage of parasite that the drug will be tested against[157] and whether the parasite will be actively dividing within the host cells. A further consideration with use of parasites is how long they have spent under *in vitro* culture conditions. It has been seen that after multiple passages the parasites adapt to *in vitro* culture, changing their biology and potentially altering the effect compounds would have on them[158].

1.5.3   Assay Endpoints

The main method of evaluating intracellular infection of macrophages by *Leishmania* is to count the number of macrophages that have been infected. An *in vitro* assay involves infecting a population of cultured cells and then, after a 24 hour period, treating with a drug over a set period of time, usually for 72 hours, before determining their infection levels and elucidating the activity of the drug. Usually this requires the host cells to be fixed and stained before observation under an oil immersion microscope[157]. This allows the counting of the number of infected cells or the number of amastigotes within each infected cell; usually over a hundred cells are counted in total. Another method that involves counting is the limiting dilution assay[159] where the number of viable intracellular pathogens can be determined by

creating a dilution series of the remaining parasites and measuring replication rates in each dilution in order to determine the number of viable parasites within the original sample.

A variation on the above counting method is to use parasites that have been transfected with a fluorescent[160&161] or bioluminescent[163] marker. This allows the parasite to produce a signal that can be measured using different techniques. With these parasites, fluorescent microscopes or confocal imaging allow for easy counting of the infection. The imaging of fluorescent parasites can be detected and evaluated in many ways, such as total fluorescent signal, size of fluorescent area or simply the number of infected cells. One advantage that fluorescent or bioluminescent parasites have over a Giemsa stained slide is the difference in contrast between parasite and host cell. Automated systems such as Opera® (PerkinElmer, UK), can count the number of infected cells when used with these transfected parasites.

A problem with using the counting method to determine infection is that it takes a long time for large data sets to be processed. A mechanised counting version as an end-point is flow cytometry, which allows cells infected with fluorescent or bioluminescent parasites to be counted[135]. Counting is also not easily compatible with 3D cell culture as the scaffolds or extracellular supports can easily stop cells from being viewed under light or fluorescent microscopes. The use of dyes, fluorescent or bioluminescent parasites and confocal microscopy would be needed. Another issue is that drug cytotoxicity can drastically change the number of cells available to count, which you would not be able to monitor until the sample is fixed and stained.

There are many assays that do not give a microscopically read estimation of infection as a final readout, but give a value that can be scaled against specific controls to give a normalised readout based on the infection levels. These may become necessary as the complexity of *in vitro* systems increases and counting becomes impossible. Colorimetric assays are assays that use a colour change or development that can be detected by either absorbance or fluorescence. A simple example of this is the use of Alamar Blue, the oxidation–reduction indicator has been used for colorimetric determination of parasite cell viability and proliferation. Alamar Blue® is non-toxic for cells even during long incubation times. In the living cell, Alamar Blue® is reduced thereby changing its colour from blue to red allowing for detection of the number of viable parasites[163]. Another chemical that has been used along the same line is 3-(4, 5-dimethylthiazol-2-yl)-2, 5-diphenyltetrazolium bromide (MTT). Surviving *Leishmania* parasites can be quantitated by their conversion of the chromophore MTT[164]. Reduction of the yellow MTT to an insoluble formazan, which has a purple colour, by

NADPH-dependent cellular oxidoreductase enzymes provides a measurable signal relating to cell viability.

Another colorimetric method that has been developed uses a parasite-specific enzyme, trypanothione reductase, which reduces trypanothione disulphide leading to a colour change through the coupled reducing activity of 5,5'-dithiobis 2-nitrobenzoic acid, which can be detected by measuring its specific absorbance[165]. The assay measures the activity of an enzyme unique to the parasite so that host cells do not affect the colour change caused by the reaction catalysed by this enzyme.

Along similar lines are assays that use reporter gene technology, where a gene has been transfected into the promastigote and produces a coloured or luminescent molecule or one that can react with an added chemical to create a measurable change in colour[162] that can be detected and used as a measure of how many parasites are present. The use of such genes, like the firefly luciferase[166] or the green fluorescent protein (GFP) gene[167], could considerably facilitate the screening of antimicrobial agents by allowing direct read outs of the remaining fluorescent signal after drug treatment. β-galactosidase[168], chloramphenicol acetyltransferase[167] and alkaline phosphatase[167] are all genes that can be transfected into the parasite causing it to produce a specific enzyme that will then be used to catalyse a reaction that produces a coloured product, which is then detected by absorbance.

Quantative polymerase chain reaction (qPCR) can be utilised as a method, which can be used to detect relative and absolute levels of parasite and host cell DNA when compared to a set of standards[169]. The results from this can show a decrease in DNA concentrations if the parasite has been cleared, whilst also giving a measure of the possible cytotoxic effects of the compound if it reduces the host cell DNA concentration. A further elaboration on this method is the use of reverse transcriptase qPCR, by adding the reverse transcriptase step you are only amplifying the RNA produced by actively viable parasites[170]. This is important, as it is possible for the DNA of parasites that have been killed to remain after the parasite has been killed.

1.5.4   High-Content Screening for Anti-leishmanial Agents

There is a strong trend towards high-content screening (HCS) of compound libraries as a tool for drug discovery[171]. High-content screening is a type of phenotypic screen, looking for changes in cells that may include increases or decreases in the production of cellular products such as proteins, changes in cell morphology or, for *Leishmania,* the presence of

parasites. High content screening includes any method that is used to analyse whole cells or components of cells with simultaneous readout of several parameters, such as parasite burden, percentage infection and number of live parasites all at the same time. Using the usual manual counting method would take a very long time for each data set to be fully evaluated, so automated image analysis is required. Even though an automated system is faster it requires greater time to set up and train the system to count as specified, even then images often have to be manually reviewed to check the results of the automated counting. A group from the Institut Pasteur Korea have used automated multidimensional analysis of macrophages infected with *Leishmania* parasites to determine drug sensitivities by studying a variety of factors[172]. Variables such as cell number, infected cell number, number of parasites per cell, cell dispersion and cell shape and texture have been analysed by an algorithm designed especially for the analysis of infection by *Leishmania* parasites. A group at the University of Dundee, conducted a similar assay, where images of fluorescent parasites in labelled macrophages were analysed and inhibition curves could be derived[173].

These high content screening methods can be used as a form of high throughput screening. Other methods, mentioned such as the colorimetric assay and reporter gene technology, also lend themselves to high-throughput screening as they can be quickly analysed and are cheap to complete[120&165], but provide less information than the high content based image analysis. Most high-throughput screens have used a reporter gene transfected strain of *Leishmania*[174].

1.5.5 *Ex Vivo* Assays

Ex vivo assays are conducted in or on tissue that is taken from an organism and moved to an external environment. Thus, there is minimal alteration of the physiological conditions within the tissue. *Ex vivo* conditions allow experimentation on an organism's cells or tissues under more controlled conditions than is possible in *in vivo* experiments; however, this is at the expense of altering the "natural" environment. A primary advantage of using *ex vivo* tissues is the ability to perform tests or measurements that would otherwise not be possible or ethical in living subjects. Tissues may be removed in many ways, including in part, or whole, organ removal. VL can be studied in splenic explants[175] and samples of blood[176] that, once removed from the body, can be cultured in a way that allows for the maintenance of the parasite. For cutaneous leishmaniasis, a skin explant model would be more relevant.

1.5.6   Standardisation among Laboratories

A major problem with current *in vitro* assays is standardization of conditions among labs. Due to the large differences that can occur, not only through the use of different strains, but also the use of parasites at different stages of its lifecycle, it is almost impossible for different labs to be testing on the same parasite. This inherent variation is also seen between host cell sources. This can mean results are hard to replicate among labs and this can inhibit the development of new assays[177].

1.6 Cellular Models for the Study of Disease

1.6.1   Why use Cellular Models

Due to concerns about animal welfare, time and cost constraints, and the ever increasing number of chemicals that need testing, establishing more predictive *in vitro* culture systems has become a priority. In addition, the predictive accuracy of rodent *in vivo* testing for human adverse health effects has become a matter of dispute in recent years[147, 178&179]. In part due to poor concordance of animal study results to disease phenotypes observed in heterogeneous human populations.

In vitro models to study disease are used for many of the same reasons mentioned in the *in vitro* assay section. There has been much development in models, over the past few years, to move from standard 2D *in vitro* static single-time point assays to model systems that are more biologically relevant.

1.6.2   Increasing Complexity

An easy first step to make a more biologically relevant system is to have a system where the cell culture medium constantly flows, transforming a 2D static system to a 2D flow system. In this way, you can mimic the fluidic conditions within the body[180]. Many tissues within the body have direct contact with moving bodies of fluid[181], from the obvious circulatory system and digestive system to the slightly less considered spinal fluid and lymphatic system. The movement of the fluid is important for a number of functions, such as nutrient delivery and waste removal[182]. In addition to this, a media perfusion system can provide the cells with biologically relevant shear stress and oxygen gradients[183], which are not reproducible in static systems. A further point to the fluid flow is that it allows for the creation of gradients, which are found in many biological environments and can be important for the function of that environment[184&185]. The flow of media through the cell culture system is especially

important as it allows for further complexity in the system to be maintained in conditions that would otherwise not easily support such complexity[182].

Along similar lines the use of bioreactors for the maintenance of cells have many of the same features as media perfusion systems. However, bioreactors can be scaled up for industrial uses producing many cells from the same growth conditions. In this method, cells can be harvested without passage and interruption of growth cycles[182].

Complexity can be increased by moving from 2D to 3D cell culture. The culture of cells in two dimensions is arguably primitive and does not reproduce the anatomy or physiology of a tissue for informative or useful study[186]. Creating a third dimension for cell culture is clearly more relevant. The 3D environment allows the cells to take a more physiologically relevant shape and volume[187]. This alters, not just the surface area to volume ratio, but fundamentally changes the availability of the cell surface for both cell-cell interactions[188] and other important cell surface activities, such as receptor presentation[188] and particle uptake[189].

Using primary cells instead of immortalized cell lines is another way to improve the predictiveness of a model. Immortalized cell lines are created by fusing a cell line with a cancer cell line which can lead to the resulting cell line taking on some of the properties of the cancer cells. For example as well as the intended immortalisation they also can take on other phenotypes[190], for example, Hepa1– 6 cells were found to be deficient in mitochondria[190]. Using primary cells can avoid this issue and also has the added benefit that the cells are much closer to the cells that are found in the body, increasing biological relevance. The choice between human or animal primary cell should depend on the purpose of the model.

Another option for cell choice, that may be more biologically relevant is the use of either stem cells or more readily available iPSCs. For the same reasons of being closer to the cells found within the body these cells could be more predictive in cellular assays[191]. The use of iPSCs has the added advantage that the cells can be donor specific and has been shown to react in the same way as the patient they are taken from. This way genetic variation is taken into account[192].

Using a cell culture system containing more than one type of cell is another way to increase the predictive strength of the model. It is obviously an understood fact that within the body, cell types do not function in isolation, and therefore, are always under the effects of surrounding cells in the tissue, some of which will be completely different cell types[193].

Knowing this it seems incredible that we still grow cells in isolation and maintain that this can provide us with enough information. Co-culture models with multiple cell types in the same culture allow for cell-cell signalling, which is important as different cells will have different functions and convey different messages though their signalling. Many examples of cells having organisational roles within tissues have been elucidated[194]. The one issue with this is that *in vitro* conditions often lack the complexities to keep the different tissue types in balance, whether this be due to nutrient needs or the ability to stop one cell type outgrowing the other.

Another important addition, that could be made to improve the realistic behaviour of the body, especially in disease models, is the incorporation of an immune response element[195]. As a minimum, a model should consider the amount and type of immune signalling molecules that can be found in the disease state environment. This aspect is missing from most currently used models.

However, the size and complexity of models can cause problems if the models are to ever be used for high throughput purposes. Considerations in the design of the model are important when high throughput is the goal. The time a model takes to construct and reach equilibrium should be considered, as high throughput requires large numbers of models and using model that takes over a month to produce is not feasible. Also important here is the price that the model costs to produce, both in resources and an expert's time.

However, for *Leishmania* there is not yet an established model that bridges the gap between static 2D cell culture and *in vivo* models.

1.6.3   Examples of Currently Used Models

The most common model used is the cancer spheroid model. First described in the early 1970s and obtained by culture of cancer cell lines under non-adherent conditions, spheroids have rapidly been accepted as a very useful model for the study of cancer[196]. Solid tumours grow in a three-dimensional spatial conformation, resulting in a heterogeneous exposure to oxygen and nutrients as well as to other physical and chemical stresses. Proliferation and hypoxia are found both at the same time in different areas of the same tumour[197]. This diffusion-limited distribution of oxygen, nutrients, metabolites, and signalling molecules is not mimicked in 2D monolayer cultures. However, it is possible to induce chemical gradients in 3D structures. In particular, the spheroid forms a necrotic core in very much the same way

as a solid tumour would and usually for the exact same reasons[198]. These similarities make the spheroid a useful model in the study of cancer[199].

Another important model of note is the model of the epidermis used for cosmetic testing[200]. The gold standard model used in the cosmetic industry is EpiDerm[tm], which is also known generically as a Reconstructed Human Epidermis[201]. EpiDerm is a ready-to-use, highly differentiated 3D tissue model consisting of normal, human-derived epidermal keratinocytes cultured on specially prepared tissue culture inserts. The process of creating the model is by the removal of all the cells from a human dermis and then re-seeding with mature keratinocytes. The model has multiple industry validations and accepted test guidelines, making it a proven *in vitro* model system for chemical, pharmaceutical and skin care product testing[201]. The model is used to study whether or not a compound is an irritant[202], corrosive[203], genotoxic[204] or affects either hydration[205] or epidermal differentiation[206], and is a suitable alternative to animal testing.

1.7 Media Perfusion Systems

1.7.1 Why use Media Perfusion

The importance of flow in physiology has been recognized for more than half a century, whether it be blood flow, media flow or interstitial flow. Since that time the understanding of fluid flow, and its effects on solute transport in biological tissues, including effects on cell-cell signalling and morphogenesis, has increased substantially. The perfusion of media in a cell culture system allows for increased nourishment and sustainability of 2D and 3D cultures, which could otherwise lead to necrotic cores in the latter case. Flow however, affects more than just cell nourishment. It can, for example, induce blood and lymphatic capillary morphogenesis *in vitro*[207-210], maintain the functional activity of chondrocytes and osteocytes[211-214], drive fibroblast differentiation[215&216] and induce cytokine production by smooth muscle cells[217].

Static systems do not offer any form of dynamic chemical or physical stimulus to cells, such as concentration gradients, flow, pressure, or mechanical stress caused by movement of fluids around them. This is a major limitation in experiments investigating cellular responses *in vitro* since the complex interplay of mechanical and biochemical factors is absent.

1.7.2 Types of Systems Available

Generally, there are two types of media perfusion systems; microfluidic and macrofluidics systems. It could be argued that large scale industrial bioreactors could be considered a third type. The first two are used mostly to conduct assays, whereas industrial bioreactors are generally considered to be for cell maintenance and growth. Simple definitions of the two main types of media perfusion system are that microfluidic systems use microliters of liquid and macrofluidics systems use millilitres of liquid and above.

Another way to categorise systems is whether the fluid is continuously circulated or has just a single pass through the system. This depends on the aim of the experiment, time duration, type of pump used and whether the system can be constructed to do either type of flow.

1.7.3 Comparison of Micro vs Macro Flow Culture Systems

Micro- (Figure 1.7.1) and Macro- (Figure 1.7.2) systems have their advantages and disadvantages, the correct decision of which system to use is largely dependent on the aims of the experiment. An obvious place to start the comparison is the volumes of liquid used. Micro fluidic systems use microliters of liquid, the benefits of this are that overall less reagents are used and this will help lower the cost of the experiment[218]. This also means experiments can be carried out on reagents that have only been produced in low quantities. A further point to the use of small volumes is that any signalling molecules produced by the cells within the system will not be diluted, which is important not only for the effects they may cause to other cells but also for measurement purposes. A disadvantage of the microfluidic systems is their difficulty of use, they are very small and therefore so are their connections and any handling must be done with care. Many microsystems have pre-attached connections to help users manipulate them more easily. Advantages of using higher volumes of liquid, in macrofluidic systems, are low concentration compounds are easier to make without potentially wasting compound in an intermediate dilution and higher confidence in dilutions.

Directly related to the different volumes of each system are the various surface area to volume ratios found between fluidic devices. A micro system will have a high surface area to volume ratio[218], this can mean that a compound that is found to stick to, or be absorbed by, the material that either the system or the connecting tubes are composed of, will represent a much higher percentage of the total concentration of compound in the system. Also in microfluidic circuits, surface adsorption can lead to nutrient or ligand depletion, so giving rise

to experimental artefacts such as increased metabolic consumption rates[219]. This effect is minimised in macro systems due to both the low surface area to volume ratio and the high amount of compound used.

It is not just the volume of liquid that is important. The size of the system also has profound effects on the behaviour of the liquid within it. Macro systems are known for their ability to re-create the low shear stress conditions found in the majority of biological environments. Conversely, micro systems can often have un-realistic levels of shear stress[220]. In addition to this issue, micro systems can be subject to air bubbles, which will cause both turbulence in the flow and increased shear stress, which is already high[221].

A larger system can support extensive cellular growth and this means that in theory macro systems can be run for longer time periods than microfluidic systems. Microfluidic systems will have a limit on the number of cells used and the size of the structures that can form within them. They will also have a maximum amount of nutrients available to absorb from the media and this could be used up near the beginning of the system, causing the cells at the end of the system to have less nutrients affecting the outcome of any assay. However, this can sometime be useful, such as when a hypoxic condition is the purpose of the model[222].

A further consideration related to the size of the systems is their ability to control the oxygen tension inside the system. A majority of micro fluidic systems are produced using polydimethylsiloxane (PDMS) a material chosen due to its property of gas permeability[223]. Additionally, PDMS has disadvantageous characteristics in terms of adsorption of small hydrophobic species[224]. Other materials are now being used but little is known about the oxygen levels within the systems. In macro systems, there is usually a reservoir compartment, which has an available air supply for re-oxygenation of the circulating media. In addition to this, they can be constructed from a variety of materials with differing properties.

The next few points can be viewed as either advantages or disadvantages, depending on the purpose of the experiment and what is hoped to be achieved by using a media perfusion system. Many micro systems, figure 1.7.1, have built-in scaffolds for 3D cell culture placed in the system during production, and whilst this is often a good thing, these scaffolds cannot be removed and may inhibit downstream analysis. Many micro systems are available custom-designed and cannot be easily modified. In contrast, macro systems are often adaptable to a range of removable scaffolds, which allows for greater manipulation and use

of existing techniques. Macro systems, figure 1.7.2, are often designed to fit with already established laboratory equipment and this can be a major bonus in both reduced cost and optimal data analysis[118]. However, the recovery of cells from the system can be essential for further analysis, and the removal of scaffolds or other inserts can be difficult and require expertise. To top this off, the ability to open the system can lead to increased chances of contamination.
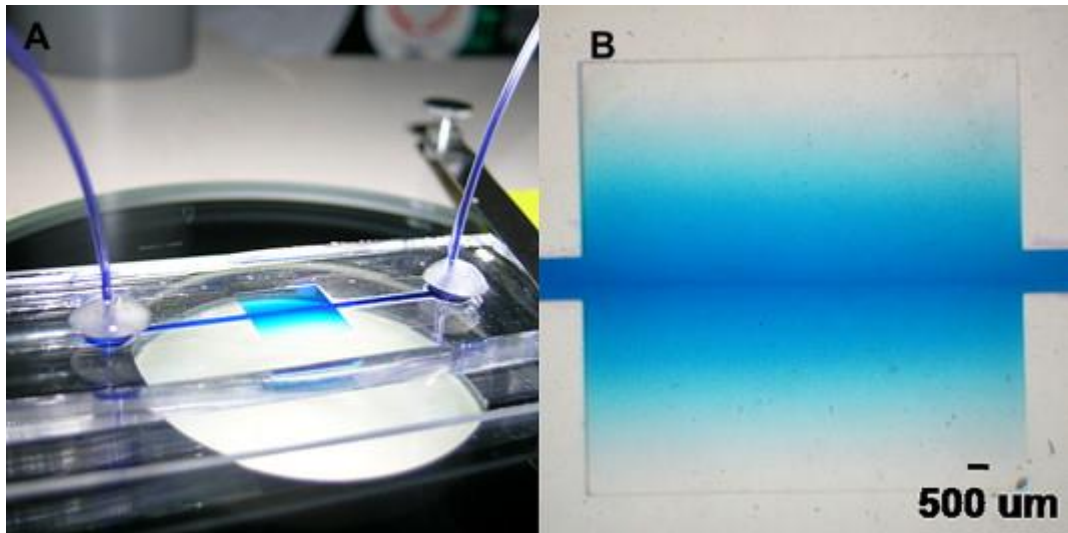
Figure 1.7-1. Multilayer microfluidic Poly (ethylene glycol) diacrylate (PEGDA) hydrogel[225]. (A) Isometric view of PDMS/PEGDA microchannel device perfused with toluidine blue, (B) Diffusion of toluidine blue into PEGDA diffusion chamber (10 × 10 mm) from a single 50 μm channel.

Figure 1.7-2. Kirkstall LTD. Quasi Vivo 900 media perfusion system in use circulating RPMI 1640 media in an incubator.

Microfluidics is a very popular technique and as mentioned, its inability to be used with existing techniques in some cases has led to the development of many new protocols and experimental guidance on how to get the most from microfluidic devices. In contrast, macrofluidic systems have seen fewer new techniques introduced, as they can be used with existing technology.

The physical size of macro fluidic systems is also important as, if the desired result is a large piece of tissue, then the system that the tissue is grown in must also be large. Another advantage to size is the ability to have enough cells in order to be able to use less sensitive assays.

1.7.4   Static Cell Culture Vs Flow Cell Culture

All cells are sensitive to their microenvironment, which is rich with chemical signals from other cells, and from mechanical stimuli due to flow, perfusion, and movement. A major limitation in experiments investigating cellular responses in static *in vitro* systems since the complex interplay of mechanical and biochemical factors is absent[219].

The ability to perfuse a chemical, whether it be drug or signal, allows for the creation of a gradient. Gradients are found all over the body and in many cases are essential for the correct physiology and behaviour. Gradients of oxygen[183&226] and pH[227&228], which are common features of tissues within the biology of the body, can also be created.

In several cases, the application of media perfusion has been shown to extend the life of spheroids[229] and help reduce the incidence of necrotic cores[230]. It also provides a means by which to remove harmful waste products that might otherwise accumulate. This could lead to chemical entities that are considered toxic to cells because of metabolites that have been shown to be less toxic than previously thought[231]. It is true that the waste removal systems of the body are efficient and do not mirror the metabolites remaining in culture and in contact with the cells that have expelled them.

The final thing that media perfusion provides is physical signals to the cell. The force of the fluid on the cells creates both mechanical and shear stress and these two factors can be interpreted by the cell as signals at the start of signalling pathways[232]. Flow alone has to be shown to aid fibroblast alignment in culture[215].

1.7.5   Interstitial Flow *in vivo*

Interstitial fluid is the fluid that is found among cells in a multicellular organism. The composition of the fluid that occupies the interstitial space also varies by location within the body. In most soft tissues, the source of fluid is the normal leakage of plasma from blood vessels, so the interstitial fluid has a composition similar to that of blood plasma. It is estimated that up to 20% of the body's mass is made up of interstitial fluid[233], and much of this fluid is in constant motion, albeit slowly. The constant movement of interstitial flow means that every cell in the body is under flow conditions to some degree. Most of this movement is a result of lymph drainage. Although the exact velocity ranges of the flow are unknown, measurements have suggested that they are of the order of 0.1–2 μms^{-1} [233-235].

1.7.6   Flow and Drugs

Another effect of fluid flow is that it could be very important to the delivery of drugs to cells. The fluid flow can be used to model the permeation of drugs to a tissue, even utilising chemical gradients or pulsatile drug delivery. A static system cannot accurately reflect the delivery of drugs to the cells or the removal of the metabolites of the drug and surrounding cells. It has been shown that the addition of flow can extend the lifetime of cells kept in culture[229&236], one way this could be possible is by the removal of toxic products.

A relevant example of the use of a media perfusion system is demonstrated in a paper by R.Bakshi[237], in which an *in vitro* system was made using a glass case and hollow fibres made by perforated dialysis tubing. The model was used for the study of *P. falciparum* and was capable of mimicking the dynamic fluctuations of a drug *in vivo*. The millimetre-sized perforations allowed free movement of drug and macromolecules between the compartments, thus providing rapid equilibration. The study was designed to use the same total dose of drug, deployed in two extremely different regimens: a short-lived high concentration bolus, where the drug is rapidly perfused followed by untreated media to remove the drug, *versus* a constant low concentration infusion. Using this method, they found that the activity of chloroquine is dependent on the time the drug concentration remains above the minimum inhibitory concentration, while the efficacy of artemisinin is driven by the maximum concentration achieved in the culture. The latter was confirmed in a mouse model of malaria. These characteristics can explain the clinical success of two antimalarial drugs with widely different kinetics in humans. Chloroquine, which persists for weeks, is ideally suited for its Time above the minimum inhibitory concentration (T_{MIC})

driven mechanism, whereas great efficacy despite short exposure is attained by C_{MAX} (Concentration maximum) driven artemisinins.

Another example of media perfusion system use is in cytotoxicity testing. Toh *et al* [238] developed a microfluidic 3D hepatocyte chip for *in vitro* drug toxicity testing to predict *in vivo* drug hepatotoxicity. The chip is formed of microfluidic channels where a 3D microenvironment is engineered in each channel to maintain the hepatocytes' synthetic and metabolic functions. The multiplexed channels allow for simultaneous administration of multiple drug doses to functional primary hepatocytes, while an incorporated concentration gradient enables the *in vitro* dose-dependent drug responses to predict *in vivo* hepatotoxicity. The IC50 values of 5 model drugs they tested correlated well with the reported *in vivo* LD50 values.

A further use of media perfusion systems is to test drug delivery vehicles such as nanoparticles. A paper by O. Farokzad *et al*[239] used a microfluidic system to study the interaction between cells and nanoparticles. Using a model system, they evaluated the interaction of polymeric nanoparticles and microparticles conjugated to aptamers that recognize the transmembrane prostate specific membrane antigen (PSMA). The binding of particles to cells that expressed or did not express the PSMA were evaluated with respect to changes in fluid shear stress and particle size. Nanoparticle-aptamer bioconjugates selectively adhered to the LNCaP cell line produced from lymph node carcinoma of the prostate, but not the prostate cancer cell line (PC3). The particles adhered to cells at static and low shear, but not higher shear conditions. Control nanoparticles and microparticles lacking aptamers and microparticle-aptamer bioconjugates did not adhere to LNCaP cells, even under very low shear conditions.

1.8 3D Cell Culture

1.8.1 Why use 3D

Cells cultured as 3D models exhibit features that are closer to the complex *in vivo* conditions[240]. The 3D culture models have proven to be more realistic for translating the study findings for *in vivo* applications. While cell lines provide us with excellent homogenous study material, culturing them as 3D models induces them to behave in a manner that is a step closer to the natural conditions. To date, the 3D culture approach has been utilized to study more than 380 cell lines. It is also known that the optimal 3D condition requirements

vary between cell types and the characteristic features of cells in 3D cultures differ in accordance to their types[241].

1.8.2   Types of 3D Systems Available

There are many ways in which to categorise the different types of 3D cell culture systems available. The simplest way to start the categorisation is whether the culture relies on an external support or scaffold system.

Common matrix-free methods employed for generating spheroids maintain the cells as suspension cultures in media. This can be done by hanging drop technology[242-244], where the cells aggregate at the bottom of a droplet of media held upside down in special plates and drawn together by gravity, figure 1.8.1. Another method uses rotary cultures or rotary bioreactors[245], the rotation of the culture stops the cells from forming attachments to the surface of the flask and means the only aggregation is between the cells forming spheroids. A further method is the use of low adhesion plates[240], which again forces adherent cells to aggregate into spheroids. The overall size of spheroids is limited to a few hundred micrometres, beyond which, necrosis ensues within the core of the spheroids[246&247]. Spheroids represent an especially good physiological 3D model for studying solid tumorigenesis and stem cell differentiation. In addition, spheroids can be readily analysed by imaging using light, fluorescence, and confocal microscopy, which is an advantage over more complex 3D cell culture models. Furthermore, it is relatively simple to mass-produce uniformly sized 3D spheroids making them highly amenable for many *in vitro* high throughput and toxicity screening applications[248].
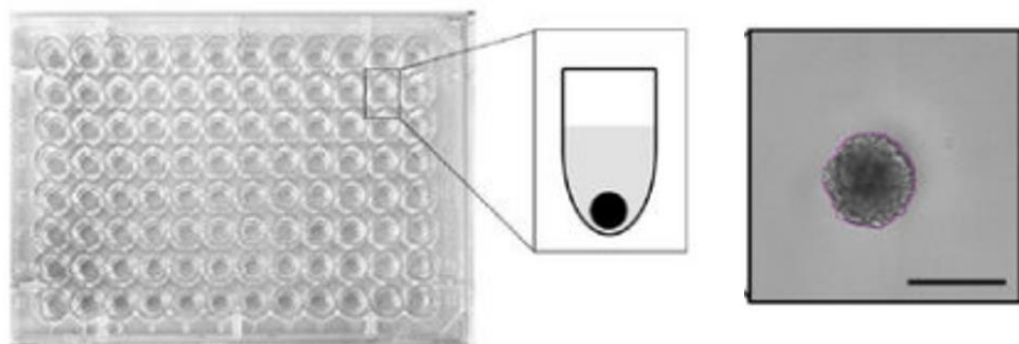
Figure 1.8-1. Generation of spheroids in a low adhesion plate (Left) and image of a spheroid formed in a single well (Right) [240].

A further development in the field of spheroids is the improvement of the model by the addition of other cell types to better simulate the situation within the body. When more than one cell type is involved, and primary cells or iPSCs, are used to allow the model to take on features of the tissue that cannot be produced in standard culture, then this is referred to as an organoid[249]. An organoid model is just the next step towards making the spheroid model "more realistic", or *in vivo* like. An organoid uses different cell types, differentiation states or sometimes includes resident immune cells, to make a structure that resembles the heterogeneous tissues found in *in vivo*.

Another type of 3D culture that does not rely on a support scaffold is explant culture[250]. This is where a section of tissue is excised from the body and kept in culture. Being taken from the body the cells can maintain their natural 3D confirmation.

With emerging technologies, it is now possible to bio-print tissues and cellular models[251&252]. This often involves the placement of cell without the need for a scaffold. Bio-printed tissues are useful for numerous reasons and can be so close to natural human tissue that they can be used for implants[253], where sourcing a tissue type may be problematic and difficult[254].

Hydrogels are comprised of networks of cross-linked polymer chains or complex protein molecules of natural or synthetic origin[255]. Due to their significant water content, hydrogels possess biophysical characteristics very similar to natural tissue, and serve as highly effective matrices for 3D cell culture. Several cell types also form spheroids in 3D hydrogels[256], and to a limited extent, in some solid scaffolds depending on the structural and physical properties of the material.

Solid scaffolds for 3D cell culture are fabricated with a broad range of materials including metal[257], ceramics[258], glass[258], and polymers[259]. In particular, polymers are a common choice for generating solid scaffolds of diverse size, varying structure, stiffness, porosity, and permeability[260]. A multitude of fabrication techniques are being utilized to generate solid scaffolds for 3D cell culture, including soft-lithography[260], electrospinning[261], micropatterning[262], printing[263], and many others. The major drawbacks of using solid scaffolds are problems with cell imaging[264] and difficulties that are encountered when recovering cells from the matrix[265].

Hollow fibre bioreactors are a 3D culture system that consist of fixed position fibres with cells typically seeded on the outside of the porous fibres and media delivered through the fibre lumen[186]. Hollow fibre type culture systems offer an *in vivo*-like environment with the fibres

mimicking blood capillaries and shielding the cells from the shear stresses associated with dynamic media delivery, while allowing defined shear stress to be applied to cells the via fluid flow outside the fibres if needed[266]. This creates a versatile culture system with superior mass transport in which high cell densities can be reached. This is a design that works particularly well with transporter[267] or drug penetration studies[268&269] as the transfer across the fibre and cells can be easily measured.

1.8.3   2D vs 3D Comparison

Main advantages of 2D cell cultures are easier environmental control, cell observation, measurement and eventual manipulation in comparison to 3D cultures. Furthermore, a rich body of literature exists to which outcome measures can be compared[186-168].

The main advantage of 3D is the conformation that the cell is able to take. Cells plated in 2D lose the natural shape that they can be found in within the body. Much of the cells surface area is lost to the culture plastic and the cell itself flattens and elongates, figure 1.8.2. 3D allows the cell to maintain a more accurate representation of its cytoarchitecture[270], which in turn can affect cell function.
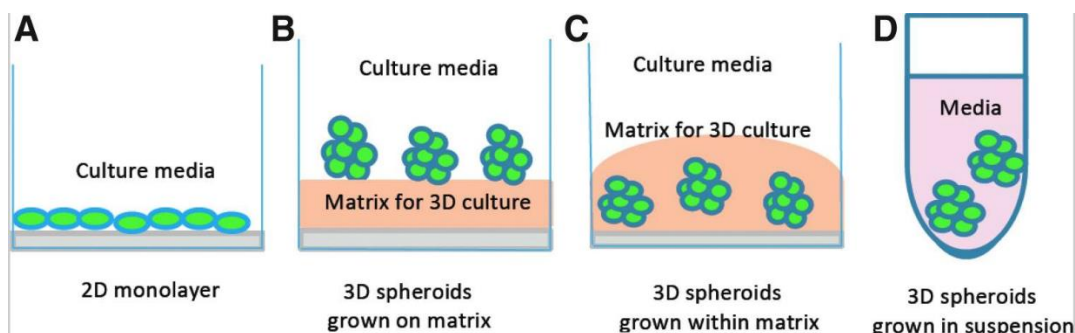
Figure 1.8-2. Diagram showing the different cellular conformation cells take in either 2D or 3D cell culture[271].

3D cell culture allows the cells to interact with other cells on all sides. This is important as it allows for more realistic interactions and the formation of important tissue components such as tight junctions[272]. Behaviour of 3D cultures is more similar to *in vivo* than 2D cultures. Cells in 3D culture have been shown to have better growth and survival than that shown by their counterparts in 2D[273].

3D cultures have been shown to take on full *in* vivo characteristics such as the production of extracellular matrix[274] and the development of bile ducts[275] in gut tissues. Another function that is essential for the study of some diseases is the ability for a culture to achieve full

polarization, such as apical-basal polarity meaning the cell has distinct microenvironments within it [242&276]. In 3D, the cells can behave more biologically in migration assays[277], through contacts with relevant cells instead of culture plastic.

Limitations of 3D culture such as, diffusional transport limitations for oxygen and other essential nutrients can cause necrotic cores[198&230] and limit the size of culture grown. Furthermore, some 3D cultures created from tissues can sometimes contain undesirable components like viruses or growth factors.

1.8.4   3D Culture and Drugs

In vitro tissue models have been developed to provide a means for systematic, repetitive, and quantitative investigation of drugs. By eliminating or reducing the need for animal subjects, these models can serve as platforms for more tightly controlled, high-throughput screening of drugs and for pharmacokinetic and pharmacodynamics analyses of drugs[278]. The results produced from 3D *in vitro* drug based assays could be more predictive than animals in certain situations as they allow for the use of human cells in a biologically relevant situation.

Culturing cells in 3D could have large effects on drug efficacies. The change in confirmation allows more of the surface to be accessible to drug molecules. In addition to this, having a working cytostructure[270] could affect how the drugs are processed. Further effects such as oxygen gradients[183] and cell cell signalling[194] could also affect drug processing. One study[279] on anticancer drug sensitivity testing on A431.H9 cells showed that cytotoxicity could be drastically different in the physiological 3D spheroids formed in the 384 hanging drop array plates compared to 2D monolayer cultures in conventional multiwell plates. Specifically, the anticancer drug 5-fluorouracil has higher anti-proliferative effects on 2D cultures whereas the hypoxia activated drug, commonly referred to as tirapazamine, is more effective against 3D cultures.

1.9 Aim and Objectives of this Research

The aim of the project is to assist the discovery and development of drugs against Leishmania, by developing *in vitro* tissue culture infection models that are more predictive of the *in vivo* infection in humans.

The objectives of the project are to:

I. Establish and compare 2D static and 2D flow cell culture models, in terms of the influence of flow on host cell infection and on drug activity.

II. Develop a 3D tissue culture model of infection.

III. Use iPSC derived macrophages to determine whether they are a valid alternative to currently used cell types.

These are detailed below:

Part 1: Establishment of 2D flow models and comparative 2D static systems. Including experiments concerning the effect of flow on infection and drug activity.

The progression of infection and treatment with control drugs was compared, using specially developed and adapted methods, in the two conditions of static and flow. Different rates of flow were used to demonstrate not only the effect of flow on the model but also the effect of the speed of the flow within the system. Then the flow was specifically tuned to match the rate of interstitial fluid flow within the skin. Measurements of macrophage status and drug accumulation were acquired to help explain the differences.

Part 2: Development of a 3D *in vitro* model.

Macrophages were grown using two scaffolds. The models were evaluated for infection and response to drugs using fluorescent parasites and confocal imaging. Comparisons of the 3D model against 2D controls will elucidate any differences between the systems.

Part 3: Utilization of iPSC derived Macrophages

Macrophages derived from iPSCs were be used for infection to show their response to drugs. The results of infection studies with a variety of parasite strains were compared against the infection rates in a panel of other widely used cell types in *Leishmania in vitro* models. Further to this, the efficacies of standard drugs used for the treatment of leishmaniasis were measured across the same range of parasites in each of the different cell types used. The results of this determined whether iPSCs are a valid alternative to these other cell types and, which widely used cell type they behave most similarly to.

Chapter 2 Materials and Methods

2.1 Materials

Table 2.1-1 *Materials used throughout*

Item	Company	Cat No.
Roswell Park Memorial Institute (RPMI-1640) medium	Sigma, Gillingham, UK	R0883
L-glutamine	Sigma, Gillingham, UK	59202C
Heat inactivated Fetal Calf Serum (HiFCS)	Harlan, Bicester, UK	
Human Macrophage Colony Stimulating Factor (hM-CSF)	Sigma, Gillingham, UK	M6518
Phosphate buffered saline (PBS)	Sigma, Gillingham, UK	P4417
Phorbol 12-myristate 13-acetate (PMA)	Sigma, Gillingham, UK	P1585
Schneider's insect medium	Sigma, Gillingham, UKb	S0146
M199 medium	Sigma, Gillingham, UK	M5017
Dulbecco's Modified Eagle's medium (DMEM)	Gibco - Thermofisher, Paisley, UK	31966-021
Penicillin and Streptomycin	Sigma, Gillingham, UK	P4333
Giemsa stain	Sigma, Gillingham, UK	G5637
miltefosine	Nycomed, Aldwych, UK	
amphotericin B	VWR international	E437
paromomycin sulphate salt	Sigma, Gillingham, UK	P9297
sodium stibogluconate	Sigma, Gillingham, UK	S5319
Dimethyl sulfoxide (DMSO)	Sigma, Gillingham, UK	D8418
Ethylenediaminetetraacetic acid (EDTA	Sigma, Gillingham, UK	E6758
Methanol	Sigma, Gillingham, UK	322415
Fatty acid free Bovine Serum Albumin (BSA)	Sigma, Gillingham, UK	A2153
Formic acid in water	Fisher, Loughborough, UK	13484269
Acetonitrile	Sigma, Gillingham, UK	360457

Item	Company	Cat No.
Tolbutamide	Sigma, Gillingham, UK	T0891
Phalloidin Cruz fluor 488	Santa Cruz Biotechnology, Heidelberg, DE	SC-363791
4',6-Diamidino-2-Phenylindole (Dapi)	Sigma, Gillingham, UK	D9542
Synthemax (Plate coating)	Corning, Wiesbaden, DE	
Gelatine	Sigma, Gillingham, UK	G1393
2-mecaptoethanol	Sigma, Gillingham, UK	M6250
4-(2-hydroxyethyl)-1-piperazineethanesulfonic acid (HEPES)	Fisher, Loughborough, UK	BP310-1
hIL-3	RnD, Abingdon, UK	203-IL-010
TrypLE™ what is this?	Thermofisher, Paisley, UK	12604013
Starch	Sigma, Gillingham, UK	33615
Alamar Blue	Sigma, Gillingham, UK	R7017
Triton x-100	Sigma, Gillingham, UK	X-100
Paraformaldehyde (PFA)	Sigma, Gillingham, UK	P6148
Fluoromount	Sigma, Gillingham, UK	F4680
Trisma base	Sigma, Gillingham, UK	T1503
Triton X-100	Sigma, Gillingham, UK	X100
phenylmethanesulfonyl fluoride (PMSF)	AppliChem, Stockport, UK	A0999
Nicotinamide adenine dinucleotide phosphate (NADPH)	Sigma, Gillingham, UK	NADPH-RO
Trypanothione disulphide (T[S]2)	BAChem, St Helens, UK	H-7510
5,5-dithio- bis 2-nitrobenzoic acid (DTNB)	Sigma, Gillingham, UK	D218200
Ethanol	Sigma, Gillingham, UK	652261
BCA protein assay kit	Thermofisher, Paisley, UK	23227
Edu assay kit	Thermofisher, Paisley, UK	C10337
NO detection kit	Thermofisher, Paisley, UK	G7921
Lipopolysaccharides *E. coli* 026:B6	Sigma, Gillingham, UK	L8274

Item	Company	Cat No.
TESR-E8 medium	StemCell Technologies, Cambridge, UK	TeSR 05940
Knockout replacement serum (KSR)	Invitrogen - Thermofisher, Paisley, UK	10828-028
Dispase:Collagenase	Sigma, Gillingham, UK	COLLDISP-RO
X-Vivo 15 plus gentamycin	Lonza, Slough, UK	04-418Q

Table 2.1-2 *Equipment used throughout*

Item	Company	Cat No.
Glass coverslips	Bellco, New Jersey, US	1943-100 12A
Peristaltic pumps	Parker, Warwick, UK	PF22x0204
96 well low adhesion round bottomed plate	Corning, Wiesbaden, DE	CLS7007
Cryovials	Greiner Bio-One, Stonehouse, UK	121263
T75 Flasks	Greiner Bio-One, Stonehouse, UK	658940
T175 Flasks	Greiner Bio-One, Stonehouse, UK	661940
Spectramax M2	Molecular Devices, Wokingham, UK	
QV500 media perfusions system	Kirkstall Ltd, Rotherham, UK	
QV900 media perfusion system	Kirkstall Ltd, Rotherham, UK	
3D printed insert for QV900	Kirkstall Ltd, Rotherham, UK	
16 well Lab-Tek™ plates	VWR International, Leicester, UK	62407-350
70 µM cell strainer	Corning, Wiesbaden, DE	CLS431751
10 cm² dish	Thermofisher, Paisley, UK	150318
24 well plates	Corning, Wiesbaden, DE	353226
96 well plates	Corning, Wiesbaden, DE	353072

Table 2.1-3. *Cells used*

Cells	Company	Cat No.
THP-1	ATCC, Teddington, UK	TIB-202
3T3 Fibroblasts	ATCC, Teddington, UK	CRL-1658
MEF CF-1 cells (mouse embryonic feeder)	Amsbio, Abingdon, UK	GSC-6001
Human bone marrow mononuclear cells	ATCC, Teddington, UK	PCS-800_013

Table 2.1-4 *Parasites used*

Parasite	Strain	Source
Leishmania major **JISH**	MHOM/SA/85/JISH118	
Leishmania amazonensis **DSRed**	IFLA/BR/1967/PH8	Eric Prina, Institut Pasteur
Leishmania mexicana	MNYC/ BZ/62/M379	
Leishmania major **mCherry**	LV39c5 (RHO/SU/59/P	Rosa Reguera, University of Leon

Table 2.1-5. *Animals used*

Animal	Source	Purpose
CD-1	Charles River, Margate, UK	Peritoneal and bone marrow macrophages
BALB/c	Charles River, Margate, UK	Parasite maintenance

2.2 Methods
2.2.1   Cell culture
2.2.1.1   THP-1 cells

THP-1 cells were maintained in RPMI-1640 medium supplemented with L-glutamine and 10% Heat inactivated Fetal Calf Serum (HiFCS). The THP-1 cell line was maintained in an incubator at 37°C and 5% CO_2 and passaged to new medium once a week (1/10 ratio).

2.2.1.2 3T3 Fibroblasts

3T3 Fibroblasts were maintained in DMEM medium supplemented with L-glutamine and 10% HiFCS. The fibroblast cell line was kept in an incubator at 37°C and 5% CO_2 and passaged to new medium once a week (1/10 ratio) using TrypLE to detach adherent cells.

2.2.1.3 Peritoneal Macrophage Isolation

Mouse peritoneal macrophages (PEM) were isolated from CD-1 mice upon peritoneal injection with 0.5 mL of 2% starch solution in sterile water. Macrophages were collected by abdominal lavage with RPMI-1640 medium containing 1% penicillin and streptomycin. The collected cells were centrifuged for 15 minutes at 500 g and 4°C, washed in RPMI-1640 medium and re-suspended in RPMI-1640 medium containing 10% HiFCS.

2.2.1.4 Leishmania Culture

L. major JISH and *L. mexicana* promastigotes were maintained in Schneider's insect medium (Sigma Aldrich, UK) supplemented with 10% HiFCS at 26°C.

L. amazonensis DSRed and *L. major* mCherry were maintained in M199 medium supplemented with 10% HiFCS at 26°C.

Parasites were maintained in a 26°C incubator and passaged to new medium once a week (1/20 ratio).

2.2.1.5 Parasite Maintenance

Female BALB/c mice of about 6-8 weeks old were purchased and housed in a controlled environment of 55% relative humidity and 26°C. They were provided with tap water and a standard laboratory diet. All *in vivo* experiments were carried out under license (PPL 70/6997 and X20014A54) at the London School of Hygiene and Tropical Medicine (LSHTM) after discussion with the veterinarian and according to UK Home Office regulations.

Female BALB/c mice had their rump shaved and injected with $2x10^7$ stationary phase promastigotes (in 200 μl of RPMI 1640 media) subcutaneously on the rump above the tail. The mice were inspected daily for the presence of a nodule. After about 7 days, a small papule at the site of injection was visible in the infected mice. When an average lesion diameter of 5 mm was reached, the mice were sacrificed and the papule was excised. The excised papule was inverted and the lesion mass in the dermis was removed from the epidermis. The dermis was cut into smaller pieces and placed in 4 mL of RPMI-1640 medium containing 10% HiFCS and 1% penicillin and streptomycin for 3-7 days. During this period

parasites transformed to promastigotes and then passaged into Schneider's insect medium supplemented with 10% HiFCS kept at 26°C

2.2.1.6   Cell and Parasite Cryo-storage

Mid exponential phase parasites were counted using a haemocytometer, then centrifuged at 700 g for 10 min (4°C) and re-suspended in RPMI-1640 medium supplemented with 20% HiFCS and 10% DMSO to a 2 x 10^8 cells/mL density. Parasites were aliquoted in 1 mL volumes into cryovials.

Cells were counted using a haemocytometer, then centrifuged at 500 g for 10 min (4°C) and re-suspended in RPMI-1640 medium supplemented with 20% HiFCS and 10% DMSO to a 2 x 10^7 cells/mL density. Cells were aliquoted in 1 mL volumes into cryovials.

Cryovials were placed in a Thermo Scientific™ Mr. Frosty™ Freezing Container, and placed in a -80°C freezer overnight. The next day cryovials were transferred into liquid nitrogen for storage.

2.3 Static vs Media Perfusion Methods

2.3.1   Kirkstall Media Perfusion Systems

Kirkstall Ltd was founded in November 2006 by **Dr J Malcolm Wilkinson** and is now based in Rotherham, UK. The company has an exclusive worldwide licence to patented cell culture technology from the University of Pisa, patent number EP2710110. The technology is the outcome of over 10 years of research by an interdisciplinary research team in Pisa. Kirkstall has developed this research into a commercially available inter-connected cell culture system, known as Quasi Vivo®, which can be set up to mimic some aspects of human metabolism, resulting in high quality, rather than just high throughput studies.

2.3.1.1   QuasiVivo 500 Media Perfusion System

The QV500 cell culture chamber (shown in Figure 2.3.1) is a highly flexible research tool, and consists of individual chambers, which allow for maximum flexibility in assay design. Produced from medical-grade silicone, the chamber provides a leak proof seal, allowing flow of cell culture media across cells. The modular design allows the flow system to be set up in a wide range of configurations to best replicate the *in vivo* environment. The internal diameter of the chamber is equal to the well diameter of a 24 well plate, table 2.3-1.
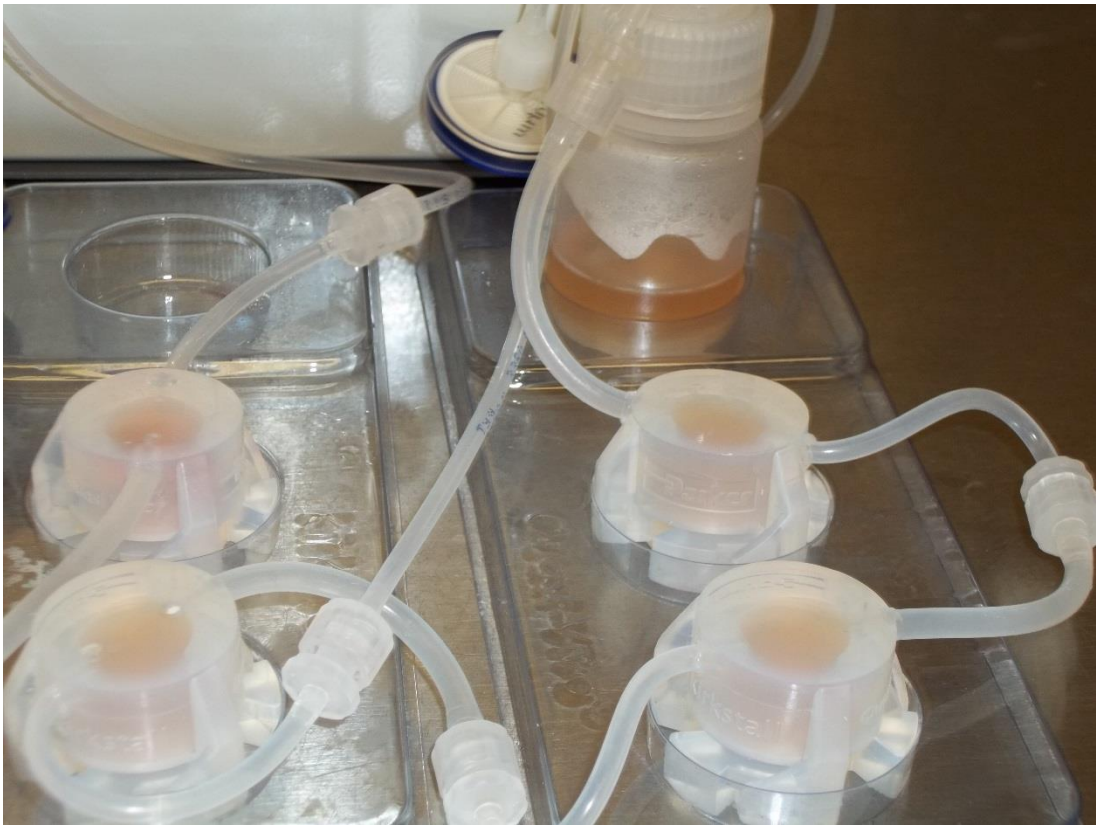
Figure 2.3-1. QuasiVivo 500 system

Table 2.3-1. *Details of QuasiVivo 500 media perfusion system[333].*

Chamber width	15 mm internal
Chamber depth	10 mm from culture surface to top of chamber base
Materials	Chamber: Polydimethylsiloxane (PDMS)
	Tubing: Tygon
	Luers and reservoir bottle: Polypropylene
Overall dimensions	23 mm height x 37 mm diameter
Diameter of tubing	Inlet: 1/16" ID
	Outlet: 3/32" ID
Volume of chamber	2 mL

2.3.1.1.1 Construction of QV500 Media Perfusion System

The QV500 system was arranged as shown in the schematic diagram below, figure 2.3.2. The various parts of the system were connected with silicon tubing joined using a luer lock system.
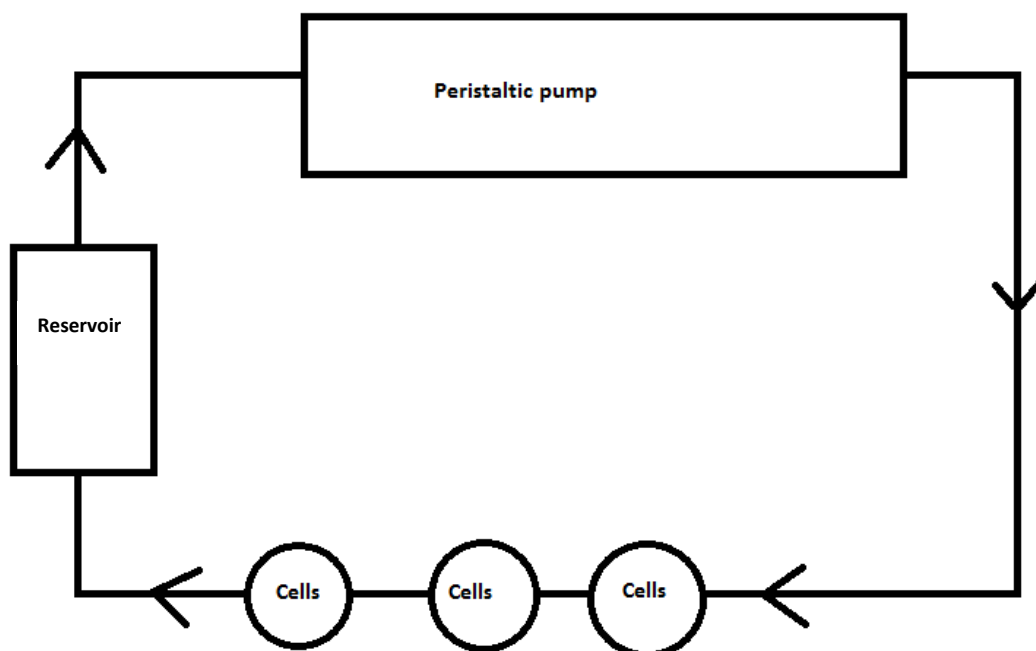
Figure 2.3-2. Schematic diagram of the QuasiVivo 500 media perfusion systems arrangement and construction

2.3.1.1.2 Evaluation of Flow Rates in the QV500 Media Perfusion System

Once the system was constructed and filled with media, the luer lock between the reservoir and the last chamber was opened. The end of the tube coming from the chamber was placed in a pre-weighed small container. The system was then run at different speed settings for different periods of time until about 1-2 mL of media had been deposited in the container. The container was then weighed and the mass of the media was calculated. From this, the rate of bulk media transfer was calculated in µL/mL, and are shown in table 2.3-2.

Table 2.3-2. *Details of bulk media transport in the QuasiVivo 500 media perfusion system at different pump settings.*

Pump Setting	Bulk media transfer rate µL/min
1	62
2	174
3	281
4	385
5	477
6	580
7	686
8	788
9	888
10	902

2.3.1.2   QuasiVivo 900 Media Perfusion System

The QV900 (shown in Figure 2.3.3) is a 6-chamber optical tray providing the same advantages of the QV500 but in a compact format. Each tray contains six chambers within the same footprint as a standard well plate, all of which have optically clear floors and ceilings to allow imaging of cultures *in situ*, table 2.3-3. Each tray is single use and this helps stop the spread of any possible contamination. The nature of the six well plates allows for a much higher throughput than the individual chambers with greater ease. A disadvantage of the system is that an error in the design before manufacturing means that the dimensions of the QV900 system does not match those of the QV500. Therefore, the bulk of the modelling conducted with QV500 was not applicable to QV900. To rectify this error, Kirkstall have produced a 3D printed insert, which will change the depth of the chambers so they match the depth of the QV500. Another disadvantage is that due to the stiffness of the material used to make the plates, leaks occur far more frequently. A recent effort to stop the plates from leaking is to use lids for the wells that have been autoclaved separately. By doing this, the lids are not deformed by the autoclave.

Figure 2.3-3. Photograph of the QV900 media perfusion system

Table 2.3-3. *Details of QuasiVivo 900 media perfusion system[334].*

Chamber width	15 mm internal
Chamber depth	22 mm
Materials	Chamber:
	Base: Altuglas SG7 – Acrylic Resin
	Lids: Melifex M8706 – Styrene TEP
	Tubing: PTFE & FEP
	Luers and reservoir bottle: Polypropylene
Overall dimensions	23 mm height x 37 mm diameter
Diameter of tubing	Inlet: 1/16" ID
	Outlet: 3/32" ID
Volume of chamber	4 mL

2.3.1.2.1   Construction of QV900 Media Perfusion System

The QV900 system was arranged as in the schematic below, figure 2.3.4. The various parts of the system were connected with Teflon tubing joined using a luer lock system. 3D printed inserts (Kirkstall Ltd) were produced using Nylon-12 and were shaped to fit the interior of the chambers. The depth of the insert was 9 mm and this reduced the depth of the well to 12 mm, including the pins at the bottom of the well previously used to hold up the glass coverslips. When 3D printed inserts were used, they were placed in the final three wells of the system, so conditions between cells with or without an insert were identical.
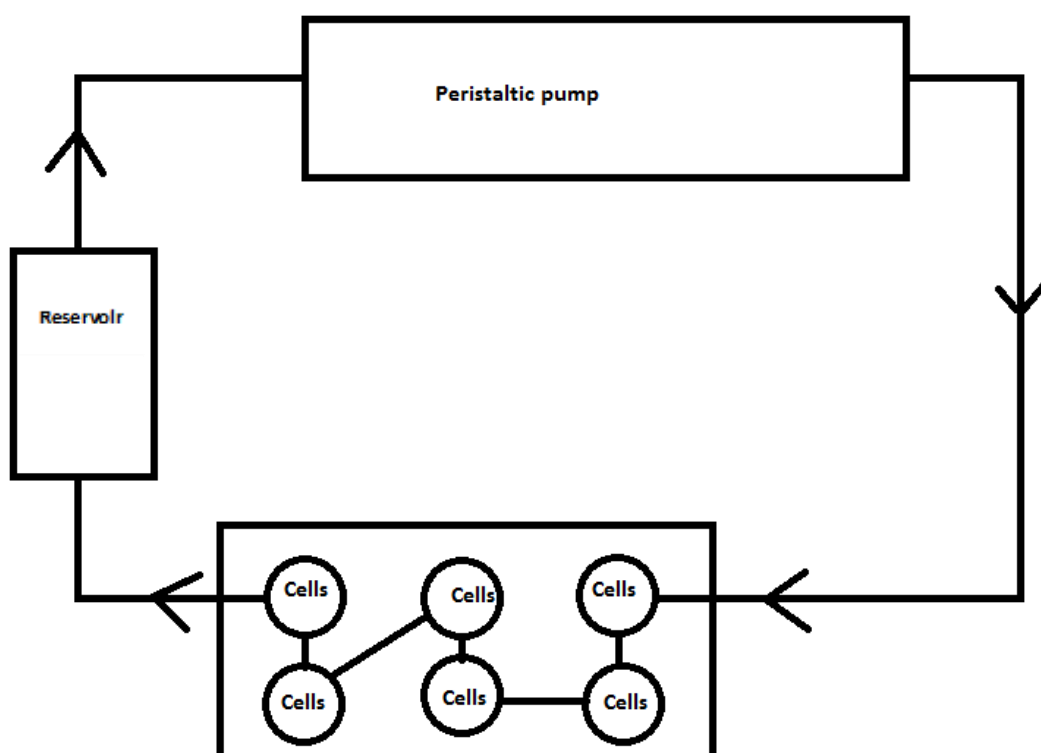
Figure 2.3-4. Schematic of the QuasiVivo 900 media perfusion systems arrangement and construction.

2.3.1.2.2   Evaluation of Flow Rates in the QV900 Media Perfusion System

Measurement of the bulk transfer rate of the QV900 system was measured using the protocol in 2.1.1.2. Results of the experiment are in table 2.3-4.

Table 2.3-4. *Details of the bulk media transport in the QuasiVivo 900 media perfusion system at different pump settings.*

Pump Setting	Bulk media transfer rate μL/min
0.5	36
1	107
2	220
2.5	280
3	360
3.5	400
4	460
5	584
6	682
7	811
8	947
9	1074
10	1169

2.3.2 Differences between Kirkstall Ltd QV500 and QV900

There are several differences between the two systems such as in the materials used in the manufacture of the systems.

- The QV500 system (Figure 3.3.1) is silicone based and liable to contamination as it was a re-useable system, whereas the QV900 system's (Figure 3.3.1) base is made from Altuglas SG7 – Acrylic Resin and the lids from Melifex M8706 – Styrene TEP.

- Another problem with the silicone is that it is known to adsorb small molecules such as drugs. The QV900 shows less drug absorption and release than the QV500 making it more suitable for drug studies.

- The QV900 system has also been equipped with Teflon tubing instead of the silicone tubing that the QV500 system uses. This again reduces the drug absorption by the system. The layout of the QV900 system allows for a higher throughput assay whilst saving time with easier handling.

- However, the main difference between these two systems is the well depth, caused by a manufacturing error. The QV500 system is 10 mm deep whereas the QV900 system is 22 mm deep. Originally, the company did not mention this difference suggesting that the two systems would behave similarly. It eventually became clear that this is not the case. After months of experimentation trying to replicate previous results, the schematics were made available and the difference in depth was discovered.

- The extra depth causes a large reduction in both media velocity across the surface of the cells and shear stress felt by the cells in the system.

- The extra depth also affects the chamber volume increasing the volume from 2 ml up to 4.4 ml.

 In order to set this problem right, Kirkstall have produced 3D printed inserts that fit within the well of the QV900 reducing its depth back to 10 mm and back to the original flow velocities and stresses. The insert is a specially designed cylinder made from Nylon-12 with a raised cross to support the glass slide on top of it.

2.3.3   Measurement of Cell Viability
2.3.3.1   Plating of cells

Cells, either THP1 or peritoneal macropahges were seeded on sterile 12 mm glass cover slips, in 24 well plates, in RPMI-1640 supplemented with 10% HiFCS at a density of $4x10^4$ per well. If the cells were THP1 cells an additional 20 ng/mL PMA was added to the media. The glass coverslips had been sterilised using an autoclave. The glass coverslips were placed in a 37°C and 5% CO_2 incubator.

2.3.3.2   Measurement of Cell Viability in Static System

THP1 cells plated as in 2.3.2.1. After 72 hours incubation at 37°C and 5% CO_2, the glass coverslips and adhered cells were transferred to a new well. 500 µL of RPMI media containing 10% Alamar blue was added to each well. An initial fluorescence reading was taken using a Spectramax M2 at 530 nm excitation and 580 nm emission, with a 550 nm cut off. The plate was incubated in the dark at 37°C and readings were taken every hour.

2.3.3.3   Measurement of Cell Viability in Kirkstall QV500 Media Perfusion System

THP1 cells plated as in 2.3.3.1. Adherent cells on the glass coverslips were transferred to the chamber of the QV500 media perfusion system, which was then placed in the 37°C and 5%

CO_2 incubator. The media transfer rate was selected and the system was run for 72 hours. Subsequently, the glass coverslips and adhered cells were transferred into a 24 well plate. Viability readings were taken as in 2.3.3.2.

2.3.4 Evaluation of *L. major* Infection Rates
2.3.4.1 Evaluation of *L. major* Infection - Static System

Mouse peritoneal macrophages (PEM) or THP1 cells were as in 2.3.3.1. After 24 hours incubation at 37°C and 5% CO_2, stationary phase promastigotes were added to the adhered cells at several promastigote : host cell ratios (1:1 to 25:1), and maintained at 34°C in a 5% CO_2 incubator. After 24h, the cell cultures were washed to remove extracellular promastigotes and one slide was fixed with methanol and stained with Giemsa to determine the initial level of infection. After a further 72 hours incubation, all slides were methanol-fixed and Giemsa-stained. The percentage infection was determined microscopically (400x magnification) by counting the number of infected macrophages in a population size of at least 100, then comparing with untreated controls.

2.3.4.2 Evaluation of Infection - Media Perfusion System

Infection under Low Flow

Protocol as in 2.3.4.1 except slides were maintained inside the media perfusion system, for 72 hours incubating at 34°C and 5% CO_2. The peristaltic pump was set to setting one (107 µL per minute), table 2.3-4.

Infection under High Flow

Experiments were carried out as above except the speed of the peristaltic pump was set to setting ten (1169 µL per minute), table 2.3-4.

Infection with Parasites in Media

Experiments were carried out as in the infection under low flow section, except the media contained stationary phase promastigotes at a variety of ratios.

Infection with and without 3D Printed Inserts

Experiments were carried out as the infection under low flow section, except the speed of the peristaltic pump was set to setting three (360 µL per minute), table 2.3-4. In addition, a 3D printed insert were placed in half of the wells of the media perfusion system.

2.3.5 Colorimetric Assay For Trypanothione

Host cells and parasites were chemically lysed by a 15 minute incubation with lysis buffer (200 μL/well), consisting of EDTA (1 mM), HEPES (40 mM), Tris (50 mM;pH 7.5), and Triton X-100 (2% vol/vol). Immediately prior to use, the buffer was supplemented with the protease inhibitor phenylmethanesulfonyl fluoride (PMSF) at a final concentration of 1 mM. TryR activity was measured in 75 μL of sample lysate. NADPH (25 μL/well), trypanothione disulphide (T[S] ^{2}) (75 μL/well) and 5, 5-dithio- bis 2-nitrobenzoic acid (DTNB) (25 μL/well) were sequentially added to the sample lysate to yield final concentrations of 200, 75, and 100 μM, respectively. A blank for each sample, consisting of sample lysate supplemented with the reaction mixture described above, in which the substrate T[S] ^{2} had been replaced by Tris (0.05 M) buffer, pH7.5, was included on every plate. Samples were incubated at 26°C for three to six hours. After incubation, absorbance was measured at a wavelength of 412 nm using a plate reader, Spectramax M2. Data was compiled in Excel and then analysed in Prism.

2.3.6 Evaluation of Anti-leishmanial Activity of Compounds

2.3.6.1 Evaluation of Anti-leishmanial Activity in the Static System

THP1 cells or PEMs were plated as in 2.3.3.1. After 24 hours incubation at 37°C and 5% CO_2, the adhered PEMs were infected with stationary phase promastigotes at a ratio of 5 (for THP1 cells) or 3 (for PEMs) *L. major* JISH promastigotes to 1 macrophage and maintained at 34°C in a 5% CO_2 incubator. After 24h, the cultures were washed to remove extracellular promastigotes and one slide was fixed with methanol and stained with Giemsa stain to determine the initial level of infection. If a sufficient level of infection, (i.e. > 50%) was obtained after 24 hours, drugs were added over a pre-determined range of concentrations. Miltefosine solutions at concentrations of 20, 5 and 1.25 μM, amphotericin B solutions at concentrations of 200, 50 and 12.5 nM, sodium stibogluconate at concentrations of 600, 200 and 60 ug of Sb^V/mL or paromomycin sulphate salt at concentrations of 300, 100 and 30 μM were added in triplicate at each concentration, on the same plate. After 72 hours incubation, all slides were methanol-fixed and Giemsa stained. The percentage reduction of inhibition was determined microscopically (400x magnification) by counting the number of infected macrophages following drug treatment. Non-linear sigmoidal curve fitting (variable slope) was conducted using Prism Software (GraphPad, Surrey, UK).

2.3.6.2 Evaluation of Anti-leishmanial Activity in the QV900 Media Perfusion System

Experiments were carried out as in 2.3.4.2 (Infection with and without 3D printed insets) except cells were infected at a 25:1 (for THP1 cells) or 6:1 (for PEMs) ratio before being maintained inside the media perfusion system for 72 hours incubating at 34°C and 5% CO_2.

The peristaltic pump was set to setting three (360 µL/ min), table 2.3-4. In addition, a 3D printed insert were placed in half of the wells of the media perfusion system.

2.3.7 Measurement of Drug Accumulation in Cells

2.3.7.1 Drug Accumulation Studies in a Static System

Experiment was conducted as in 2.3.6.1 except MIL at 20 µM or AmB at 1 µM were added to each well. Cultures were maintained for either 4, 8, 12 or 24 hours at 34°C and 5% CO_2.

Slides were transferred to a new 24 well plate and washed three times with PBS. If miltefosine was used a back-exchange step to remove membrane-bound miltefosine was completed by adding 3% (w/v) fatty acid-free BSA in PBS. Then the cells are washed again in PBS. To lyse the cells, 0.1% (v/v) formic acid in water was added and vigorously mixed by pipetting up and down every five minutes during a 30 minute incubation at room temperature. Lysates were transferred to a microcentrifuge tube with 250 µL acetonitrile, if miltefosine was used, or 250 µL of 16% DMSO in methanol, if amphotericin B was used. 200 ng/mL tolbutamide was used as an internal standard for both drugs. Tubes were then placed on a shaker for 10 minutes before being centrifuged 15 min at 4150 g at 4°C. Supernatant was transferred into 96 well plates and stored at -80°C.

A calibration curve was created using untreated cell lysates spiked with known miltefosine or amphotericin B concentrations. A further set of blanks were prepared using acetonitrile without tolbutamide.

Frozen plates were taken to Pharmidex Ltd (Stevenage UK), a company specialising in ADMET assays with experience in miltefosine and amphotericin B drug accumulation in cells studies. Plates were analysed for drug concentration using HPLC-MSMS using an electro-spray ionisation on an Agilent 1200 HPLC/Agilent 6410 triple quad under positive ion MSMS mode. Data was extracted into Excel files and analysed in both Excel and Prism.

The remaining lysate was used to measure protein concentration as a measure of cell number using a Pierce™ BCA protein assay kit.

2.3.7.2 Drug Accumulation in the Kirkstall QV900 Media Perfusion System

Experiment conducted as in 2.3.6.2 except PEMs were infected with stationary phase promastigotes at a ratio of 6 *L. major* promastigotes to 1 macrophage and maintained inside the QV900 media perfusion system, either at the chamber base or on top of the 3D printed inserts.

2.3.7.3　　　Protein Determination Assay

A working reagent was prepared by mixing 50 parts of BCA reagent A with 1 part of BCA reagent B. A standard curve between 0 and 2 mg/mL BSA was constructed. 25 µL of lysate or standard curve was added to 200 µL of the working reagent, in a 96 well plate. The plate was covered in tin foil and incubated at 37°C for 30 minutes. Absorbance was measured at 562 nm using the Spectramax M2 plate reader. A standard curve was created in Graphpad Prism and values for the samples were interpolated.

2.3.8　Cell Proliferation - Edu Incorporation Assay

Invitrogen Click-iT® EdU Imaging Kit was used to measure 5-ethynyl-2´-deoxyuridine (Edu) incorporation as a measure of cell proliferation. The kit supplies a labelled DNA base that is incorporated only into the cell's DNA as they synthesise new DNA for cellular division, this can then be detected by attaching a fluorescent marker to the label. Experiment conducted as in 2.3.3.1 and 2.3.3.2, using the section infection with and without 3D printed inserts, except PEMs were infected with a ratio of 3 *L. major* promastigotes to 1 macrophage and maintained at 34°C in a 5% CO_2 for 24 hours. Media used contained 50 µM Edu. After 24 hours, cells were placed in a new 24 well plate and were fixed in 4% PFA for 15 minutes at room temperature. The samples were treated with 0.2% Triton X-100 in PBS for 20 minutes and then 1% BSA in PBS for 10 minutes. Click-iT® reaction cocktail was prepared according to instructions in Invitrogen Click-iT® EdU Imaging Kit. 0.5 mL of Click-iT® reaction cocktail was added to each well containing a coverslip. Cells were incubated for 30 minutes at room temperature, protected from light. Cells were then washed with 1 mL of 3% BSA in PBS. Cells were incubated with 300 mM DAPI stain for 10 minutes. Coverslips were mounted onto slides and imaged using a confocal microscope (Zeiss LSM510 Axiovert). Images taken were 40x magnification. The lasers used were Laser Diode: 405 nm for DAPI excitation and Argon laser: 458, 488, 514 nm for Edu excitation. Images captured were analysed using Volocity software (PerkinElmer) to automatically count nuclei for total cell number and then the images were manually viewed to count number of fluorescent and non-fluorescent parasites within each cell. The results were exported and analysed with Graphpad Prism.

2.3.9　Nitrite Ion Detection using the Griess Assay

The Griess test detects the presence of nitrite ion in solution, in this case detecting nitrites released by the cells as a defence mechanism. The purpose of this experiment is to determine if the media perfusion increases the cells response to parasites. PEMs were plated as in 2.3.3.1 and maintained for 24 hours at 34°C 5% CO_2 in either the QV900 media perfusion system set to 360 µL/min, using depth reducing inserts in half the wells or in a static plate.

All cells were then transferred to a new well in a static 24 well plate and treated with 10ng/mL lipopolysaccharides, which has been shown to stimulate nitrite release[326], for 24 hours at 34°C 5% CO_2. Then 250 µL of media was removed from the wells and an equal volume of Griess reagent, made as specified in NO detection kit, was added in a new plate. The plate was incubated for 1 hour in the dark at 37°C and then the absorbance at 548 nm was found using a plate reader. Values were determined by comparing to a standard curve made using sodium nitrite, provided in the NO detection kit.

2.3.10 Modelling of the Kirkstall QV900 System

The following section was provided by Lauren Hyndman and Dr Sean McGinty of the University of Glasgow who developed a mathematical model of the fluid flow and oxygen transport within the QV900 media perfusion system. The purpose of the model was to aid in the configuration of the experiments and to quantify the oxygen concentrations and shear stresses found within the system. COMSOL Multiphysics, a commercially available finite element analysis software, was used to perform simulations for six chambers connected in series with cells placed (i) at the base of each chamber, and (ii) on a solid 9 mm insert placed at the base of each chamber. Figure 2.3.5 illustrates the computational geometry (of a single chamber) which was used in each case. Note that the geometry on the right is shorter because the computational domain only includes the parts of the chamber that contain fluid, and since the 9 mm insert is solid it is assumed that there is no fluid flow within this region.
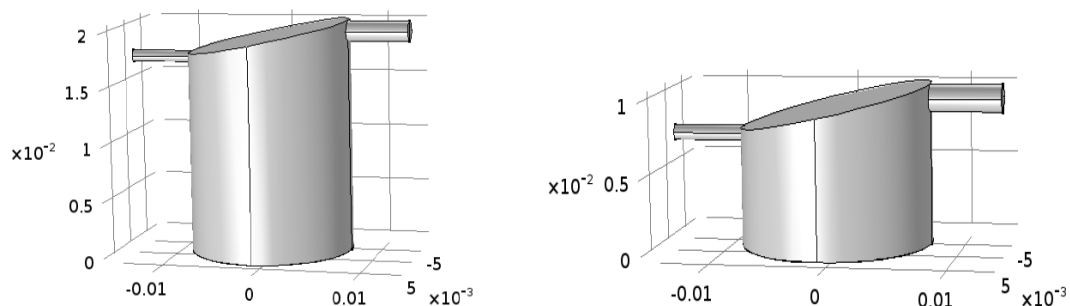
Figure 2.3-5. Idealised 3D geometry of a single QV900 chamber. Note that length scales are in m. **Left**: Geometry for cells placed at the base of the chamber. **Right**: Geometry for cells place on the insert.

The fluid flow was modelled using the Navier-Stokes equations, assuming that the medium is an incompressible Newtonian fluid. The transport of oxygen throughout the fluid was modelled by convection and diffusion, and within the cells, the oxygen consumption was modelled according to Michaelis-Menten kinetics. For simplicity, the values of the parameters in these equations were chosen under the assumption that the fluid is water. table 2.3-5 lists all the parameter values that were used in the simulations. As the exact value of V_{max} was unknown for macrophages, the minimum and maximum values of an accepted range were chosen in order to demonstrate the effect of varying this parameter. The thickness of the cell layer was calculated by dividing the total cell volume by the area covered by the cells.

Table 2.3-5 Parameter values used in the simulations.

Parameter	Description	Value	Unit
ρ	Fluid density	1×10^3	$kg\ m^{-3}$
μ	Fluid dynamic viscosity	1×10^{-3}	$Pa\ s$
p	Pressure	1×10^3	Pa
D	Oxygen diffusion coefficient in water	3×10^{-9}	$m^2\ s^{-1}$
D_c	Oxygen diffusion coefficient in cells	1×10^{-9}	$m^2\ s^{-1}$
h_c	Thickness of cell layer	5×10^{-6}	m
V_{max}	Maximum oxygen consumption rate	1×10^{-2} or 1×10^{-3}	$mol\ m^{-3}\ s^{-1}$
K_m	Michaelis-Menten constant	6.3×10^{-3}	$mol\ m^{-3}$
c_i	Inlet oxygen concentration (20% O_2)	0.2	$mol\ m^{-3}$
Q	Volumetric flow rate	360	$\mu L\ min^{-1}$

2.4 3D vs 2D methods
2.4.1 3D Scaffold Selection
2.4.1.1 Alvetex (UK)

Reinnervate Ltd was founded in 2002 by Professor Stefan Przyborski as a spinout biotechnology company from Durham University, UK. Reinnervate was acquired by ReproCELL in 2014 and was merged with Biopta to form ReproCELL Europe Ltd in July 2016.

Reinnervate's core strength was in its Alvetex® family of 3D cell culture products, providing a flexible platform that allows scientists in any life science laboratory to easily establish improved *in vitro* assays and tissue models that better mimic the *in vivo* growth of cells. Alvetex® is a highly porous polystyrene scaffold designed for 3D cell culture. Each disc of

spun polystyrene is engineered to a thickness of just 200 microns with pore sizes of 36-40 microns. No cell is ever further than 100 microns from the nutrient source enabling easy exchange of nutrients, gases and waste products by passive diffusion across short distances. Alvetex is completely inert so there is no chance of contaminating biological material that can sometimes be found in animal derived scaffolds.

Alvetex has been designed for simple and routine use. It uses conventional cell culture plasticware. It requires no specialist equipment, changes to media or optimized cell feeding protocols and is compatible with the majority of downstream analytical techniques. Alvetex 3D cell culture enables cells to maintain their *in vivo* morphology, behaviour and responsiveness within an *in vitro* model system.

2.4.1.2 Invitrocue (Singapore)

Invitrocue Ltd Singapore is a leading provider of bio-analytic solutions including *in vitro* cell-based testing technologies and image analytics software for use in digital pathology. Invitrocue's technology originated in Singapore's Agency for Science, Technology and Research (A*STAR). Invitrocue have been developed and validated in partnerships with leading biopharmaceutical companies and scientific collaborators.

The 3D CelluSponge[254] is an innovative *in vitro* platform for 3D cell culture. It is fabricated from inert hydroxypropyl cellulose, has a uniform macroporosity of 80 – 150 µm and each disk is 1 mm thick. The controlled macroporosity allows the formation of uniformly sized spheroids. This thereby prevents necrosis in the spheroid core by allowing access to nutrients without mass transfer limitations. The constrained spheroids have shown excellent maintenance of 3D cell morphology, viability, cell-cell interaction, cell polarity, synthetic and metabolic functions[335]. The 3D CelluSponge exhibits minimal drug absorption and offers new possibilities for *in vitro* drug safety testing.

2.4.2 Cell Seeding Protocols

2.4.2.1 Alvetex

Alvetex scaffolds were submerged in 70% ethanol for 10 seconds, then washed in RPMI-1640. Scaffolds were then placed in a 24 well plate. Cells were washed, centrifuged and re-suspended at $2x10^7$ per mL in RPMI-1640 supplemented with 10% HiFCS. Cells were seeded by pipetting 50 µL directly on to the scaffold. Scaffolds were left at 37°C and 5% CO_2 for 45 minutes then wells were topped up with in RPMI-1640 supplemented with 10% HiFCS and replaced in the incubator.

2.4.2.2   InvitroCue

Cells were washed, centrifuged and re-suspended at 4×10^7 per mL in RPMI-1640 supplemented with 10% HiFCS. Sponges were placed in the centre of a well in a 24 well plate. Cells were seeded by pipetting 25 µL directly on top of the sponge. Sponges were left at 37°C and 5% CO_2 for 45 minutes then wells were topped up with in RPMI-1640 supplemented with 10% HiFCS and replaced in the incubator.

2.4.3   Measurement of Cell Viability

2.4.3.1   Measurement of Cell Viability in 2D Cultures

Peritoneal macrophages were seeded in 96 well plates at 1×10^6 cells/well per mL in RPMI-1640 supplemented with 10% HiFCS. Cells were incubated in a 37°C and 5% CO_2 incubator. To take a reading, the media was removed and 100 µL of media containing 10% Alamar blue was added to each well. The plate was incubated in the dark at 37°C for an hour. After an hour, samples of media were taken and fluorescence was read using a Spectramax M2 at 530 nm excitation and 580 nm emission with a 550 nm cut off. The media was replaced with 100 µL of fresh media before cells were replaced in the incubator.

2.4.3.2   Measurement of Cell Viability in 3D

Peritoneal macrophages were seeded as in 2.4.2.2 and viability was measured as in 2.4.3.1.

2.4.4   Evaluation of *Leishmania* Infection in 3D Cell Culture

Peritoneal macrophages were plated as in 2.4.2.1 and 2.4.2.2. After 24 hours incubation at 37°C and 5% CO_2, the adhered PEMs in both scaffolds were infected with stationary phase promastigotes, by removing the media in the well and replacing with fresh media containing promastigotes, at a variety of ratios (0.5:1 to 6:1). Cells were maintained at 34°C and 5% CO_2 for a further 72 hours. The scaffolds were then fixed in 4% PFA overnight at 4°C. The next day the scaffolds were treated with 0.2% Triton X-100 in PBS for 10 minutes and then 1% BSA in PBS for 10 minutes. Scaffolds were then stained with phalloidin Cruz fluor Actin labelling antibody overnight at 4°C on a plate shaker. The next day scaffolds were washed and treated with 300 mM DAPI stain for 10 minutes. The percentage infection was determined microscopically using Zeiss LSM510 confocal (40x magnification) by counting the number of infected macrophages.

2.4.5   Evaluation of Anti-leishmanial Activity in 3D Cell Culture

Peritoneal macrophages were plated as in 2.4.2.2. After 24 hours, the adhered PEMs in the Invitrocue scaffold were infected with stationary phase promastigotes at a ratio of 5 *L. major* (mCherry) promastigotes or 7 *L. amazonensis* (DSred2) to 1 macrophage and maintained at

34°C in a 5% CO_2 for 24 hours. After 24 hours, media was removed from all wells and miltefosine at concentrations of 20, 5 and 1.25 µM or amphotericin B at concentrations of 200, 50 and 12.5 nM were added in triplicate at each concentration. A set of un-drugged controls were included in triplicate, by adding just fresh media. After 72 hours, percentage infection was assessed as in 2.4.4.

2.4.6   Confocal Microscopy

The confocal microscope used was a Zeiss LSM510 Axiovert (Zeiss, Germany) contained within an incubation chamber, which can be temperature and CO_2 regulated, it uses Zeiss 510 software for image acquisition. Images taken with the microscope were usually 40x but it is also equipped with x10, x20, x63 and x100 lenses. The following lasers were used Laser Diode: 405 nm for DAPI excitation, Argon laser: 458, 488, 514 nm for phalliodin excitation and HeNe1 laser: 543 nm for parasite mCherry and RFP excitation. The optical slice was set to 1 µm for all lasers, scan speed was set to 8 and image size was set to 512 pixels. Cells were found visually using the laser that excites the DAPI stain and then intensities of the lasers were adjusted using the software to provide equal intensities for each colour detected. The total depth of the z-stack was selected to capture the complete 3D structure of the cells. Images captured were analysed either completely automatically by Invitrocue or semi-automatically at the LSHTM using Volocity software (PerkinElmer) to automatically count nuclei for total cell number and then the images were manually viewed to count number of infected cells. The results were exported and analysed using Microsoft Excel and Graphpad Prism.

2.5 Cell Choice Methods

2.5.1   Cell Culture

2.5.1.1   Induced Pluripotent Stem Cells

Induced pluripotent stem cells are reprogrammed adult, specialized cells[320]. The reprogramming turns them into pluripotent stem cells meaning they can make any type of cell in the body. IPS cells and embryonic stem cells are similar[321]. They are self-renewing, meaning they can divide and produce copies of themselves indefinitely. Both types of stem cell can be used to derive nearly any kind of specialized cell under precisely controlled conditions in the laboratory. For our purposes, the iPSCs were differentiated to make iPSC derived macrophages[322 & 323].

Dr Christine Hale provided training on the culture, differentiation and use of iPSCs at the Wellcome Trust Sanger Institute, Genome Research Limited.

2.5.1.1.1   iPSC Culture

iPSCs were removed from cyrostorage and thawed. Cells were washed once with TESR-E8 medium and plated on Synthemax coated 6 well plates and maintained at 37 ˚C 5% CO_2 in TESR-E8. Once the cells reach about 80% confluence they were harvested with TrypLE and divided onto four Synthemax coated $10cm^2$ dishes. When the cells reached 80% confluence they were transferred to a second Synthemax coated 10 cm^2 dish. During the culture on Synthemax coated plates media was changed daily.

A vial of MEF CF-1 cells (mouse embryonic feeder) was defrosted and cultured in 2 x 10 cm^2 round tissue culture dishes coated in 0.1% gelatine in MEF media, Advanced DMEM F12 with 10% HiFCS, L-glutamate and 3.5 µl 2-mecaptoethanol.

After the cells reached 80% confluence on Synthemax they were harvested with TrypLE, washed twice with huiPS base medium (Advanced DMEM/F12, 20% Knockout replacement serum (KSR), 1x L-glutamine, 3.5 µL B-mercaptoethanol containing fibroblast growth factor (FGF) (7.5 µL per 50 mL) and transferred to 16 MEF CF-1 containing 10 cm^2 dishes. This process was repeated again after a couple days. After the second passage, the cells were isolated with a 1:1 Dispase: Collagenase solution and centrifuged. The pellet after resuspension in huiPS base medium at 4 x 10^5 cells/mL and was then plated at 100 µL per well between the well in a 96 well low adhesion round bottomed plate. The plate was then centrifuged to stimulate embryo body formation. The plate was then left for 3-4 days in a humidified CO_2 incubator.

After 3-4 days, the embryoid bodies were harvested and 16 bodies were placed in each 10 cm^2 dish.

2.5.1.1.2   iPSC Differentiation

Embryoid bodies were plated onto 10 cm^2 round dishes in monocyte differentiation media, X-Vivo 15 plus gentamycin with L-glutamine, B-mercapto-ethanol, hM-CSF (50 ng/mL) and hIL-3(25 ng/mL). Media was changed every 7 days and the resulting floating monocytes were ready to be harvested after day 21. Harvesting was repeated once a week for up to 100 days.

Monocytes were harvested and contaminating clumps of stem cells were removed by collecting the media and straining through a 70 µM cell strainer (Corning CLS431751). Monocytes were centrifuged, re-suspended in macrophage differentiation media, RPMI with 10% FCS, l-glutamine and hM-CSF (100 ng/mL), prior to re-plating in 10 cm^2 round dishes. Differentiated macrophages were isolated between day 7-14, TrypLE (5 minutes at 37 ºC), to remove them from the surface of the dish.

2.5.1.2 Mouse Bone Marrow Monocytes
2.5.1.2.1 Mouse Bone Marrow Monocyte Isolation

Mice were euthanized by schedule 1 killing, then using aseptic technique, the femurs were removed and placed in a plastic dish containing sterile PBS. Femurs were stripped of further skin and muscle from legs by holding the end of the bone with forceps and using scissors to push muscle downward away from forceps. Leg bones were severed proximal to each joint. A 25G needle was used to flush the bone cavity with 5mL of ice cold DMEM, until the bone cavity appeared white. Flushed RPMI was collected and then centrifuged before re-suspending the bone marrow progenitor cells in RPMI 1640 + 10% FCS and penicillin/streptomycin.

2.5.1.2.2 Mouse Bone Marrow Monocyte Differentiation

The mouse bone marrow monocytes were plated at a concentration of 25 million cells per T175 flask. Then extra DMEM + 10% FCS and pen/strep containing macrophage colony stimulating factor (m-CSF) was added to give a final concentration of 50 ng/mL of m-CSF. The cells were incubated for 7 days in a 37°C incubator before mature macrophages were harvested.

2.5.1.3 Human Bone Marrow Monocytes

Human bone marrow mononuclear cells were purchased from ATCC (PCS-800_013). 25 million cells were delivered cryopreserved, these were defrosted and plated. The ATCC have characterised these cells to be CD45, CD3, CD8, CD58, CD14, CD19 and CD34 positive immediately before freezing.

2.5.1.3.1 Human Bone Marrow Monocyte Differentiation

The human bone marrow monocytes were plated at a concentration of 8.3 million cell per T175 flask in RPMI 1640 + 10% FCS, pen/strep and 50ng/mL macrophage colony stimulating factor m-CSF. The cells were incubated for 7 days in a 37°C incubator before mature macrophages were harvested.

2.5.2 Evaluation of Infection Potential of Cells

Cells (THP1, Human and mouse bone marrow macrophages and iPSC derived macrophages) were seeded in 16 well Lab-Tek™ plates in RPMI-1640 supplemented with 10% HiFCS at a density of $2x10^4$ per well. After 24 hours incubation at 37°C and 5% CO_2, cells were infected with stationary phase promastigotes. A variety of ratios (0.5:1 to 10:1) of *L. major* JISH 118, *L. major* mCherry, *L. mexicana* M379 and *L. amazonensis* DSred2 were used and maintained at 34°C in a 5% CO_2. After 24h, the cultures had the media replaced to remove extracellular promastigotes and one slide was fixed with methanol and stained with Giemsa to determine

the initial level of infection. After a further 72 hours incubation, all slides were methanol-fixed and either Giemsa-stained or stained for use with the confocal microscope. The percentage inhibition was determined microscopically (400x magnification) by counting the infected macrophages.

2.5.3 Evaluation of anti-leishmanial drug activity

Experiment conducted as in 2.5.2. Except, after 24 hours incubation at 37°C and 5% CO_2, cells were infected with stationary phase promastigotes at a ratio of promastigotes to macrophage, pre-selected using the results of the 2.5.2. Parasite strains *L. major* JISH 118, *L. major* mCherry, *L. mexicana* M379 and *L. amazonensis* DSred2 were used. In addition, drugs were added for the 72 hours incubation at a variety of concentrations. Miltefosine solutions at concentrations of 30, 10, 5 and 1.25 µM, amphotericin B solutions at concentrations of 300, 100, 50 and 10 nM or sodium stibogluconate at concentrations of 600, 300, 100 and 50 ug of Sb/mL were added in triplicate at each concentration.

2.6 Statistical Analysis and Computer Packages

2.6.1 General Statistics

Data was first formatted and normalised in Microsoft excel and then transferred into Prism Software. The Hill coefficient, EC_{50} and EC_{90} values were determined by non-linear sigmoidal curve fitting (variable slope) and statistics carried out using the built in functions.

2.6.2 3D Imaging Software

As previously mentioned, images were taken using Zeiss 510 software. The images were then processed in either Zeiss image browser or Volocity. Zeiss image browser was used to view images, add scale bars, make videos and publish images in other file formats. The Volocity software was used to analyse the images to quantify infection.

2.7 Ethical Clearance

All animal experiments were conducted under license (project license 70/6997 or X20014A54) in accordance with UK Home Office approval, EU regulations, EU directive 2010/63/EU and the ethics committee at the LSHTM. At all stages the 3Rs (replacement, reduction and refinement) were taken into consideration. The overall aim of the project was to help develop models that could be used as a replacement for some animal experiments.

Chapter 3 Development of a Media Perfusion System Model for Leishmaniasis

3.1 Introduction

The aim of this thesis is to investigate different ways in which the current *in vitro* model systems could be more predictive of *in vivo* results. Current approaches are based upon both 2D cell assays and *in vivo* mouse models, both of which may not accurately reflect the infection in humans. Three methods of potentially improving reliability and predictability in models are investigated in this thesis. In this first results chapter the development of a dynamic media perfusion system for *in vitro* assays is addressed.

Static systems have been the most commonly used *in vitro* assay to measure the infection rates and drug activities against *Leishmania* parasites in most laboratories. A variety of plates with different well numbers, from 2 wells per plate up to 6144 wells, are widely available for purchase and have been used in Leishmaniasis assays[173]. This form of *in vitro* assay is based upon continuous exposure of infected cells for 48/72 hours. However, it does not offer any form of dynamic chemical or physical stimulus to cells. This is a major limitation in experiments investigating cellular responses *in vitro* since the complex interplay of mechanical and biochemical factors is absent.

The use of a dynamic media perfusion system can stimulate cells by creating: concentration gradients, flow, pressure and mechanical stress caused by movement of fluids around them[133]. The media can be set to a single pass or used in a re-circulating system depending on the purpose of the assay. With enough knowledge of the system, the exact conditions can be carefully controlled to simulate several aspects of an *in vivo* system.

For the introduction of fluid flow into the *in vitro* model, a macro fluidic system was chosen over microfluidic systems, as this would allow easier manipulation of the parameters of the system. One important factor for the choice of a macro system is that it would allow for the eventual creation and sustainment of a reconstituted skin model that was large enough for use in the testing of topical medicines. Another important consideration was the retrieval of cells post experiment, this is critical for the study of *Leishmania* parasites *in vitro*, as the main method of evaluation is microscopic counting of infected cells[157].

The Quasi Vivo system from Kirkstall Ltd was selected as not only is it a macro fluidic system, but also because it can provide a variety of fluid flow rates which includes the range of

interstitial fluid flow rates in the skin and at the same time a low shear stress environment. For CL, the interstitial fluid flow rate in the skin is the condition that the system aims to replicate. Interstitial fluid is the fluid that is found between the cells in a multicellular organism, the movement of the fluid in the skin is caused by the normal leakage of plasma from blood vessels and drainage into the lymphatic system. Although the exact velocity of this flow may vary, measurements have suggested that the interstitial fluid flow rates in human skin are of the order of 0.1–2 μms^{-1} [233-235]. The Quasi vivo systems are able to produce this rate of fluid flow consistently and were designed specially with easy inter-changeable layouts and the ability to remove cells after the completion of the experiment.

The work covered in this section for *Leishmania* has almost no precedence in the literature and almost all of the experiments conducted have never been previously reported to the best of my knowledge. Notable work in the area of *Leishmania* by Miller and Twohy[280], involved using a perfusion model for the infection of mouse peritoneal macrophages with *L. donovani*. They used a media perfusion system to observe the infection of the macrophages by leptomonads, however they did not, include the rate of media perfusion, the reasons behind the experiment, or comment on any differences between their experiment and the static alternative.

Other examples of media perfusion systems used in other infectious disease areas are also rare, although the use of microfluidics in this area is growing. The malaria and *Leishmania* parasites are both vector-borne protozoan parasites with different life cycle stages. The malaria parasite has a specific blood stage to its life cycle and this environment is highly dynamic. Microfluidic devices have been used to model this dynamic environment to study the maturation of *P. falciparum* and its effect on the deformability of infected red blood cells[281&282]. One study showed that *P. falciparum* decreases the deformability of infected red blood cells, increasing their clearance as they attempt to pass through endothelial slits of the splenic sinus[281]. Another previous study on *P. vivax* infected erythrocytes reached different conclusion with respect to cellular deformability[282]. A variety of bacterial models, such as ones simulating the dynamic environments in the gut exist. One such model is used to model bacterial attachment[283] and another colonisation[284] of *E. coli*. Media perfusion is used in these models to simulate gut movements and demonstrate the strength of binding between bacteria and the gut wall. In some cases, a media perfusion system is used for the maintenance and production of cells before the testing of infectious disease[285]. One example

where the media perfusion is just as important for the function of the host cells is in the liver and in models of hepatitis C[286]. A direct modelling of hepatitis replication was studied using a microfluidic device and showed that it is an adequate system for virus infection[286]. Other infections by viruses have been studied with microfluidic devices, one such example is the infection of cells from *Spodoptera frugiperda* by baculovirus[287].

The objectives of this study were:

    I.   To set up an *in vitro* media perfused model of macrophages in the skin.

    II.   To determine viability of host cells in the Quasi Vivo macrofluidic system.

    III.   To establish methods to detect the infection within the system.

    IV.   To establish an infection and determine the infection potential within the system.

3.2 Investigation of Cell Viability Differences between Cells Maintained under Static or Media Perfusion Conditions

Media perfusion systems have been reported[288&289] to maintain cell viability for longer in both 2D and 3D cell culture systems. To investigate if the same effect was seen using the Kirkstall QV500 system THP1 macrophages were plated and maintained either under media perfusion or static conditions. The system was then left to run for 72 hours, which is the same period used in a standard three day drug assay. The viability of the cells was assessed using an Alamar blue assay, which is a measure of mitochondrial metabolism[290]. The Alamar blue assay is based upon the compound resazurin (7-Hydroxy-3H-phenoxazin-3-one 10-oxide) which is weakly fluorescent. The conversion of resazurin to resorufin (7-Hydroxyphenoxazin-3-one) by the cells is an irreversible reduction giving a red fluorescent molecule. Mitochondrial metabolism is a good measure of cell viability as non-viable cells will not be able to process and metabolise the dye. Resazurin based assays show excellent correlation[332] to other viability assays such as formazan-based assays, whilst being easier and safer to use. If the media perfusion maintains the cell viability better than the static system then the fluorescent signal produced by the resorufin will be higher.

3.2.1 Cell Viability Differences between Cells Maintained under Static or Media Perfusion Conditions

In the first experiment, shown in figure 3.2-1, after four hours of incubation with Alamar blue, the fluorescent reading of the cells maintained under media perfusion conditions had increased to an average of 1210 RFU. Whereas, the fluorescence reading of cells maintained in static conditions, had increased to an average of 390 RFU. Using a student T-test, to

compare viability between the static system and media perfusion, set to 50 µL/min, viability in the media perfusion system is statistically higher (p<0.0001).

In the second experiment (0-7 hours), figure 3.2-1, cells maintained under media perfusion conditions and a bulk transfer rate of 50 µl/min had increased this fluorescent read out to an average of 5308 RFU after 7 hours, whereas the cells maintained in a static system had only increased the read out to an average of 3273 RFU. The cells maintained under media perfusion conditions with a bulk transfer rate of 100 µL/min had increased this fluorescent read out to an average of 8115 RFU after 7 hours. Using a student T-test viability was compared between the static system and the QV500 media perfusion system, set to 50 µL/min, viability in the media perfusion system was statistically higher (p<0.0001). When the perfusion system was set to 100 µL/min, viability in the media perfusion system was again statistically higher, p<0.0001. If the two speeds of the media perfusion system were compared viability at 100 µL/min was statistically higher than the 50 µL/min, p<0.0001. A linear relationship between fluorescent signal and time for each of the three conditions can be seen in figure 3.2-1. This shows that the assay is in the linear stage of the reaction and has not reached the limit of detection of the plate reader after 7 hours.
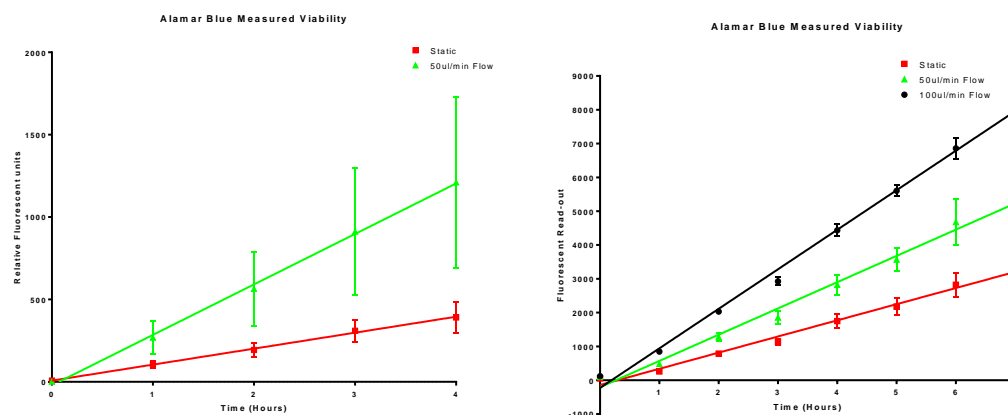
Figure 3.2-1. Turnover of Alamar blue by cells maintained under either static or media perfusion conditions (50 µL/min or 100 µL/min) measured over a period of 0-7 hours. N =3 Error bars show SD

3.2.2   Discussion of Cell Viability Differences between Cells Maintained under Static or Media Perfusion Conditions

The data shows that even at a speed of 50 µL/min the media perfusion system better maintains the viability of the cells when compared to the static condition. This is further evident when increasing the flow speed. A reason for this difference in viability could be an increased availability of nutrients in the media or the increased rate of potentially harmful

waste products removal. From the literature, it is clear that different types of cells have different responses to media perfusion and are comfortable over a particular range of speeds. Thus, it can be expected that whilst increasing the speed of media perfusion better maintains the viability of these macrophages, the increase will not continue exponentially and eventually the increased media perfusion speed will cause damage to the cells and a decrease in cell viability[291&292].

3.3 Change of Media Perfusion Systems from Kirkstall Ltd QV500 to QV900

3.3.1 Rationale behind Change of Media Perfusion System

The QV media perfusion system is a complex system with many interchangeable parts; one challenge when using this system is maintaining sterility. The QV500 media perfusion system is a multi-use system, which can be re-used if cleaned correctly between uses. Cleaning the system before and after each experiment is meant to maintain sterility but the deconstruction and re-construction of the system each time allows contaminants an opportunity to enter the system. The problem of bacterial contamination caused a series of failed and aborted experiments, this problem was then investigated. Despite the QV500 system being regularly flushed with both 70% and 100% ethanol and autoclaved between uses, the bacterial contamination was still present. A test of the system, using nothing but filtered RPMI-1640, still yielded a contaminated system. The result of the experiments was realisation the bacterial contamination was coming from the system itself. After contact with the Kirkstall Ltd, who produce the system, it was concluded that the bacteria had grown into the systems silicone pores and autoclaving would not be effective to remove the colonies.

Due to the contamination issues, it was decided to switch to the QV900 system, relying on single use disposable plates, which would avoid any recurrence of contamination between assays.

3.4 *In Silico* Modelling of Media Perfusion Systems

3.4.1 Modelling of the Kirkstall Ltd QV500 Media Perfusion System

The modelling of the fluid flow rates and the stresses that this causes for cells within the QV500 system was first reported in two publications: Ahluwalia (2010)[219]: A low shear stress modular bioreactor for connected cell culture under high flow rates and Ahluwalia (2014)[360]: Design Criteria for Generating Physiologically Relevant *In Vitro* Models in Bioreactors. Authors of these papers were part of the original team who designed the

QV500 system before Kirkstall Ltd spun out from the project. The modelling in these papers was used to choose a bulk flow speed that matched the flow velocity at the cell surface to the interstitial fluid flow rate. The selected value from the papers was 360 µL/min bulk flow. This translates to 1 µm/s in flow velocity across the cell surface, which is the value for interstitial fluid flow rate in human skin[233-235].

3.4.2 Modelling of the Kirkstall Ltd QV900 Media Perfusion System

3.4.2.1 Modelling of Cells Maintained at the Base of the Well when the Maximum Rate of Oxygen Consumption (Vmax) = 1e^{-3} mol/m^3/s

Visual representations of the results of the modelling conducted in COMSOL, which is a modelling software, are shown in figure 3.4-1. The figure shows the modelling of the first chamber, of six chambers, each containing cells connected in series with the maximum oxygen consumption rate of the cells set to 1 x 10^{-3} mol/m^3/s. The top left image of figure 3.4-1 shows the oxygen concentrations throughout the first chamber in the series, showing a decrease in the oxygen concentration moving from the inlet of the chamber to the bottom of the chamber. This is partially due to the oxygen diffusion and convection within the system. In addition, the cells at the bottom of the well are using the oxygen for metabolism and this further reduces the oxygen concentration within the media at the bottom of the chamber. The middle left image of figure 3.4-1 is a 2D representation of the oxygen concentrations at the bottom of the well. Oxygen concentrations reduce from left to right across the bottom of the well due to this being the direction of travel of the media, and the oxygen being used up by the cells. This reduction in oxygen concentration is graphically displayed in the bottom left image of figure 3.4-1. The oxygen concentrations range from 0.1898 mol/m^3 down to 0.1864 mol/m^3 across the base of the chamber. Values showing the oxygen concentrations for each of the six chambers connected in series are shown on the bottom right of figure 3.4-1. The oxygen concentrations are lower in each consecutive chamber but the pattern of the spread of oxygen concentrations across the base of the chamber is the same in each chamber. By the time the final chamber is measured, the maximum oxygen concentration has fallen to 0.1889 mol/m^3 and the minimum to 0.1855 mol/m^3.

The top right image of figure 3.4-1 shows a representation of the streamlines, showing how the media travels through the chamber. It also shows the flow velocity of the media throughout the chamber. The depth of the well allows flow recirculation zones at the bottom of the well. In this area, the media is recirculated and this could result in oxygen or drug molecules being trapped. The image shows that the media velocity is fastest at

the inlet and outlet. The flow velocity of the media at the base of the well where the cells are is 1.74 x 10^{-9} m/s. The flow velocity across all six chambers is consistent and is, on average, 1.75 ± 0.01 x 10^{-9} m/s.

The middle right image of figure 3.4-1 shows a 2D representation of the magnitude of shear stress the cells are under at the bottom of the well. The shear stress is highest in the centre of the well and was reduced nearer the edges. The shear stress values range from 3.52 x 10^{-7} Pa, at the centre of the chamber, down to 1.51 x 10^{-11} Pa, at the edges of the chamber. The shear stress across all six chambers is consistent and is on average 3.53 ± 0.03 x 10^{-7} Pa, at its maximum value, and the minimum value is identical across all wells at 1.51 x 10^{-11} Pa.

Vmax = 1e-3 and cells at base
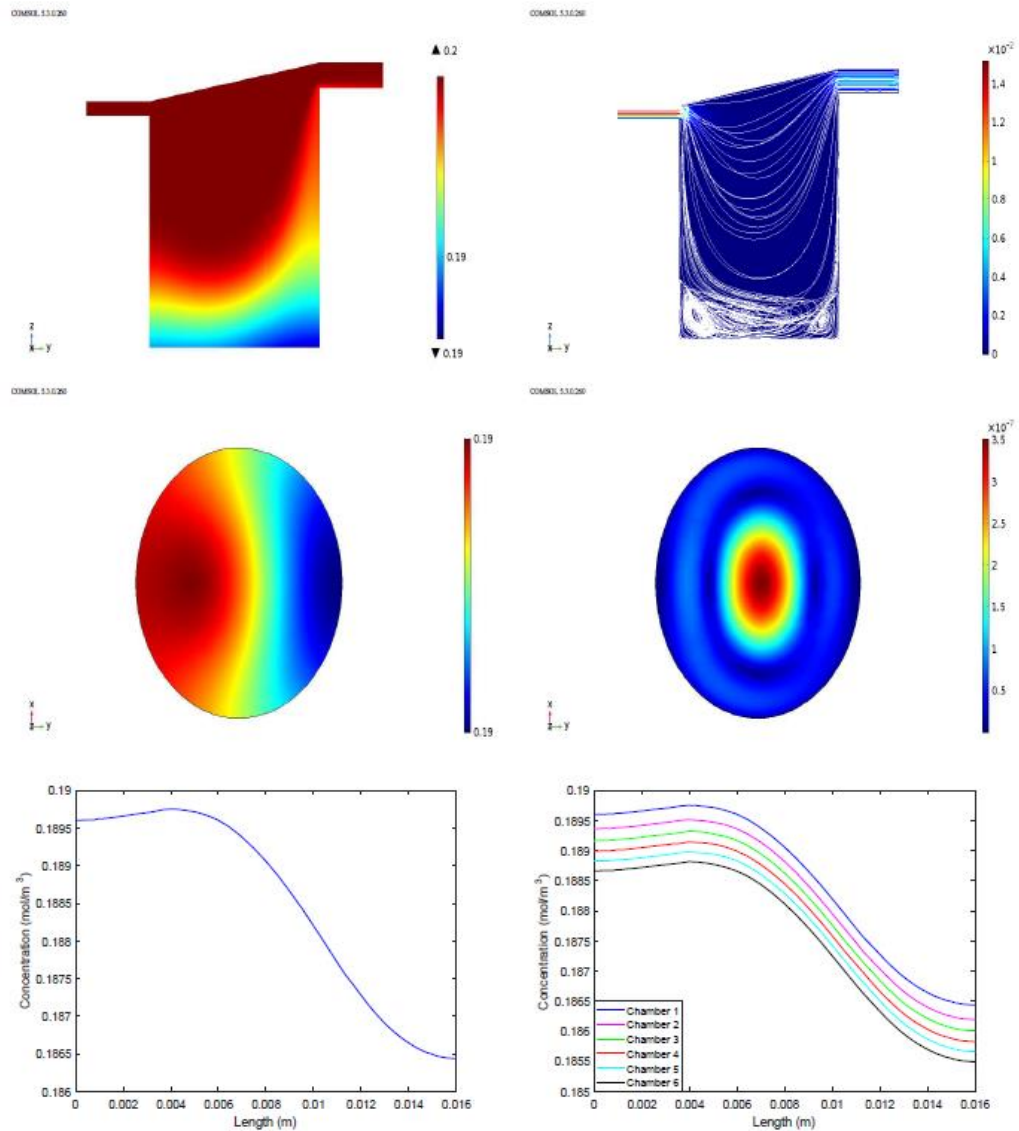
Figure 3.4-1. COMSOL results for cells at the base of the chamber and V_{max} = 1 x 10^{-3} mol/m^3/s. **Upper left**: Oxygen concentration in chamber 1. **Upper right**: Flow profile in chamber 1. **Middle left**: Cell surface oxygen concentration in chamber 1. **Middle right**: Magnitude of the cell surface shear stress in chamber 1. **Bottom left**: Cell surface oxygen concentration profile in chamber 1. **Bottom right**: Cell surface oxygen concentration profiles for all 6 chambers.

3.4.2.2 Modelling of Cells Maintained at the Base of the Well when the Maximum Rate of Oxygen Consumption (Vmax) = 1e^{-2} mol/m^3/s

Visual representations of the results of the modelling are shown in figure 3.4-2. The figure shows the modelling of the first chamber of six chambers each containing cells connected in series with the maximum oxygen consumption rate of the cells set to 1 x 10^{-2} mol/m^3/s. The images show the same results as before. The pattern of results is

identical; however, the values produced by this simulation are different. Oxygen concentrations range from 0.1009 mol/m^3 down to 0.0703 mol/m^3 across the bottom of the chamber. The oxygen concentrations are lower in each consecutive chamber but the pattern of the spread of oxygen concentrations across the base of the chamber is the same in each chamber. By the time the final chamber is measured, the maximum oxygen concentration has fallen to 0.0925 mol/m^3 and the minimum to 0.0623 mol/m^3.

The flow velocity of the media at the base of the well where the cells are is 1.74 x 10^{-9} m/s. This is identical to the previous (figure 3.4-1) above with a lower maximum oxygen consumption. The shear stress values range from 3.52 x 10^{-7} Pa at the centre of the chamber down to 1.51 x 10^{-11} Pa at the edges of the chamber. This is also identical and follows directly from the fact that the flow velocities are identical as in the previous simulation. The flow velocity and shear stress values in each of the six chambers are identical to the values produced in the previous simulation.
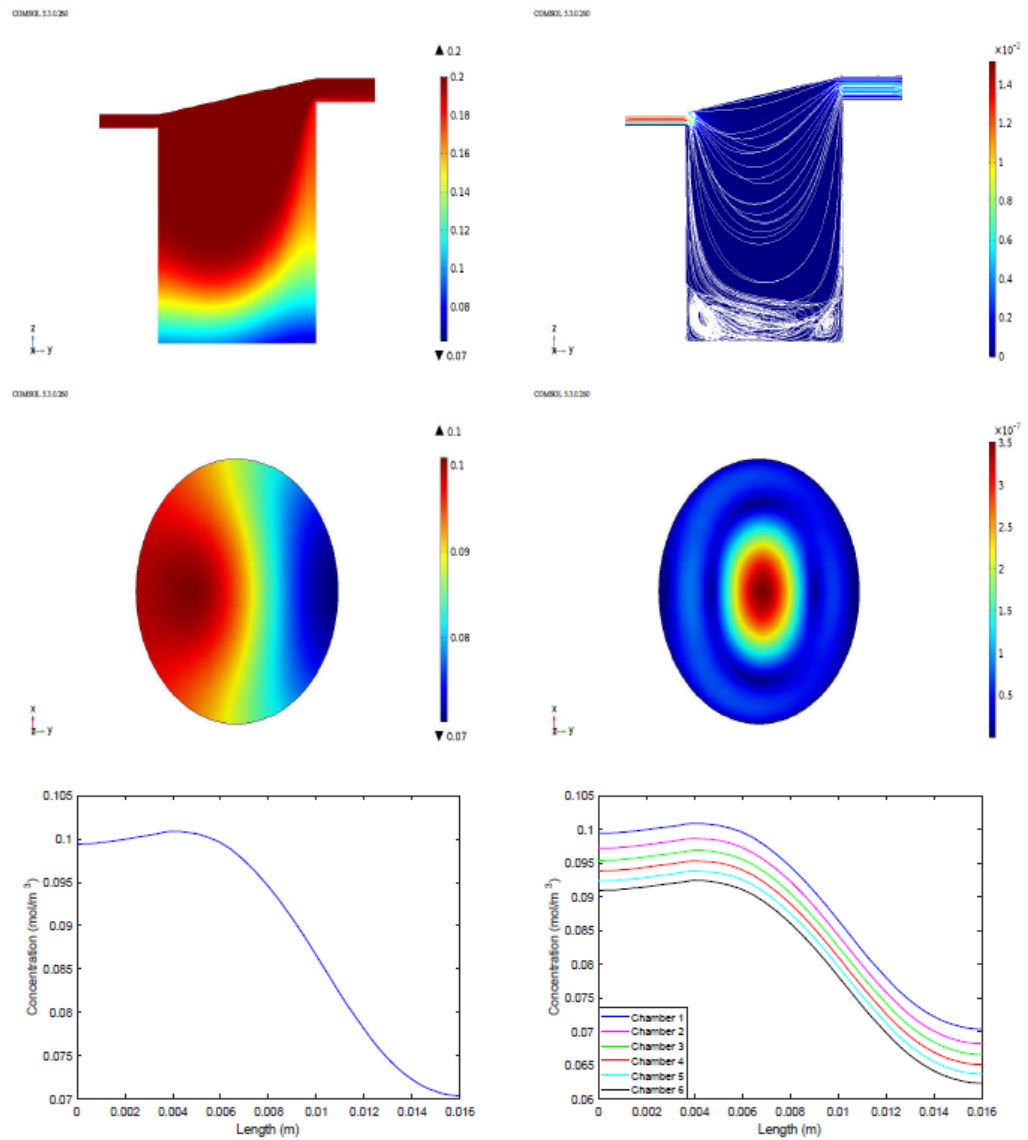
Figure 3.4-2. COMSOL results for cells at the base of the chamber and V_{max} = 1 x 10^{-2} mol/m^3/s. **Upper left**: Oxygen concentration in chamber 1. **Upper right**: Flow profile in chamber 1. **Middle left**: Cell surface oxygen concentration in chamber 1. **Middle right**: Magnitude of the cell surface shear stress in chamber 1. **Lower left**: Cell surface oxygen concentration profile in chamber 1. **Lower right**: Cell surface oxygen concentration profiles for all 6 chambers.

3.4.2.3 Modelling of Cells Maintained on Top of the 9mm Insert when the Maximum Rate of Oxygen Consumption (Vmax) = 1e^{-3} mol/m^3/s

Visual representations of the results of the modelling, conducted in COMSOL, on the first chamber of six chambers connected in series, each with a 9 mm insert placed inside the chamber to reduce its depth, are shown in figure 3.4-3. The maximum oxygen consumption rate was set to 1 x 10^{-3} mol/m^3/s, the accepted value for HEPG2 cells, as the value for macrophages is unknown. The images shown represent the same parameters as before, oxygen concentration, flow velocity and shear stress. When the 9 mm insert was placed inside the chambers, the insert changed both the pattern of results observed and the values produced in the simulation. The top left image of figure 3.4-3 showing the oxygen concentrations throughout the chamber. The reduction in the height of the well means that the oxygen concentration seen is higher throughout the whole chamber. There is reduced oxygen concentrations at the edges of the chamber caused by recirculation of the media, leading to maximum oxygen concentrations being found closer to the centre of the chamber. The oxygen concentrations range from 0.1979 mol/m^3 at the centre of the well down to 0.1937 mol/m^3 at the far right hand side of the chamber. Values showing the oxygen concentrations for each of the six chambers connected in series are shown in the bottom right of figure 3.4-3. The oxygen in the final chamber ranges from 0.1969 mol/m^3 to 0.1927 mol/m^3.

The top right image of figure 3.4-3 shows a representation of the streamlines of the movement of the media in the chamber. The streamlines in the reduced depth well (figure 3.4-3) are clearly more horizontal to the base of the chamber than in the deeper well (figure 3.4-1). The flow velocity of the media at the base of the well where the cells are is 1.46 x 10^{-7} m/s. The flow velocity across all six chambers is consistent and, is on average, 1.46 ± 0.01 x 10^{-7} m/s.

The middle right image of figure 3.4-3 shows a 2D representation of the magnitude of the shear stress the cells are under across the bottom of the well. This variation in shear stress is graphically displayed in the bottom right image of figure 3.4-3. The shear stress values range from 2.95 x 10^{-5} Pa at the centre of the chamber down to 4.42 x 10^{-11} Pa at the edges of the chamber. The shear stress across all six chambers is consistent, and is on average 2.96 ± 0.02 x 10^{-5} Pa at its maximum value and the minimum value is on average 4.35 ± 0.92 x 10^{-11} Pa, across all wells.
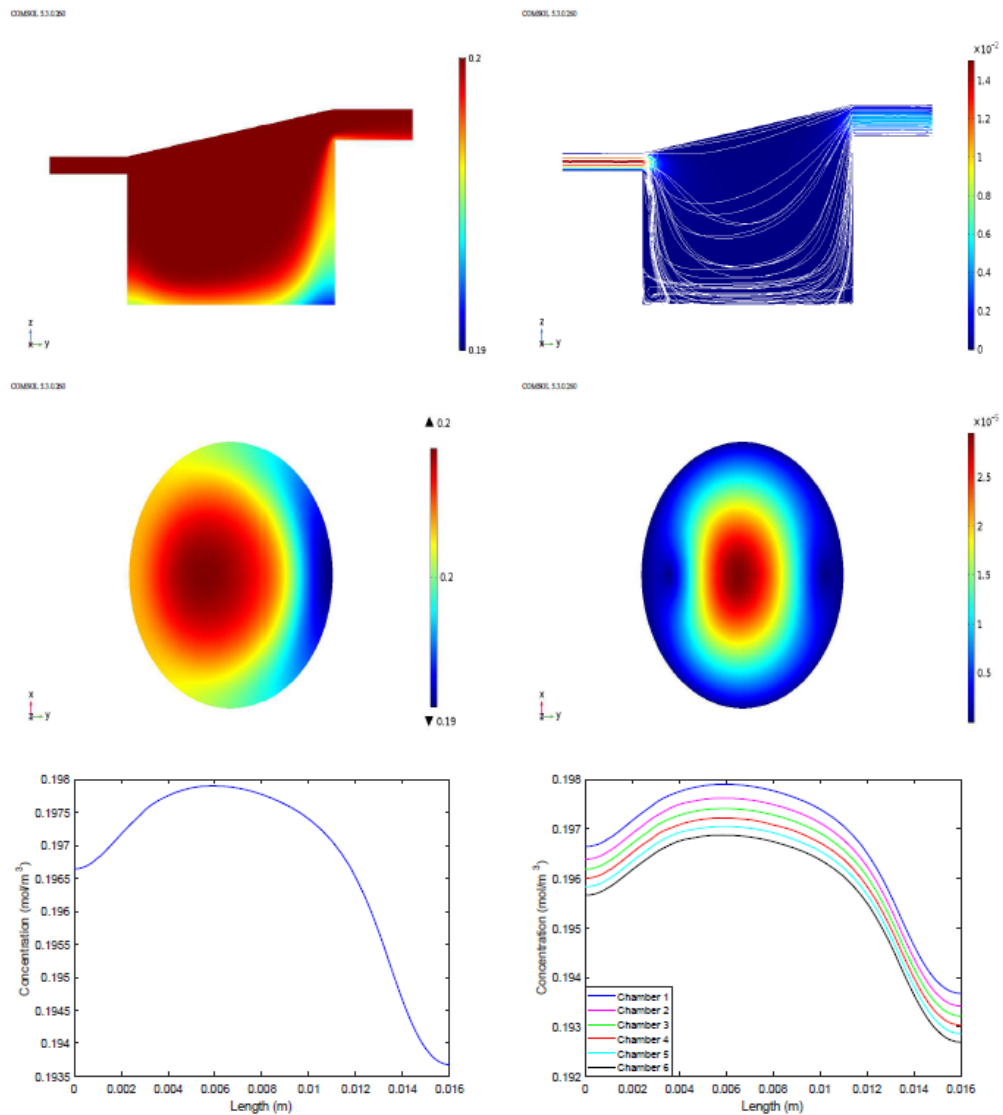
Figure 3.4-3. COMSOL results for cells on top of the 9mm insert and V_{max} = 1 x 10^{-3} mol/m^3/s. **Upper left**: Oxygen concentration in chamber 1. **Upper right**: Flow profile in chamber 1. **Middle left**: Cell surface oxygen concentration in chamber 1. **Middle right**: Magnitude of the cell surface shear stress in chamber 1. **Lower left**: Cell surface oxygen concentration profile in chamber 1. **Lower right**: Cell surface oxygen concentration profiles for all 6 chambers.

3.4.2.4 Modelling of Cells Maintained on Top of the 9mm Insert when the Maximum Rate of Oxygen Consumption (Vmax) = 1e^{-2} mol/m^3/s

Visual representations of the results of the modelling conducted are shown in figure 3.4-4. The maximum oxygen consumption rate set to 1 x 10^{-2} mol/m^3/s. The images show the same results as before. The pattern of results is identical; however, the values

produced by this simulation are different. The oxygen concentrations range from 0.1797 mol/m^3 at the centre of the chamber down to 0.1382 mol/m^3 at the far right hand side of the chamber. Values showing the oxygen concentrations for each of the six chambers connected in series are shown in the bottom right of figure 3.4-4. By the time the final chamber is measured, the maximum oxygen concentration has fallen to 0.1696 mol/m^3 and the minimum to 0.1285 mol/m^3.

The top right image of figure 3.4-4 shows the flow velocity of the media at the base of the well where the cells are is 1.46 x 10^{-7} m/s. The shear stress values range from 2.95 x 10^{-5} Pa down to 4.42 x 10^{-11} Pa. The flow velocity and shear stress values in each of the six chambers are identical to the values produced in the previous simulation.

Vmax = 1e-2 and cells on insert
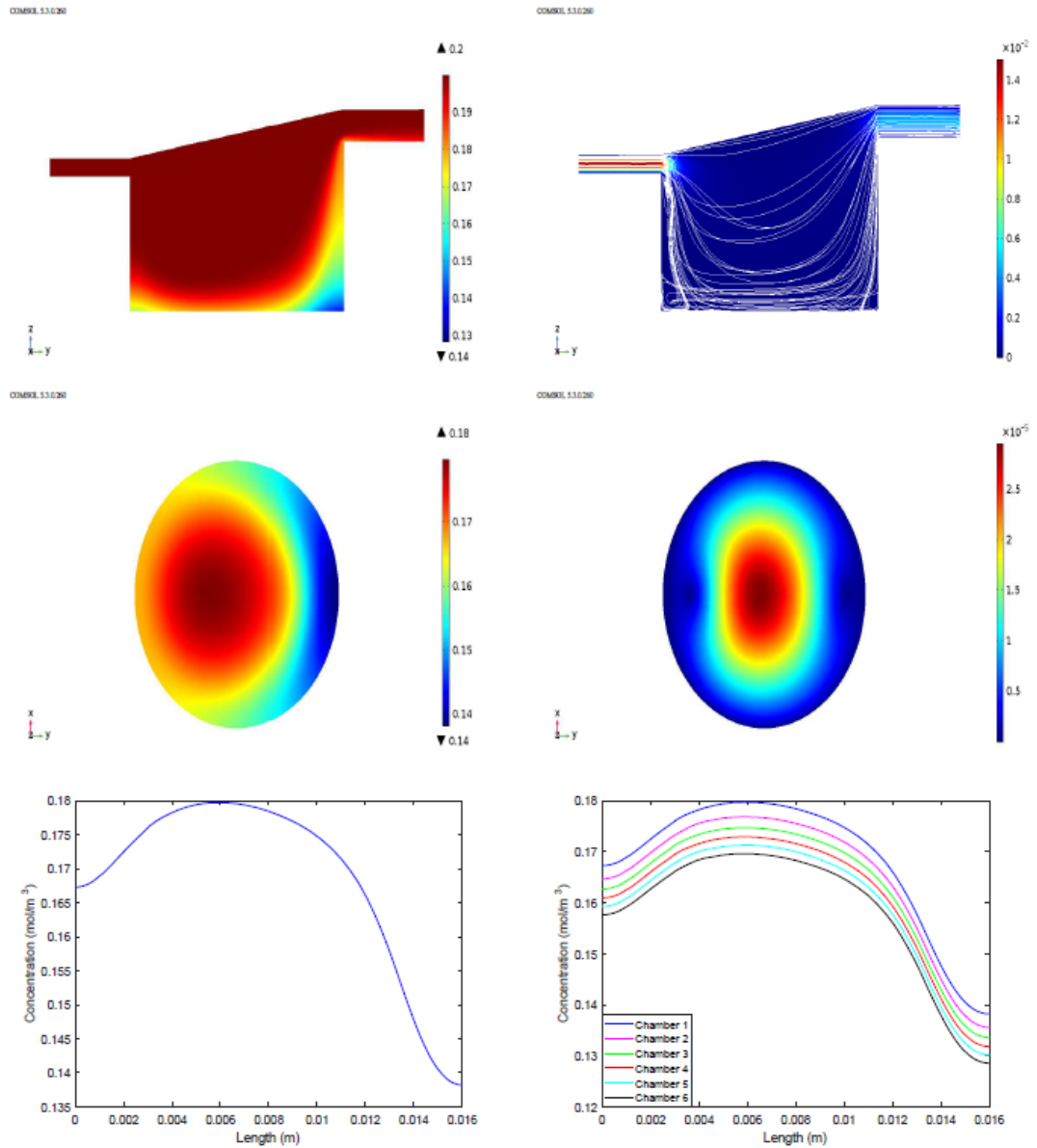
Figure 3.4-4. COMSOL results for cells on top of the 9mm insert and $V_{max} = 1 \times 10^{-3}$ mol/m^3/s. **Upper left**: Oxygen concentration in chamber 1. **Upper right**: Flow profile in chamber 1. **Middle left**: Cell surface oxygen concentration in chamber 1. **Middle right**: Magnitude of the cell surface shear stress in chamber 1. **Lower left**: Cell surface oxygen concentration profile in chamber 1. **Lower right**: Cell surface oxygen concentration profiles for all 6 chambers.

3.4.3 Comparisons between the Kirkstall Ltd QV500 and QV900 Media Perfusion Systems

A range of values are quoted in the literature for the speed of interstitial fluid flow in the skin under normal conditions. These values are between 0.1 and 2 μm/s[233-235], this is the range that the velocity of media in the system should aim to be within. As stated, the value selected for bulk media transfer based from the equations, in the papers that modelled the QV500 system, was 360 μL/min. According to the equations in the papers, this translates to a media velocity of 1 μm/s across the surface of the cell in the QV500 media perfusion system. This was chosen to be in the middle of the range using a pump set to setting three on the controls. It was assumed that the systems would have the same chamber size and depth. Therefore, a bulk media transfer rate of 360 μL/min was also chosen, as the bulk media transfer rate in the QV900 system. However, the results from the modelling of the QV900 show that the velocity of the media at the surface of the cells is actually 1.75±0.01 nm/s. This is 1000 times less than the media velocity that the system was expected to produce. This explains why the results of the earlier viability studies in the QV500 system could not be repeated in the QV900 system.

When comparing the QV500 system to the QV900 system with the depth correcting insert the maximum velocity of the media again does not match that of the original system. Using the same 360 μL/min bulk media transfer rate gives a media velocity across the surface of the cells of 0.15 μm/s. This value is about seven times less than what was expected. Despite this, the value for media velocity across the cell surface produced by the QV900 system with an insert included in each chamber still fits within the reported range of interstitial fluid flow rates within human skin.

3.4.4 Comparisons between the Kirkstall Ltd QV900 Media Perfusion System with or without an Insert

The results from the modelling analysis of the QV900 shows that when the cells are placed on the bottom of the chamber, the velocity of the media at the surface of the cells is 1.75±0.01 nm/s and the sheer stress is 36.4±0.2 nPa. When a 3D printed insert is included in the well, in order to reduce the depth back to matching the QV500 depth, the results from the modelling show the velocity of the media at the cell surface to be 146±1 nm/s, and the sheer stress is on average 3.76±0.02 μPa. The values from the system with the inserts included are about 100 times higher than without the insert. When the oxygen concentration values are compared, the values are very similar when the maximum oxygen consumption is set to 1 x 10^{-2} mol/m^3/s. Although, when the maximum oxygen consumption rate is set to 1 x 10^{-3} mol/m^3/s the oxygen concentration in the chambers with an insert is nearly twice as

high. In chambers without an insert, the maximum oxygen concentration is 0.1 mol/m^3 and the minimum is 0.07 mol/m^3. When comparing to the values of oxygen concentration in chambers with an insert, 0.1797 mol/m^3 at maximum and 0.1382 mol/m^3 as a minimum value, a difference is seen that is dependent on both chamber depth and maximum oxygen consumption rate.

3.4.5   Limitations of the Model

Whilst the modelling provides us with a calculated estimation of the system, it is only as good as the parameters used in its construction. All models require an iterative process of improvement to become closer to the *in vivo* situation. The parameters concerning the behaviour of the media is modelled using parameters from water, a change which is widely used in fluidic models. We have also set the maximum oxygen consumptions to the accepted value for HEPG2 cells, and then raised the value by one order of magnitude in order to assess the effect that an increased oxygen consumption may have on the model. The Michaelis-Menten constant, a constraint of a well-characterised kinetic model used in this case for measuring the rate of oxygen consumption, is set to a value accepted for many cell types. However, these are all estimates of the true values hence the data produced by the model is also an estimate of how the system functions with regards to oxygen consumption.

3.5 Development of a Colorimetric Assay to Measure the Influence of Drugs on the Infection of Cells by *Leishmania*

3.5.1   Introduction

Colorimetric assays are assays that use a colour change or colour development that can be detected either by absorbance or fluorescence. Advantages of a colorimetric screening method are a reduction in both time taken and cost. Results can be produced in a much shorter time allowing a much larger number of compounds to be tested in each experiment. They are also compatible with the development of *in vitro* 3D cell culture methods, where conventional microscopy is more difficult.

A trypanothione reductase (TryR) based assay was carried out as detailed in Van den Bogaart *et al* (2014)[165]. The assay is based on the fact that TryR is only found in kinetoplasts, such as *Leishmania,* and has a specific substrate allowing a measurement of substrate turnover to be directly relatable to number of parasites in a culture. Trypanothione reductase is an essential component of the unique kinetoplast thiol-redox metabolism, and was used to assess the viability of the *Leishmania* parasites by monitoring the colour change of 5,5-dithio- bis 2-

nitrobenzoic acid (DTNB) as it is reduced. This reaction combines the TryR-catalysed reduction of trypanothione disulphide ($T[S]_2$) with its *in situ* regeneration through DTNB, as shown in figure 3.5-1.
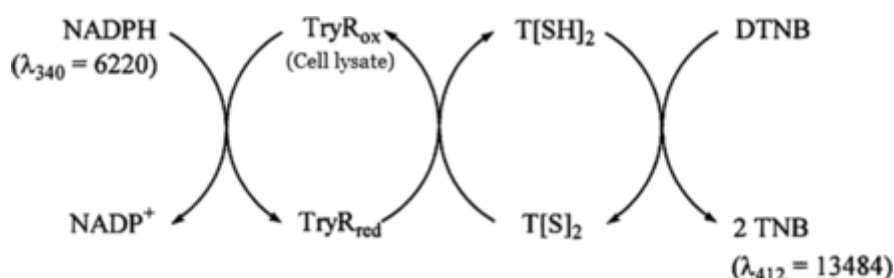
Figure 3.5-1. Schematic of the DTNB-coupled reaction[165].

The optical density of the blank, which consisted of all the reaction components except the DNTB, was subtracted from the corresponding sample signal, yielding the TryR activity, which correlated to the number of parasites present in each sample. As only the parasite contains TryR, the assay directly measures the number of parasites in the culture with no interference from the host cells.

3.5.2   Method Development for the Colorimetric Assay

Initially we were unable to reproduce the assay reported by van den Bogart *et al* (2014). Therefore, the assay was tested using different concentrations of promastigotes ($2 \times 10^5 - 1.2 \times 10^6$ per mL), different durations of incubation (1 hour to 48 hours) and different species of parasite. To start with, no signal was produced at any concentration of promastigote, after any duration of incubation with the reagents. Eventually a signal was detected using a high concentration of promastigotes (8×10^7), which was being used as a positive control and this enabled validation of the assay and the data recording sensitivity of the plate reader.

The first goal was to determine whether there was a correlation between parasite number and the colorimetric titre. Initial experiments yielded little data, as only very high concentrations of parasite ($1-8 \times 10^7$ cells) gave a signal. This meant our assay had a problem with sensitivity. The results from high concentrations of parasites allowed us to confirm the linearity of the signal over a concentration range of parasites and the use of a cell-only negative control.

A visit to the group who developed the assay gave a better understanding of the assay. The sensitivity problem had been caused by the degradation of the trypanothine reductase as the protease inhibitor; phenylmethanesulfonyl fluoride (PMSF) was insoluble in water and

therefore not available in solution. This was not mentioned in the paper and an alternative solvent, isopropanol was subsequently selected.

As the final step in the development of the assay, the results from the colorimetric assay were matched to the results from an identical experiment where percentage infection was determined by microscopic counting. An assay measuring the activity of amphotericin B on *L. major* infected THP1 cells was conducted, using both the colorimetric assay and the established counting assay; results were compared allowing validation of the colorimetric assay for the measurement of drug activity. There was a difference between the two methods, with the counting method consistently giving lower EC_{50} values. The difference between the results from the colorimetric assay and the counting was caused by the measurement of extracellular parasites during the colorimetric assay. To overcome this problem, the cells were incubated with media containing horse serum, which is known to remove the extracellular parasites as horse serum is less rich in nutrients and growth factors than fetal calf serum. Another difference between the detection methods is that the colorimetric method measures parasite burden i.e. total number of parasites. Whereas, the microscopic counting shows percentage infection i.e. number of cells that are infected. Burden could be counted, but in certain cells the quality of the dye, overlapping of parasites and cells make this difficult and time consuming.

3.5.3 Development Results for the Colorimetric Assay

3.5.3.1 Determination of the Correlation between Parasite Number and the Colorimetric Titre

L. major JISH 118 parasites at different concentrations ($1 \times 10^5 - 7 \times 10^5$ per mL) were lysed and tested for signal using the colorimetric assay. Correlation between parasite number and colorimetric result can be seen in figure 3.5-2. A linear increase was seen showing that the signal produced was directly proportional to the number of parasites within the sample.
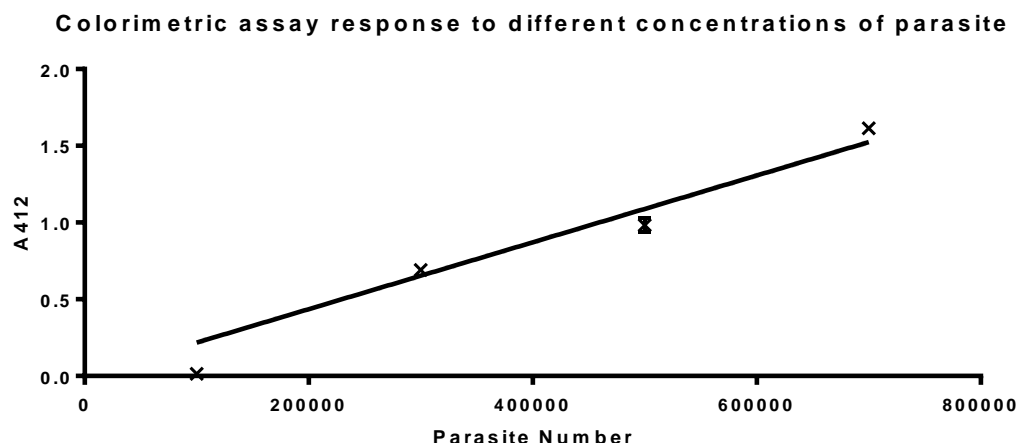
Figure 3.5-2. Graph showing a linear increase in signal with increasing concentration of parasite. Graph shows A412 reading after 6 hours of incubation. N =3 Error bars show SD, error bars are excluded if smaller then symbols.

3.5.3.2   Validation of the Colorimetric Assay against Microscopic Counting

To validate the use of the trypanothione reductase based assay for assessing viability of the intracellular *Leishmania* amastigote, the activity of the two reference drugs, figure 3.5-3, was measured against *L. major*. Light microscopy was used in comparison, as it is the conventional method to measure drug efficacies in *Leishmania* dose-response assays.

Table 3.5-1 EC$_{50}$ determined by Graphpad Prism

EC$_{50}$	Colorimetric assay 1	Colorimetric assay 2	Counting
amphotericin B (95% CI) (nM)	34.54 (28.74 to 41.51)	28.42 (23.21 to 34.79)	22.15 (21.29 to 23.04)
Miltefosine (95% CI) (μM)	8.49 (6.25 to 11.54)	8.56 (6.37 to 11.49)	2.98 (2.64 to 3.36)

EC$_{50}$ values seen, table 3.5-1, are similar to previously reported values in the literature[330]. A one-way repeated measure ANOVA shows that there were significant differences between the curves (figure 3.5-2) for the treatment of THP-1 cells with amphotericin B. Statistically significant differences were seen between both colorimetric assays and the counting method ($p < 0.01$).

EC$_{50}$ values for the activity of miltefosine, seen in table 3.5-1, given in this assay are lower than what is often reported in the literature[72 &331,] but does still fit with previously produced

values. Significant differences are seen between the results of the counting method and the colorimetric assay (p<0.0001, one-way repeated measure ANOVA).

 The results from the colorimetric assay show a lower reduction in the percentage infection than the counting analysis suggests. The reason for this was the resulting signal from extracellular parasites still attached to the cells. When microscopically counting these extracellular parasites are not counted. In the colorimetric assay, the extracellular parasites contribute to overall signal, which would make it appear higher than it should be and less of a reduction would be seen. To improve the assay extracellular promastigotes need to be removed, this can be done with horse serum treatment post drugging as part of the experiment[296].
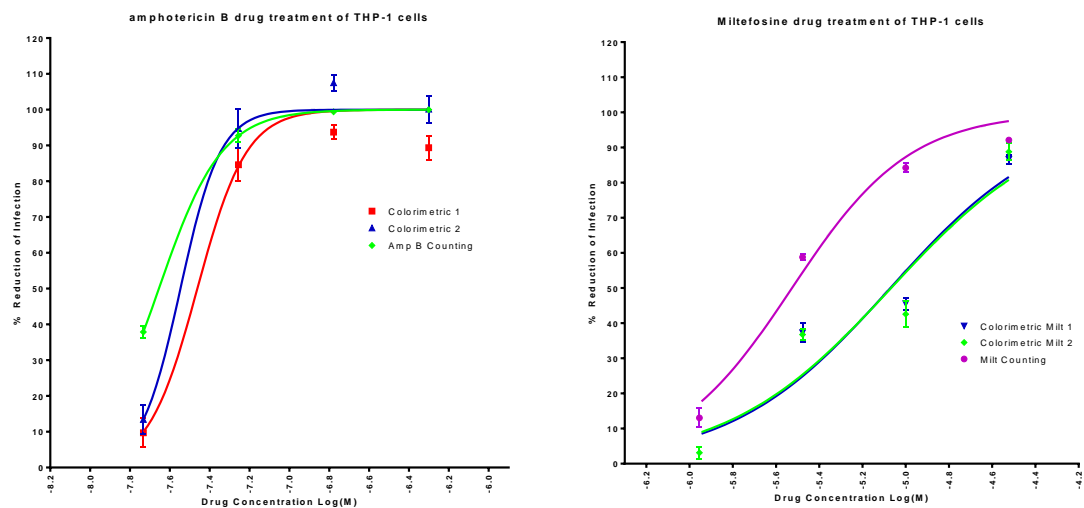
Figure 3.5-3. Dose-response curves showing the reduction in infection of THP-1 cells produced by treatment with amphotericin B (Left) or miltefosine (right). Curves were fitted by Prism with a variable slope and maximum and minimum set to 0 and 100%. The reduction in infection was measured either by the colorimetric assay or by microscopic counting and scaled to a reduction in total infection seen in the untreated control. N =3 Error bars show SD

3.5.4 Colorimetric Assay with Horse Serum Treatment to Remove Extracellular Promastigotes

The activity of the two reference drugs, figure 3.5-4, was measured against *L. major*; horse serum was used to reduce extracellular promastigotes. The process by which the horse serum reduces the number of extracellular promastigotes is not known, however, it is known that horse serum is less rich in nutrients and growth factors than fetal bovine serum, and this could contribute to the observed effect[296].

Table 3.5-2 *EC$_{50}$ by Graphpad Prism*

EC$_{50}$	Colorimetric	Counting
amphotericin B (95% CI) (nM)	29.93 (23.79 to 37.64)	23.44 (22.48 to 24.45)
Miltefosine (95% CI) (µM)	5.96 (4.33 to 8.20)	3.81 (3.48 to 4.17)

The EC$_{50}$ value for the activity of amphotericin B, seen in table 3.5-2 and figure 3.5-4, using the colorimetric assay closely matches the EC$_{50}$ value when the reduction in infection was measured by microscopic counting. These values are both similar to what is reported in the literature[330]. The EC$_{50}$ values produced after the addition of horse serum show a stronger similarity than in the previous experiment. EC$_{50}$ values of the counting method were not affected by the horse serum treatment. The horse serum treatment, however, does produce a difference in the colorimetric assay, giving a more comparable result to the counting method. A student t-test shows that there was still significant differences ($p < 0.01$), between the colorimetric assay and the counting method.

The EC$_{50}$ value for the activity of miltefosine, seen in figure 3.5-4 and table 3.5-2, are closer in value than in previous assays. The EC$_{50}$ values produced by this experiment are much closer to what is seen in the literature[72]. The horse serum treatment has reduced the signal generated by extracellular promastigotes and this has reduced the EC$_{50}$ value produced by the colorimetric assay, reducing the differences between the two assays. A two-way student t-test shows that there was still a significant difference ($p < 0.0001$), between the two methods of analysis, but to a much lower degree than in the previous experiments without a horse serum treatment post experiment. There may still some extracellular promastigotes detected by the colorimetric assay interfering with the results of the experiment.
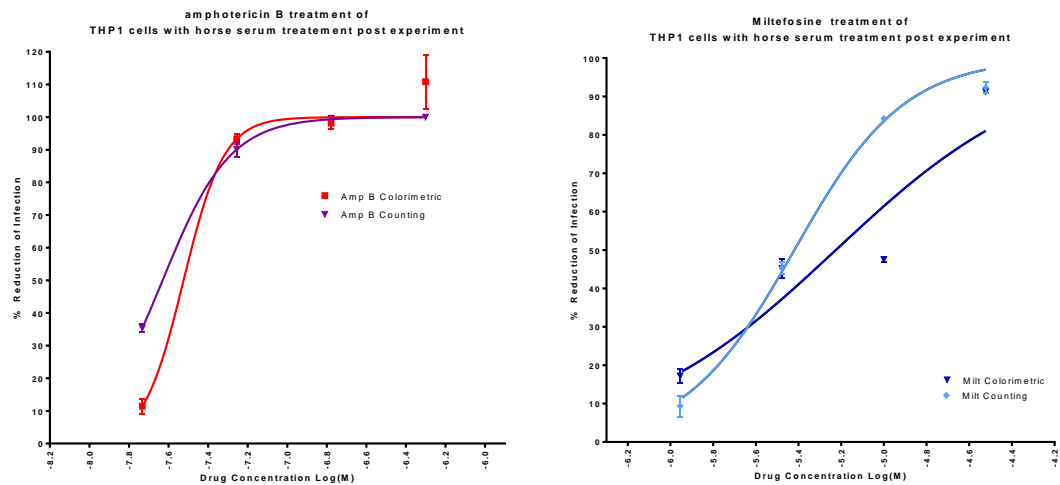
Figure 3.5-4. Dose response curves showing the reduction in *L. major* infection of THP-1 cells produced by treatment with amphotericin B or miltefosine. Curves were fitted by Prism with a variable slope and maximum and minimum set to 0 and 100%. The reduction in infection was measured either by the colorimetric assay or by microscopic counting and scaled to a reduction in total infection seen in the untreated control. N =3 Error bars show SD

To prove that the colorimetric assay would also work when mouse peritoneal macrophages were used instead of THP1 cells, an experiment to determine the efficacy of amphotericin B was conducted using peritoneal macrophages, shown in figure 3.5-5. An EC_{50} value of 29.6 nM (95% CI = 22.17 to 39.42 nM) was seen using the colorimetric assay without horse serum treatment and 74.1 nM (95% CI = 46.6 to 117.7 nM) with a horse serum treatment. The EC_{50} value when the reduction in infection was measured by microscopic counting was 55.2 nM (95% CI = 52.9 to 57.5 nM). The EC_{50} values produced by this experiment are similar to what is seen in the literature[72]. Significant differences are seen when comparing the counting method to both of the colorimetric assays, ($p<0.0001$).
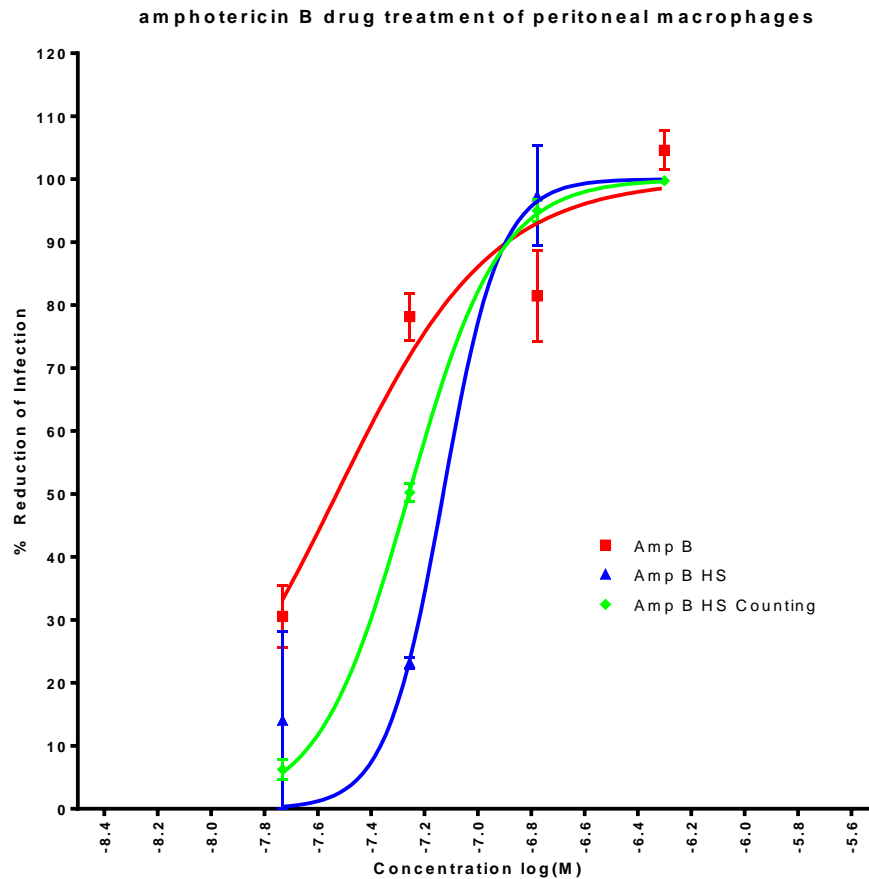
Figure 3.5-5. Dose-response curves showing the reduction of *L. major* infection of mouse peritoneal macrophages produced by treatment using amphotericin B. Curves were fitted by Prism with a variable slope and maximum and minimum set to 0 and 100%. The reduction in infection was measured either by the colorimetric assay or by microscopic counting and scaled to a reduction in total infection seen in the untreated control. N =3 Error bars show SD

Despite wash steps, it can be seen under the microscope that promastigotes are still present in the culture around the host cells. If the number of wash steps are increased then this could lead to the cells being damaged. The horse serum treatment has been shown to reduce the number of extracellular promastigotes[296] whilst having no effect on the host cells. When the horse serum was used, the signal produced by the colorimetric assay was more closely related to the values achieved by microscopic counting. The use of horse serum to remove extracellular parasites is both important to the assay and better than alternatives such as repeated wash steps.

3.5.5 Evaluation of the Colorimetric Assay for Determining Drug Efficacies

This colorimetric assay works, the signal produced by the assay was proportional to the number of parasites in the system. It has also been used to produce results in a drug efficacy determination assay, which can be matched to microscopic counting. This validated the assay for use with this specific strain of *L. major*. This assay is useful and reduces the time taken from the start of analysis to results.

The results produced in this section do both match and reinforce the data shown in the paper describing the use of this trypanothione reductase based assay[165]. Both have shown the relationship between the numbers of *Leishmania* parasites and the signal produced by the colorimetric assay. Both have also used the assay to assess drug efficacies and produced values that match microscopic counting methods and figures seen in literature [72&165].

However, the colorimetric assay is a continuous recording method that measures total parasite burden, whereas microscopic counting is a discrete method that measures the number of infected cells. Whilst these two measures should show the same trend, they will never perfectly line up due to the differences in what the assays measure.

3.5.6 Using the Colorimetric Assay for Screening of Compounds

This colorimetric assay was used to screen eleven unknown compounds from the pathogen box, produced by the Medicines for Malaria Venture. The pathogen box contains 400 diverse, drug-like molecules active against neglected diseases of interest and is available free of charge. The compounds had previously had their EC_{50} values determined by microscopic counting, table 3.5-3, and were used in order to measure the ability of the colorimetric assay to rank compounds in potency order and further validate its ability to produce results table 3.5-3, that match those produced using the conventional counting method.

Determination of the EC_{50} values for some compounds displaying weak anti-leishmanial activities and poorly fitted dose-response curves, were not always feasible, and hence were classified as >30 µM. The level of correlation and agreement between the trypanothione reductase based assay, and the microscopic assessments was analysed with a scatter plot and the Bland-Altman plot. The scatter plot showed a significantly high level of correlation between the results from the two assays giving an R squared value of 0.9492 and a p<0.0001 in a Spearman's rank correlation test. In the Bland-Altman plot (Figure 3.5-6), all points were scattered around a mean difference of 0.097, and all but one point fell within one standard

deviation of this mean. This mean difference was the average difference seen between the two methods of drug efficacy determination. If the values fall between one standard deviation then this is considered noise. The Bland-Altman plot allows assay bias to be taken into account and results can be scaled between assays to give more representative values. Overall, the correlation between the colorimetric assay and the counting method, considered the gold standard for *in vitro* assays, was strong. This validates its use in screening assays as a quicker and more efficient way to rank the strength of compounds against *Leishmania.* Doing the colorimetric assay first would allow compounds that were weak, or showed no anti-leishmanial activity, to be removed before time is wasted on the compounds used in other (more time-consuming) assays.

Table 3.5-3 *EC$_{50}$ values (95% confidence interval) for 11 compounds from the pathogen box and standard drug controls of amphotericin B and miltefosine. N =3*

L. major JISH 118		
	Trypanothione assay (µM)	**Microscopic assay (µM)**
Standard drugs		
amphotericin B	0.04 (0.02-0.08)	0.03 (0.03-0.04)
miltefosine	8.00 (3.25-20.90)	19.59 (17.45-21.99)
Pathogen box compounds		
MMV676158	>30	>30
MMV676057	7.25 (3.71-13.49)	13.02 (11.46-14.79)
MMV676005	>30	>30
MMV676001	2.95 (2.10-3.81)	9.00 (wide)
MMV676169	>30	>30
S2621	3.46 (1.70-5.70)	3.15 (wide)
MMV688263	23.65 (19.59-27.70)	>30
MMV688274	8.66 (6.51-12.07)	12.37 (9.88-15.49)
MMV688273	9.52 (4.45-14.22)	10.43 (wide)
MMV688283	7.13 (4.17-12.98)	8.51 (wide)
MMV688272	>30	>30
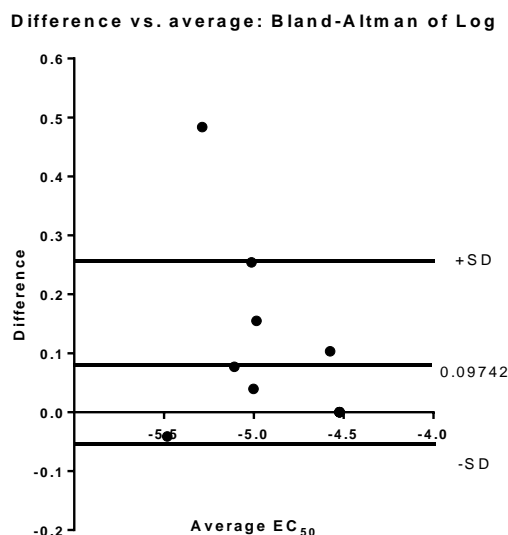
Figure 3.5-6. A Bland-Altman plot of the EC$_{50}$ values of 11 selected compounds of the pathogen box between the TryR-based assay and the microscopic assessments. The mean difference of the Bland-Altman plot was 0.097. The upper and lower limits of agreement (mean ± SD) are 0.25 and -0.06, respectively.

3.6 Evaluation of Infection

3.6.1 Rationale

The first step in exploring how the media perfusion system affects the treatment of a *Leishmania* infection was to establish an infection within the system. To demonstrate the direct effect of flow on the process of infection with *L. major* parasites, a variety of flow rates have been studied. Initial conditions have been varied to try to establish a high infection that will reflect and match the infection seen in the static system. It is important that the overall levels of infection match, as they will need to be the same to avoid dose inoculum effects when testing drug efficacy.

3.6.2 Evaluation of Infection in a Static System

3.6.2.1 Evaluation of *L. major* Infection of THP1 Cells

Increasing the initial ratio of parasite to host cell increases the percentage infection after 72 hours of co-incubation, shown in figure 3.6-1. At the lowest ratio of parasites to THP1 cells, the 1:1 infection ratio, the infection after 72 hours is, on average, 37%. The overall percentage infection using initial infection ratios from 6:1 up to 15:1 are all very similar and have essentially reached the maximum infection possible. The ideal percentage infection is between 80-90% hence the best infection ratio for THP-1 cells is a 4:1 ratio of parasites to THP-1 cells.

A one-way ANOVA showed a significant difference between ratio 1:1 and all other results, $p<0.0001$. There are also significant differences between ratio 3:1 and 4:1, $p<0.05$ and all other data sets $p<0.0001$. The data set from infection using an initial ratio of 4:1 shows a significant difference from 6:1, $p<0.01$, 10:1 and 12:1, $p<0.001$ and 15:1, $p<0.05$. The other data sets show no significant differences.

Figure 3.6-1. Box and whisker diagram showing the percentage of THP-1 cells infected after 72 hours co-incubation with different ratios of *L. major* promastigotes. N =9

3.6.2.2 Evaluation of *L. major* Infection in Mouse Peritoneal Macrophages

The trend of an increase in initial infection ratio giving an increase in percentage infection after 72 hours was also found for mouse peritoneal macrophages (table 3.6-1). When the initial infection ratio was 1:1 the average percentage infection was 86%, which is the optimum level of infection and therefore 1:1 is the optimum infection ratio. When the data was analysed, using a one-way ANOVA, all ratios are significantly different from each other, $p<0.0001$, apart from ratio 3:1 when compared to ratio 6:1.

Table 3.6-1 *Percentage infection of mouse peritoneal macrophage when exposed to L. major promastigotes at different ratios. N =9*

	0.5:1 Static	1:1 Static	3:1 Static	6:1 Static
Minimum	53.00	82.00	100.00	100.00
Maximum	67.00	86.00	100.00	100.00
Mean	58.50	84.17	100.00	100.00
Std. Deviation	5.96	1.47	0.00	0.00

3.6.3 Evaluation of *L. major* Infection in THP1 Cells in the QV900 Media Perfusion System using a Media Flow Rate of 50 µl/min

THP-1 cells were infected with different ratios of a mixed population of stationary phase *L. major* promastigotes then maintained in static culture for 24 hours. This was to allow the establishment of infection. Subsequently, the QV900 media perfusion system was set to a bulk media transfer rate of 50µL/min, which was the minimum reproducible rate of bulk media transfer possible using the peristaltic pumps available at this time.

Once again, increasing the initial ratio of parasite to host cell increases the percentage infection after 72 hours in both the static, conducted in parallel to test the influence of flow, and the media perfusion system, shown in figure 3.6-2. Although, the percentage infection increases as the initial infection ratio increases, the percentage infection seen in the cells maintained under media perfusions conditions was consistently lower. At a 1:1 infection ratio, the infection after 72 hours was on average 37% in the static system; however, it was only 16% in the media perfusion system. This pattern of a higher infection in the static system compared to the media perfusion system continues with each different initial ratio used. At a 3:1 infection ratio, the infection after 72 hours was on average 74% in the static system whereas; it was only 29% in the media perfusion system. Similarly, at a 4:1 infection ratio, the infection after 72 hours was on average 83% in the static system; however, it was 32% in the media perfusion system. The overall percentage infection using initial infection ratios of 6:1 up to 15:1 are all very similar, around 100% infection for the static system, having essentially reached the maximum infection possible. However, the media perfusion system, even at the highest initial infection ratio of 15:1, only reaches an infection percentage of 81%

after 72 hours of incubation. A ratio of 15:1, in the media perfusion system, the percentage infection in the media perfusion system was still rather lower than optimum.

When comparing the same initial infection ratio between the two conditions of static or media perfusion, significant differences, $p<0.0001$, are seen in a one-way ANOVA. An interesting example where there was no significant difference was seen between 1:1 ratio in the static system and the 3:1, 4:1 and 6:1 infection ratios under media perfusion conditions. This shows that the percentage infection after 72 hours when using a 1:1 infection ratio in the static system was equivalent to the percentage infection seen when infecting with an initial ratio of either 3:1, 4:1 or 6:1 in the media perfusion system. Similarly, a 3:1 ratio of infection in the static system was not significantly different from 10:1, 12:1 and 15:1 infection ratios under media perfusion conditions.
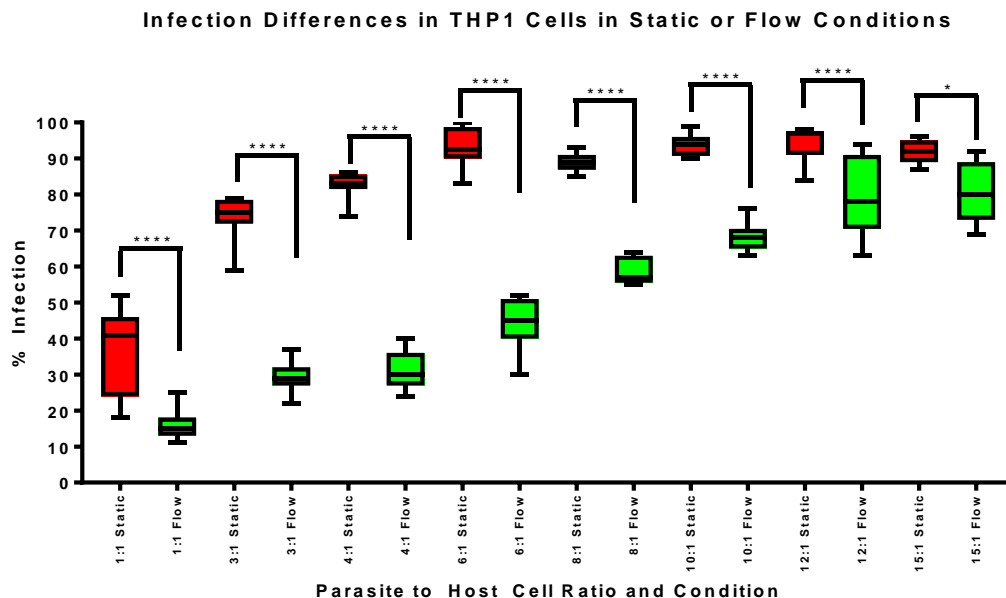
Figure 3.6-2. Percentage of THP-1 cells infected after 72 hours co-incubation with different ratios of *L. major* promastigotes in static or flow conditions. * = p<0.05 **** = p<0.0001 Error bars = maximum and minimum values N =9

3.6.4 Evaluation of *L. major* Infection in THP1 Cells in the QV900 Media Perfusion System under a Flow Rate of 1000 μl/min

The results of the previous experiment showed that media perfusion decreased the overall percentage infection after 72 hours. In this set of experiments using a higher rate of bulk media transfer (1000 vs 50 μL/min), higher initial infection ratios were used. Once again, the percentage infection seen in the cells, which have been maintained in the media perfusion

system, was consistently lower than the infection seen in the static system, using the same initial infection ratios, as seen in figure 3.6-3. At an 8:1 infection ratio, the infection after 72 hours was on average 89% in the static system; however, it was only 30% in the media perfusion system. This pattern of a higher infection in the static system compared to the media perfusion system continues with each different initial ratio used. At a 10:1 infection ratio, the infection after 72 hours was on average 94% in the static system whereas; it was only 44% in the media perfusion system. Similarly, at a 12:1 infection ratio, the infection after 72 hours was on average 94% in the static system; however, it was 70% in the media perfusion system. At 15:1 in the static system 92% after 72 hours of incubation compared to the media perfusion system where the overall average infection was 77%. All matching ratio data sets are significantly different from each other when static and flow are compared, using a one-way ANOVA, p<0.0001.
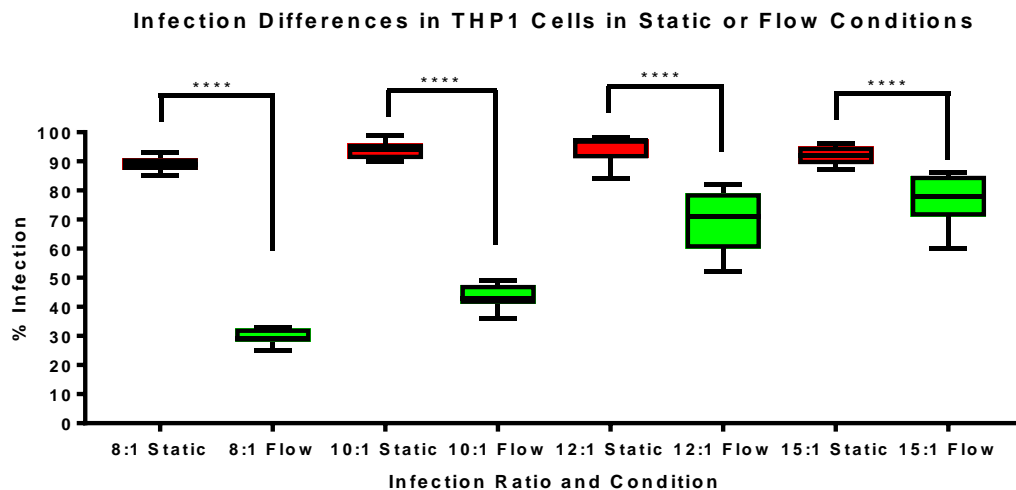
Figure 3.6-3. Box and whisker diagram showing the percentage of THP-1 cells infected after 72 hours co-incubation with different ratios of *L. major* promastigotes either in static or flow conditions. **** = p<0.0001 Error bars = maximum and minimum values N =9

3.6.5   Evaluation of *L. major* Infection of THP1 Cells with *Leishmania* Parasites in the Perfusion Media

The QV900 media perfusion system was set to a bulk media transfer rate of 50 µL/min. Increasing the initial ratio of parasite to host cell increases the percentage infection after 72 hours in both the static and the media perfusion system, shown in figure 3.6-4. However, the cells maintained for 72 hours in the QV900 media perfusion system with parasites in the media have achieved a higher percentage infection when compared to the static system. The percentage infection of the cells maintained in the static system was on average 23%. When

compared to the 55% infection seen in the cells maintained under the media perfusion system, it was clear that there was a much higher overall percentage infection after 72 hours in the media perfusion system. This result was repeated using an initial infection ratio of 3:1, when the static system shows 49% infection compared to the media perfusions systems 84%. All matching ratio data sets are significantly different from each other when static and flow are compared, using a one-way ANOVA, $p < 0.0001$.

Infection differences between static and media perfusion systems when the parasites are in the perfusion medium
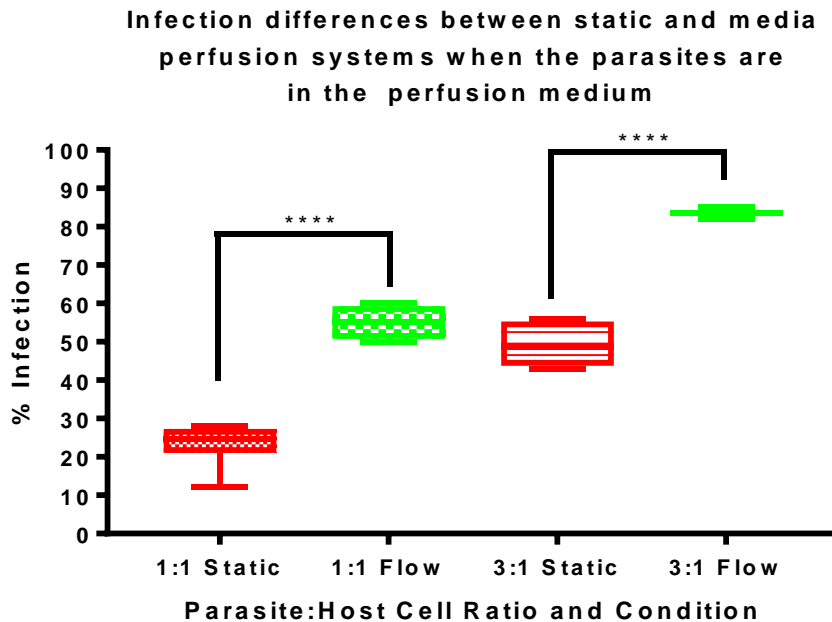
Figure 3.6-4. Box and whisker diagram showing the percentage of THP-1 cells infected after 72 hours co-incubation with different ratios of *L. major* promastigotes either in static or flow conditions. **** = $p < 0.0001$ Error bars = maximum and minimum values N = 9

In the experiment where parasites are in the circulating media, the infection percentage after 72 hours was higher in the media perfusion system than in the static system, seen in figure 3.6-4. In this model, the circulating media has a constant ratio of parasites per mL: number of host cells per mL in the initial plating media. This method leads to a good infection rate in the media perfusion system, however, there would be a vast difference between total number of parasites used between flow and static systems. What appears to happen is the parasites are carried in the perfusion media, pushed into the wells and then, as flow velocity reduces a number of parasites remain at the bottom of the well, trapped in recirculation zones. This causes a local increase of parasite number in the bottom of the wells and increases the effective parasite to host cell ratio. This could be why the infection in flow conditions were much higher than in the static conditions. However, using this method

meant that there was many extracellular promastigotes in the media. Drug used to treat infected cells in this system will also have an effect on the extracellular promastigotes. Another problem would be with so many promastigotes around the cells, the possibility for re-infection would be high. For this reason, it was concluded that, this model of the system using promastigotes in the perfusion media would not be the model that would be used in future experiments.

3.6.6 Evaluation of *L. major* Infection with and without 3D Printed Inserts Included in the QV900 Media Perfusion System

3.6.6.1 Evaluation of *L. major* Infection in THP1 Cells with and without 3D Printed Inserts Included in the QV900 Media Perfusion System

The QV900 media perfusion system was set to a bulk media transfer rate of 50µL/min. Depth reducing inserts were included in the QV900 system's chambers to increase the flow velocity by reducing the depth, providing additional conditions for the experiment. Previous observations can be seen again in figure 3.6-5; showing increasing the initial ratio of parasite to host cell increases the percentage infection after 72 hours and that the application of flow reduces the overall percentage infection after 72 hours. In addition to this, the inclusion of a depth-reducing insert further reduces the overall percentage infection seen in the cells after 72 hours. At a 15:1 infection ratio, the infection after 72 hours was on average 100% in the static system, 81% in the media perfusion system without insert and 67% in the media perfusion system when an insert was included. This pattern of a higher infection in the static system compared to the media perfusion system was seen again at a 25:1 infection ratio. Here the infection after 72 hours was on average 100% in the static system; 86% in the media perfusion system and 75% when the chamber contains an insert. The optimal percentage infection is between 80-90% hence the best infection ratio for THP-1 cells in the media perfusion system is an initial infection of a 25:1 parasite to host cell ratio, with no insert and a bulk transfer speed of 50µL/min. The optimum percentage infection, using an insert and a bulk media transfer rate of 50µL/min, was not achieved in the range of infection ratios tested.

All matching ratio data sets are significantly different from each other when static and flow, with or without an insert, are compared, using a one-way ANOVA. Achieving the required percentage infection level after 72 hours, under media perfusion conditions with an insert, would involve a higher parasite to host cell ratio, which would not be representative of the situation in the body[360].
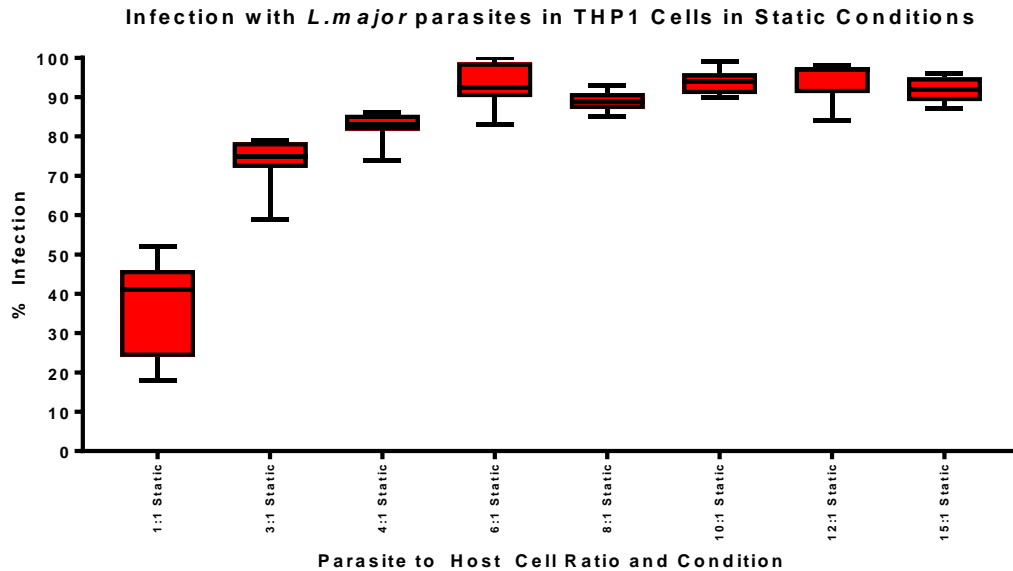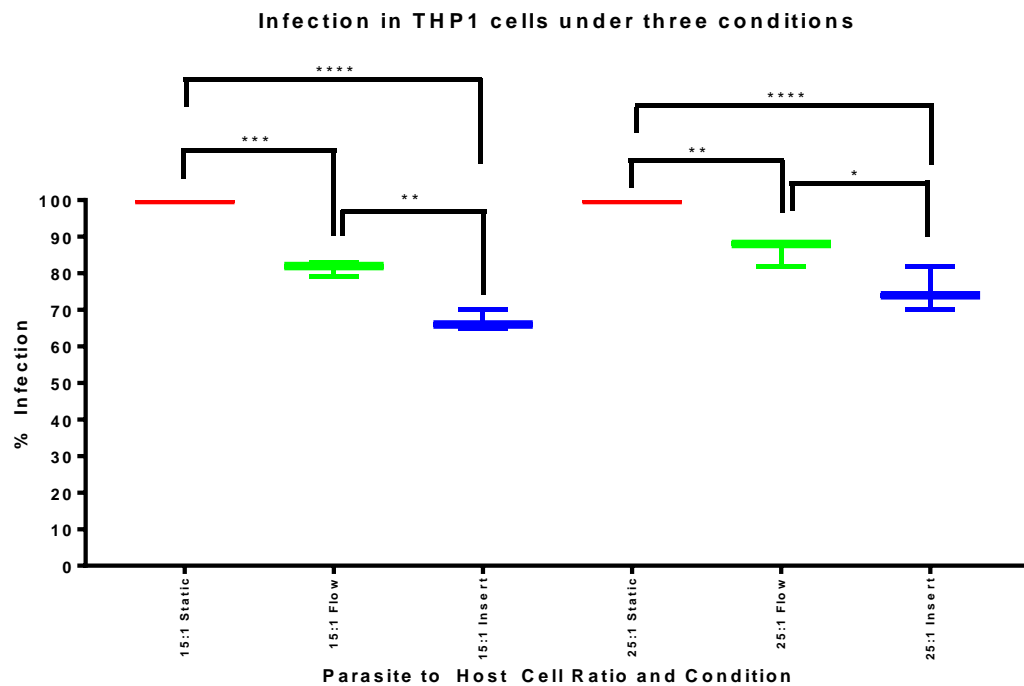
Figure 3.6-5. Percentage of THP-1 cells infected after 72 hours co-incubation with different ratios of *L. major* promastigotes either in static or flow conditions, with or without an insert. * = p<0.05 ** = p<0.01 *** = p<0.01 **** = p<0.0001 Error bars = maximum and minimum values N =9

3.6.6.2 Evaluation of *L. major* Infection in Mouse Peritoneal Macrophages with and without 3D Printed Inserts Included in the QV900 Media Perfusion System

Mouse peritoneal macrophages were chosen, to test if suitable overall percentage infection after 72 hours can be reached. The QV900 media perfusion system was kept at a bulk media transfer rate of 360 µL/min. As before, depth reducing inserts were placed in the QV900 system's chambers to increase the flow velocity and provide additional conditions for the experiment. Peritoneal macrophages show the exact same trend as the THP-1 cells but with lower initial infection ratios, figure 3.6-6. At a 0.5:1 infection ratio, the infection after 72 hours was on average 59% in the static system, 40% in the media perfusion system without insert and 24% in the media perfusion system with an insert. At a 1:1 infection ratio the infection after 72 hours was on average 85% in the static system; 62% in the media perfusion system and 55% in the presence of an insert. As the static system nears maximum infection, the differences between the three conditions grow smaller. At a 3:1 infection ratio, the infection after 72 hours was on average 100% in the static system, 93% in the media

perfusion system without insert and 83% in the media perfusion system with an insert. When a 6:1 infection ratio was used all three conditions show similar infection percentages. The optimal initial infection ratio for mouse peritoneal macrophages in the media perfusion system was a 3:1 parasite to host cell ratio.

Comparing the data, using a one-way ANOVA, all matching data sets showed significant differences from each other except the data sets from the 6:1 ratio comparisons.
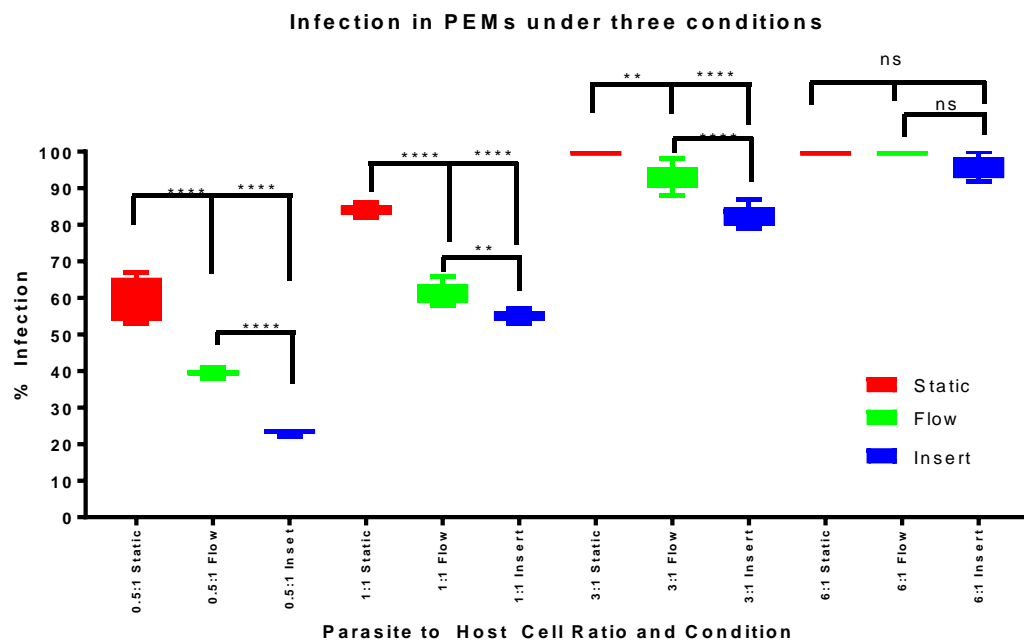
Figure 3.6-6. Box and whisker diagram showing the percentage of mouse peritoneal macrophages infected after 72 hours co-incubation with different ratios of *L. major* promastigotes either in static or flow conditions, with or without an insert. **** = p<0.0001 ** = p<0.01 Error bars = maximum and minimum values N =9.

3.6.7   Comparison of *L. major* Infection in THP1 Cells at Different Media Perfusion Velocities

A comparison of *L. major* infections in THP1 cells at an initial infection ratio of 15:1 across all the different conditions, except experiments where parasites were included in the media for the 72-hour incubation, is seen in figure 3.6-7. The higher the velocity of the media across the surface of the cells the lower the percentage infection. The percentage infection in the static condition was on average 93%. When a bulk flow of 50 µL/min was applied, the percentage infection was on average 81%. The mean percentage infection of the cells under higher bulk transfer rates, 360 µL/min and 1000µL/min are similar to the percentage infection when the bulk transfer rate was 50 µL/min. When the flow velocity across the cell

surface was increased by presence of an insert the average level of infection falls to 67%. When comparing the two conditions that are under the same volume of bulk flow, 360μL/min, but with or without an insert the average infection drops from 81% down to 67%. This shows the increased velocity of media across the surface of the cells must cause this reduction of infection.

When the data was compared, using a one-way ANOVA, all data sets show significant differences from the static condition. In addition to this the percentage infection levels are significantly different between the conditions of a bulk media transfer of 50μL/min and 360μl/min when using an insert, $p < 0.05$.
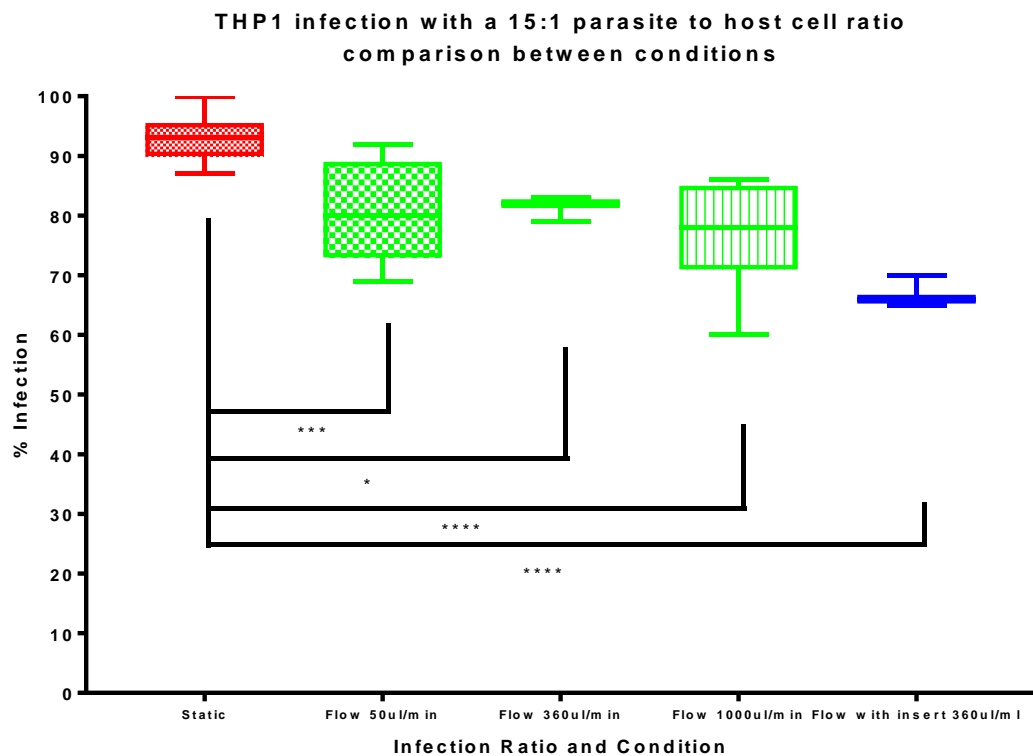
Figure 3.6-7. Box and whisker diagram showing a comparison of the percentage infection of THP-1 cells after 72 hours infected with an initial 15:1 infection ratio with *L. major* promastigotes either in all conditions tested using either a static system or a media perfusion system. * = $p < 0.05$ *** = $p < 0.001$ **** = $p < 0.0001$ Error bars = maximum and minimum values N =9

3.6.8 Discussion

It is important to produce a high infection of between 80-90% in each condition in order to have a large population of infected macrophages available for treatment with compounds in efficacy experiments. If a system has too many external parasites, often found when using a

high infection ratio, then re-infection by promastigotes may bias the data. If a system has too few parasites then there will not be a large enough population of infected cells in order for drugs to have a measurable effect on. It is important to produce similar levels of infection between the two systems, to avoid dose inoculum effects, which is where a difference in infection levels and amastigote number could alter the EC_{50} and EC_{90} values in a drug assay. A drug that is able to reduce the percentage infection level from 100% down to 50% may appear the same as a different drug that has reduced the percentage infection from 50% down to 25%, as they both have halved the percentage of infected host cells. However, the first 50% reduction will have cleared a different parasite load whilst appearing the same in terms of overall reduction in percentage infection.

It is clear from the experiments that for future assays the initial infection ratios used in the static and flow systems will need to be different, in order to provide the same level of percentage infection after 72 hours. The model that uses a 24-hour pre-incubation of the cells with parasites, before transfer to the media perfusion system, matches the schematic of the static experiment; both have a 24-hour pre-incubation before the addition of drug. This means that the cells, treated with the same infection ratio, have similar percentage infection levels after 24-hours, before they are transferred to the media perfusion system. Therefore, the difference between the two systems must be either due to a difference in parasite division within the host cell or a difference in invasion of host cell by any parasites remaining in the culture after the transfer to the media perfusion system or to a new well in the static culture.

The data shows the progression of the infection was hindered by the application of flow, and that the faster the media velocity across the surface of the cells, the lower the percentage infection resulting from the same initial infection ratio. This could possibly be because the movement of the flow would limit the chances of successful parasite phagocytosis by the host cell, by causing the parasites to be rapidly moving and keeping them away from the cell surface[293 & 294]. A reduction in the time the parasites spend in contact with the cells could stop successful phagocytosis.

Another reason could be that the cells are more viable in the media perfusion systems and hence are more quickly able to adapt and resist infection or able to naturally kill the parasite. Media perfusion systems have been used to show up-regulation or maintenance of gene regulation in HEPG2 cells[295]. If this was similar in macrophages then there is potential for the cells to either be primed by the media perfusion having a much faster response when the parasites are detected.

A further possibility is that the parasites struggle to survive in the dynamic flow conditions. The parasites that have remained on the glass slide during the transfer to the media perfusion system could be wasting energy swimming against the flow of the media, to reach the cells. If the parasites have less energy, they could be less able to divide.

Another conclusion from this set of experiments was that the choice of cell used in experiments needs consideration. Data shows that the mouse peritoneal macrophages are more easily infected, and lower initial ratios of parasite to host cell can be used when compared to the THP1 cells. An infection ratio of 1:1 using THP1 cells gives an average of 36.67% infection compared to an infection rate of 84.67% when using peritoneal macrophages. For this reason, it was decided that in future experiments peritoneal macrophages would be the cell used.

3.7 Investigation of *L. major* Amastigote Division in the QV900 Media Perfusion System

3.7.1 Rationale

The reduced percentage infection seen in the media perfusion system could be related to the rate of parasite division within the system. To determine whether this was the case, a 5-ethynyl-2´-deoxyuridine (Edu) incorporation assay was conducted. The principle of the Edu assay is that only cells that are actively dividing will incorporate the Edu, a nucleoside analog of thymidine. The Edu contains an alkyne that an Alexa Fluor® dye will bind to for fluorescent detection. If the parasites are dividing slower in the media perfusion system then there will be a lower percentage of Edu incorporation amongst the amastigote population.

3.7.2 Incorporation of Edu in *L. major* Amastigotes in the QV900 Media Perfusion System

The percentage of *L. major* amastigotes in mouse peritoneal macrophages, incorporating Edu was much lower in the QV900 media perfusion system, figure 3.7-1. On average the percentage of amastigotes that have incorporated Edu into their DNA, and hence are dividing parasites, was 26%. When the infected cells are maintained at the bottom of the QV900 chamber, they are under a media velocity rate of 1.74 nm/sec. The average percentage incorporating Edu into their DNA, at this flow velocity was 12%. This was less than half of the percentage that are dividing in the static system. When the infected cells are maintained on top of an insert in the QV900 chamber, they are under a media velocity rate of 0.15 µm/sec. The average percentage incorporating Edu into their DNA, at this flow velocity was 11%. Comparing the data using a one-way ANOVA shows there to be significant differences between the static system and the two flow velocities in the QV900 media perfusion system,

p<0.05. The average burden of the mouse peritoneal macrophages was the same across all three conditions, figure 3.7-1, only the number of dividing parasites changes. The reduction of Edu incorporation shows that there are less dividing parasites in the media perfusion system compared to the static system, this could lead to the differences in percentage infection seen.
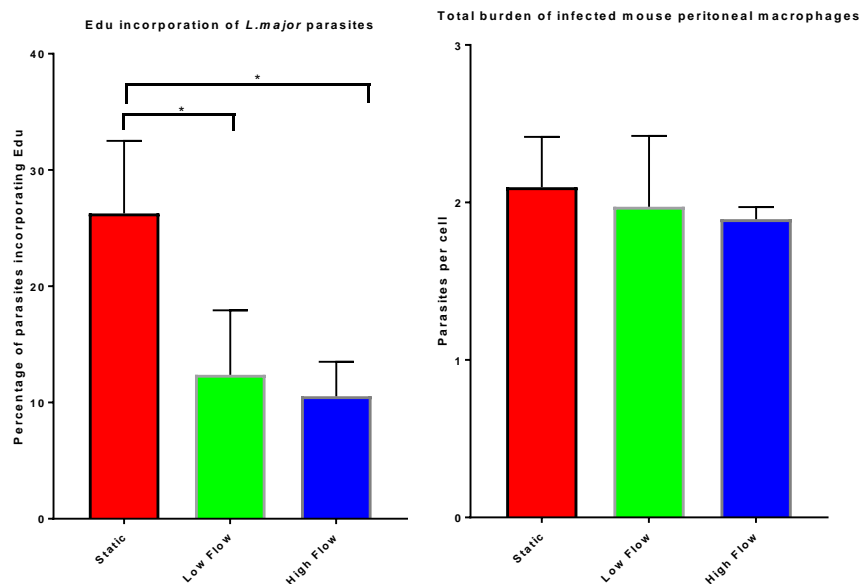
Figure 3.7-1. Bar graph showing the percentage of *L. major* amastigotes that have incorporated the Edu marker into their DNA (Left), across three different conditions. A bar graph showing the parasite burden of mouse peritoneal macrophages, across three conditions. * = p<0.05 Error bars show SD N =3

3.7.3   Incorporation of Edu into Mouse Peritoneal Macrophages in the QV900 Media Perfusion System

Interestingly, another difference was seen when the Edu assay was conducted. The mouse peritoneal macrophages should not incorporate any Edu into their DNA, as they should be fully differentiated non-dividing cells. In the course of this thesis, it has been observed that cells maintained in the media perfusion system are more differentiated than the same cells maintained in a static system. Previously only visual observations had been made, but the Edu assay provided a quantifiable result. The percentage of cells that incorporated Edu was higher in the cells maintained under static conditions, figure 3.7-2. On average the percentage of mouse peritoneal macrophages that have incorporated Edu into their DNA, and hence are dividing, was 7%. When the infected cells are maintained at the bottom of the QV900. The average percentage of cells incorporating Edu into their DNA, at this flow velocity was 0.7%. When the infected cells are maintained on top of an insert in the QV900 chamber.

The average percentage incorporating Edu into their DNA was 1%. The results from this experiment show, that the mouse peritoneal macrophages maintained under media perfusion conditions are incorporating less Edu, and as a whole population are more differentiated than the same cells maintained in a static system.
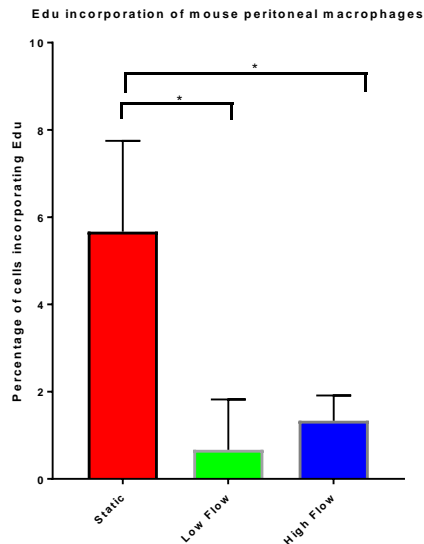
Figure 3.7-2. Bar graph showing the percentage of mouse peritoneal macrophages that have incorporated the Edu marker into their DNA (Left), across three different conditions. * = $p < 0.05$ Error bars = SD N = 3

3.8 Conclusion

The application of media perfusion to a static *in vitro* system has been shown to increase cell viability, longevity and metabolism in the literature[288&289]. In this section it has been shown that media perfusion in the Kirkstall QV500 system increases the cell viability, using a measure of mitochondrial metabolism as cell health. Whilst this may also be the case in the QV900 system the differences in flow velocity and time constrains caused by the contamination of the QV500 system have meant that this has not been measured with the QV900 system.

The modelling of the QV900 system allowed for the direct comparison of the QV500 and QV900 media perfusion systems. It allowed for the calculation of the exact flow velocities and shear stress effect that the cells are under, whether they are either at the bottom of the well or raised on top of a 3D printed insert. The modelling shows that the chosen flow rate of 360μL/min is equal to a flow velocity of 0.14 μm/s when the cells are on top of the insert, which fits within the range of interstitial fluid flow rates within the skin, which was between 2 and 0.1 μm/s.

Experiments on the initiation and progression of an infection with *Leishmania* parasites have shown that media perfusion inhibits the progression of the infection. Overall infection rates after 72 hours are significantly lower in the media perfusion system than in the static system. The results show the higher the flow velocity the lower the infection caused, using the same initial infection ratio. An Edu incorporation assay demonstrated that fewer parasites are actively dividing under media perfusion conditions.

Chapter 4 Evaluation of Anti-leishmanial Activity in a Media Perfusion System

4.1 Introduction

In this second results chapter, the media perfusion model developed in the previous section was used for the evaluation of anti-leishmanial drugs. Methods developed in the previous section were used to elucidate the anti-leishmanial activity of standard drugs and to show any differences between the media perfusion model and the standard static assays.

The objectives were to:

I.   To use the infected macrophage model to determine the activity of standard drugs in the flow system in comparison to the currently used static system.

II.   To understand potential differences found in the activities of the standard drugs through drug accumulation studies.

III. Finally, to understand potential differences found in the activities of the standard drugs by measuring the cell's activation status.

4.2 Evaluation of Anti-leishmanial Activity using the Colorimetric Assay in the Kirkstall QV900 Media Perfusion system

The anti-leishmanial drug activity of two standard drugs, amphotericin B and miltefosine was assessed in infected THP1 cells, under flow conditions using the QV900 media perfusion system. QV900 media perfusion system was set to a bulk media transfer rate of 360 µL/min, giving a media velocity rate of 1.75 ± 0.01 nm/s at the cell surface in this system. Static controls were used as a comparison to measure any difference from the standard procedure.

Dose-response curves for amphotericin B and miltefosine, figure 4.2-1, were produced in both a static and media perfusion system and measured by two different methods. EC_{50} and EC_{90} values for amphotericin B, table 4.2-1, and miltefosine, table 4.2-2, were calculated using Graphpad Prism. A repeated measure one-way ANOVA showed no significant differences between any of the conditions, when the culture was dosed with amphotericin B. Using a two-way ANOVA, significant differences were detected at the middle concentration, between the two methods of counting and colorimetric when cells dosed with amphotericin B, and maintained under flow, where media velocity was 1.75 nm/sec, $p < 0.01$. Significant differences are seen between the static and flow results measured by the colorimetric assay at the lowest concentration, $p < 0.05$.

A one-way repeated measure ANOVA shows no significant difference between any of the conditions, when the culture was dosed with miltefosine. A two-way ANOVA showed no significant differences between the static and media perfusion system.

Table 4.2-1 *Table of EC_{50} and EC_{90} values of amphotericin B treatment against L. major infected THP1 cells, measured by both microscopic counting and the colorimetric assay.*

amphotericin B	EC_{50} (nM)		EC_{90} (nM)	
	Colorimetric	Counting	Colorimetric	Counting
Static (0 m/s)	55.2	52.3	220.2	129.4
Media Perfusion (1.75 nm/s)	94.6	49.8	268.9	143.9

Table 4.2-2 *Table of EC50 and EC90 values of miltefosine treatment against L. major infected THP1 cells, measured by both microscopic counting and the colorimetric assay.*

miltefosine	EC_{50} (µM)		EC_{90} (µM)	
	Colorimetric	Counting	Colorimetric	Counting
Static (0 m/s)	4.11	4.38	12.7	16.8
Media Perfusion (1.75 nm/s)	7.08	5.28	90.9	18.4
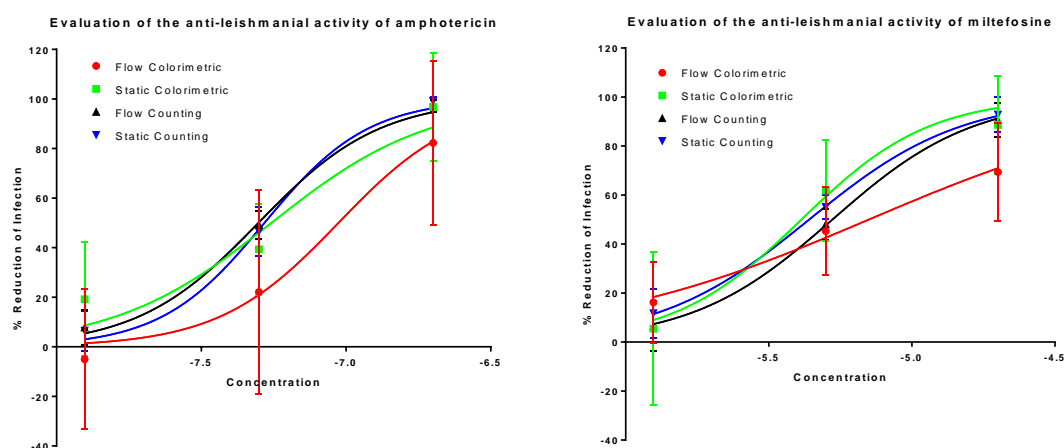
Figure 4.2-1. Dose-response curves showing the reduction in infection of THP-1 cells produced by treatment using amphotericin B (left) and miltefosine (right) with a variable slope and maximum and minimum set to 0 and 100%. The reduction in infection was measured either by the colorimetric assay or by microscopic counting and scaled to a reduction in total infection seen in the untreated control. N = 9 Error bars show SD

4.2.1 Comparison

No significant differences were seen between the static and media perfusion systems, when compared as a data set. When the EC_{50} and EC_{90} values of either drug are compared, using a one-way ANOVA this also showed no significant difference. Despite this, it is clear for both

drugs tested that, whilst the EC_{50} values are very similar, the EC_{90} values show more variation. EC_{90} values are higher in the media perfusion system than their corresponding values in the static system using both detection methods for each drug tested.

4.2.2   Discussion

The modelling conducted on the QV900 system shows that the flow velocity of the media across the surface of the cells was 1.74 nm/s^{-1}, which is actually below the range of values used for interstitial flow within the skin. This means the system was running at a sub-optimal speed and it was no surprise that only a small non-significant difference was seen when comparing static and flow. In order to correct the flow velocity, a 3D printed insert was included in the chamber of the QV900 system, for future experiments. Currently, an experiment takes four QV900 media perfusion systems to run, one for each drug concentration and a control. Each QV900 system provides six samples, three for colorimetric and three for counting. However, to include the insert would require the use of double the number of media perfusion systems, as another six samples would need to be provided for each concentration. If the colorimetric assay was still used, and this would be unmanageable. Therefore, only the counting method was used in further experiments as it shows a lower variation in the results, and was more comparable to values in literature.

4.3 Evaluation of Anti-leishmanial activity – Three Levels of Media Velocity

Three levels of flow were used, static or zero media velocity, low flow which was 1.74 nm/sec and high flow of 0.146 μm/sec, using the inserts. For consistency, both the previous flow velocities, low flow and static were repeated for comparison with the higher flow rate. Having two media velocities in the QV900 system will allow comparison of the magnitude of effect of the speed of flow. In order for the results to be directly comparable, the inserts were placed in 3 out of 6 wells of the same plate. This way the cells, in the QV900 system, were maintained under identical conditions. These experiments measured drug efficacies against *L. major* in mouse peritoneal macrophages.

4.3.1   Amphotericin B

Dose response curves for amphotericin B dosing of *L. major* infected mouse peritoneal macrophages are seen in figure 4.3-1. The data shows that the addition of media perfusion reduces the activity of amphotericin B at certain conditions. EC_{50} values are similar across all three media velocities, table 4.3-1. EC_{90} values increase in value as the speed of media velocity increases, table 4.3-1. This effect was only seen minimally, as the drug is highly

effective and concentration driven. Despite this, there was clearly an upward trend in the EC_{90} value between the three conditions.

A one-way repeated measure ANOVA showed no significant difference between any of the conditions. A two-way ANOVA showed significant differences between the static system and the QV900 system with inserts in the chambers at the highest, $p < 0.001$, and middle, $p < 0.01$, concentrations tested.

Table 4.3-1 *Table of EC_{50} and EC_{90} values of amphotericin B treatment against L. major infected mouse peritoneal macrophages.*

amphotericin B	EC_{50} (95% CI) (nM)	EC_{90} (95% CI) (nM)
Static (0 m/s)	53.7 (51.2 to 56.5)	128.3 (100.3 to 154.1)
Media Perfusion (1.75 nm/s)	58.6 (52.0 to 66.9)	172.6 (114.4 to 244.1)
Insert (146 nm/s)	67.3 (60.8 to 74.8)	237.2 (185.1 to 305.0)
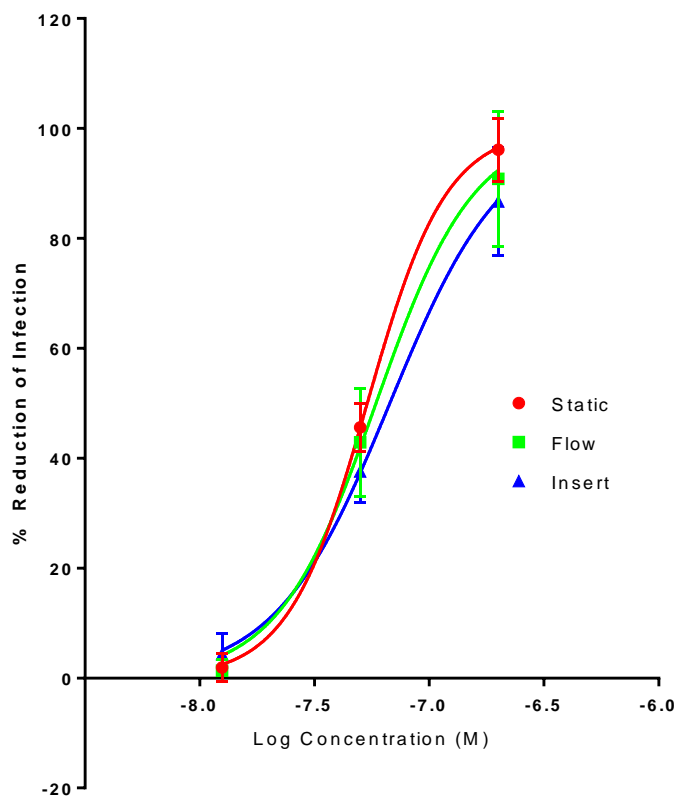
Figure 4.3-1. Dose-response curves showing the reduction in infection of mouse peritoneal macrophages produced by treatment using amphotericin B with a variable slope and maximum and minimum set to 0 and 100% respectively. The reduction in infection was measured by microscopic counting and scaled to a reduction in total infection seen in the untreated control. N = 9 Error bars show SD

4.3.2   Miltefosine

Whilst the dose-response curves for miltefosine, figure 4.3-2, all start in the same place a clear separation of the curves was seen as the concentration increases. The data shows that the addition of media perfusion reduces the activity of miltefosine. EC_{50} values, table 4.3-2, generated show the higher the media velocity the higher the EC_{50} value. EC_{90} values generated show a similar pattern, table 4.3-2. The effect of media perfusion on the cell culture system was seen more easily using miltefosine, when compared to amphotericin B. This could be because the drug is less efficacious than amphotericin B and it has a time dependent mode of action, meaning a larger effect could be seen if the concentration was lower in the media perfusion system.

A one-way repeated measure ANOVA shows no significant difference between any of the conditions. A two-way ANOVA showed a significant difference between the static system and the QV900 system both with and without an insert at the highest concentrations tested, $p<0.0001$. Significant differences can also be seen between the different media velocities in the media perfusion system at the highest drug concentration, $p<0.01$. Significant differences can be seen between the static system and the QV900 system with an insert at the middle concentration, $p<0.01$. Again, significant differences can be seen between the two media velocities of the QV900 system at the middle concentration, $p<0.01$.

Table 4.3-2 *Table of EC_{50} and EC_{90} values of miltefosine treatment against L. major infected mouse peritoneal macrophages.*

miltefosine	EC_{50} (95% CI) (µM)	EC_{90} (95% CI) (µM)
Static (0 m/s)	13.0 (11.1 to 15.2)	59.6 (42.9 to 91.7)
Media Perfusion (1.75 nm/s)	20.5 (18.5 to 23.1)	161.0 119.0 to 231.9
Insert (146 nm/s)	29.5 (26.3 to 34.2)	177.0 121.4 to 276.3
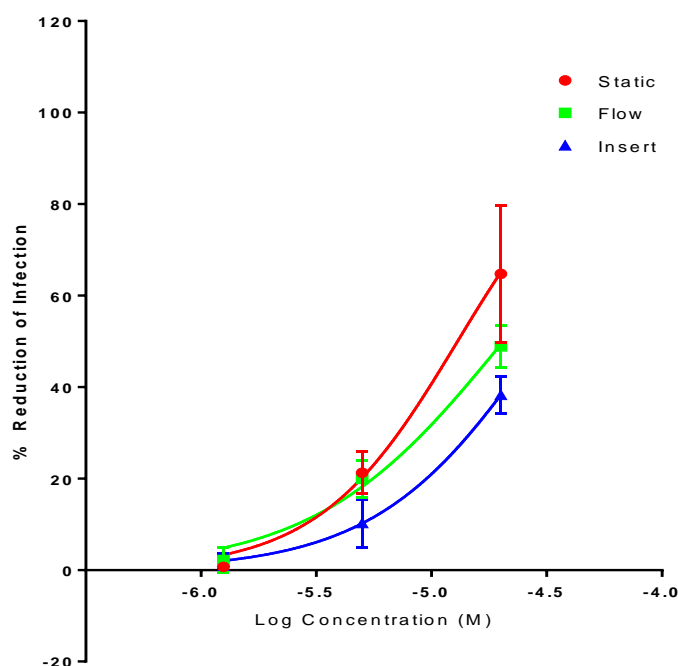
Figure 4.3-2. Dose-response curves showing the reduction in infection of mouse peritoneal macrophages produced by treatment using miltefosine with a variable slope and maximum and minimum set to 0 and 100% respectively. The reduction in infection was measured by microscopic counting and scaled to a reduction in total infection seen in the untreated control. N = 9 Error bars show SD

4.3.3 Sodium stibogluconate

Dose-response curves for sodium stibogluconate, figure 4.3-3, showed a unique profile. The order of the efficacy of the drug across the three media velocity conditions are reversed when increasing the concentration from low to high. The experiments using sodium stibogluconate show again significant differences between the three conditions. The data shows that the addition of media perfusion reduces the activity of sodium stibogluconate at certain higher drug concentrations. The EC_{50} values for the three conditions are similar, table 4.3-3. Whilst at higher concentrations, the activity appears to be weaker in the media perfusion systems. This reduction in activity also appears to correlate with velocity of media perfusion across the surface of the cells. However, it also shows at low drug concentration the activity was increased by the media perfusion. The other previously tested drugs, the higher the velocity of the media flow at the cell surface the lower the activity. The trend seen in this set of experiments fits with what was seen in the previous drugs studied.

A one-way repeated measure ANOVA showed no significant difference between any of the conditions. A two-way ANOVA shows significant differences between the static system and

the QV900 system with inserts in the chambers at all concentrations. At the highest and lowest concentrations a significant difference was seen, $p<0.01$. At the middle concentration, the significant difference seen was $p<0.05$.

Table 4.3-3 Table of EC_{50} and EC_{90} values of sodium stibogluconate treatment against *L. major* infected mouse peritoneal macrophages.

sodium stibogluconate	EC_{10} (95% CI) (µg of Sb^v/ml)	EC_{50} (95% CI) (µg of Sb^v/ml)	EC_{90} (95% CI) (µg of Sb^v/ml)
Static (0 m/s)	136.0 (114.9 to N/A)	223.0(N/A to 237.1)	368.0 (N/A to 465.3)
Media Perfusion (1.75 nm/s)	98.0 (81.6 to 115.6)	212.0 (214.4 to 242.3)	532.0 (435.9 to 635.2)
Insert (146 nm/s)	63.0 (49.5 to 79.3)	228.0 (192.5 to 232.5)	709.0 (571.7 to 892.4)

Figure 4.3-3. Dose-response curves showing the reduction in infection of mouse peritoneal macrophages produced by treatment using sodium stibogluconate with a variable slope and maximum and minimum set to 0 and 100% respectively. The reduction in infection was measured by microscopic counting and scaled to a reduction in total infection seen in the untreated control. N = 9 Error bars show SD

4.3.4   Paromomycin

Partial dose-response curves for paramomycin are shown in figure 4.3-4. In the *L. major* infected macrophage assays, paromomycin had low efficacy. EC_{50} values generated, table 4.3-4, show the trend seen in the previous drugs studied in the QV900 media perfusion system, but the two media perfusion conditions are similar in concentration. The general trend seen in previous drug studies of higher efficacies in the static system compared to the media perfusions system was replicated again.

A repeated measure one-way ANOVA shows no significant difference between any of the conditions. A two-way ANOVA shows significant differences between the static system and the QV900 system without inserts at the highest and middle concentrations tested, $p < 0.0001$. There was also a significant difference seen between the static system and the QV900 system with inserts at the highest, $p < 0.0001$, and middle concentrations tested, $p < 0.01$. There was no significant difference seen between the two different media velocities of media flow at any concentration tested.

Table 4.3-4 *Table of EC_{50} and EC_{90} values of paromomycin treatment against L. major infected mouse peritoneal macrophages.*

paromomycin	EC_{50} (95% CI) (µM)	EC_{90} (µM)
Static (0 m/s)	84.9 (64.5 to 110.8)	N/A
Media Perfusion (1.75 nm/s)	198.0 (161.6 to 254.2)	N/A
Insert (146 nm/s)	188.0 (157.6 to 229.9)	N/A
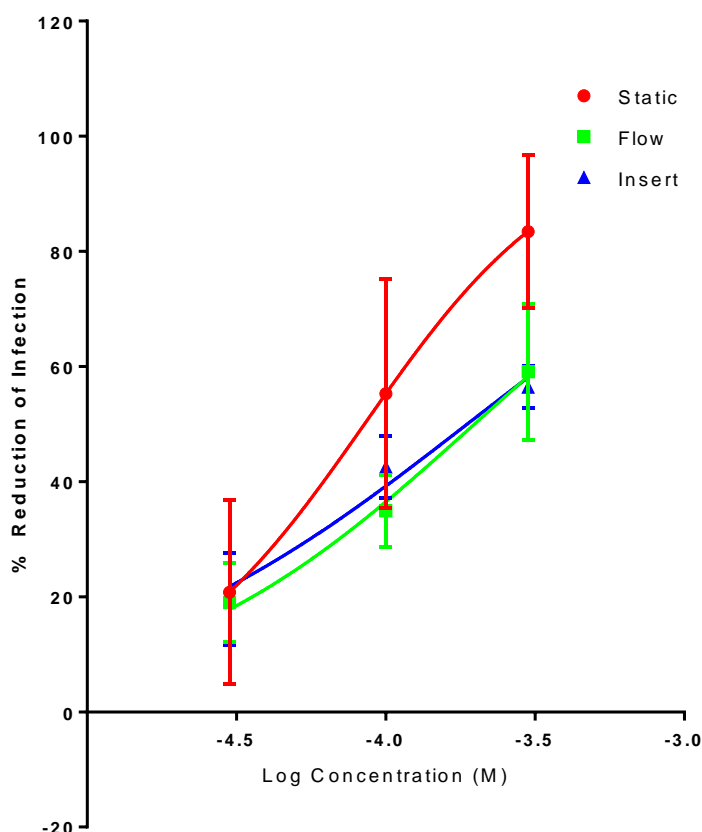
Figure 4.3-4. Dose-response curves showing the reduction in infection of mouse peritoneal macrophages produced by treatment using paromomycin with a variable slope and maximum and minimum set to 0 and 100% respectively. The reduction in infection was measured by microscopic counting and scaled to a reduction in total infection seen in the untreated control. N = 9 Error bars show SD

4.3.5   Discussion

The trend seen across all drugs used was that the higher the media velocity at the cell surface the lower the efficacy of the drug in that system. A Wilcoxon matched-pairs signed rank test was conducted comparing the EC_{50} and EC_{90} values produced by each individual assay, analysing the trend seen across all four drugs used. Using this, a significant difference was seen when comparing the EC_{50} values, between the static and media perfusion system without an insert, $p<0.05$. Much of the effect that flow has on the activities of the drugs was only seen at higher concentrations. When this statistical test was used to compare EC_{90} values, significant differences were seen between the static system and both the media velocities in the QV900 media perfusion system. The static condition shows significant differences, $p<0.001$, from the media perfusion system without inserts. The static condition also shows significant differences, $p<0.001$, from the media perfusion system with inserts.

The values of EC_{50} for all drugs used in the static system fit within previously studies and values reported within the literature[72, 325 & 330]. The main difference between the different conditions across all four drugs was an increased EC_{90} values in conditions that have a higher flow velocity at the cell surface. The EC_{90} values are also important for the treatment of parasites, as this signals a log reduction in parasite and this level of treatment is required to successfully kill enough parasites to inhibit a resurgence of the population. This trend was seen in all four drugs tested to differing degrees, depending on the efficacy and mode of action of the compound used.

A special effect produced by the media perfusion system was seen when using sodium stibogluconate to treat the *Leishmania* infection. The media perfusion increased the activity of the drug at low concentrations, whilst decreasing its activity at higher concentrations. A possible reason behind this is that media perfusion increases the metabolism of the host cell and therefore the metabolism of the drug. In order for sodium stibogluconate to be active against *Leishmania* parasites, metabolism is required for the pentavalent to be converted to its more active trivalent form[362]. Therefore, the higher the metabolism the more active agent is produced, and the stronger the reduction in parasite burden should be. This appears to be the case at low concentrations, although this effect was lost at higher concentrations. The reason for this was that when only a small amount of drug was present, a small increase in the production of the active metabolite can largely increase the effect. However, when a large amount of drug was present, enough to be in excess, then a small increase in the secondary metabolite due to the increase in metabolism, would make little difference as the concentration of this secondary metabolite would already be maximal and the additional effect would be a less significant addition. Additionally, with a large concentration of drug it is possible that the enzyme turnover has reached saturation.

The main effect caused by the addition of media perfusion was the reduction in activity of the standard drugs tested. The trend was that the higher the velocity of the media the higher the reduction in activity of the drug. Potential theories of why this effect was observed would require further investigation, but some suggestions can be outlined. As previously discussed the cells maintained under flow conditions show a higher cell metabolism and have better viability than their static counterparts. This effect could mean that the cell could produce more ATP for use in efflux pumps, removing the drug from the cell. Faster drug removal would allow the parasite to survive better[346].

Another factor that could be important is the media perfusion could also cause a reduction in drug molecule uptake. The flow velocity could interfere with the drug molecules binding to external receptors and this could lead to a lower level of accumulation of the drug within the cell. This lower accumulation could present as a lower activity, as less drug is available within the cell. Another possibility is that the zones of recirculating media found in the QV900 media perfusion system could lead to localised reductions in drug availability.

This effect could be extremely important when considering the purpose of this model. The purpose of these experiments was to elucidate the effect that media perfusion would have on a complete *in vitro* model, when both media perfusion and 3D co-culture of cells had been incorporated. The model would help to bridge the gap between static *in vitro* assays and *in vivo* experimentation. Fluid movement around the cells in *in vivo* in would affect compounds tested in animals. If we do not understand the effect that this fluid movement has, it could cost a lot of money, as drugs that appeared to work in static *in vitro* systems may lose some of their activity *in vivo* and could be unnecessarily discarded after being tested at a sub-optimal range. The findings from this chapter show a higher dose than expected may be required *in vivo*. In addition to this, *in vivo* experiments may be able to withstand a higher dose before cytotoxicity is seen[347]. Another thing that needs to be taken into consideration is that many disease states cause an increase in local fluid flow velocities[348]. By increasing the fluid velocity this could again effect the concentration of drug that is required to successfully treat the disease.

4.4 Drug Accumulation Studies in the QV900 System
4.4.1 Rationale

One way to find out if the difference in activity levels of the drugs tested in the media perfusion system, was caused by a reduced accumulation of drug molecules, was to carry out a drug accumulation assay. A protein assay was run on the samples to determine protein concentrations and allow for standardisation of the results by an estimate of cell number. After a 24-hour incubation with the drugs, the drugs were extracted from the *L. major* infected mouse peritoneal cells and analysed using HPLC-MSMS mass spectrometry using electrospray ionisation. The results were then compared to a standard curve of drug concentrations included as a reference. The results are a measure of how much drug had accumulated intracellularly

4.4.2 Comparison of Drug Accumulation in the Static or Media Perfusion System

Different amounts of drug had accumulated in the cells that were maintained in three different velocities of media perfusion, figure 4.4-1. The accumulation of both drugs was significantly higher in the static system relative to the media perfusion system, after 24 hours, table 4.4-1 and 4.4-2. Within the media perfusion system, cells maintained on top of the insert also showed a lower concentration of intracellular drug compared with the cells that were incubated at the bottom of the QV900 chamber.

Accumulation of amphotericin B increased over time, figure 4.4-1, at first the concentrations in the cells were similar but eventually it can be seen that the highest concentration of amphotericin B within the cell maintained in the static system. The next highest concentrations were found in the low flow conditions. Finally, the lowest concentrations were found in the high flow conditions. Using a one-way repeated measure ANOVA test significant differences in the concentration of amphotericin B accumulated can be seen between the low flow and high flow conditions, $p < 0.05$. Using a two-way ANOVA significant differences can be seen after 8 hours between static and low flow conditions, $p < 0.01$, and between low flow and high flow conditions, $p < 0.05$. At the 12-hour time point a significant difference was seen between the static system and the drug accumulation under high flow conditions, $p < 0.01$. After 24 hours significant differences can be seen between the static and low flow condition, $p < 0.001$, and between the static and high flow conditions, $p < 0.0001$.

The intracellular concentrations of miltefosine increased very slightly over time, as demonstrated in figure 4.4-1. Initially the cells had the same concentration of miltefosine within them at all three media velocities. By the end of the time course, the same pattern seen with amphotericin B was seen with miltefosine. There was no significant differences seen between the concentrations of miltefosine accumulated using a one-way ANOVA test. Using a two-way ANOVA significant differences can be seen after 8 hours between static and high flow conditions, $p < 0.05$, and between low flow and high flow conditions, $p < 0.001$. At the 12-hour time point, no significant difference was seen. After 24 hours significant differences can be seen between the static and low flow condition, $p < 0.01$, and between the static and high flow conditions, $p < 0.001$.

Table 4.4-1 *Table showing intracellular drug accumulation concentrations of amphotericin B (with standard deviations) in the three different velocities of media perfusion.*

Time (h)	Static (ng per μg of protein) 0 m/s	Low flow (ng per μg of protein) 1.75 ± 0.01 nm/s	High flow (ng per μg of protein) 0.146 ± 0.001 μm/s
4	0.68 ± 0.15	0.8 ± 0.25	0.62 ± 0.20
8	1.1 ± 0.31	1.66 ± 0.60	1.19 ± 0.51
12	1.56 ± 0.33	1.28 ± 0.23	0.96 ± 0.18
24	2.56 ± 1.21	1.83 ± 0.66	1.56 ± 0.49

Table 4.4-2 *Table showing intracellular drug accumulation concentrations of miltefosine (with standard deviations) in the three different velocities of media perfusion*

Time (h)	Static (ng per μg of protein) 0 m/s	Low flow (ng per μg of protein) 1.75 ± 0.01 nm/s	High flow (ng per μg of protein) 0.146 ± 0.001 μm/s
4	0.19 ± 0.02	0.20 ± 0.03	0.19 ± 0.02
8	0.26 ± 0.03	0.24 ± 0.03	0.20 ± 0.04
12	0.26 ± 0.05	0.23 ± 0.05	0.22 ± 0.04
24	0.35 ± 0.04	0.27 ± 0.02	0.24 ± 0.04
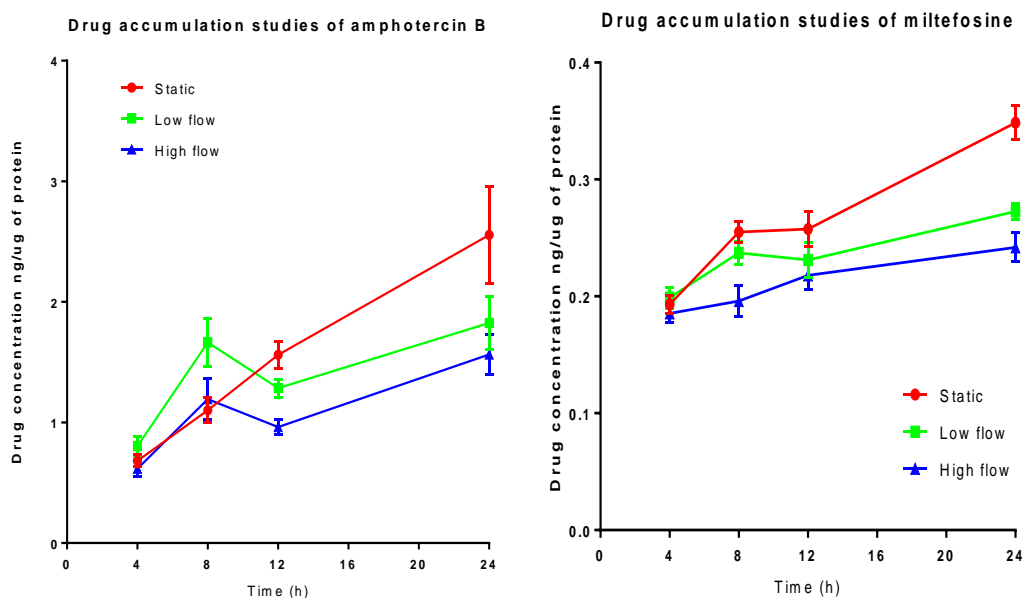
Figure 4.4-1. Accumulation of amphotericin B (left) and miltefosine (right) over time in peritoneal macrophages maintained either in static conditions or in the QV900 media perfusion system. Low flow was a media velocity of 1.75 ± 0.01 nm/s and high flow was media velocity of 0.146 ± 0.001 μm/s. Graphpad prism was used to display the data and connecting lines are drawn between points. N = 9 Error bars show SD

4.4.3   Discussion

One caveat of these experiments was that the drug concentration used was higher than the highest concentration used in previous assays throughout this thesis. The concentration used was also high enough to kill over 90% of the *Leishmania* parasites present within the cells. This was because otherwise the results fall below the lower limit of detection of the HPLC-MSMS system. Initially development of this method involved a range of relevant concentrations used over the same period; however, the results were below the lower limit of detection. The literature on the specific method used was checked and it was found that the concentrations used were too low for detection. It was decided that the use of higher concentrations would still be able to demonstrate any differences between the three conditions. There was no point in using a range of higher concentrations as they would all have the same effect on the infection and could lead to cytotoxic effects, hence a time course was chosen to study rates of absorption and accumulation.

Both data sets show that, the cells maintained under flow conditions have accumulated less drug than the static alternative. Considering the media perfusion systems have 36 mL of drug containing media in total, compared to the static system's 1 mL of drugged media, this was a surprising result, as there are more molecules of drug in the media perfusion systems. The data also shows the higher the flow velocity of the media, at the surface of the cells, the less drug was found accumulated within the cells.

A higher cell metabolism, found in cells maintained under media perfusion conditions, could cause the cell to be more active and have a higher rate of drug molecules breakdown[361]. The faster turnover would lead to less accumulation as the rate at which the cells metabolise the drug in flow could cause a local decrease in concentration of the drug within the cell. The reduction in drug accumulation could also be due to a reduction in the rate of drug uptake. If the media perfusion effected the binding of the drug molecules to their receptors, either by reducing the time spent in contact with the receptor, or by affecting the probability of molecules coming in contact with the surface receptors. Another idea was that the media perfusion causes localised re-circulation within the media perfusion system, which could lead to the cells being surrounded by media containing a lower concentration of drug. These two things would reduce the probability of drug uptake and hence reduce the drug accumulation within the cell.

4.5 Nitrite Ion Release Following Cell Stimulation in the QV900 System

4.5.1 Rationale

Nitric oxide (NO) from activated macrophages has been shown to be one of the mechanisms by which macrophages kill *Leishmania* parasites[349]. Nitric oxide has an important role in cytotoxicity and has been shown to be toxic for a variety of pathogens, including *Leishmania*. One method for the indirect determination of NO is the Griess assay. The Griess assay involves the spectrophotometric measurement of its stable decomposition products NO^-_3 and NO^-_2[350].

In this experiment, mouse PEMs were incubated under the three different flow conditions for 24 hours, and then stimulated with lipopolysaccharide (LPS), known to elicit a NO response. The response was then measured using the Griess assay. The reason that the assay was conducted this way was that, if the cells were stimulated with LPS whilst inside the media perfusion system, the NO released would be diluted by the volume of media within the system. This dilution would most likely mean that the NO release would be below the limit of detection for the Griess assay.

4.5.2 Comparison of Nitrite Ion Release in Cells Conditioned either in the QV900 Media Perfusion or Static System

The cells maintained under static conditions show a higher release of nitrite ion, hence nitric oxide release when challenged with LPS, figure 4.5-1. Cultures maintained in the QV900 media perfusion system show a similar concentration of nitrite ion release regardless of the speed of media velocity. On average, the concentration of nitrite ion in the media surrounding the cells maintained in static conditions was 1.882 ± 0.006 µM. In comparison to this the concentration of nitrite ion in the media surrounding the cells maintained in media perfusion system was 1.815 ± 0.034 and 1.813 ± 0.026 µM, with and without a 3D printed insert. A one-way ANOVA showed statistically significant differences between the static condition and both of the two media velocities in the QV900 media perfusion system, $p < 0.001$.
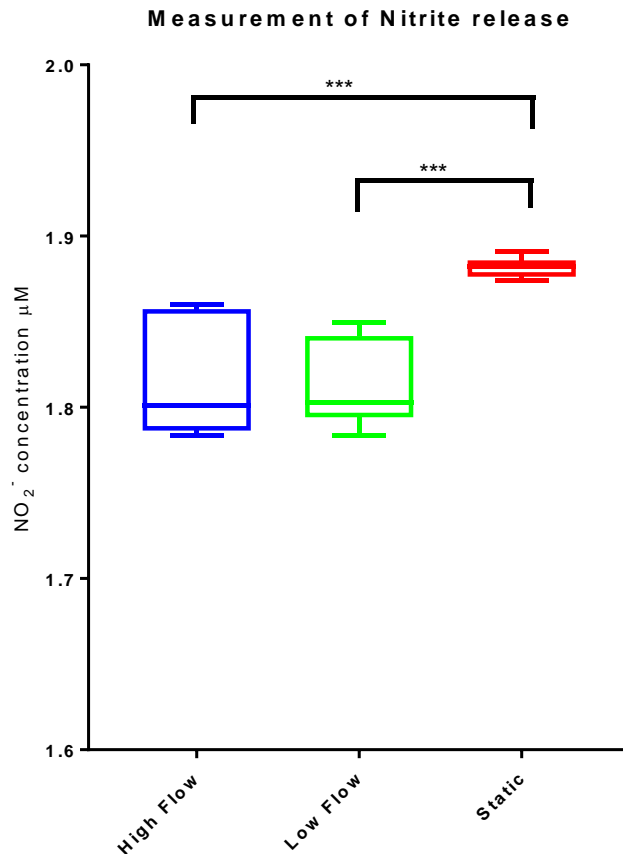
Figure 4.5-1. A box and whisker diagram showing the concentration of nitrite ion in sample after incubation under the three different media flow velocities. *** = p<0.001 N = 3

4.5.3   Discussion

The results show that cells maintained under static conditions produced more NO when activated with LPS, compared to the cells maintained in the media perfusion system. The values of nitrite ion detected in the media surrounding the cell that had been maintained under static conditions match values found in the literature[351 & 352]. The more NO released the better a cell will be able to kill an invading parasite. One hypothesis behind this experiment is that cells maintained under media perfusion conditions may be more able to kill the *Leishmania* parasites due to their increased viability. This appears not to be the case as they have been shown to produce a lower concentration of NO, when challenged with LPS. This result does reflect what was seen when the parasites are treated with drugs. When using the media perfusion system the efficacy of drugs was lower, there are less parasites killed by the cells maintained under flow conditions than under static conditions when using the same drug concentration. The reduced concentration of nitric oxide produced by cells in

the media perfusion system could be a contributing factor in the reduced ability to kill the parasites.

4.6 Conclusion

The effect that media perfusion had on the treatment of cells infected with *Leishmania* parasites was non-significant in the experiments measured by two different methods. Whilst the colorimetric assay was shown to work, and matched to microscopic counting, it still has a large variation in its results. The experiments were conducted on cells maintained under very low flow velocity and shear stress. This meant that the differences seen between the static and flow systems were minimal, and the colorimetric assay struggled to detect the differences. Visually it appeared to show that the media perfusion makes treatment of leishmaniasis less effective when compared to the static system.

With the introduction of the 3D printed insert, the effect of an interstitial fluid flow rate and the comparisons of two different flow rates was possible in the QV900 system. The results show that in the media perfusion systems the effectiveness of the drug treatment was statistically lower, in comparison to a static model. A reduction in the uptake of drug molecules, or an increase in metabolism leading to a higher efflux of drug, both lead to a reduced effectiveness of the drug treatment. The results also show that the higher the velocity of the media across the cell surface, the less effective the drug treatment was against a *Leishmania* infection.

To investigate whether the differences in infection rates and drug treatments are to do with the rate of uptake into the cell, drug accumulation studies were carried out. The results from this show that less drug was accumulated by the cells maintained under the flow conditions. The data shows that the faster the flow velocity the lower the concentration of drug within the cells. A measure of nitric oxide release also showed that there was a reduced concentration of nitric oxide in cells maintained in the media perfusion system. This would mean that the cells were less able to kill the parasites and reduce the infection.

Work in this area of testing drug efficacies in an *in vitro* model, that has a media perfusion aspect to it, is rare. The examples of these models in literature concentrate on establishing the model and measuring how the cell functions are maintained. A recent study (unpublished data) showed the application of media perfusion used the drug diclofenac and showed different EC_{50} values in static and media perfusion culture. The media perfusion system increased the sensitivity of the cells to the drug. In doing so, it brought the results from the

in vitro models closer to the results from *in vivo* studies and correctly identifies diclofenac as a cytotoxic drug.

In conclusion, the application of media perfusion has wide-ranging effects on both the infection by *Leishmania* parasites and the treatment of infected macrophages. It is important to realise that in biological situations almost all cells are under some form of fluid flow, causing both movement of nutrient and a mechanistic shear stress effect. These factors are not taken into account in most *in vitro* assays and hence they can often give misleading results. The use of a media perfusion system is a key part in the creation of a more predictive and more biologically relevant *in vitro* model.

Chapter 5 Development of a 3D Cell Culture Model for Leishmaniasis

5.1 Introduction

The aim of this thesis was to investigate different ways in which the current *in vitro* model systems could be more predictive of *in vivo* results. Current approaches are based upon 2D cell assays and *in* vivo mouse models, both of which do not, in several ways, accurately reflect the infection in humans. In this third results chapter, the use of a 3D cell culture model for *in vitro* assays was investigated.

2D cell culture systems have been used for *in vitro* assays to measure the infection rates and drug efficacies against *Leishmania* parasites since 1974[327]. In 2D cell culture systems, cells are plated out into the bottom of the well and left to settle and attach to the flat surface of the bottom of the well. When the cells form attachments to the flat surface of the well, they spread out becoming wider and flatter. The cells rearrange their cyto-architecture and internal structure to reflect the new environment. In contrast, cells found within the body will be found in a 3D conformation or will have assembled to form 3D architecture. It has been shown that maintaining the cells in 3D provide a more predictive model, as cells are more representative of the *in vivo* situation[187&243], as discussed in more detail in the introduction.

Maintaining the cells in 3D allows the cells to take a more physiologically relevant shape and volume. The change from 3D to 2D, alters the surface area to volume ratio and completely changes the availability of the cell surface, both for cell-cell interactions and receptor presentation. When the cell is maintained in 2D, much of the cell surface area is in contact with the culture plastic or glass and not available for interactions with other cells or signals from the environment. 3D maintenance of cells allows cells to maintain a natural shape and conformation and allows the cells to have a larger area where signals can be received or sent. In this project, two solid scaffolds were chosen for use in 3D cell culture of macrophages, their infection with *Leishmania* parasites and the evaluation of drugs against amastigotes within infected macrophages. A solid scaffold, rather than a hydrogel or free floating 3D structure such as a spheroid, was chosen for two reasons. Firstly, the free swimming nature of the *Leishmania* promastigotes was taken into consideration. The parasites might have had a problem moving through the hydrogel and the spheroid may not allow access to the cells in the centre of the spheroid giving an uneven infection. A solid scaffold with a well-organised pore system would allow the parasites to move through the scaffold and reach cells that are

within the scaffold. Another reason for this choice of scaffold was the extent of literature on solid scaffolds and specifically the use of the scaffold for the creation of skin models[206 & 319]. The two scaffolds chosen for this work were the 3D CelluSponge from Invitrocue, referred to in future as the Invitrocue scaffold. The second is a polystyrene spun scaffold from Alvetex®, referred to in future as the Alvetex scaffold. Both are discussed in more detail in the materials and methods section.

The work covered in this section is novel and previously unreported. Notable work in the area of *Leishmania* involving 3D models for the infection mainly focused on *ex vivo* models. A *Leishmania* and HIV co-culture model used tissue explants from human tonsils to study the modulation of the HIV replication cycle by *Leishmania* parasites[297]. The paper uses the naturally occurring 3D structure of the tissue to provide a better microenvironment for the replication of the natural interactions between the parasite and the virus and detect the signals, as they could be happening within the body. Another paper[298] demonstrates the ability of *Leishmania* parasites to migrate through an extracellular matrix like substance made using a 3D environment mainly composed of collagen I. In this paper, the promastigotes demonstrate a new type of migration dynamics compared to the free-swimming forms found in 2D cultures. Their behaviour was altered by the 3D environment; the promastigotes showed a different pattern of migration and the collagen matrix increased the time taken for the parasites to infect the cells. This was despite the fact that parasites moved faster into the collagen matrix when cells were present. Another area of *Leishmania* research where a 3D environment is actively being used is for the development of labelled fluorescent or bioluminescent parasites. In another paper[299], splenic explants were removed from infected mice and the parasite loads were measured, by measuring the fluorescence of the parasites before culture of the explants led to release of parasites.

Examples of 3D systems being used in other infectious disease research areas are more common. Viral infections have been studied with the use of 3D cell culture systems. A paper by Straub *et al*[300] showed that noroviruses could infect and replicate in a 3D organoid model of human small intestinal epithelium. Cells were grown on porous collagen-coated beads and differentiated into 3D architectures that resembled both the morphologic and physiologic function of *in vivo* tissues. A fully differentiated 3D cell culture model could support the natural growth of human noroviruses, whereas previous attempts using differentiated monolayer cultures had failed. Another example is the culture of Hepatitis C virus in 3D Huh7 cells that were morphologically and transcriptionally distinct from more standard Huh7 2D monolayers[301]. These 3D cultures are highly permissive for HCV infection, thus providing an

opportunity to study HCV entry and the effects of HCV infection on host cell function in a more physiologically relevant cell culture system. More recently, the effects of Zika virus infection in human neural stem cells growing as neurospheres and brain organoids were studied[302]. 3D cell culture systems have been used extensively with bacteria. One example is a tuberculosis model of granuloma[303]. The paper describes the development of a biomimetic *in vitro* model of human tuberculosis granuloma using human primary leukocytes, in which the tuberculosis exhibited characteristics of dormant mycobacteria. The cells were maintained in 3D confirmation in an extracellular matrix mimic. In a study of *Pseudomonas aeruginosa,* 3D reconstituted lung models are regularly used[304&305]. *Salmonella typhimurium* was used with 3D small intestine[306] and colon models[307]. For parasites, the technique is far less common and the literature reflects this. A paper on *Cryptosporidium parvum*[308,] shows the development of a three-dimensional human intestinal model for long-term infection. Asexual and sexual stages and the formation of new oocysts were observed during the course of infection in a 3D silk scaffold. A paper on *Plasmodium*[309] incorporated primary human hepatocytes into engineered polyethylene glycol based macroporous human ectopic artificial livers; they demonstrated that porous livers support liver stage human malaria (*P. falciparum*) infection *in vitro*.

A key example of a model that is relevant for the disease area that this thesis covers is a reconstituted skin model used to test the efficacy of miltefosine against *Acanthamoeba*[310]. As skin is the host organ infected by *Leishmania* parasites in cutaneous leishmaniasis, this model was of particular interest. A key difference however is that *Leishmania* parasites infect macrophages within the skin, whereas the *Acanthamoeba* model[310] was largely based around keratinocytes. The model allowed the study of the infection caused by *Acanthamoeba* and to show that subsequent dosing with miltefosine was successful.

The objectives of the work discussed in this chapter are:

I. To establish methods to determine viability of host cells and of parasite in 3D models.
II. To establish an infection in mouse peritoneal macrophages maintained in the 3D culture.
III. To determine the infection potential within the system compared to a 2D alternative.
IV. To use the infected macrophage model to determine the activity of standard drugs in 3D models compared to the currently used model system.

5.2 Viability Studies on Invitrocue Scaffold

Comparisons of 2D and 3D cell culture models in literature[311] have indicated differences in cellular morphology and metabolism, commonly attributed to the closer representation of *in vivo* conditions of the 3D cell culture environment. To study the influence of 2D or 3D cell culture on cell viability, an Alamar blue assay was used on one million mouse peritoneal macrophages.

The results, figure 5.2-1, show that initially the 3D system seems to confer lower cell viability compared to the 2D system. However, this may be due to the ease of cell adherence to a flat surface compared to a 3D scaffold. Cells in 3D may not have completely recovered from the initial plating. The next phase from about 72 hours to about 300 hours shows the cells having similar viabilities in 2D and 3D. Finally, by 300 to 400 hours the cell viability in the 3D was higher. When the data was compared using a t-test, no significant difference was seen. When comparing the data using a two-way ANOVA there was significant difference seen at the 24 hour time point, $p<0.05$. No significant difference was seen at any other time point. The conclusions we can draw from this is that the cells have similar viability and hence metabolic processes in either 2D or 3D. However, the 3D systems show a better maintenance of viable cells over the long term. This result was similar to Bonnier *et al*[312] who conclude that there was little difference between 2D and 3D conditions after 24 hours. Another paper[313] showed over a longer period of time, 14 days, that there was only minimal differences in cell viability when maintained in 3D rather than 2D.

3D vs 2D Viability ratio
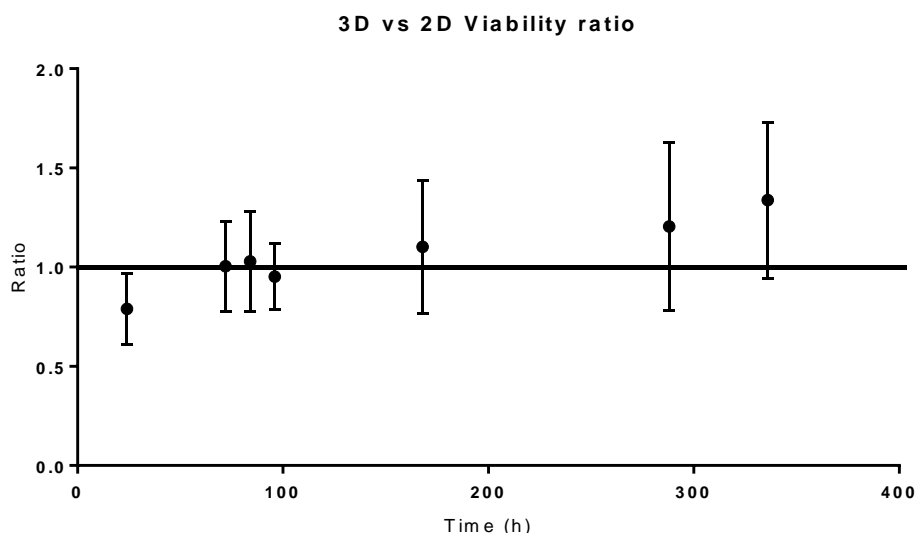
Figure 5.2-1. Graph showing the ratio of viability of mouse peritoneal macrophages maintained in the Invitrocue sponge (N=9) compared to the viability of mouse peritoneal macrophages maintained in 2D (N=9) A ratio of 1 means that they are equally viable. Error bars show SD

5.3 Imaging the Scaffolds

Cells were imaged in 3D to prove they had adopted a 3D configuration and to analyse the formation of any 3D tissue-like structures they formed within the scaffold. Cells can form many different larger structures in 3D as demonstrated by Kenny *et al* (2007)[314] and Ingram *et al* (1997)[245] and it is important to see what the microenvironment does to the different cell types used in experiments. Cells were stained with DAPI (Blue), a nuclear stain and phalloidin (Green), which stains actin fibres giving a general outline of the cell. Images were taken using a confocal microscope, as described in the methods section, both single plane and z-stacks.

5.3.1 Culture of THP-1 Cells in 3D

THP-1 cells were seeded at a density of 1 million cells per scaffold, shown in figure 5.3-1. The THP-1 cells settled in the Alvetex scaffold and whilst they can be seen to be in 3D and throughout the scaffold, they seem to not have formed any kind of secondary structure.

The THP-1 cells settled in the pores of the Invitrocue scaffold, figure 5.3-1, and formed a secondary structure. Using the Kenny *et al* (2007)[313] descriptions of the different forms that cells take as a secondary structure in 3D cell culture (figure 5.3-2), the cells in the Invitrocue scaffold most resemble a grape like structure. The phalloidin staining in figure 5.3-1 was not as strong and consistent as the cells seen in other images (figure 5.3-1 and 5.3-3), this was

because the phalloidin has more difficulty penetrating the Invitrocue sponge scaffold and reaching the cells. Incubation times with the phalloidin were increased to adjust for the extra time taken to diffuse throughout the sponge scaffold, and this improved staining of the fixed cells.
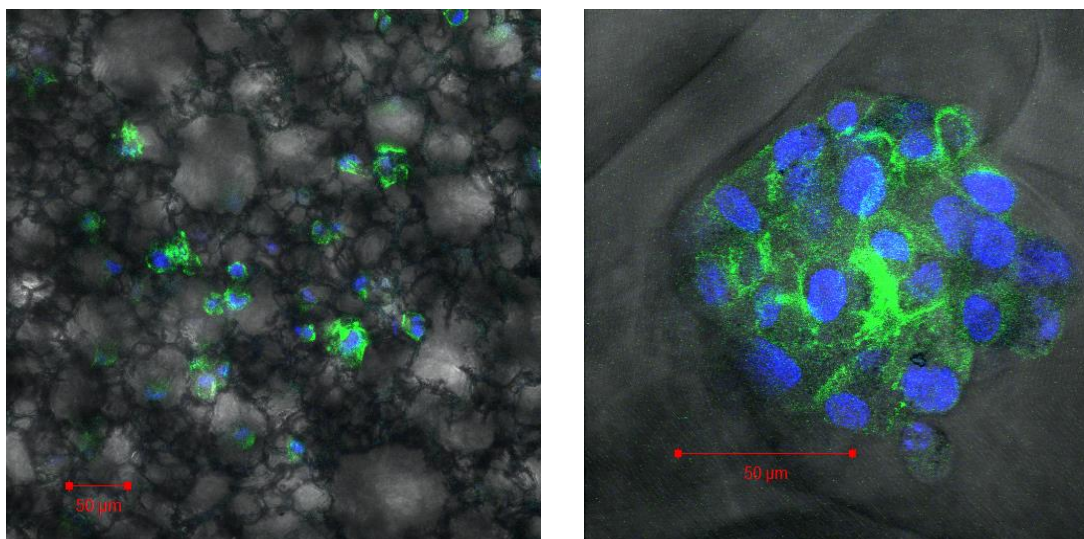
Figure 5.3-1. Confocal image of THP-1 cells grown in an Alvetex scaffold (Left) and Invitrocue scaffold (Right). Cells stained with DAPI (Blue) and phalloidin (Green).

Figure 5.3-2. Figure from Kenny *et al* (2007)[313] showing different morphologies found in 3D cell culture

5.3.2 Culture of Mouse Peritoneal Macrophages in 3D

Peritoneal macrophages settle on the Alvetex scaffold, figure 5.3-3, and whilst they can be seen to be in 3D and throughout the scaffold, they have not formed any kind of secondary structure. The peritoneal macrophages appear to act in a similar manner to the THP-1 cells.

When the peritoneal macrophages settle in the pores of the Invitrocue scaffold, figure 5.3-3 they form the same grape like secondary structure seen when using the THP-1 cells. The size for a grape like bundle varies greatly but is summarised in table 5.3-1.
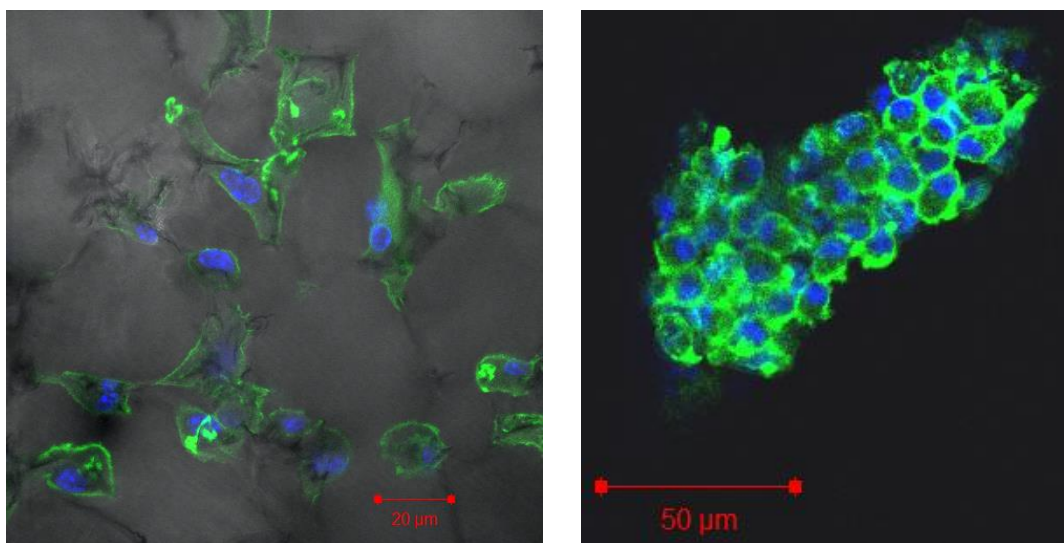
Figure 5.3-3. Confocal image of mouse peritoneal macrophages grown in an Alvetex scaffold (Left) or Invitrocue scaffold (Right). Cells stained with DAPI (Blue) and phalloidin (Green).

Table 5.3-1 *Maximum and minimum dimensions of observed 3D structures created by mouse peritoneal macrophages in the Invitrocue scaffold. N = 24*

Category	Maximum	Minimum	Mean
Height (No. of Cells)	17	3	8
Width (No. of Cells)	20	2	7
Depth (No. of Cells)	3	1	2
Volume µm³	1,326,438	11,239	271,142
Total number of cells	100	13	39

Considering the peritoneal macrophages form the same structures in the two different scaffolds as the THP-1 cells but are easier to infect, it was decided to carry out further development of a drug assay with only mouse peritoneal macrophages.

5.3.3   Culture of Fibroblasts in 3D

Cutaneous leishmaniasis infections are found in the dermis, which is largely made up of fibroblasts. A further test of the scaffolds ability to sustain cells in 3D was carried out using cells that are still dividing. Fibroblasts grow in flat sheets and their natural conformation shows a different pattern of structuring, compared the macrophages.

In comparison to the fully differentiated macrophages, the actively dividing fibroblasts were left for 3 days to grow within the scaffold. It can be seen in figure 5.3-4, that the fibroblasts have proliferated and have nearly colonised the Alvetex scaffold. The cells have taken a flat elongated confirmation and have spread out to form full layers across the surface and slightly below it. Figure 5.3-5, demonstrates the position of the fibroblast within the scaffold. The majority of the fibroblasts sit on top of the scaffold to form a confluent layer but some do penetrate further into the scaffold.
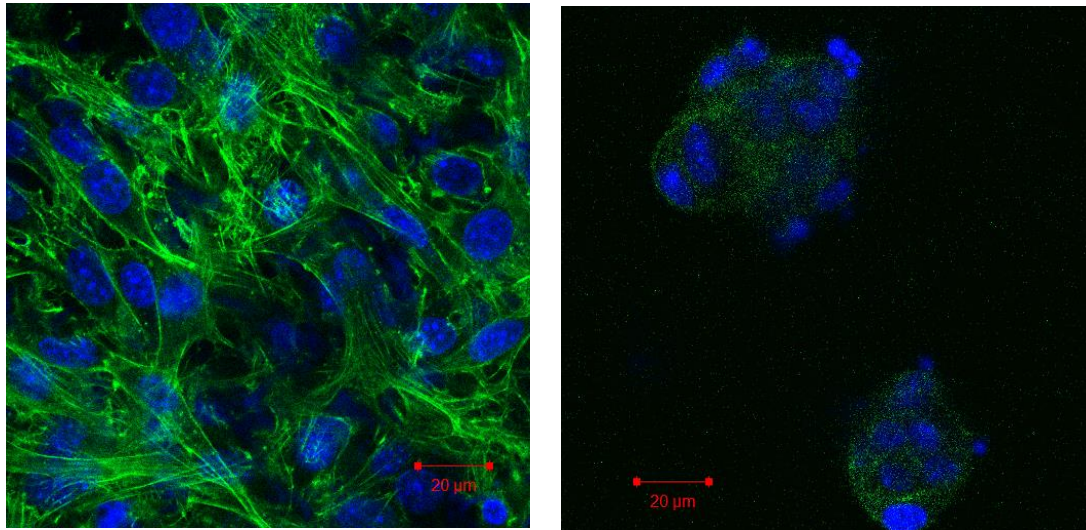
Figure 5.3-4. Confocal image of 3T3 fibroblasts grown in an Alvetex scaffold (Left) and Invitrocue scaffold (Right). Cells stained with DAPI (Blue) and phalloidin (Green).
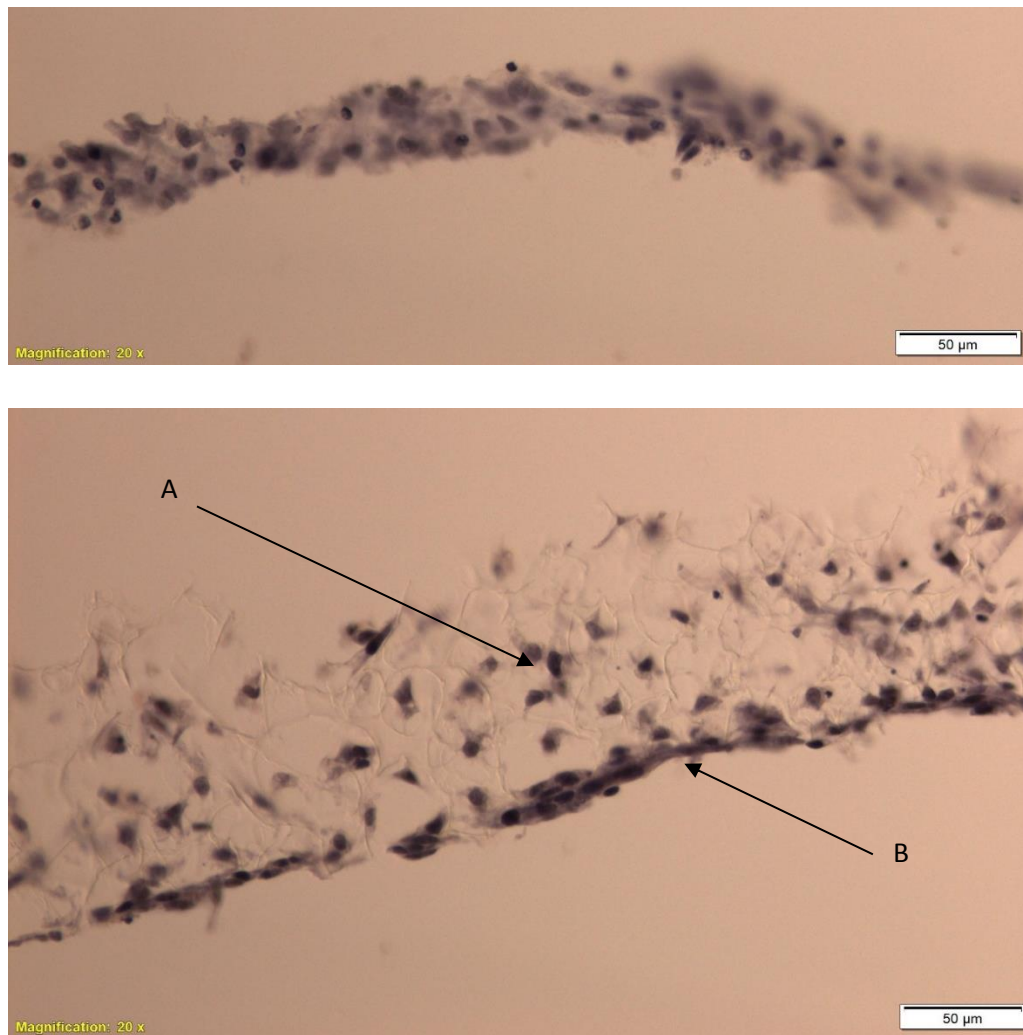
Figure 5.3-5. Microscopic images of 3T3 fibroblasts grown in an Alvetex scaffold. Cells stained with Hematoxylin and Eosin stains. A = Fibroblasts that have penetrated through the scaffold. B = Layer of fibroblasts that has formed at the surface of the scaffold.

The fibroblasts cultured in the Invitrocue scaffold take on the previously seen grape like structures. It can be seen in figure 5.3-4, that the fibroblasts have not proliferated but have formed the same grape like bundles similar to those seen with macrophages. The cells in this scaffold have not taken the usual flat elongated conformation seen for fibroblasts in most culture systems. The cells have not spread out to form layers as seen in the body, and seen when plated on the Alvetex scaffold. The fibroblasts have also not proliferated as seen in the Alvetex scaffold suggesting they might not be as suited to this scaffold.

5.3.4 Fluorescent *L. major* Parasites for use in 3D

A group at the Universidad de León, León, Spain engineered a transgenic *L. major* strain, figure 5.3-6, expressing the mCherry red-fluorescent protein for real-time monitoring of the parasitic load[161]. *L. major* LV39c5 (RHO/SU/59/P) strain was used for generating mCherry transgenic promastigotes, transfecting it with the 711-bp mCherry coding region. This

parasite has a maximum emission peak at 610 nm with a 587 nm excitation wavelength, giving it a red fluorescent signal, allowing the signal to be detected as a separate signal from the blue DAPI and green phalloidin.
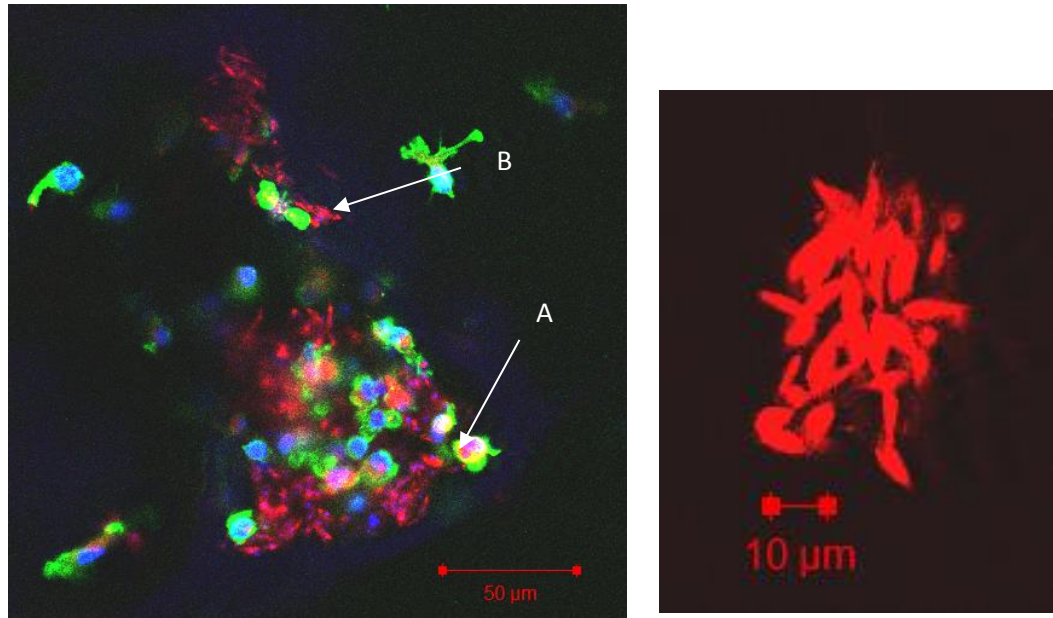
Figure 5.3-6. Confocal image of *L. major* mCherry parasites infecting peritoneal macrophages in the Invitrocue scaffold (Left) and free in the media (Right). An infected cell containing a *L. major* mCherry amastigote is shown by A. An external *L. major* mCherry parasite is shown by B. This strain was kindly gifted to us courtesy of Prof Rosa Reguera, University of Leon.

5.3.5   Fluorescent *L. amazonensis* Parasites for use in 3D

The World Health Organization (WHO) reference strain *L.* amazonensis (IFLA/BR/1967/PH8) was used to create a red fluorescent parasite, figure 5.3-7. The *L. amazonensis* parasites were transfected with the constructs pIR1SAT-LUC(a) DsRed2(b) (B5947) to create a red fluorescent protein expressing strain of *Leishmania*[316]. This strain was kindly provided to us by Eric Prina, Institute Pasteur Paris.
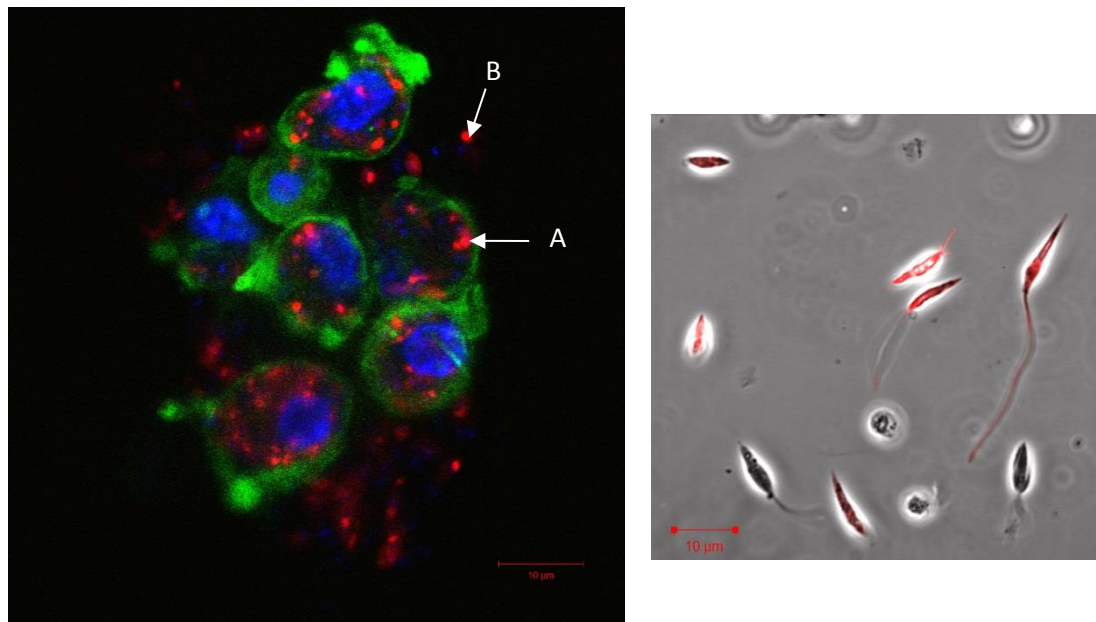
Figure 5.3-7. Confocal image of *L. amazonensis* DSRed2 parasites infecting peritoneal macrophages (Left) and free in the media (Right). An infected cell containing an *L. amazonensis* DSRed2 amastigote is shown by arrow A. An external *L. amazonensis* DSRed2 parasite is shown by arrow B.

5.4 Counting Methodology Development

One problem that 3D cell culture causes, is the need to adapt current evaluation methods that have historically been developed for 2D cell culture. In the case of *Leishmania,* the main method of evaluation is microscopic counting of the number of infected cells. Once they have been fixed and stained. This cannot be used with 3D cell culture for several reasons, primarily the fact that the scaffold is opaque and cells cannot be directly visualised within it. Another issue was that the microscopes used for counting fixed and stained cells are oil immersion microscopes that could easily damage the scaffold. The most important reason is as the cells are in a 3D conformation, the whole of the cell will need to be imaged, as parasites could be located anywhere within the cell. To get around this, a confocal microscope and the z-stack capability will need to be utilised. This also means that fluorescent dyes will need to be used so that any image that is captured will be clear, and infected cells will be easy to identify. Once the samples have been fixed and stained, z-stacks are taken and stored for later analysis.

5.4.1   Determination of the Level of Infection using Volocity

The images and z-stacks taken on the confocal microscope were loaded into Volocity, an image analysis software package from PerkinElmer, as mentioned in the methods section.

The number of cells in each image was calculated using the automated measurements section of the Volocity program. The find objects command of Volocity was used in the DAPI (blue) channel to select all cell nuclei. Settings were adjusted by offsetting the threshold, if the threshold was too close to the initial peak of the signal and the minimum object size was set to 500 μm^3. This produces a list of objects detailing volume and other parameters, each object was a possible nucleus that the program has counted. The list of objects was manually checked for volumes that were above 1000 μm^3, if a volume above 1000 μm^3 was found then the selected object was manually checked to make sure it represents only one nucleus. If the highlighted section was made of more than one nucleus then how many extra cells need to be added to the count once at the end of the list was recorded. Then all the objects on the list were highlighted and the image checked to see if any cell nuclei has been missed by the automated count. If there were nuclei that have been missed, they were added to the total count of number of cells present in the image.

Once the number of cells in an image was determined, the image tab was selected and visualisation set to XYZ mode. Then the z-stack was manually advanced counting the number of infected cells. Intensities of the red parasite channel were maintained but on occasion, the phalloidin (green) channel can be reduced to make it easier to see if the red signal was inside or outside the cell. The percentage infection was calculated by comparing the number of infected cells to the total number of cells in the image.

One limitation of this system was the time and concentration it takes to semi-automatically count the cells in each image. Another problem is that the Volocity method has more subjectivity than the Invitrocue method of counting. It has the advantage over the Invitrocue computational analysis that the decision-making behind whether a cell is infected is more experienced, and can make decisions on situations where the computational method would be unable to decide. Cells near the edges of the image are not ignored as if they are infected then it is obvious that they should count. The human aspect of this method makes up for some of the shortcomings of the computer analysis. This method also allows for the analysis of single plane images, which the computer analysis cannot do. It can also detect anomalies such as z-stack drift, which can cause the computer problems.

5.4.2 Determination of the Level of Infection - Computer Analysis from Invitrocue

The number of parasites per cell was counted using the ImarisCell module of Imaris 8.2.0 (Bitplane AG). Imaris cell detection consists of three parts, namely nucleus detection, cell

body detection and vesicles detection, which in this case will detect the parasites. In our analysis, the red channel labelling the parasite was inputted as the vesicle channel so the number of parasites per cell can be determined directly from the measurements called number of vesicles per cell.

Nucleus detection was performed on the DAPI channel. Local background subtraction with a region width of 2.8 µm was applied. Nucleus was detected using an estimated diameter of 7 µm and an intensity threshold of 40.

Cell body was detected using the green channel, which detects the signal from phalloidin that has labelled the actin. Local background subtraction with a region width of 12 µm was performed before applying an intensity threshold of 29. The cell splitting was done by enforcing the rule of one nucleus per cell. Extremely small nuclei and cells that resulted from wrong segmentation were removed by setting minimum size thresholds.

For parasite (vesicles) detection, background subtraction was performed and an estimated diameter of 3 µm and an intensity threshold of 6.7 were used in the detection.

The intensity threshold for all these three were set based on visual inspection of a few stained samples to get most desired segmentation. One of the limitations of this approach is that there might be variations in images obtained from samples stained and imaged on different days. To overcome this limitation, we tried to make sure that all samples were stained similarly so that same segmentation scheme can be applied to all samples. Other limitations of this system are that the algorithm used does not detect cells that are touching the edges of the image and it cannot process single plane images. Where the major difference is seen between the two different counting methods was the quantification of total cell number. This was partly due to cells not being detected as they are too close to the edge but also because of nuclei that are in close proximity of to each other being mistaken as a single object by the analysis.

Advantages of this method of counting are the speed of detection and how rapidly images can be analysed and results produced. The algorithm has been through many cycles of improvement and can count both the percentage infection and the burden of parasites within the cells at the same time, producing high quality data on the infection status.

5.5 Determination of Level of Infection in 3D Cultures

5.5.1 Rationale

The differences between 2D and 3D cell culture models in cellular morphology, metabolism and the microenvironment lead to differences in infection potential. In 3D, the cells present more surface area for the parasite to attach to; this could increase the ease of parasite entry into the cell. To study the difference in infection rates between 2D and 3D, experiments were conducted using the two strains of fluorescent parasite.

5.5.2 Evaluation of Infection Rates in 3D

As the infection ratio was increased, the percentage infection after 72 hours also increases in all three conditions, figure 5.5-1. The mean value at an initial infection ratio of 0.5 *L. major* parasites to each cell in the 2D system was 72.3±2.2% infection after 72 hours. In the 3D systems, the mean infection percentage was 8.0±3.1% in the Alvetex scaffold and 67.2±17.6% in the Invitrocue scaffold. The values are similar between the 2D and the Invitrocue scaffold. However, the Alvetex scaffold shows a much lower level of infection after 72 hours. This pattern continues when the initial infection ratio of *L. major* was increased. When the data was compared using a one-way ANOVA, a significant difference was seen between the 2D and Alvetex scaffold, p<0.001. A significant difference was also seen between the Alvetex and the Invitrocue scaffold but to a lesser degree, p<0.01.

The mean value at an initial infection ratio of 0.5 *L. amazonensis parasites* per cell in the 2D system was 54.8±1.0% infection after 72 hours, figure 5.5-1. In the 3D systems, the mean infection percentage was 5.4±3.4% in the Alvetex scaffold and 51.4±5.7% in the Invitrocue scaffold. Again, the values are similar between the 2D and the Invitrocue scaffold; however, the Alvetex scaffold shows a much lower level of infection after 72 hours. When the data was compared using a one-way ANOVA significant difference was seen between the 2D and Alvetex scaffold, p<0.01. In addition, significant difference was seen between the Alvetex and the Invitrocue scaffold, p<0.01.
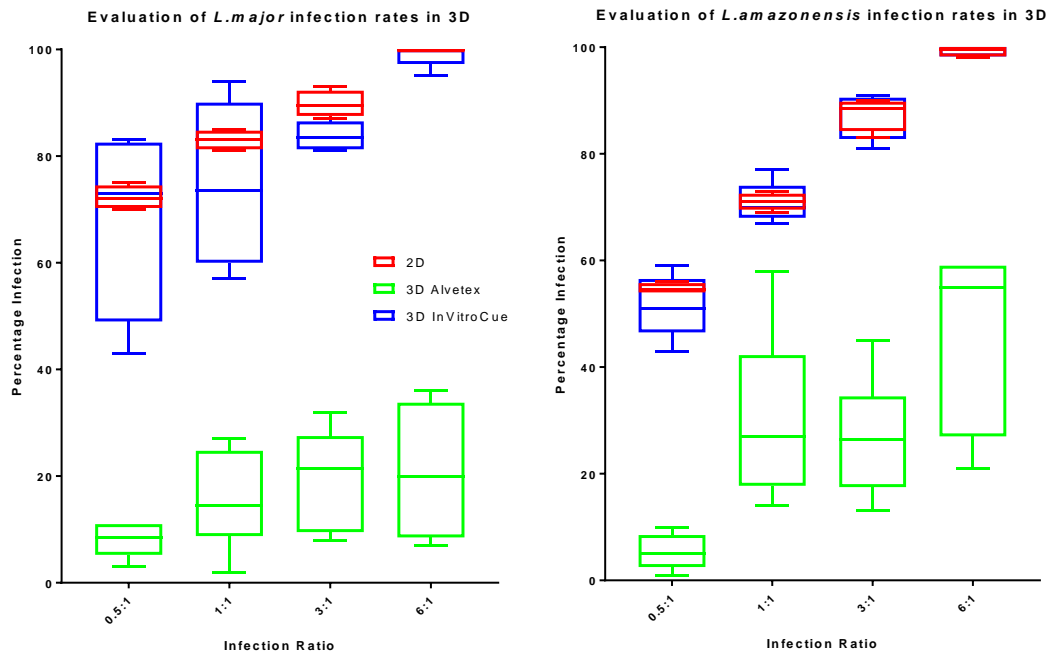
Figure 5.5-1. Box and whisker charts showing the infection rates of *L. major* (left) and *L. amazonensis* (right) in both 2D (N=6) and 3D cell (N=6) culture. 3D cell culture was conducted in both the Invitrocue and Alvetex scaffolds. Red = 2D, Blue = 3D Invitrocue and Green = 3D Alvetex. Error bars show maximum and minimum values.

5.5.3   Discussion

As initial infection ratio, of either parasite, was increased the overall percentage infection after 72 hours increased. This was true of all three conditions. It can be seen that there was a higher variation of the final infection rate after 72 hours in the 3D scaffolds compared to the 2D system. The boxes in figure 5.5-1 are much larger for the 3D scaffolds. The variation in the Invitrocue scaffold gives rise to values that fall either side of the values produced by the 2D assay and they show similar average infection rates. In contrast, the Alvetex scaffold shows significantly less infection than the other two conditions. A reason for this could be the smaller pore size[336] in the Alvetex scaffold. The smaller pores mean the scaffold blocks more of the cell surface and this may make it difficult for the parasite to enter the cell. If the cells are blocking the pores then the parasites will have trouble reaching cells deeper in the scaffold.

Leishmania infection in the Alvetex scaffold was very variable and difficult to achieve. For this reason, experiments from this point onwards will be conducted using only the Invitrocue scaffold.

5.6 3D Infection Dynamics

5.6.1 Rationale

Once the optimum infection ratio was chosen, the progression of the infection could be studied. In three dimensions, the cells have a different confirmation and cytoarchitecture, these differences could affect the division rate of the parasite. Infections were conducted using the two strains of fluorescent parasite on both 2D and 3D cell culture and the progression of the infection was measured.

5.6.2 Evaluation of Infection Progression

The change in percentage infection of either parasite over time, when maintained in either 2D or 3D, is shown in figure 5.6-1. The mean value after 24 hours for *L. major* parasites in the 2D system was 70.3±1.5% compared to the 3D systems that shows a mean infection percentage was 71.7±3.2% in the Invitrocue scaffold. This increased to 91.3±1.5% and 89.0±5.2%, for the 2D and 3D respectively, after 48 hours of incubation. After 72 hours, the percentage infection rates were 89.8±2.5 percent for 2D and 83.8±2.8 percent for 3D. Values are similar between the 2D and the Invitrocue scaffold at each time point. When the data was compared using a student's t-test no significant difference was seen between the 2D and the Invitrocue scaffold.

The infection pattern was seen again, when the infection was caused by the *L. amazonensis* parasite, figure 5.6-1. The mean value after 24 hours in the 2D system was 64.3±1.2% compared to the 3D system, which shows a mean infection percentage of 63.7±0.6% in the Invitrocue scaffold. This increased to 83.7±4.5% and 82.7±0.5% for the 2D and 3D respectively, after 48 hours of incubation. After 72 hours, the percentage infection rates were 87.5±3.1 percent for 2D and 87.3±4.3 percent for 3D. Values are very similar between the 2D and the Invitrocue scaffold at each time point. When the data was compared using a student's t-test no significant difference was seen between the 2D and the Invitrocue scaffold.
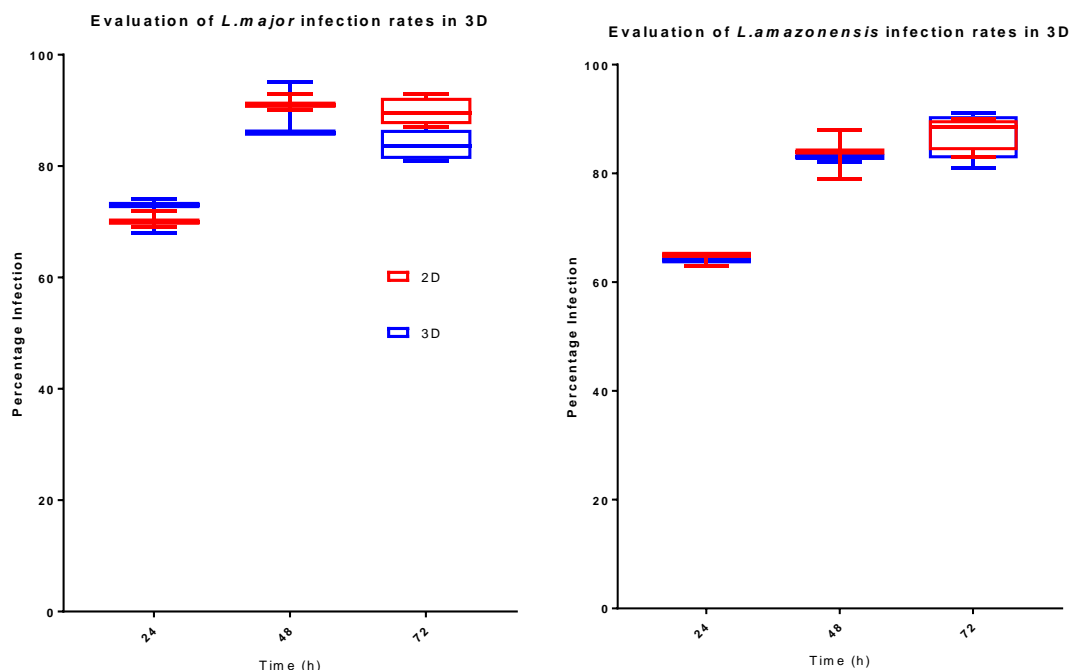
Figure 5.6-1. Box and whisker charts showing the infection rates of *L. major* (left) and *L. amazonensis* (right) in both 2D (N=6) and 3D (N=6) cell culture. 3D cell culture was conducted in the Invitrocue scaffolds. Red = 2D and Blue = 3D Invitrocue Error bars show maximum and minimum values.

5.6.3   Discussion

As expected, considering the similar infection after 72 hours in the previous experiment, the progression of infection was similar in both the 2D and the 3D Invitrocue scaffold. They also showed similar overall infection rates after 72 hours (figure 5.5-1).

5.7 Determination of Drug Efficacies in 3D

5.7.1   Rationale

The effect of culturing cells in 3D on drug efficacies was determined. Changes to the cells confirmation allows a higher percentage of the surface area of the cell to be accessible to drug molecules. A larger surface area accessible could also affect the availability of transporters and may affect permeability. A more biologically relevant cyto-structure compared to cells in 2D could affect how the drugs are trafficked and processed within the cell. To study the differences between drug efficacies in 2D and 3D cell culture systems, AmB and MIL were evaluated against the *L. major* and *L. amazonensis* fluorescent strains.

Drug efficacies were determined measuring reduction in both percentage infection and the number of parasites within each cell; this measurement of burden could be very different between macrophages cultured in 3D compared to 2D. Cells cultured in 3D have very

different appearances compared to those in 2D, which have spread out and flattened. This change in cell shape may not affect the overall number of infected cells but could have an effect on how many parasites have accumulated within each cell.

Images taken in the course of the experiments were analysed computationally, both by Invitrocue and using the Volocity software, to produce values for both percentage infection and the number of parasites per cell for the 3D data. 2D counts were done manually using a microscope to determine both the percentage infection the average number of amastigotes per cells after 100 cells were counted.

5.7.2 Determination of Drug Efficacies against *L. major*
5.7.2.1 amphotericin B

A clear reduction in percentage infection caused by dosing with amphotericin B concentrations between 200 nM and 12.5 nM was seen in both 2D and 3D, figure 5.7-1. EC_{50} and EC_{90} values can be seen in table 5.7.1. When the 2D and the 3D data, that has been manually counted, was compared using a one-way ANOVA there was a statistical difference, $p<0.05$.

Parasite burden is reduced with AmB and Mil treatment, figure 5.7-1. The reduction in average burden with *L. major* shows that initially there are more parasites per cell at the lowest concentration of amphotericin B in 2D than in 3D. When the concentration of amphotericin B was increased past 50 nM, the two cell culture systems show very similar parasite burdens.

No significant difference was seen in parasite burden between the two data sets when comparing with a one-way ANOVA. When a two-way ANOVA was used no significant difference was seen at any concentration.
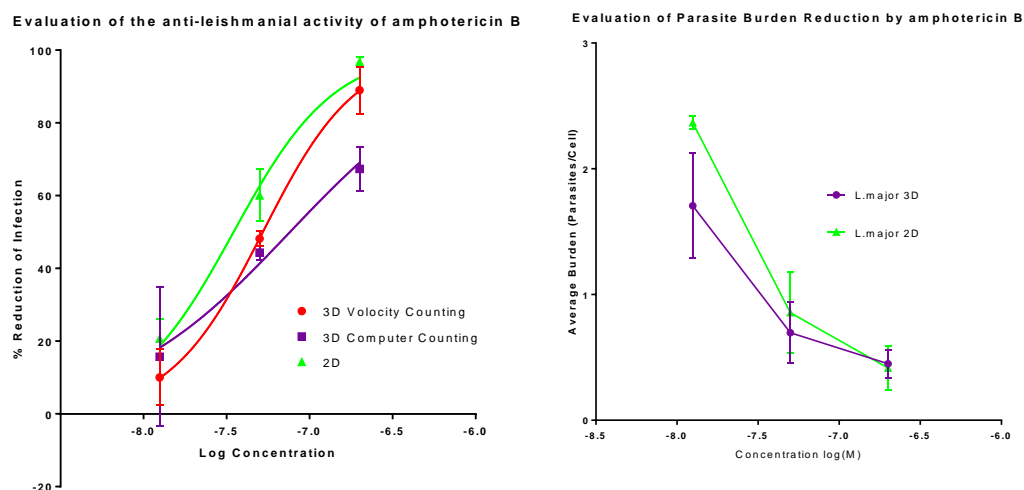
Figure 5.7-1. (Left) Dose-response curves for 2D (N=6) and 3D (N=6) cell culture showing the reduction in percentage infection of peritoneal macrophages by *L. major* produced by treatment using amphotericin B. The reduction in infection was scaled to a reduction in total infection seen in the untreated controls in either condition. (Right) Reduction in *L. major* parasite burden of peritoneal macrophages for 2D (N=6) and 3D (N=6) cell culture, produced by dosing with amphotericin B. Error bars show standard deviation

Table 5.7-1 *Table summarising the results of dosing with amphotericin B on the reduction in percentage infection, seen in peritoneal macrophages infected with L. major amastigotes, in either 2D or 3D cell culture.*

	3D Velocity Counting	**3D Computer Counting**	**2D**
EC50 (95% CI) (nM)	52.3 (46.6 to 58.7)	76.2 (37.7 to 203.5)	34.9 (31.4 to 38.6)
EC90 (95% CI) (nM)	216.6 (165.5 to 288.2)	1070.0 (237.3 to N/A)	161.5 (132.4 to 201.2)

5.7.2.2 miltefosine

A reduction in infection caused by treatment with miltefosine was seen in both 2D and 3D, figure 5.7-2. EC_{50} and EC_{90} values are shown in table 5.7-2. When the data was compared using a one-way ANOVA there was no a statistical difference seen.

The graph showing the parasite burden of peritoneal macrophages that have been dosed with miltefosine shows, the average number of parasites per cell decreases as the concentration of miltefosine increases. The reduction in average burden with *L. major* shows that initially there are more parasites per cell at the lowest concentration of miltefosine in 2D than in 3D. When the concentration of miltefosine was increased past 50 nM, the two cell culture systems show very similar parasite burdens. This was the same pattern seen in the amphotericin B treated cultures; the reason for this may be partly due to the limitations of

the computation counting methods ability to differentiate parasites from each other in highly infected cells, where the fluorescent signal may overlap. Treatment of infected cells with miltefosine does not always show a concentration dependent reduction in a linear fashion. For the *L. major* infected macrophages the average burden per cell appears to rise between the lowest and the middle concentration. This was despite the percentage infection decreasing, meaning cells that have not been cleared by miltefosine treatment have more parasites in them. No significant difference was seen between the conditions when comparing with a one-way ANOVA. When a two-way ANOVA was used there are significant differences at the lowest amphotericin B concentration between the burden of *L. major* in 2D and 3D, $p < 0.05$.
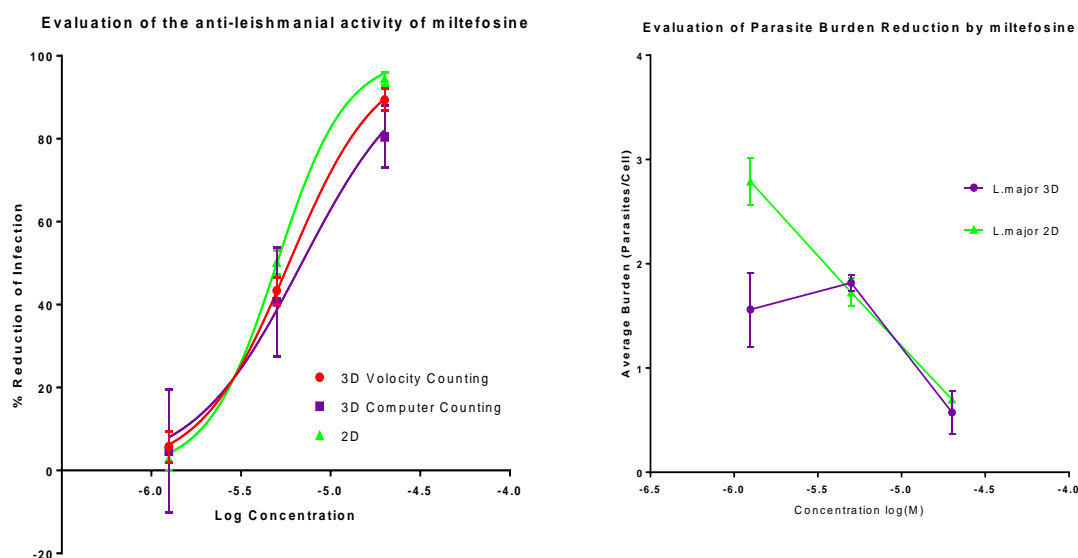
Figure 5.7-2. (Left) Dose-response curves for 2D (N=6) and 3D (N=6) cell culture showing the reduction in percentage infection of peritoneal macrophages by *L. major* produced by treatment using miltefosine. The reduction in infection was scaled to a reduction in total infection seen in the untreated controls in either condition. (Right) Reduction in *L. major* parasite burden of peritoneal macrophages for 2D (N=6) and 3D (N=6) cell culture, produced by dosing with miltefosine. Error bars show SD

Table 5.7-2 *Table summarising the results of dosing with amphotericin B on the reduction of percentage infection, seen in peritoneal macrophages infected with L. major amastigotes, in either 2D or 3D cell culture.*

	3D Volocity Counting	3D Computer Counting	2D
EC50 (95% CI) (µM)	5.85 (5.52 to 6.21)	6.90 (4.09 to 12.22)	5.02 (4.88 to 5.16)
EC90 (95% CI) (µM)	20.4 (17.6 to 23.7)	32.0 (N/A to 189.0)	13.2 (12.0 to 14.5)

5.7.3 Determination of Drug Efficacies against *L. amazonensis*
5.7.3.1 amphotericin B

Amphotericin B treatment gave a reduction in percentage infection in both 2D and 3D, figure 5.7-3. EC_{50} and EC_{90} values are shown in table 5.7-3. When the data was compared, using a one-way ANOVA there was no statistically relevant difference seen.

When comparing the burden of *L. amazonensis* in amphotericin B treated cultures the burden was always lower in cells maintained in 2D than it was in cells kept in 3D. All treatments of infected cells with amphotericin B show a concentration dependent reduction in parasite burden. No significant difference was seen in parasite burden between the two data sets when comparing with a one-way ANOVA. When a two-way ANOVA was used there are significant differences at the lowest amphotericin B concentration between the burden of *L. amazonensis* in 2D and 3D, $p < 0.05$.
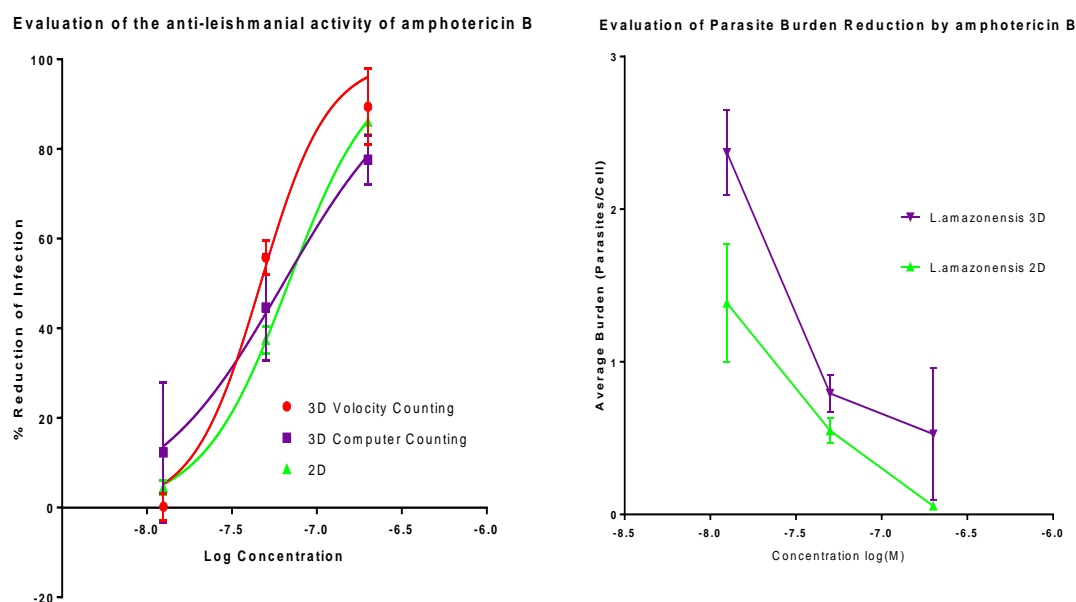
Figure 5.7-3. (Left) Dose-response curves for 2D (N=6) and 3D (N=6) cell culture showing the reduction in percentage infection of peritoneal macrophages with *L. amazonensis* produced by treatment using amphotericin B with a variable slope and maximum and minimum set to 0 and 100% respectively. The reduction in infection was scaled to a reduction in total infection seen in the untreated controls in either condition. (Right) Reduction in *L. amazonensis* parasite burden of peritoneal macrophages for 2D (N=6) and 3D (N=6) cell culture, produced by dosing with amphotericin B. Error bars show standard deviation

Table 5.7-3 *Table summarising the results of dosing with amphotericin B on the reduction of percentage infection, seen in peritoneal macrophages infected with L. amazonensis amastigotes, in either 2D or 3D cell culture.*

	3D Volocity Counting	3D Computer Counting	2D
EC50(95% CI) (nM)	46.65 (41.48 to 52.95)	63.47 (36.06 to 117.0)	68.00 (65.33 to 70.81)
EC90 (95% Ci) (nM)	126.8 (N/A to 189.3)	441.7 (134.9 to 4002.0)	245.4 (223.1 to 270.2)

5.7.3.2 Miltefosine

A reduction in infection caused by dosing with miltefosine was seen in both 2D and 3D, figure 5.7-4. EC_{50} and EC_{90} values are shown in table 5.7-4. EC_{90} values generated are extrapolated and may not be a true indicator of the data collected. When the data was compared, using a one-way ANOVA there was no statistical difference seen.

When comparing the burden of *L. amazonensis* in miltefosine treated cultures the burden was always higher in cells maintained in 2D than it was in cells maintained in 3D. The average burden of the *L. amazonensis* infected macrophages show a very slight decrease in value compared to the decrease seen in the *L. major* infected macrophages. This matches the percentage infection data, as miltefosine treatment at the concentrations used in the experiment only manage to reduce the percentage infection by about 50%.

No significant difference was seen between the conditions when comparing with a one-way ANOVA. When a two-way ANOVA no significant differences observed at any concentration of miltefosine.
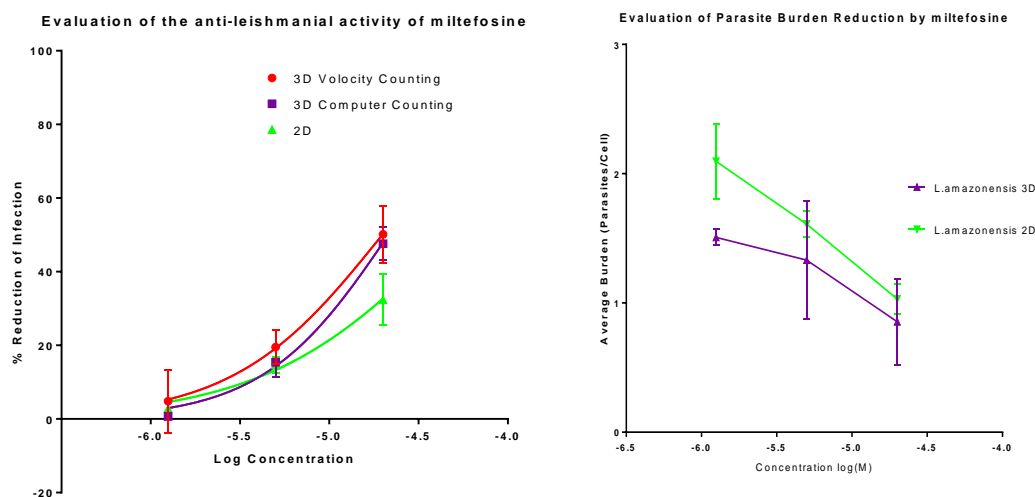
Figure 5.7-4. (Left) Dose-response curves for 2D (N=6) and 3D (N=6) cell culture showing the reduction in percentage infection of peritoneal macrophages with *L. amazonensis* produced by dosing with miltefosine with a variable slope and maximum and minimum set to 0 and 100% respectively. The reduction in infection was scaled to a reduction in total infection seen in the untreated controls in either condition. (Right) Reduction in *L. amazonensis* parasite burden of peritoneal macrophages for 2D (N=6) and 3D (N=6) cell culture, produced by dosing with miltefosine. Error bars show standard deviation

Table 5.7-4 *Table summarising the results of dosing with amphotericin B on the reduction of percentage infection, seen in peritoneal macrophages infected with L. amazonensis amastigotes, in either 2D or 3D cell culture.*

	3D Velocity Counting	3D Computer Counting	2D
EC50 (95% CI) (µM)	19.8 (16.2 to 25.9)	21.4 (17.4 to 28.7)	47.6 (37.2 to 66.8)

5.7.4 Comparison of the Two Counting Methods used

When the results from the two different counting methods, Volocity and Invitrocue's computational counting method, for assessment of *Leishmania* infection in 3D cell culture system were compared, no significant difference was seen in any experiment when the data was analysed using a one-way ANOVA. The two methods show a good similarity in the values they produce (table 5.7-5) and hence in all cases produce similar curves. The main difference seen between the two methods is found at the extremities of the curves affecting the EC$_{90}$ values. A possible reason behind this was the Invitrocue computational method returned results with slightly less infection seen in the positive controls. This meant that when percentage infection rates were calculated the values were scaled up giving higher values for lower infection rates. This has led to a reduction in the Hill slope for some of the curves.

Despite the difference in analysis methods, the results show a striking similarity and either method could be used for future analysis.

Table 5.7-5 *Table summarising the values produced by fitting a curve to the data when analysed in Graphpad Prism by either Volocity or Invitrocue automated counting methods*

Species	EC$_{50}$ of drug:	Volocity Counting (µM)	Invitrocue Counting (µM)
L. major mCherry	Amphotericin	0.052	0.076
	Miltefosine	5.85	6.90
L. amazonensis DSRed2	Amphotericin	0.047	0.063
	Miltefosine	19.8	21.4

5.7.5 Discussion

There was only one case of statistically significant differences between the 2D and 3D cell culture systems, seen when amphotericin B was used to treat a *L. major* infection, and the data for 3D was manually counted. Whilst the rest of the results lack statistical significance, patterns in the data emerge. When the peritoneal macrophages were infected with *L. major* then treatment with either amphotericin B or miltefosine appears to be weaker, but not significantly, in the 3D cell culture system than in the 2D cell culture system. The EC$_{50}$ value for amphotericin B when used against *L. major* in 2D was lower than in 3D. The values for miltefosine show the same pattern. EC$_{50}$ values produced by both the 2D and 3D assays match the range of values seen in the literature[50 & 161].

Interestingly, peritoneal macrophages that are infected with *L. amazonensis* responded differently. Treatment with either amphotericin B or miltefosine appears to be more potent in the 3D cell culture system than in the 2D cell culture system. EC$_{50}$ values generated by treatment of the infected macrophages with amphotericin B show the 2D system to have an EC$_{50}$ value higher than the 3D system, when measured using the Volocity counting method or the Invitrocue computational counting method. Miltefosine shows the same pattern of higher EC$_{50}$ values in the 2D system than in the 3D system. EC$_{50}$ values produced by both the 2D and 3D assays match the range of values seen in the literature[316 & 325]. The data shows that the small effect that using a 3D cell culture system has, in this experiment over a 2D cell culture system, is reliant on the strain of *Leishmania* parasite used.

Patterns of reduction in average parasite burden between 2D and 3D are similar but there are some differences in the values that each system generates. As previously mentioned the

burden of the 3D system was computationally counted by Invitrocue and the algorithm for this may have problems discerning the true number of parasites per cell in a highly infected cell. The fluorescent signal from the parasites may overlap, and the images captured at the LSHTM were not of very high quality due to the equipment used. The time and memory constraints if extra quality were to be added were a problem in the capture of each image as part of a z-stack.

This difference in drug sensitivities between stains seen in these experiments have been previously reported in the literature[50, 161, 316 & 325]. Even in the 2D cell culture systems, the two different strains show different efficacies to the drugs tested. Infected peritoneal macrophages treated with amphotericin B show EC_{50} values of 34.9 nM and 68.0 nM, when infected with *L. major* or *L. amazonensis* respectively. Infected peritoneal macrophages treated with miltefosine show EC_{50} values of 5.0 μM and 47.6 μM, when infected with *L. major* or *L. amazonensis* respectively. It was clear that the two standard drugs tested show a higher efficacy against the *L. major* parasite than the *L. amazonensis* parasite.

When comparing the average parasite burden data, it was clear that amphotericin B was more effective at reducing the parasite burden and clearing the parasite from the cells. It was the only drug that was able to reduce the burden below an average of 0.5 parasites per cell, which was seen for amphotericin in both strains and both 2D and 3D conditions. Whilst the miltefosine was able to reduce the percentage infection[328], cells that remain infected show high parasite burden in comparison of those cells still infected when treated with amphotericin B. This high parasite burden may be able to re-establish a higher infection rate if treatment is not continued. This is because miltefosine shows a time and concentration dependent mechanism of killing, and in order to show the same reduction in burden the treatment time would need to be extended.

The results shown in this experiment are largely seen when other compounds are compared between 2D and 3D models. Bielecka *et al*[329], tested various anti tuberculosis drugs in a 2D and 3D system showing 3D has no effect on the use some compounds to treat infection, when compared to 2D cell culture. They also show a number of compounds that are effected by the switch from a 2D to a 3D cell culture system. Whether a compound changes its efficacy when used in 3D compared to 2D is dependent on the compound used.

5.8 Conclusion

The main difference in the use of 3D cell culture is the physical shape that the cells are able to take. This was demonstrated by the different cell types tested in the two scaffolds. Another point made in the development of the 3D culture systems, was that the morphology and secondary structures that the cells can take are different depending on the type of 3D cell culture or scaffold used. Here, the two types of solid support scaffold used show drastic differences in the behaviour of the cells and the shapes that form within them. Another important distinction was that different types of scaffold are more suited for different cell types. Macrophages are fully differentiated cells that are infected more naturally in the Invitrocue sponge. In the Invitrocue sponge, they have formed large grape like structures allowing the parasites a loci of cells to infect or re-infect. The large pore size is perfect for the cells to accumulate grouping together forming a secondary structure with only the cells in the periphery forming contacts to the sponge. The cells can be maintained in each pore without the cells multiplying forcing the cells to move out of the pore to find more space. Alternatively, the macrophages are more difficult to infect in the Alvetex scaffold, the cells are more spread out and can be seen to stick fully to the scaffold and its smaller pore system. Hence, for the establishment of infection and treatment of infection, the Invitrocue sponge was the obvious choice.

The switch from 2D to 3D cell culture showed no difference in the viability of the cells over short periods of time. The period of time where there was no obvious difference between the viability in the two systems covers the standard time taken for a 3 day drugging experiment. Whilst opinions vary on whether 2D and 3D cell culture differ in cell viability, at least when using the Invitrocue sponge it can been seen that there was no significant difference over the period that all experiments were run. After this period, the 3D cell culture seems to maintain the cells for longer than the 2D cell culture, another observation reported in the literature[317-319].

The infection of the macrophages by *Leishmania* parasites, either in 2D or 3D cell culture systems, show no difference in the total percentage infection after 72 hours or in the development of that infection. This was not surprising, as the 3D cell culture system has large pores, which allow the *Leishmania* parasites easy access to the macrophages. Additionally, the secondary grape like structure that the cells form was on average only a few cells thick, meaning almost every cell is freely accessible to the parasites direct from the media. The way that the parasites encounter the macrophages is similar in the 2D and 3D cell culture systems

used here. Another study[337] using the Invitrocue scaffold with Hepatitis C virus showed that the virus accumulated more in the cell maintained in 3D. This however, may be due to the cell type used, hepatocytes in 3D has been shown to maintain their function better[238, 301 & 311], and this may lead to a higher accumulation of virus.

With no differences in viability or infection potential between the 2D and 3D cell culture systems, the starting point of the experiments for determining drug efficacies are the same in both 2D and 3D. The slight differences seen in either 2D or 3D cell culture systems appear to be dependent on the species of parasite used. *L. major* parasites are less susceptible to treatment with drugs when cultured in 3D, when compared to a 2D cell culture system. Whereas, *L. amazonensis* parasites appear to be more susceptible to treatment when cultured in 3D. However, there was no statistically significant differences between the two different culture systems when comparing percentage infection. When comparing reduction of parasite burden, there are some significant differences at certain concentrations of drug. This could be due to the differences between the counting methods and when compared as a whole trend of parasite reduction, no significant difference in the trend was seen.

In other studies in this area, a variety of differences in sensitivity to drug exposure between cells grown in 2D and 3D are seen. One study[279] showed, A431.H9 cells grown in 2D and 3D show differences in viability when treated with the same concentrations of 5-fluorouracil and tirapazamine. In the case of 5-fluorouracil, 2D cultures showed a reduced viability compared 3D spheroids. Additionally, cells treated with tirapazamine showed a higher viability in 2D compared to 3D. This research highlights the fact that cells in 3D do not necessarily exhibit a higher drug resistance, but that it is a combination of the specific drug and the cellular environment that influence the cells reaction. Another paper[338] showed that fibroblast in 3D exhibited a higher resistance to doxorubicin compared to 2D controls and cells grown in 3D and then treated with tamoxifen are less susceptible to the cytotoxic effects of the drug than cells grown in 2D.

In conclusion, the transition from 2D cell culture to 3D cell culture has large effects on the morphology and the dynamics of cell to cell contact, depending on the type of 3D system used. The choice of 3D scaffold can alter the pattern of infection by *Leishmania* parasites. Therefore, selection of scaffold to suit the purposes of the model is very important.

There was little to no effect on the infection of macrophages maintained in the Invitrocue scaffold by *Leishmania* parasites. Additionally, the treatment of infected macrophages in

mouse peritoneal macrophages, in the Invitrocue scaffold appears to be largely unaffected by being maintained in a 3D cell culture system. It is important to realise that in biological situations cells will be far more similar to the cells maintained in the 3D cell culture systems than cells maintained in 2D. This section shows that the differences between 2D and 3D cell culture are not enough to show a statistically relevant difference when comparing the results of the experiments. Differences between 2D and 3D cell culture systems may have effects in other areas but in the context of the experiments conducted, no significant differences are seen. The use of a 3D cell culture system may take on a more important role when combined with other aspects in the creation of a more predictive and more biologically relevant *in vitro* model.

Chapter 6 Evaluation of Cell Choice for an *In Vitro* Model

6.1 Introduction

The aim of this thesis is to investigate different ways in which the current *In vitro* model systems could be more predictive of *in vivo* results. Current *in vitro* approaches use a variety of different cell types. From cell lines to primary cells, the choice of cell for use in an assay can depend on availability and personal preferences. In this results chapter, the use of induced pluripotent stem cells are compared to mouse and human bone marrow derived macrophages and to THP1 cells for their suitability in *in vitro* assays.

In 2006, Takahashi and Yamanaka[320] showed that the forced expression of four transcription factors (Oct4, Sox2, Klf4, and c-Myc) was sufficient to convert fibroblast cells into embryonic stem cell-like cells, which were called induced pluripotent stem cells (iPSC). A process called reprogramming, where timed expression of master regulator factors changed differentiated cells into iPSCs. Since then, a variety of starting cell types, different combinations of main transcription factors and techniques used to deliver the transcription factors into cells have been used successfully.

Pluripotent stem cells allow the production of primary human cells of any lineage in a way that can be constantly replenished, just as with cell lines. iPSC derived macrophages are genetically highly related to their original donor cells, sharing phenotypic and functional similarities with primary human macrophages. Being closer to the cells found within the human body, these cells could be more predictive in cellular assays[191]. The use of iPSCs has the added advantage that the cells can be donor specific and have been shown to react in the same way as the macrophages taken from the patient. However, the potential of iPSC derived macrophages in host-pathogen interaction has not been fully investigated.

In the past, a large range of cell types and sources have been used to study infection by *Leishmania* parasites and determination of anti-leishmanial drug activity. Cell lines such as the Sticker dog sarcoma fibroblasts cell line[155], transformed rodent macrophage cell lines[156] and human monocytic cell line, derived from an acute monocytic leukaemia patient (THP-1), have been widely used due to their immortalised status. Cell lines have advantages such as unlimited division potential and are easy to maintain in culture. Cell lines however, are usually immortalised because of a mutation in the controls of the cell cycle; this can affect the response of the cell and its functions. Immortalized cell lines can be created by fusing a primary cell with a cancer cell line. This can lead to the resulting cell line having some of the

properties of the cancer, such as the intended immortalisation but also other phenotypes[190]. The mutation means that the cell line, whilst easy to obtain and use, may not be the same as the cell that they are representing within an *in vitro* system.

Primary isolated cells are cells taken directly from the body, such as mouse peritoneal or bone marrow macrophages and human monocyte-derived macrophages. These cells are normally used straight away, as they only maintain the functionality and similarity to cells within the body for a short period[229]. The main problem with primary cells is that they are difficult to obtain. Human primary cells are mainly generated from surgery and require the patient's permission for research. Mouse cells are more easily obtainable but a Home Office license and training are required for use of animals in experimentation, as well as a specialised unit for the animals. A finite number of cells are obtained from each animal, and this means that multiple animals are needed to generate the number of cells required.

iPSC derived macrophages are both able to proliferate and are primary cells showing similarity to the native cell. They are more difficult to obtain than cell lines and more expensive to maintain. When compared to primary cells, their expansion potential is a great advantage but they can occasionally mutate into a cancer phenotype due to their unrestricted growth cycle[321], caused by the additions of stem cell transcription factors.

There is currently no literature, to the best of my knowledge, on the use of iPSC derived macrophages and *Leishmania* parasites. However, iPSC derived macrophages have been used for other infectious diseases. Such as *Chlamydia trachomatis*[322] and *Salmonella enterica*[323]. A recent paper showed that iPSC derived macrophages support the full infectious life cycle of *C. trachomatis* mimicking the infection of human blood-derived macrophages *in vivo*[322]. Transcriptomic and proteomic profiling of the macrophage response to chlamydial infection highlighted the role of the type I interferon and interleukin 10-mediated responses, as in the body. The researchers used human iPSCs in combination with CRISPR/Cas9 gene editing technology, to knock out genes making the macrophages more susceptible and showing the importance of the gene in resistance to the pathogen, which would be difficult to do on primary cells. They showed the iPSC to be suitable for gene editing with CRISPR/Cas9 and *C. trachomatis* infections, allowing the study of pathogen host interactions[322]. Another group explored the potential of human iPSC derived macrophages to study *S. enterica* interactions[323]. They showed iPSC derived macrophages express a panel of established macrophage specific markers, produce cytokines, and polarise into classical and alternative activation states in response to IFN-γ and IL-4 stimulation, respectively. iPSC derived

macrophages also efficiently phagocytosed inactivated bacterial particles as well as live *Salmonella typhi* and *S. typhimurium* and were able to kill these pathogens. It was concluded that iPSC derived macrophages can support productive *Salmonella* infection and propose this as a flexible system to study host/pathogen interactions[323].

Other groups have used iPSC derived macrophages to study viruses. In one study, researchers generated iPSCs and edited their genome to give a phenotype of resistance to HIV-1 infection. These modified iPSCs were then differentiated into macrophages and demonstrated their resistance to a HIV-1 challenge. It was concluded that this strategy might provide an approach toward a functional cure of HIV-1 infection[324].

The objectives of the work discussed in this Chapter are to:

I.   Establish an infection in iPSC derived macrophages with *Leishmania* parasites and compare with that in other cells that are commonly used in *in vitro* assays.

II. Determine the activity of standard drugs in iPSC derived macrophages and compare with results in other cell lines.

III. Determine the suitability of iPSC derived macrophages as a host cell in *in vitro* assays to investigate the anti-leishmanial activity of compounds.

6.2 Cell Comparison

As mentioned in the previous chapter, the conformation of a cell is important to its function and response to *Leishmania* parasites. Whilst all the cells used in this chapter are cultured in 2D and are all macrophages, they are not all equal. In this section, the different cells were compared, table 6.2-1, showing they come in a variety of sizes and whether this has any effect on the infection with *Leishmania* parasites.

Table 6.2-1 *Table comparing the properties of the four cell types used in this chapter*.

	THP-1 cells	Mouse bone marrow macrophages	Human bone marrow macrophages	iPSC
Abbreviation	THP1	MBMM	HBMM	iPSC
Species	Human	Mouse	Human	Human
Cell type	Monocyte	Mononuclear	Mononuclear	Monocyte
Category	Cell line	Primary cell	Primary cell	iPSC
Source	Acute monocytic leukaemia	Mouse femur and tibia	Bone	Originally Skin
Supplier	ATCC	LSHTM	ATCC	Wellcome Trust Sanger Institute
Differentiation signal	phorbol 12-myristate 13-acetate	Human m-CSF	Human m-CSF	Human m-CSf

6.2.1　Cell Size

The average size of each cell type was measured using two different methods. Firstly, the protein content of the cells was determined using a BCA protein assay, figure 6.2-1, the theory being that the larger the cell, the more protein it will contain. The second method of size determination was to culture each cell type in 3D, then capture images of the cells using the confocal microscope, then analyse the images with the Volocity software to determine cell volume, shown in figure 6.2-1.
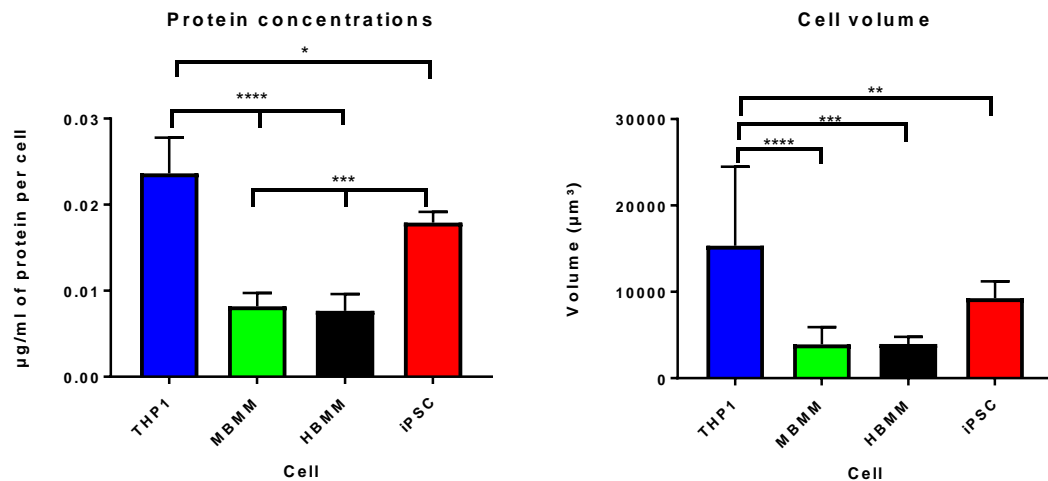
Figure 6.2-1. Protein concentrations of single cells (Left) (N=9) and cell volume (Right) (N=9) for each cell type. Statistical significance in a one-way ANOVA * = p<0.05 ** = p<0.01 *** = p<0.001 **** = p<0.0001. Error bars show SD.

The four cell types can be seen to have the same size order in both measures of cell size, shown in figure 6.2-1. THP-1 cells are the largest, followed by iPSCs while the mouse and human bone marrow macrophages are the smallest and are similar to each other. There are statistical differences among the cells when the data was compared using a one-way ANOVA. The protein concentration of THP-1 cells show a statistical difference when compared to mouse bone marrow macrophages, p<0.0001, human bone marrow macrophages, p<0.0001, and iPSCs, p<0.05. iPSC protein concentrations show statistical differences when compared with the protein concentrations in mouse bone marrow macrophages and human bone marrow macrophages, p<0.001. When comparing the volume of the cells statistical difference was seen only between THP-1 cells and the other three cell types. The volume of THP-1 cells shows a statistical difference when compared to mouse bone marrow macrophages, p<0.0001, human bone marrow macrophages, p<0.001, and iPSCs, p<0.01.

6.2.2   Parasite Burden

To give a representation of how the cell size affects the parasite burden, *L. major* JISH samples from the establishing infection potential section, Chapter 6 Section 3, were re-analysed. The number of parasites in a population of infected cells were counted to give an average parasite burden.
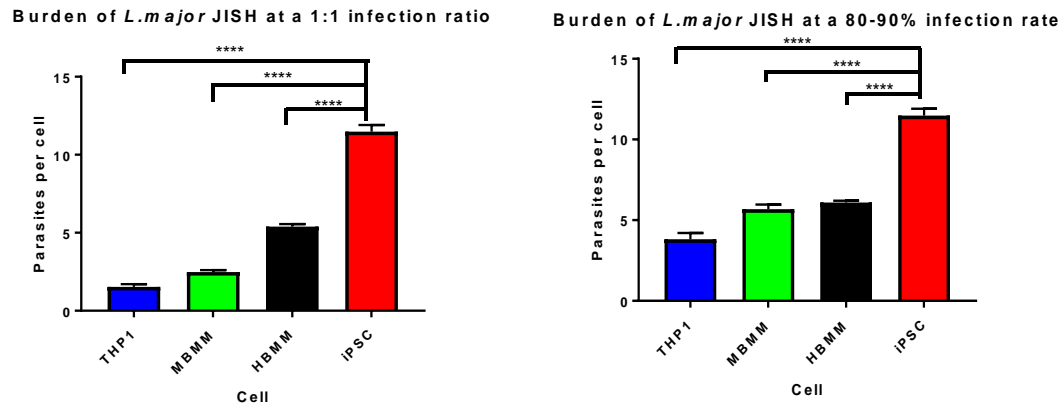
Figure 6.2-2. Two measurements of parasite burden, parasite burden across different cell types when using the same initial infection ratio (Left) (N=3) and parasite burden when 72 hour percentage infection rate was kept within ± 5% (Right) (N=3) in each cell type. Statistical significance in a one-way ANOVA * = $p<0.05$ ** = $p<0.01$ *** = $p<0.001$ **** = $p<0.0001$. Error bars show SD.

When comparing the parasite burden per cell (figure 6.2-2), the same pattern emerges whether burdens are compared across cell types with the same initial infection ratio or cell with the same final infection rate. The pattern shows that parasite burden was highest in iPSC derived macrophages. The next highest burden was in HBMM closely followed by MBMM. Finally, THP1 cells show the lowest parasite burden.

Using a one-way ANOVA, comparing the burden data for the data set generated using samples which all had the same initial infection ratio, statistical significant differences are seen between all cell types, $p<0.0001$, except between THP1 cells and MBMM which have a significance value of $p<0.01$. Using a one-way ANOVA, to compare the burden data for the data set generated using samples which all had the same final infection rate, statistical significant differences are seen between iPSC derived macrophages and all other cell types, $p<0.0001$. Significant differences are also seen between THP1 cells and both MBMM and HBMM, $p<0.001$. No difference was seen between HBMM and MBMM.

The pattern observed in the burden of the cells was that the easier the cell type was to infect the higher the burden is in both sample sets. Cell size has no effect on the parasite burden, this is clear as THP1 cells are the largest cell and show the lowest burden.

6.3 Establishing the Infection Potential

The first step in exploring how the different cell types respond to *Leishmania* infection was to establish an infection within the system. A variety of initial infection ratios have been studied using four different parasite strains to try to establish a high infection rate that is

equivalent across all cell types, for each parasite. An optimal infection rate would be between 80-95%, as this is high enough for reductions to be easily seen, but not so high that the cells are over infected. It is important that the overall levels of infection match, as they will need to be the same to avoid dose inoculum effects when treating with drugs.

6.3.1 Infection Rates

As the initial infection ratio was increased, an increase in percentage infection after 72 hours was seen (figure 6.3-1) for all four parasites strains. The percentage infection after 72 hours showed variation between both strains and cell types. In the *L. major* JISH graph the infection rates, when an initial infection ratio of 0.5 parasites per cell was used, are 11.3, 46.0, 66.4 and 75.1% for the four cells types, THP1, MBMM, HBMM and iPSC derived macrophages respectively. iPSC derived macrophages pass over the 80% mark at a 1:1 ratio and reach 100% infection at an initial infection ratio of 2:1. The HBMM exceed the 80% infection rate at the 3:1 ratio and reach their peak infection at 7:1. The MBMM exceed the 80% infection rate at the 3:1 ratio and reach their peak infection at 5:1. The THP1 cells pass over the 80% infection rate at the 5:1 ratio.

In the *L. major* mCherry graph (figure 6.3-1), the infection rates, when an initial infection ratio of 0.5 parasites per cell was used, are 12.1, 38.2, 67.7 and 70.8% for the four cells types, THP1, MBMM, iPSC derived macrophages and HBMM respectively. iPSC derived macrophages pass over the 80% mark at a 2:1 ratio and reach 100% infection at an initial infection ratio of 3:1. The HBMM pass over the 80% infection rate at the 2:1 ratio and reach their peak infection at 7:1. The MBMM pass over the 80% infection rate at the 5:1 ratio and reach their peak infection at 10:1. The THP1 cells pass over the 80% infection rate at the 5:1 ratio and reach their peak infection at 10:1.

In the *L. amazonensis* graph (figure 6.3-1) the infection rates, when an initial infection ratio of 0.5 parasites per cell was used, are 12.0, 32.7, 42.2 and 50.3% for the four cells types, THP1, MBMM, HBMM and iPSC derived macrophages respectively. iPSC derived macrophages pass over the 80% mark at a 3:1 ratio and reach 100% infection at an initial infection ratio of 7:1. The HBMM pass over the 80% infection rate at the 5:1 ratio and never reach their peak infection, in the tested range. The MBMM pass over the 80% infection rate at the 7:1 ratio and never reach their peak infection, in the tested range. The THP1 cells pass over the 80% infection rate at the 10:1 ratio.

In the *L. mexicana* graph (figure 6.3-1) the infection rates, when an initial infection ratio of 0.5 parasites per cell was used, are 28.8, 44.6, 52.8 and 78.8% for the four cells types, THP1,

HBMM, iPSC derived macrophages and MBMM respectively. iPSC derived macrophages pass over the 80% mark at a 2:1 ratio and reach 100% infection at an initial infection ratio of 5:1. The HBMM pass over the 80% infection rate at the 5:1 ratio and reach their peak infection at 7:1. The MBMM pass over the 80% infection rate at the 1:1 ratio and reach their peak infection at 2:1. The THP1 cells pass over the 80% infection rate at the 7:1 ratio and reach their peak infection at 10:1.
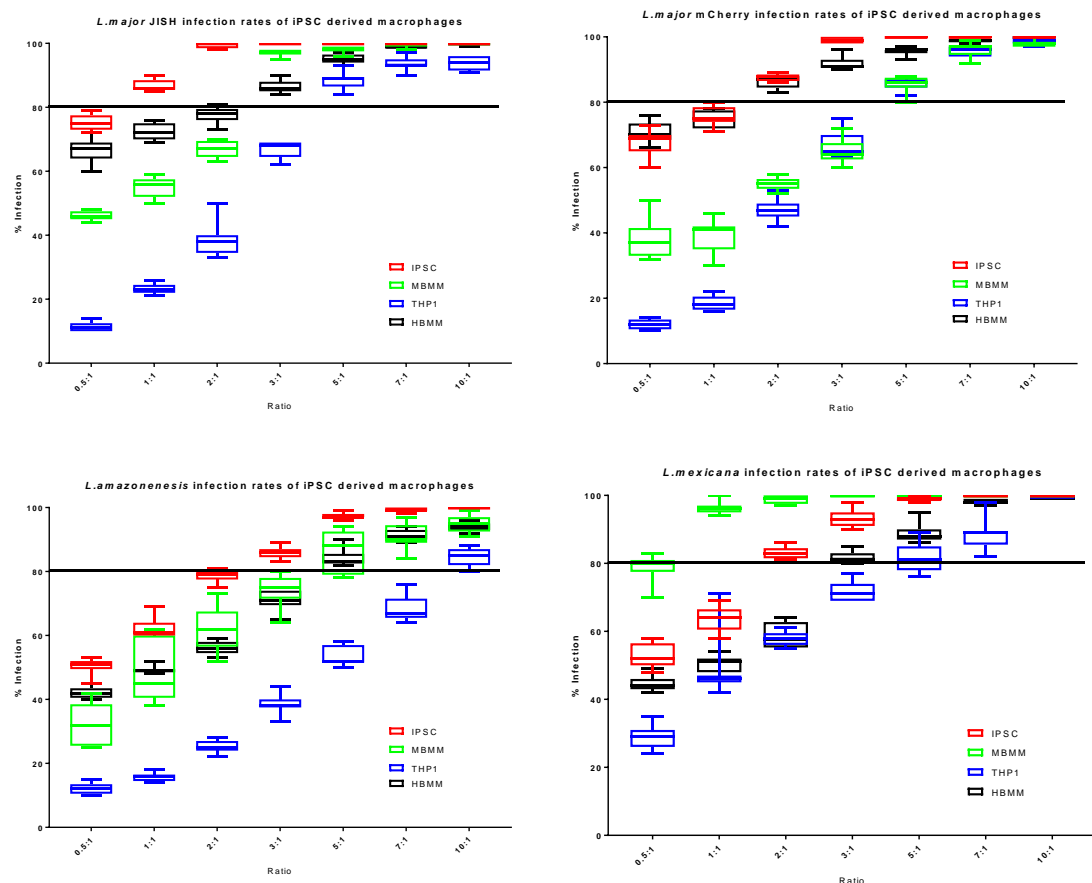
Figure 6.3-1. Percentage infections of *L. major* JISH (Top Left), *L. major* mCherry (Top Right), *L. amazonensis* (Bottom Left) and *L. mexicana* (Bottom Right) after 72 hours measured in each of the four cell types. N = 9. Line shows 80% infection. Error bars show maximum and minimum values.

6.3.2   Strain Variation

Differences in the percentage infection after 72 hours were seen between the four different parasite strains, figure 6.3-1. In THP1 cells, *L. mexicana* gave the highest percentage infection after 72 hours when initial infection ratios of parasite:cell between 0.5:1 to 2:1 were used. At these concentrations the percentage of cells infected with *L. mexicana* was statistically significantly higher than all other parasites used, p<0.0001. Between initial infection ratios of 3:1 and 10:1 in THP1 cells *L. mexicana* had a similar percentage infection after 72 hours as

L. major JISH and *L. major* mCherry. *L. amazonensis* was consistently giving the lowest percentage infection after 72 hours, figure 6.3-1, and was statistically lower than all other parasite strains between initial infection ratios of 2:1 up to 10:1, p<0.0001.

In mouse bone marrow macrophages, *L. mexicana* gave the highest percentage infection after 72 hours at all initial infection ratios. *L. mexicana* gave statistically significantly higher percentage infection than all other parasites used, p<0.0001, until the 3:1 ratio, where *L. major* JISH becomes statistically the same. At an initial infection ratio of 7:1 the *L. major* mCherry becomes statistically the same as the *L. mexicana*. At an initial infection ratio of 10:1 percentage infection with *L. mexicana* showed a smaller statistical significance when compared with *L. amazonensis*, p<0.01. *L. amazonensis* was consistently giving the lowest percentage infection after 72 hours, and was statistically lower than all other parasite strains, except *L. major* mCherry, at initial ratios of 5:1 and 10:1.

In human bone marrow macrophages, *L. major* JISH and *L. major* mCherry gave the highest percentage infections after 72 hours at all initial infection ratios, figure 6.3-1. The two strains gave a statistically significantly higher percentage infection than other parasites used, until the 7:1 ratio. After this, all parasites gave near 100% infection rates after 72 hours. *L. mexicana* and *L. amazonensis* showed similarity in the percentage infection between an initial infection ratios of 0.5:1 to 2:1. After this *L. amazonensis,* again, becomes the strain that causes the lowest percentage infection.

In iPSC derived macrophages, *L. major* JISH gave the highest percentage infections after 72 hours, at all initial infection ratios, figure 6.3-1. The two *L. major* strains gave a statistically significantly higher percentage infection, p<0.0001, than other parasites used until the 3:1 ratio, when the infection rate reaches 100%. At 5:1, all parasite strains gave infection rates near 100% after 72 hours. *L. major* mCherry gave the next strongest infection rates, at the lower initial infection ratios, followed by *L. mexicana. L. amazonensis* again showed the lowest percentage infection of all strains at any initial infection ratio.

To give an overall perspective, *L. amazonensis* consistently gave the lowest percentage infection at most initial infection ratios. *L. mexicana* gave the highest infection in both THP1 cells and mouse bone marrow macrophages. *L. major* JISH gave the strongest infection in iPSC derived macrophages and *L. major* mCherry gave the strongest infection in human bone marrow macrophages. In general, *L. major* JISH*, L. major* mCherry and *L. mexicana* all gave over 80% infection rates at the same initial infection ratio across the different cell types.

6.3.3 Discussion

THP1 cells consistently showed the lowest percentage infection when infected at any ratio of parasites to cells. They are the cell type that was most resistant to infection by *Leishmania* parasites. The iPSC derived macrophages showed the highest percentage infection for most of the infection ratios, across the four parasites used. Mouse and human bone marrow macrophages showed similar infection when using *L. major* JISH and *L. amazonensis*, but when using *L. mexicana* mouse bone marrow macrophages showed a higher infection than human bone marrow macrophages. The opposite was seen when using *L. major* mCherry, with human bone marrow macrophages showing a higher infection than mouse bone marrow macrophages.

All cell types used were successfully able to phagocytose *Leishmania* parasites, and infection was sustained up to 72 hours. Each cell has the required receptors for *Leishmania* entry to the cells; however, the number of receptors may differ between cell types. Another difference between the cell types could be the survival process for the *Leishmania*. A study[339] has shown that the iPSC derived macrophages and THP1 cells are both able to phagocytose inert particles at similar rates. Further to this, a study[340] on the differential gene expression in macrophages upon polarization looked at the gene expression of all four cell types used here. They concluded that the iPSC derived macrophages were most similar to the human bone marrow macrophages. The results of the experiments in this chapter show the same, with infection rates similar between the iPSC derived macrophages and the human bone marrow macrophages. The paper's[340] findings, for the classical M1 type activation, shows that the mouse bone marrow macrophages show the most difference when compared to the other cell types. This result, of mouse bone marrow macrophages showing the most difference, was not replicated in the experiments in this chapter, as the data produced shows THP1 cells to have the largest difference in response to *Leishmania* parasites.

In a previous study[341], *L. infantum* was used to infect macrophages derived from human peripheral blood, macrophages differentiated from human cell line U-937, mouse bone marrow derived macrophages, mouse peritoneal macrophages and canine monocyte-macrophage cell line DH82. The study showed mouse peritoneal macrophages and DH82 macrophages were less permissive to *Leishmania* infection. The other three showed similar infection rates. Although these are not the same cells as those used in our study, the results in this thesis agree by showing similar percentage infection between mouse and human bone marrow macrophages, whilst the cell line show the lowest infection.

The goal of this set of experiments was to elucidate the initial infection ratio that would give an overall infection percentage after 72 hours of between 80-90%. This is important as it means that future experiments can be standardised, giving similar percentage infections in all wells after 72 hours, using any parasite strain or cell type. Using the information in table 6.3-1, dose inoculum effects can be avoided and treatment with drugs can be compared fairly.

Table 6.3-1 *Table showing the optimal initial infection ratio for each parasite strain for each of the four different cell types used in this results chapter.*

Species	THP1	mBMM	hBMM	iPSC
L. major JISH	5:1	3:1	3:1	1:1
L. major mCherry	5:1	5:1	2:1	2:1
L. amazonensis	10:1	7:1	7:1	3:1
L. mexicana	7:1	1:1	5:1	2:1

6.4 Determining the Efficacy of Standard Drugs
6.4.1 amphotericin B

A dose-response was seen when amphotericin B was used to treat the infected macrophages (figure 6.4-1). EC_{50} and EC_{90} values for the amphotericin B treatment, of each cell type infected with each parasite are shown in table 6.4-1.

Table 6.4-1 *EC_{50} and EC_{90} results for amphotericin B against different parasites in different cell types.*

Parasite/Cell	Value	IPSC (nM)	MBMM (nM)	THP1 (nM)	HBMM (nM)
L. major JISH	EC_{50}	35.9	33.5	46.4	33.6
	EC_{90}	105.2	62.9	69.8	54.4
L. major mCherry	EC_{50}	70.7	44.1	69.0	38.2
	EC_{90}	182.0	85.0	102.8	78.5
L. amazonensis	EC_{50}	79.8	60.9	63.4	51.1
	EC_{90}	229.2	251.6	163.5	188.8
L. mexicana	EC_{50}	59.8	55.4	76.5	67.8
	EC_{90}	102.4	109.2	140.1	131.5

A two-way ANOVA, testing the influence of cell type on the treatment of *L. major* JISH parasite infection, showed a statistical difference between iPSC derived macrophages and

THP1 cells at the highest drug concentration used, $p < 0.05$. At the second highest concentration statistical difference was seen in the percentage reduction between iPSC derived macrophages and all other cell types, $p < 0.0001$. At the second lowest concentration statistical difference was seen in the percentage reduction between all cell types, $p < 0.0001$. At the lowest concentration statistical difference was seen in the percentage reduction between iPSC derived macrophages and all other cell types, $p < 0.001$.

When a two-way ANOVA, testing the influence of cell type on the treatment of *L. major* mCherry parasite infection, was used a statistical difference was seen between iPSC derived macrophages and all other cell types at the highest concentration used, $p < 0.0001$. At the second highest concentration, statistical difference was seen in the percentage reduction between all cell types, $p < 0.0001$, except when comparing MBMM and HBMM. At the second lowest concentration, statistical difference was seen in the percentage reduction between all cell types, $p < 0.0001$. At the lowest concentration, no statistical difference was seen.

When a two-way ANOVA was used, testing the influence of cell type on the treatment of *L. amazonensis* parasite infection, no statistical difference was seen at the highest concentration used. At the second highest concentration, statistical difference was seen in the percentage reduction between all cell types $p < 0.01$, except between iPSC derived macrophages and MBMM and between THP1 cells and HBMM. At the second lowest concentration, statistical difference was seen in the percentage reduction between all cell types, $p < 0.001$. At the lowest concentration, statistical difference was seen in the percentage reduction between MBMM and all other cell types, $p < 0.05$.

When a two-way ANOVA, testing the influence of cell type on the treatment of *L. mexicana* parasite infection, was used no significant difference was seen between any of the cell types used at the highest concentration. At the second highest concentration, statistical difference was seen in the percentage reduction between all cell types, $p < 0.01$, except when comparing iPSC derived macrophages and MBMM. At the second lowest concentration, statistical difference was seen in the percentage reduction between all cell types, $p < 0.01$. At the lowest concentration, no significant difference was seen in the percentage reduction when comparing all cell types, except between HBMM and THP1 cells, $p < 0.01$.
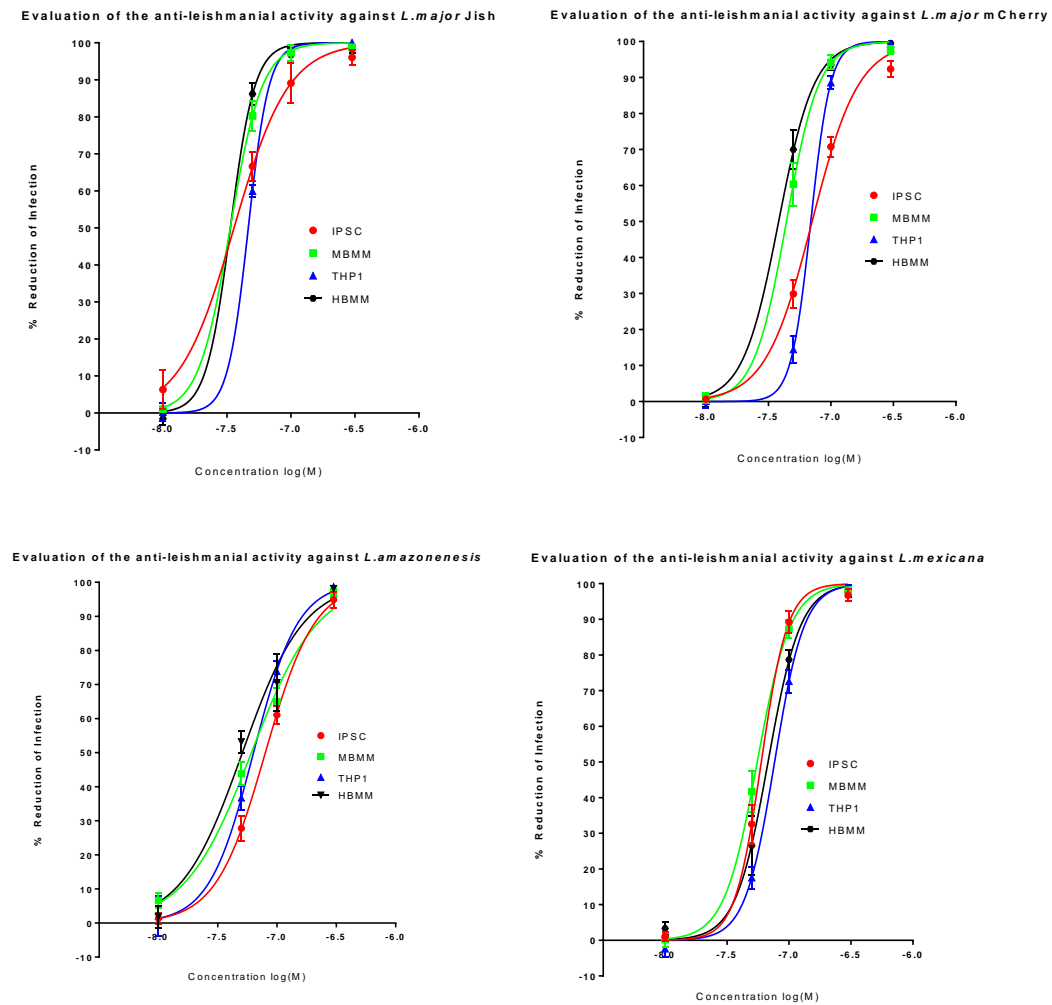
Figure 6.4-1. Reduction of percentage infections of *L. major* JISH (Top Left), *L. major* mCherry (Top Right), *L. amazonensis* (Bottom Left) and *L. mexicana* (Bottom Right) after 72 hours caused by treatment with amphotericin B measured in each of the four cell types. N = 9 Error bars show Standard deviation (SD)

6.4.2   Miltefosine

A dose-response was seen when miltefosine was used to treat the infected macrophages, figure 6.4-2. EC_{50} and EC_{90} values for the miltefosine treatment of each cell type infected with each parasite are seen in table 6.4-2.

Table 6.4-2 *EC_{50} and EC_{90} results for miltefosine against all parasites in all cell types used.*

Parasite/Cell	Value	IPSC (µM)	MBMM (µM)	THP1 (µM)	HBMM (µM)
L. major JISH	EC_{50}	5.8	6.4	7.7	7.4
	EC_{90}	37.0	19.2	17.4	34.2
L. major mCherry	EC_{50}	15.3	14.9	9.6	4.9
	EC_{90}	105.2	170.3	67.7	16.1
L. amazonensis	EC_{50}	76.6	25.3	28.2	14.3
	EC_{90}	229.2	251.6	163.5	188.8
L. mexicana	EC_{50}	5.3	5.0	4.8	6.0
	EC_{90}	17.2	16.1	15.8	25.1

A reduction in percentage infection was seen when increasing the concentration of miltefosine used to dose, across all cell types and all *Leishmania* species used, although it was noticeably weaker against *L. amazonensis*. When a two-way ANOVA was used, testing the influence of cell type on the treatment of *L. major* JISH parasite infection, statistical difference was seen between all cell types used, $p < 0.0001$, at the highest concentration, except between iPSC derived macrophages and HBMM and between THP1 cells and MBMM. At the second highest concentration, statistical difference was seen in the percentage reduction between MBMM and all other cell types, $p < 0.05$. At the second lowest concentration, statistical difference was seen in the percentage reduction between all cell types, $p < 0.0001$, except between MBMM and HBMM. At the lowest concentration, statistical difference was seen in the percentage reduction between iPSC derived macrophages and both MBMM and THP1 cells, $p < 0.01$. Significant differences are also seen between THP1 cells and HBMM, $p < 0.01$.

When a two-way ANOVA was used, testing the influence of cell type on the treatment of *L. major* mCherry parasite infection using miltefosine, statistical difference was seen between HBMM and all other cell types at the highest concentration used, $p < 0.0001$. A significant difference was also seen when comparing MBMM and THP1 cells at the highest concentration of miltefosine. At the second highest concentration, statistical difference was seen in the percentage reduction when comparing all cell types, $p < 0.0001$, except when comparing MBMM and iPSC derived macrophages. At the second lowest concentration, statistical difference was seen in the percentage reduction between all cell types, $p < 0.0001$, except when comparing MBMM to either HBMM or THP1 cells. At the lowest concentration,

statistical difference was seen when comparing HBMM to the other cell types, p<0.05, same comment as above, group

When a two-way ANOVA, testing the influence of cell type on miltefosine treatment of *L. amazonensis* parasite infection, statistical difference was seen at the highest concentration used between all cell types, p<0.0001, except between MBMM and THP1 cells. At the second highest concentration, statistical difference was seen between all cell types p<0.05, except between HBMM and MBMM. At the second lowest concentration, statistical difference was seen in the percentage reduction between iPSC derived macrophages and both HBMM and MBMM, p<0.001. Significant differences are also seen between THP1 cells and HBMM, p<0.001, at the second lowest concentration. At the lowest concentration, no statistical difference was seen in the percentage reduction any of the cell types.

When a two-way ANOVA was used, to test the influence of cell type on the treatment of *L. mexicana* parasite infection with MIL, no significant difference was seen between any of the cell types used at any concentration except the second highest. At the second highest concentration, statistical difference was seen in the percentage reduction between HBMM and all other cells types, p<0.0001.
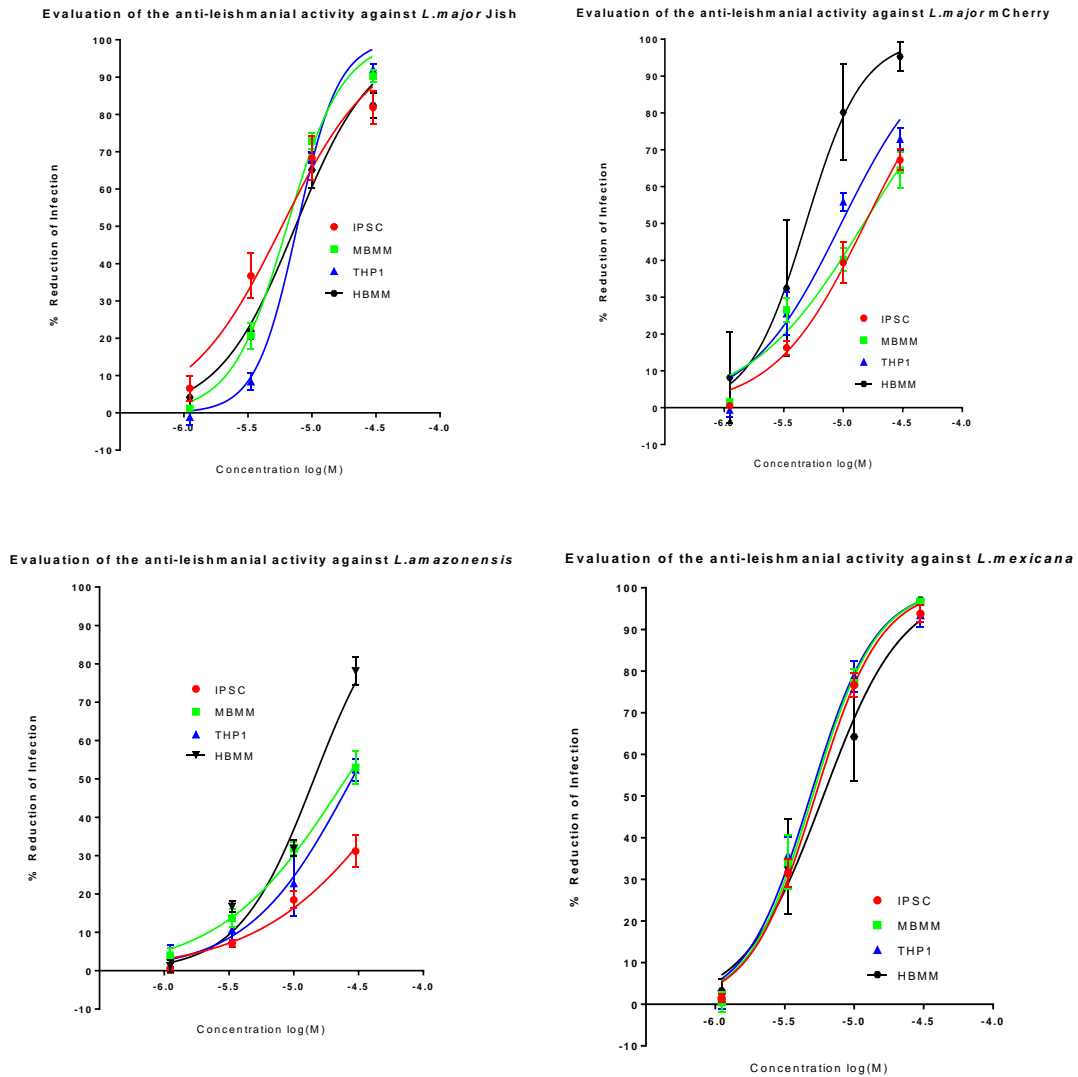
Figure 6.4-2. Reduction of percentage infections of *L. major* JISH (Top Left), *L. major* mCherry (Top Right), *L. amazonensis* (Bottom Left) and *L. mexicana* (Bottom Right) after 72 hours caused by treatment with miltefosine measured in each of four cell types. N = 9 Error bars show SD.

6.4.3   Sodium Stibogluconate

A dose-response was seen when sodium stibogluconate was used to treat the infected macrophages, figure 6.4-3. EC_{50} and EC_{90} values for the sodium stibogluconate treatment of each cell type infected with each parasite are seen in table 6.4-3.

Table 6.4-3 *EC_{50} and EC_{90} results for sodium stibogluconate against all parasites in all cell types used.*

Parasite/Cell	Value	IPSC (µg of SB^V/ml)	MBMM (µg of SB^V/ml)	THP1 (µg of SB^V/ml)	HBMM (µg of SB^V/ml)
L. major JISH	EC_{50}	355	2770	186	348
	EC_{90}	N/A	N/A	N/A	N/A
L. major mCherry	EC_{50}	220	730	253	434
	EC_{90}	N/A	N/A	N/A	N/A
L. amazonensis	EC_{50}	306	503	459	255
	EC_{90}	N/A	N/A	N/A	N/A
L. mexicana	EC_{50}	347	435	1840	299
	EC_{90}	N/A	N/A	N/A	N/A

When a two-way ANOVA was used, to test the influence of cell type on the treatment of *L. major* JISH parasite infection with sodium stibogluconate, statistical difference was seen between all cell types at the highest concentration used, $p<0.0001$. At the second highest concentration, statistical difference was seen in the percentage reduction between iPSC derived macrophages and all other cell types, $p<0.0001$, except between iPSC derived macrophages and HBMM, which only gave a p value less than 0.05. At the second lowest concentration, statistical difference was seen in the percentage reduction between all cell types, $p<0.0001$, except between THP1 cells and HBMM. At the lowest concentration, no statistical difference was seen in the percentage reduction between any of the cell types, except between MBMM and THP1 cells, $p<0.01$.

When a two-way ANOVA was used, to test the influence of cell type on the sodium stibogluconate treatment of *L. major* mCherry parasite infection, statistical difference was seen between all cell types at the highest concentration used, $p<0.0001$. At the second highest concentration, statistical difference was seen in the percentage reduction between all cell types, $p<0.0001$, except when comparing THP1 cells and iPSC derived macrophages. At the second lowest concentration, statistical difference was seen in the percentage reduction between MBMM and all cell types, $p<0.0001$. At the lowest concentration, statistical difference was seen between iPSC derived macrophages and MBMM and THP1 cells, $p<0.05$.

When a two-way ANOVA was used to test the influence of cell type on the treatment of *L. amazonensis* parasite infection with sodium stibogluconate, statistical difference was seen at the highest concentration used, between the different cell types used, $p < 0.0001$. At the second highest concentration, statistical difference was seen in the percentage reduction between all cell types $p < 0.01$. At the second lowest concentration, statistical difference was seen in the percentage reduction between all cell types, $p < 0.0001$, except when comparing MBMM and THP1 cells. At the lowest concentration, statistical difference was seen in the percentage reduction between HBMM and THP1 cells, $p < 0.05$.

When a two-way ANOVA was used, to test the influence of cell type on the dosing of *L. major* JISH parasite infection with sodium stibogluconate, significant differences are seen between all of the cell types, $p < 0.0001$, at the highest concentration, except when comparing iPSC derived macrophages and MBMM, $p < 0.05$. At the second highest concentration, statistical difference was seen in the percentage reduction between all cell types, $p < 0.01$, except when comparing iPSC derived macrophages and MBMM. At the second highest concentration, statistical difference was seen in the percentage reduction between all cell types, $p < 0.01$, except between iPSC derived macrophages and HBMM. At the second lowest concentration, statistical difference was seen in the percentage reduction between all cell types, $p < 0.01$, except between iPSC derived macrophages and both HBMM and MBMM. At the lowest concentration, no significant difference was seen in the percentage reduction when comparing all cell types.

Figure 6.4-3. Reduction of percentage infections of *L. major* JISH (Top Left), *L. major* mCherry (Top Right), *L. amazonensis* (Bottom Left) and *L. mexicana* (Bottom Right) after 72 hours caused by treatment with sodium stibogluconate measured in each of four cell types. N = 9 Error bars show SD

6.5 Discussion

When using AmB the EC_{50} values generated were similar to each other, across all cell types. There was no set, or repeated order, that was conserved amongst infection using the different species of parasite.

EC_{50} values for MIL show similarity when *L. major* JISH or *L. mexicana* cause the infection. When *L. major* mCherry was used, responses are more variable. However, when *L. amazonensi*s was used, the MIL was seen to be ineffective in treating the infection. There was no repeated pattern seen in the data, no one cell type that responds better to the treatment with MIL no matter the species used. When EC_{90} values were compared, THP1

cells show the lowest EC_{90} values and iPSC derived macrophages showed the highest EC_{90} values.

EC_{50} values for SSG treatment of infected macrophages show relative similarity between cell types with a couple outliers. MBMM gave a very high value for the EC_{50} values when SSG was used to treat *L. major* JISH or *L. major* mCherry infections. Another high EC_{50} value was seen when THP1 cells were infected with *L. mexicana* parasites.

A study[342] on three cell types; THP1 cells, human peripheral blood mononuclear cell derived macrophages and mouse peritoneal macrophages infected with *L. donovani*, tested numerous drug compounds. They showed that the efficacy of the drug molecules changed depending on the cell type used. This was shown in the data presented here, also shown in the paper was that there was no pattern of ranking between the cell types. In the paper, miltefosine was used as a control and the paper showed that it was most potent in mouse peritoneal macrophages, and least potent in THP1 cells. This pattern is replicated when using *L. major* JISH but not for any other parasite species.

Another paper[344] discusses the use of THP1 cells as a model for macrophages, comparing them to circulating monocytes. They found that using THP1 cells had many limitations. THP1 cells have a lower response to lipopolysaccharide due to a low expression of CD14 in comparison to circulating monocytes. This in turn leads to low IL-8 production and a lower response to bacteria. This shows that although the THP1 cell line may be useful it does not always respond as expected of human macrophages. Indeed, in the experiments in this thesis it is shown to require a higher number of parasites to achieve infection, when compared to other cell types.

A much larger variation was seen when comparing the EC_{50} and EC_{90} values between *Leishmania* species in the same cell type. Overall, when comparing the efficacies of all three drugs, to all of the parasites, in each cell type, there is no obvious pattern. When the drugs are considered separately then patterns are more obvious. When using amphotericin B, *L. major* JISH shows the lowest EC_{50} values across all cell types. The highest EC_{50} value are produced when amphotericin is used against either *L. amazonensis* or *L. mexicana.* When miltefosine was used, *L. amazonensis* always showed the highest EC_{50} value. The next highest EC_{50} values was usually seen when using miltefosine to dose *L. major* mCherry infected macrophages. There was no species pattern seen when using sodium stibogluconate.

What can be seen in this section is that iPSC derived macrophages respond just as well to drug treatment as other cell types commonly used in *in vitro* assays[325]. The curves generated do not look out of place next to the curves generated by the other cell types, the same patterns in reduction of infection is seen in all cell types, when using the same parasite species. The EC_{50} values produced match values seen in the literature[50, 316 & 325] and produced in other labs using the same cell types. When comparing the iPSC derived macrophages to the range of values seen in the literature, when the standard drugs were used, the iPSC fit within the range of accepted values.

The amount of literature on iPSCs, and more specifically iPSC derived macrophages, is relatively small at the moment. Those papers that do use iPSC derived macrophages are usually papers that are establishing them as a model for a disease, specifically showing that they can be infected and respond as expected. The papers rarely compare the iPSC model to other models using different cell types, and never do this in a quantified experiment. The work in this thesis is novel for many reasons; not only does it show iPSC derived macrophages as a model for *Leishmania,* it quantitatively compares them to other cell types used in this area. However, the literature comparing the infection and treatment of *Leishmania* in different cell types is also difficult to find. A low number of papers use numerous cell types, and an even lower number use a panel of cell types for comparison. With different laboratories actively using different cell types and different species, then data produced by one lab is very difficult to validate.

6.6 Conclusion

Whilst each cell type was a different size, and required slightly different conditions to grow and differentiate, this did not have an effect on how easily the cells were infected or how heavy the parasite burden was.

It has been shown that iPSC derived macrophages are capable of successfully supporting an infection with *Leishmania* parasites of a variety of species. The studies show that the iPSC derived macrophages are often the easiest cell to infect.

It has also been shown that infected iPSC derived macrophages respond as expected to treatment with standard drugs. The response shown provides EC_{50} and EC_{90} values that are similar to those obtained using other cell types.

As iPSC derived macrophages were easily infected with *Leishmania* parasites, and the infection was reduced with treatment using standard drugs, they represent a useful cell type that could be used in *in vitro* models.

Chapter 7: Conclusion

7.1 Conclusion

The aim of the project was to assist the discovery and development of drugs against *Leishmania* by developing *in vitro* tissue culture infection models, which are more predictive of the *in vivo* infection.

The objectives of the project were to:

I.   Establish and compare 2D static and 2D flow cell culture models, in terms of the influence of flow on host cell infection and on drug activity.

II.   Develop a 3D tissue culture model of infection.

III.   Use iPSC derived macrophages to determine whether they offer a valid alternative to currently used cell types.

To date, there is no literature on *in vitro* models for *Leishmania* infection in the skin, or on drug screening in *in vitro* models incorporating media perfusion, 3D cell culture or iPSC derived stem cells. An *in vitro* model with such added complexity could be extremely useful, and the aim of this work was to develop and characterise more complex models for drug discovery. A complex *in vitro* model (compared to the standard 2D cell line based one) could be more predictive, by providing a more advanced/complete infection for drug screening, and this is expected to enhance *in vitro-in vivo* correlations.

In Chapter 3, the objective was to establish a 2D media perfusion cell culture model and establish methods to study *Leishmania* infection. I compared the Kirkstall Ltd Quasi Vivo 500 and the Quasi Vivo 900 media perfusion systems, eventually choosing the QV900 media perfusion system. *In silico* modelling was conducted on the QV900 to compare the two media perfusion systems and to justify the chosen flow rate. Interstitial flow rates between 0.1–2 μms^{-1} have been reported in the literature[233-235], the QV900 modelling showed that our chosen flow rate was 0.15 μms^{-1} when a 3D printed insert was placed in the chamber of the media perfusion system. A colorimetric method was adapted for use with *L. major* JISH parasites and the media perfusion system. Infection studies showed that the media perfusion system inhibited the progression of infection. When infection studies were conducted in the media perfusion system, the percentage infection counted after 72 hours was lower than the percentage infection seen in static controls. The data showed the higher the velocity of the

media at the cells' surface the lower the percentage infection was after 72 hours. To investigate this the proliferation of the *Leishmania* parasites in the host cell was measured, showing the parasites in the media perfusion system were dividing at a slower rate. This lower rate of proliferation could result in a lower infection after 72 hours, seen within the media perfusion system.

In Chapter 4, I compared 2D static and 2D flow cell culture models, in terms of the influence of flow on drug activity, using the models and methods developed in the previous chapter. I showed that the activities of four standard anti-leishmanial drugs were reduced when cells were treated in the media perfusion systems. To investigate why, I conducted drug accumulation studies, which showed a reduced accumulation of drugs in cells in the media perfusion system. In addition, studies on the production of nitric oxide showed a lower production of nitric oxide in the media perfusion system compared to the static controls.

In vitro cell culture models that incorporate media perfusion are far less common than 3D models. In fact, most models using media perfusion to maintain the cells within the 3D culture. The media perfusion provides a continuous flow of media, reducing the need for daily media changes and providing constant nutrients matching the higher demands of the 3D culture. Media perfusion has been most often incorporated into organoid models, such as the kidney and liver, enabling cells such as hepatocytes to maintain their function *in vitro*. Another field where media perfusion is extensively used is bone cell culture and bone regeneration. For direct comparison with the work undertaken in this thesis, a few papers are of special note. In one paper[358], the authors measured the viability of HepG2 hepatocytes and GBM cancer cells at different media flow velocities, and found the lowest flow velocity to be optimal. In this thesis, I took a different approach, and used the most biologically relevant flow velocity rather than the velocity which enabled the highest cell viability. The complex interplay between increased nutrients and increased shear stress generated by media flow can create a window of optimum flow rates that will differ among media perfusion systems. Another paper[236] shows similar results but compares it to the static conditions showing a better viability in the media perfused culture. A field in which drug transport via media perfusion is important is in models of human placental transfer. Initially, the media perfusion model, produced by Hutson *et al*[363] (2011), did not fully predict the transport of drugs across the placental barrier. After adjusting for differences in maternal and fetal protein binding and blood pH, the perfusion results were able to accurately predict *in vivo* transfer under steady state conditions. The field of microfluidics is new and still

expanding, while organ models with media perfusion are becoming more common, drug testing in these models, especially for infectious diseases, are rare. When microfluidic devices are used for infectious disease, it is far more common for them to be used as diagnostic tools. The results from the comparisons of the media perfusion system to static culture, showed vast differences between the two systems. This is in agreement with what is found in the literature[359], which suggests that the application of media flow contributes far more than 3D cell culture to the outcome of a model. In the paper[359], they showed that with both oral and dermal fibroblasts physiological levels of fluid flow induced widespread changes in gene expression compared to static cultures, including up-regulation of genes.

In Chapter 5, I established a 3D cell culture model on two different scaffolds, then proceeded to try and infect the 3D models. I then developed methods to determine the percentage infection in mouse peritoneal macrophages maintained in the 3D culture. A Volocity based counting method was compared to a computer based analysis method, developed by the 3D scaffold provider, Invitrocue. I then used the infected macrophage model to determine the activity of standard drugs in 3D models and compared it to the currently used model system. I showed that the activity of standard drugs was similar between the 3D model developed and the 2D control.

Complex 3D co-culture skin models have been used to successfully determine skin irritation and cytotoxicity[202] with high rates of accuracy when compared to the *in vivo*[203] studies. The models have been so successful that they have replaced animal models in some areas of cosmetics and toxicity testing[353]. Many commercial examples of *in vitro* skin models are commercially available and many research groups have developed their own model for use in a specific disease state[356]. In terms of the work in this thesis, the 3D model we use is rudimentary in comparison, using only macrophages to study the main relevant *Leishmania* interaction with the host. Having said that, the model we have developed for infection and determination of drug efficacy is a first in the field for *Leishmania.* Skin based models for infectious diseases are far less common, with most of them being used to study the interaction between the invading pathogen and host skin[355&356], and treatment of such an infection is usually only a future plan once the model has been fully characterised. An example where treatment has been examined, as described in a paper by Andrei *et al*[357] (2005) where compounds were tested against a variety of viruses that had colonised an *in vitro* skin model. The authors showed that the compounds reduced virus titre, with

comparative efficacies to those seen in 2D culture. Our results reflect this; we showed drug efficacies were similar in 2D and 3D cell cultures.

In Chapter 6, I aimed to determine whether iPSC derived macrophages are a valid alternative to currently used cell types. I did this by establishing an infection in iPSC derived macrophages with *Leishmania* parasites, which was compared with other cells that are commonly used cells in *in vitro* assays. I showed that the iPSC derived macrophages were capable of maintaining a *Leishmania* infection. Percentage infection was higher in iPSC derived macrophages for several different *Leishmania* species/strains. I then determined the activity of standard drugs in iPSC derived macrophages to compare with results in other cell lines. iPSC derived macrophages showed the expected response to standard drugs, and showed similar EC_{50} values to those that have been reported in literature for other cell types. I concluded that iPSC derived macrophages are a suitable model cell type for use in the study of *Leishmania*.

The development of iPSCs is a recent development, and their full potential is still being fully explored. Most papers discuss the possibility of using the iPSCs to derive cells that could then be used in infections, and some go as far as showing that the cells will sustain an infection just as well as previous models. The focus then switches to the interaction between the pathogen and the cells, or to the cellular response to the infection. Groups working in this area are categorising the responses seen in the model, to understand the biology before moving forward with treatment. The work conducted in this thesis is the only work conducted on *Leishmania* infections and treatment in iPSC derived macrophages. To date, there is no literature available comparing the efficacies of drug compounds in iPSC derived macrophages to a range of different cell types, using a range of *Leishmania* strains.

The ultimate goal of biomedical research is to develop new and improved therapies, vaccines or diagnostics. Advances have been made in developing disease models, like the development of transgenic mice for *in vivo* studies. Advances in *in vitro* modelling have also been made in several fields, where the use of 3D cell culture, microfluidic devices and stem cell technologies have led to an improvement in the design of disease models. However, many of these models fail to fully reproduce the human condition. Another problem is that while some scientific fields have fully adopted these advances to bring complexity into the models used, such as toxicology, other fields have not responded to the changes created by recent advances. While in the field of infectious disease modelling, efforts have been made to improve the predictivity of models using recent advances, we are still a long way behind

other fields. Even when models incorporating more complexity have been produced, they are considered to be novel and are not adopted for use by other researchers in the field. The field of drug discovery using infectious disease models has not fully accepted that by improving their models, the outcome may also be improved. A more predictive disease model would not just give a better indication of whether a potential drug candidate will be successful; it will also allow compounds that may not fare well in simple *in vitro* cell culture to be discovered.

A recent review[345] on the opportunities and challenges in phenotypic drug discovery suggests that a resurgence of phenotypic drug screening may be occurring. They suggest that the reason for this is the existence of more advanced and complex disease models, which better reflects the disease *in vivo*. This opens up new opportunities to discover novel drug entities, as phenotypic screening in complex models could identify interactions that were previously uncaptured in simpler models, which can then become targets.

The aim of this project was to develop a more predictive *in vitro* model (compared to the current 2D macrophage cell lines), which could be used as an extra step between *in vitro* and *in vivo* studies, giving another chance for low potency compounds to be discovered. The model could help reduce animal usage and save both time and money spent pursuing poor compounds. It could also provide a new platform for drug discovery, as new interactions are incorporated within the model and the biological system is better replicated. The work presented in this thesis as a whole is both novel in substance and viewpoint, no literature exists on an *in vitro* model that has been broken down to its component parts, and then tested to see the effect each component brings to the model. In the field of *Leishmania*, the work conducted on *Leishmania* infections in 3D, under flow conditions or in iPSC derived macrophages is all first of its kind.

7.2 Future Work

In the context of improving existing models and elucidating how each increase in complexity will affect the model as a whole, as shown in this thesis, one area has been overlooked. The addition of other cell types to a model could be very important. Co-culture models incorporate the complex interaction between different cell types that is found *in vivo*. Originally, this was part of the work in this thesis but the questions raised by experiments led us to appreciate that the time and resources needed were not possible within this PhD. Plans for using co-culture in the model for *Leishmania* involved the culture of macrophages in co-culture with fibroblasts and keratinocytes. This would effectively capture the

environment of the skin and allow a simulation of cutaneous leishmaniasis to be established. *Leishmania* parasites are capable of infecting any cell that can carry out phagocytosis, this includes fibroblasts. This infection of fibroblasts may affect the infection profile of the cell culture and may have long term ramifications. It has been suggested that fibroblast may act as a reservoir for *Leishmania* parasites, which can thus hide from the immune system[20].

Another reason this section of work was left until last was that it would be the starting point of bringing all the different parts of the thesis together, figure 7.2-1. Further plans were to assess whether a model where macrophages and fibroblasts were mixed together inside a 3D scaffold and then layered with keratinocytes would correctly mimic skin. The layered model would then be maintained in the media perfusion system, first submerged to allow cell growth and differentiation, and then raised to an air liquid interface to allow keratinisation of the keratinocytes at the top of the model[365]. Another option would be to create the skin substitute 3D model with fibroblasts and keratinocytes, created using the media perfusion system and an air liquid interface, then have the macrophages circulating in the media perfusion system as monocytes and see if they would be attracted to the signals generated from the infected skin. Another option would be to incorporate the use of iPSC derived cells into the model. The iPSCs could be derived into macrophages, fibroblasts and keratinocytes for the model. Using cells that are all from a single source, and share the same DNA, might give the most relevant model. This model would have reduced variability, in comparison to models created from multiple cell lines. In addition, the iPSC derived models would be identical to each other each time they were produced, providing a reproducible model that would hopefully lead to more reproducible results.

Infection studies using this model would be used to determine the best way to apply promastigotes; whether by injection with a needle or potentially using infected sand flies. To determine infection levels in these models new methods of detection would have to be utilised. The colorimetric assay used in this thesis could be used to detect the levels of infection, as conventional microscopy would be impossible, and confocal microscopy would require many more specific cell labels to identify each cell type. Another option would be the use of a reverse transcriptase quantitative polymerase chain reaction assay (RTqPCR)[169]. This could be used to detect the RNA of the parasites and the macrophages to give an accurate reading of how many host cells and parasites were present within the sample. The reverse transcriptase part of the assay has the advantage over standard qPCR that only live cells are producing RNA and the RNA, from dead cells will be rapidly degraded.

Once an infection model has been established, the next step would be to test its application for the determination of drug efficacies. Again, the complexity of the model allows for the route of drug administration to be varied. The dose of compound could be applied to the model through a topical application of the compound, possible now due to the size and nature of the model and its ability to mimic skin functions. Another option could be through the media circulating in the media perfusion system, which would mimic a systemic route of administration. This systemic route has implications for the pharmacokinetic and pharmacodynamics modelling of the compound within the system. PK/PD modelling and simulation can be used to provide answers on efficacy and safety of new drugs faster and at a lower cost[366]. Using the media perfusion system, the compound could be applied either in a continuous manner or in a pulsed scenario, mimicking the fluctuating levels of drug found within the body. These drug level fluctuations could be tailored, in both concentration and duration, allowing the fluctuations of drug seen within the body to be replicated. An example where this method has already been utilised in seen in papers by Bakshi *et al*[237 &364], which studied the different profiles of anti-malarial drugs when they were applied in a media perfusion system in either a bolus or continuous manner. This method requirement for efficacy showing the drugs match pharmacokinetics obtained *in vivo*. Data provided by this PK/PD study can be used to make changes to the computer modelling, allowing for better predictions in both the *in silico* and *in vitro* models.

The most important next step for this project would be to validate the model in comparison to both existing *in vitro* and *in vivo* models. Whilst direct comparisons could be difficult, a selection of unknown compounds could be blindly tested in the different models to determine if the rank order of their efficacies was the same. This would help to prove the predictability and validity of the model, and mean that in future it could be used before *in vivo* studies in animals.
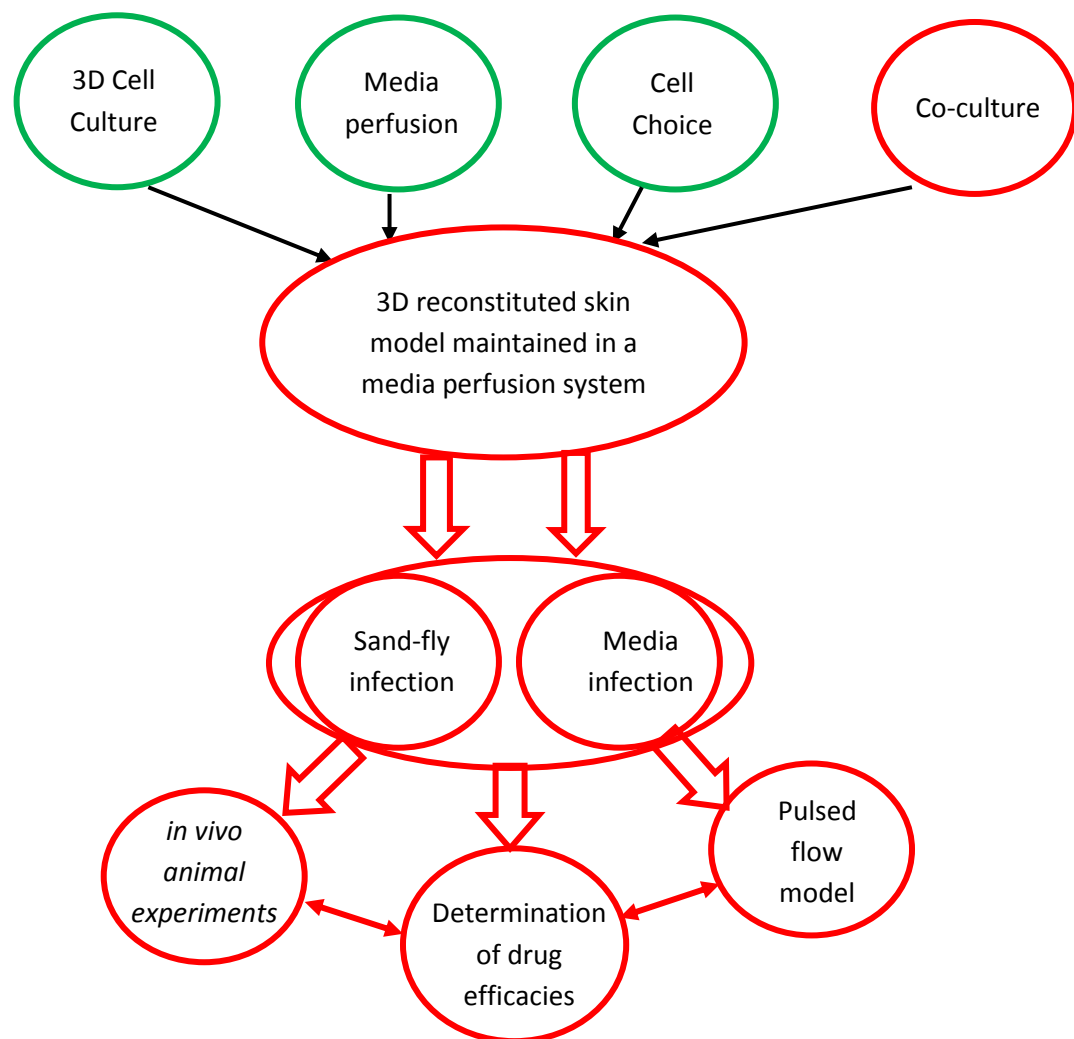
Figure 7.2-1. Schematic of possible future work

References

1. Kevric, I., Cappel, M. A., & Keeling, J. H. (2015). New World and Old World *Leishmania* Infections. *Dermatologic clinics*, *33*(3), 579-593.

2. Desjeux, P. (2004). Leishmaniasis: current situation and new perspectives. *Comparative immunology, microbiology and infectious diseases*, *27*(5), 305-318.

3. Leishman, W. B. (1903). On the possibility of the occurrence of trypanosomiasis in India. *British medical journal*, *1*(2213), 1252.

4. Boyd, J. S. (1963). Leonard Rogers. 1868-1962. *Biographical Memoirs of Fellows of the Royal Society*, 261-285.

5. Ross, R. (1903). Further notes on Leishman's bodies. *British medical journal*, *2*(2239), 1401.

6. Alvar, J., Vélez, I. D., Bern, C., Herrero, M., Desjeux, P., Cano, J. & WHO Leishmaniasis Control Team. (2012). Leishmaniasis worldwide and global estimates of its incidence. *PloS one*, *7*(5), e35671.

7. Garnier, T., & Croft, S. L. (2002). Topical treatment of cutaneous leishmaniasis. *Current Opinion in Investigational Drugs*. 3(4): © PharmaPress ISSN 1472-4472

8. WHO, *Leishmaniasis: worldwide epidemiological and drug access update*. 2012, World Health Organisation.

9. Kaye, P., & Scott, P. (2011). Leishmaniasis: complexity at the host-pathogen interface. *Nature reviews. Microbiology*, *9*(8), 604.

10. Bates, P. A. (2007). Transmission of Leishmania metacyclic promastigotes by phlebotomine sand flies. *International journal for parasitology*, *37*(10), 1097-1106.

11. Killick-Kendrick, R. (1986). Part I. IV The Transmission of Leishmaniasis by the Bite of the Sandfly. *Journal of the Royal Army Medical Corps*, *132*(3), 134-140.

12. Rogers, M. E., Ilg, T., Nikolaev, A. V., Ferguson, M. A., & Bates, P. A. (2004). Transmission of cutaneous leishmaniasis by sand flies is enhanced by regurgitation of fPPG. *Nature*, *430*(6998), 463.

13. Peters, N. C., & Sacks, D. L. (2009). The impact of vector-mediated neutrophil recruitment on cutaneous leishmaniasis. *Cellular microbiology*, *11*(9), 1290-1296.

14. Tacchini-Cottier, F., Zweifel, C., Belkaid, Y., Mukankundiye, C., Vasei, M., Launois, P. & Louis, J. A. (2000). An immunomodulatory function for neutrophils during the

References

induction of a CD4+ Th2 response in BALB/c mice infected with *Leishmania major*. *The Journal of Immunology*, *165*(5), 2628-2636.

15. Peters, N. C., Egen, J. G., Secundino, N., Debrabant, A., Kimblin, N., Kamhawi, S. & Sacks, D. (2008). In vivo imaging reveals an essential role for neutrophils in leishmaniasis transmitted by sand flies. *Science*, *321*(5891), 970-974.

16. Moore, K. J., & Matlashewski, G. (1994). Intracellular infection by *Leishmania donovani* inhibits macrophage apoptosis. *The Journal of Immunology*, *152*(6), 2930-2937.

17. Carrera, L., Gazzinelli, R. T., Badolato, R., Hieny, S., Muller, W., Kuhn, R., & Sacks, D. L. (1996). *Leishmania* promastigotes selectively inhibit interleukin 12 induction in bone marrow-derived macrophages from susceptible and resistant mice. *Journal of Experimental Medicine*, *183*(2), 515-526.

18. Zilberstein, D., & Shapira, M. (1994). The role of pH and temperature in the development of Leishmania parasites. *Annual Reviews in Microbiology*, *48*(1), 449-470.

19. Alexander, J., & Vickerman, K. (1975). Fusion of Host Cell Secondary Lysosomes with the Parasitophorous Vacuoles of Leishmania mexicana-inlected Macrophages. *Journal of Eukaryotic Microbiology*, *22*(4), 502-508.

20. Bogdan, C., Donhauser, N., Döring, R., Röllinghoff, M., Diefenbach, A., & Rittig, M. G. (2000). Fibroblasts as host cells in latent leishmaniosis. *Journal of Experimental Medicine*, *191*(12), 2121-2130.

21. Svensson, M., Maroof, A., Ato, M., & Kaye, P. M. (2004). Stromal cells direct local differentiation of regulatory dendritic cells. *Immunity*, *21*(6), 805-816.

22. Hendrickx, S., Guerin, P. J., Caljon, G., Croft, S. L., & Maes, L. (2016). Evaluating drug resistance in visceral leishmaniasis: the challenges. *Parasitology*, 1-11.

23. Garnier, T., Mäntylä, A., Järvinen, T., Lawrence, M. J., Brown, M. B., & Croft, S. L. (2007). Topical buparvaquone formulations for the treatment of cutaneous leishmaniasis. *Journal of pharmacy and pharmacology*, *59*(1), 41-49.

24. Markle, W. H., & Makhoul, K. (2004). Cutaneous leishmaniasis: recognition and treatment. *American family physician*, *69*(6), 1455-1460.

25. Al-Kamel, M. A. (2016). Impact of leishmaniasis in women: a practical review with an update on my ISD-supported initiative to combat leishmaniasis in Yemen (ELYP). *International Journal of Women's Dermatology*, *2*(3), 93-101.

26. Reithinger, R., Dujardin, J. C., Louzir, H., Pirmez, C., Alexander, B., & Brooker, S. (2007). Cutaneous leishmaniasis. *The Lancet infectious diseases*, *7*(9), 581-596.

27. Edrissian, G. H., Mohammadi, M., Kanani, A., Afshar, A., Hafezi, R., Ghorbani, M., & Gharagozloo, A. R. (1990). Bacterial infections in suspected cutaneous leishmaniasis lesions. *Bulletin of the world health organization*, *68*(4), 473.

28. Kharfi, M., Fazaa, B., Chaker, E., & Kamoun, M. R. (2003, January). Mucosal localization of leishmaniasis in Tunisia: 5 cases. In *Annales de Dermatologie et de Vénéréologie*. *130*(1) Pt 1,27-30.

29. Akilov, O. E., Khachemoune, A., & Hasan, T. (2007). Clinical manifestations and classification of Old World cutaneous leishmaniasis. *International journal of dermatology*, *46*(2), 132-142.

30. Goto, H., & Lindoso, J. A. L. (2010). Current diagnosis and treatment of cutaneous and mucocutaneous leishmaniasis. *Expert review of anti-infective therapy*, *8*(4), 419-433.

31. WHO, *Control of the leishmaniases* 2010, World Health Organisation: Geneva. p. 186.

32. Zerpa, O., Ulrich, M., Blanco, B., Polegre, M., Avila, A., Matos, N. & Convit, J. (2007). Diffuse cutaneous leishmaniasis responds to miltefosine but then relapses. *British Journal of Dermatology*, *156*(6), 1328-1335.

33. Sypek, J. P., Chung, C. L., Mayor, S. E., Subramanyam, J. M., Goldman, S. J., Sieburth, D. S. & Schaub, R. G. (1993). Resolution of cutaneous leishmaniasis: interleukin 12 initiates a protective T helper type 1 immune response. *Journal of Experimental Medicine*, *177*(6), 1797-1802.

34. González, U., Pinart, M., Reveiz, L., & Alvar, J. (2008). Interventions for Old World cutaneous leishmaniasis. *Cochrane Database Syst Rev*, *4* (issue), CD005067.

35. González, U., Pinart, M., Rengifo-Pardo, M., Macaya, A., Alvar, J., & Tweed, J. (2009). Interventions for American cutaneous and mucocutaneous leishmaniasis. The Cochrane Collaboration, Issue 2, Wiley Publishers.

36. DiMasi, J. A., Hansen, R. W., & Grabowski, H. G. (2003). The price of innovation: new estimates of drug development costs. *Journal of health economics*, *22*(2), 151-185.

37. Morgan, S., Grootendorst, P., Lexchin, J., Cunningham, C., & Greyson, D. (2011). The cost of drug development: a systematic review. *Health Policy*, *100*(1), 4-17.

38. Pedrique, B., Strub-Wourgaft, N., Some, C., Olliaro, P., Trouiller, P., Ford, N. & Bradol, J. H. (2013). The drug and vaccine landscape for neglected diseases (2000–11): a systematic assessment. *The Lancet Global Health*, *1*(6), e371-e379.

39. Ashburn, T. T., & Thor, K. B. (2004). Drug repositioning: identifying and developing new uses for existing drugs. *Nature reviews. Drug discovery*, *3*(8), 673-683.

40. Sundar, S., & Olliaro, P. L. (2007). Miltefosine in the treatment of leishmaniasis: clinical evidence for informed clinical risk management. *Therapeutics and clinical risk management*, *3*(5), 733-740.

41. Allen, U. D. (2010). Antifungal agents for the treatment of systemic fungal infections in children. *Paediatrics & child health*, *15*(9), 603-608.

42. Nagata, N., Marriott, D., Harkness, J., Ellis, J. T., & Stark, D. (2012). Current treatment options for Dientamoeba fragilis infections. *International Journal for Parasitology: Drugs and Drug Resistance*, *2*, 204-215.

43. Prajapati, V. K., Mehrotra, S., Gautam, S., Rai, M., & Sundar, S. (2012). In vitro antileishmanial drug susceptibility of clinical isolates from patients with Indian visceral leishmaniasis—status of newly introduced drugs. *The American journal of tropical medicine and hygiene*, *87*(4), 655-657.

44. Blessy, M. R. D. P., Patel, R. D., Prajapati, P. N., & Agrawal, Y. K. (2014). Development of forced degradation and stability indicating studies of drugs—A review. *Journal of Pharmaceutical Analysis*, *4*(3), 159-165.

45. Silva, S. Y., Rueda, L. C., López, M., Vélez, I. D., Rueda-Clausen, C. F., Smith, D. J. & Díaz, H. (2006). Double blind randomized controlled trial, to evaluate the effectiveness of a controlled nitric oxide releasing patch versus meglumine antimoniate in the treatment of cutaneous leishmaniasis [NCT00317629]. *Trials*, *7*(1), 14.

46. Nandha, B., Srinivasan, R., & Jambulingam, P. (2014). Cutaneous leishmaniasis: knowledge, attitude and practices of the inhabitants of the Kani forest tribal settlements of Tiruvananthapuram district, Kerala, India. *Health education research*, *29*(6), 1049-1057.

47. Abazid, N., Jones, C., & Davies, C. R. (2012). Knowledge, attitudes and practices about leishmaniasis among cutaneous leishmaniasis patients in Aleppo, Syrian Arab Republic. *Eastern Mediterranean Health Journal*, *18*(1), 7.

48. Ruoti, M., Oddone, R., Lampert, N., Orué, E., Miles, M. A., Alexander, N. & Sinclair, B. (2013). Mucocutaneous leishmaniasis: knowledge, attitudes, and practices among paraguayan communities, patients, and health professionals. *Journal of tropical medicine*, *2013*. Article ID 538629

49. Treatment recommendation: Extracted from The control of the leishmaniases. WHO Technical Report Series N°949, 2010. (PP 67–71)

50. Goodwin, L. G. (1995). Pentostam®(sodium stibogluconate); a 50-year personal reminiscence. *Transactions of the Royal Society of Tropical Medicine and Hygiene*, *89*(3), 339-341.

51. Wyllie, S., Cunningham, M. L., & Fairlamb, A. H. (2004). Dual action of antimonial drugs on thiol redox metabolism in the human pathogen *Leishmania donovani*. *Journal of Biological Chemistry*, *279*(38), 39925-39932.

52. Krauth-Siegel, R. L., & Comini, M. A. (2008). Redox control in trypanosomatids, parasitic protozoa with trypanothione-based thiol metabolism. *Biochimica et Biophysica Acta (BBA)-General Subjects*, *1780*(11), 1236-1248.

53. Sereno, D., Holzmuller, P., Mangot, I., Cuny, G., Ouaissi, A., & Lemesre, J. L. (2001). Antimonial-Mediated DNA Fragmentation in *Leishmania infantum* Amastigotes. *Antimicrobial agents and chemotherapy*, *45*(7), 2064-2069.

54. Sudhandiran, G., & Shaha, C. (2003). Antimonial-induced increase in intracellular Ca2+ through non-selective cation channels in the host and the parasite is responsible for apoptosis of intracellular *Leishmania donovani* amastigotes. *Journal of Biological Chemistry*, *278*(27), 25120-25132.

55. Demicheli, C., Frézard, F., Lecouvey, M., & Garnier-Suillerot, A. (2002). Antimony (V) complex formation with adenine nucleosides in aqueous solution. *Biochimica et Biophysica Acta (BBA)-General Subjects*, *1570*(3), 192-198.

56. Herman, J. D., Gallalee, J. V., & Best, J. M. (1987). Sodium stibogluconate (Pentostam) inhibition of glucose catabolism via the glycolytic pathway, and fatty acid β-oxidation in *Leishmania mexicana* amastigotes. *Biochemical pharmacology*, *36*(2), 197-201.

57. Balana-Fouce, R., Reguera, R. M., Cubrıa, J. C., & Ordonez, D. (1998). The pharmacology of leishmaniasis. *General Pharmacology: The Vascular System*, *30*(4), 435-443.

58. Frézard, F., Demicheli, C., & Ribeiro, R. R. (2009). Pentavalent antimonials: new perspectives for old drugs. *Molecules*, *14*(7), 2317-2336.

59. Sharquie, K. E., Al-Talib, K. K., & Chu, A. C. (1988). Intralesional therapy of cutaneous leishmaniasis with sodium stibogluconate antimony. *British Journal of Dermatology*, *119*(1), 53-57.

60. Grogl, M., Thomason, T. N., & Franke, E. D. (1992). Drug resistance in leishmaniasis: its implication in systemic chemotherapy of cutaneous and mucocutaneous disease. *The American journal of tropical medicine and hygiene*, *47*(1), 117-126.

References

61. Berman, J. D., Chulay, J. D., Hendricks, L. D., & Oster, C. N. (1982). Susceptibility of clinically sensitive and resistant *Leishmania* to pentavalent antimony in vitro. *The American journal of tropical medicine and hygiene*, *31*(3), 459-465.

62. Allen, S., & Neal, R. A. (1989). The in vitro susceptibility of macrophages infected with amastigotes of *Leishmania spp.* to pentavalent antimonial drugs and other compounds with special relevance to cutaneous isolates. In *Leishmaniasis* Springer US. p. 711-720.

63. Navin, T. R., Arana, B. A., Arana, F. E., Berman, J. D., & Chajón, J. F. (1992). Placebo-controlled clinical trial of sodium stibogluconate (Pentostam) versus ketoconazole for treating cutaneous leishmaniasis in Guatemala. *Journal of Infectious Diseases*, *165*(3), 528-534.

64. Corral, M. J., González-Sánchez, E., Cuquerella, M., & Alunda, J. M. (2014). In vitro synergistic effect of amphotericin B and allicin on *Leishmania donovani* and *L. infantum*. *Antimicrobial agents and chemotherapy*, *58*(3), 1596-1602.

65. Cohen, B. E. (2016). The role of signaling via aqueous pore formation in resistance responses to amphotericin B. *Antimicrobial agents and chemotherapy*, *60*(9), 5122-5129.

66. Cohen, B. E., Ramos, H., Gamargo, M., & Urbina, J. (1986). The water and ionic permeability induced by polyene antibiotics across plasma membrane vesicles from *Leishmania sp*. *Biochimica et Biophysica Acta (BBA)-Biomembranes*, *860*(1), 57-65.

67. Saha, A. K., Mukherjee, T., & Bhaduri, A. (1986). Mechanism of action of amphotericin B on *Leishmania donovani* promastigotes. *Molecular and biochemical parasitology*, *19*(3), 195-200.

68. Sampaio, R. N., & Marsden, P. D. (1997). Treatment of the mucosal form of leishmaniasis without response to glucantime, with liposomal amphotericin B. *Revista da Sociedade Brasileira de Medicina Tropical*, *30*(2), 125-128.

69. Balasegaram, M., Ritmeijer, K., Lima, M. A., Burza, S., Ortiz Genovese, G., Milani, B. & Chappuis, F. (2012). Liposomal amphotericin B as a treatment for human leishmaniasis. *Expert opinion on emerging drugs*, *17*(4), 493-510.

70. Neves, L. O., Talhari, A. C., Gadelha, E. P. N., Júnior, S., Guerra, J. A. D. O., Ferreira, L. C. D. L., & Talhari, S. (2011). A randomized clinical trial comparing meglumine antimoniate, pentamidine and amphotericin B for the treatment of cutaneous leishmaniasis by *Leishmania guyanensis*. *Anais brasileiros de dermatologia*, *86*(6), 1092-1101.

71. Dorlo, T. P., Balasegaram, M., Beijnen, J. H., & de Vries, P. J. (2012). Miltefosine: a review of its pharmacology and therapeutic efficacy in the treatment of leishmaniasis. *Journal of Antimicrobial Chemotherapy*, *67*(11), 2576-2597.

72. Escobar, P., Matu, S., Marques, C., & Croft, S. L. (2002). Sensitivities of *Leishmania* species to hexadecylphosphocholine (miltefosine), ET-18-OCH 3 (edelfosine) and amphotericin B. *Acta tropica*, *81*(2), 151-157.

73. Überall, F., Oberhuber, H., Maly, K., Zaknun, J., Demuth, L., & Grunicke, H. H. (1991). Hexadecylphosphocholine inhibits inositol phosphate formation and protein kinase C activity. *Cancer research*, *51*(3), 807-812.

74. Achterberg, V., & Gercken, G. (1987). Cytotoxicity of ester and ether lysophospholipids on *Leishmania donovani* promastigotes. *Molecular and biochemical parasitology*, *23*(2), 117-122.

75. Croft, S. L., & Engel, J. (2006). Miltefosine—discovery of the antileishmanial activity of phospholipid derivatives. *Transactions of the Royal Society of Tropical Medicine and Hygiene*, *100*(Supplement_1), S4-S8.

76. Croft, S. L., Neal, R. A., Pendergast, W., & Chan, J. H. (1987). The activity of alkyl phosphorylcholines and related derivatives against *Leishmania donovani*. *Biochemical pharmacology*, *36*(16), 2633-2636.

77. Rakotomanga, M., Blanc, S., Gaudin, K., Chaminade, P., & Loiseau, P. M. (2007). Miltefosine affects lipid metabolism in *Leishmania donovani* promastigotes. *Antimicrobial agents and chemotherapy*, *51*(4), 1425-1430.

78. Lucas, A., Kim, Y., Rivera-Pabon, O., Chae, S., Kim, D. H., & Kim, B. (2010). Targeting the PI3K/Akt cell survival pathway to induce cell death of HIV-1 infected macrophages with alkylphospholipid compounds. *PloS one*, *5*(9), e13121.

79. Bryceson, A. (2001). A policy for leishmaniasis with respect to the prevention and control of drug resistance. *Tropical medicine & international health*, *6*(11), 928-934.

80. Sundar, S., & Murray, H. W. (2005). Availability of miltefosine for the treatment of kala-azar in India. *Bulletin of the World Health Organization*, *83*(5), 394-395.

81. Escobar, P., Matu, S., Marques, C., & Croft, S. L. (2002). Sensitivities of *Leishmania* species to hexadecylphosphocholine (miltefosine), ET-18-OCH 3 (edelfosine) and amphotericin B. *Acta tropica*, *81*(2), 151-157.

82. Yardley, V., Croft, S. L., De Doncker, S., Dujardin, J. C., Koirala, S., Rijal, S. & Chappuis, F. (2005). The sensitivity of clinical isolates of *Leishmania* from Peru and Nepal to miltefosine. *The American journal of tropical medicine and hygiene*, *73*(2), 272-275.

References

83. Soto, J., Arana, B. A., Toledo, J., Rizzo, N., Vega, J. C., Diaz, A. & Junge, K. (2004). Miltefosine for new world cutaneous leishmaniasis. *Clinical infectious diseases*, *38*(9), 1266-1272.

84. Neal, R. A. (1968). The effect of antibiotics of the neomycin group on experimental cutaneous leishmaniasis. *Annals of Tropical Medicine & Parasitology*, *62*(1), 54-62.

85. Maarouf, M., Lawrence, F., Croft, S. L., & Robert-Gero, M. (1995). Ribosomes of *Leishmania* are a target for the aminoglycosides. *Parasitology research*, *81*(5), 421-425.

86. Fernández, M. M., Malchiodi, E. L., & Algranati, I. D. (2011). Differential effects of paromomycin on ribosomes of *Leishmania mexicana* and mammalian cells. *Antimicrobial agents and chemotherapy*, *55*(1), 86-93.

87. Maarouf, M., Lawrence, F., Brown, S., & Robert-Gero, M. (1997). Biochemical alterations in paromomycin-treated *Leishmania donovani* promastigotes. *Parasitology research*, *83*(2), 198-202.

88. El-On, J., Jacobs, G. P., Witztum, E., & Greenblatt, C. L. (1984). Development of topical treatment for cutaneous leishmaniasis caused by *Leishmania major* in experimental animals. *Antimicrobial Agents and Chemotherapy*, *26*(5), 745-751.

89. Kim, D. H., Chung, H. J., Bleys, J., & Ghohestani, R. F. (2009). Is paromomycin an effective and safe treatment against cutaneous leishmaniasis? A meta-analysis of 14 randomized controlled trials. *PLoS neglected tropical diseases*, *3*(2), e381.

90. Neal, R. A., Murphy, A. G., Olliaro, P., & Croft, S. L. (1994). Aminosidine ointments for the treatment of experimental cutaneous leishmaniasis. *Transactions of the Royal Society of Tropical Medicine and Hygiene*, *88*(2), 223-225.

91. Bailey, M. S. (2013). Editorial commentary: local treatments for cutaneous leishmaniasis. *Clinical Infectious Diseases, 57*,381–383.

92. Corpas-López, V., Merino-Espinosa, G., López-Viota, M., Gijón-Robles, P., Morillas-Mancilla, M. J., López-Viota, J. & Martín-Sánchez, J. (2016). Topical Treatment of *Leishmania tropica* Infection Using (−)-α-Bisabolol Ointment in a Hamster Model: Effectiveness and Safety Assessment. *Journal of natural products*, *79*(9), 2403-2407.

93. Clinical trials government register https://clinicaltrials.gov/ct2/show/NCT01845727 acessed 27/06/17

94. Asilian, A., Sadeghinia, A., Faghihi, G., & Momeni, A. (2004). Comparative study of the efficacy of combined cryotherapy and intralesional meglumine antimoniate (Glucantime®) vs. cryotherapy and intralesional meglumine antimoniate

(Glucantime®) alone for the treatment of cutaneous leishmaniasis. *International journal of dermatology*, *43*(4), 281-283.

95. Salmanpour, R., Razmavar, M. R., & Abtahi, N. (2006). Comparison of intralesional meglumine antimoniate, cryotherapy and their combination in the treatment of cutaneous leishmaniasis. *International journal of dermatology*, *45*(9), 1115-1116.

96. Sadeghian, G., Nilfroushzadeh, M. A., & Iraji, F. (2007). Efficacy of local heat therapy by radiofrequency in the treatment of cutaneous leishmaniasis, compared with intralesional injection of meglumine antimoniate. *Clinical and experimental dermatology*, *32*(4), 371-374.

97. Reithinger, R., Mohsen, M., Wahid, M., Bismullah, M., Quinnell, R. J., Davies, C. R. & David, J. R. (2005). Efficacy of thermotherapy to treat cutaneous leishmaniasis caused by *Leishmania tropica* in Kabul, Afghanistan: a randomized, controlled trial. *Clinical infectious diseases*, *40*(8), 1148-1155.

98. Buates, S., & Matlashewski, G. (1999). Treatment of experimental leishmaniasis with the immunomodulators imiquimod and S-28463: efficacy and mode of action. *The Journal of infectious diseases*, *179*(6), 1485-1494.

99. Parihar, S. P., Hartley, M. A., Hurdayal, R., Guler, R., & Brombacher, F. (2016). Topical Simvastatin as Host-Directed Therapy against Severity of Cutaneous Leishmaniasis in Mice. *Scientific reports*, *6*, Article no 33458.

100. Brito, G., Dourado, M., Polari, L., Celestino, D., Carvalho, L. P., Queiroz, A. & Passos, S. (2014). Clinical and immunological outcome in cutaneous leishmaniasis patients treated with pentoxifylline. *The American journal of tropical medicine and hygiene*, *90*(4), 617-620.

101. DNDI-5421 & DNDI-5610 OXABOROLES http://www.dndi.org/diseases-projects/portfolio/oxaleish/ accessed 27/06/17

102. AMINOPYRAZOLES http://www.dndi.org/diseases-projects/portfolio/aminopyrazoles/ accessed 27/06/17

103. DNDI-0690 NITROIMIDAZOLE http://www.dndi.org/diseases-projects/portfolio/nitroimidazole/ accessed 27/06/17

104. Mukherjee, S., Mukherjee, B., Mukhopadhyay, R., Naskar, K., Sundar, S., Dujardin, J. C. & Roy, S. (2012). Imipramine is an orally active drug against both antimony sensitive and resistant *Leishmania donovani* clinical isolates in experimental infection. *PLoS neglected tropical diseases*, *6*(12), e1987.

105. Wyllie, S., Patterson, S., Stojanovski, L., Simeons, F. R., Norval, S., Kime, R. & Fairlamb, A. H. (2012). The anti-trypanosome drug fexinidazole shows potential for treating visceral leishmaniasis. *Science translational medicine*, *4*(119), 119re1-119re1.

106. Miguel, D. C., Yokoyama-Yasunaka, J. K., Andreoli, W. K., Mortara, R. A., & Uliana, S. R. (2007). Tamoxifen is effective against *Leishmania* and induces a rapid alkalinization of parasitophorous vacuoles harbouring *Leishmania (Leishmania) amazonensis* amastigotes. *Journal of Antimicrobial Chemotherapy*, *60*(3), 526-534.

107. Carvalho, L., Luque-Ortega, J. R., Manzano, J. I., Castanys, S., Rivas, L., & Gamarro, F. (2010). Tafenoquine, an antiplasmodial 8-aminoquinoline, targets *Leishmania* respiratory complex III and induces apoptosis. *Antimicrobial agents and chemotherapy*, *54*(12), 5344-5351.

108. Clinical trials government register https://www.clinicaltrials.gov/ct2/show/NCT02687971 accessed 29/06/17

109. Aït-Oudhia, K., Gazanion, E., Vergnes, B., Oury, B., & Sereno, D. (2011). *Leishmania* antimony resistance: what we know what we can learn from the field. *Parasitology research*, *109*(5), 1225-1232.

110. Choudhury, K., Zander, D., Kube, M., Reinhardt, R., & Clos, J. (2008). Identification of a *Leishmania infantum* gene mediating resistance to 'and Sb III. *International journal for parasitology*, *38*(12), 1411-1423.

111. Srivastava, P., Prajapati, V. K., Rai, M., & Sundar, S. (2011). Unusual case of resistance to amphotericin B in visceral leishmaniasis in a region in India where leishmaniasis is not endemic. *Journal of clinical microbiology*, *49*(8), 3088-3091.

112. Purkait, B., Kumar, A., Nandi, N., Sardar, A. H., Das, S., Kumar, S. & Singh, D. (2012). Mechanism of amphotericin B resistance in clinical isolates of *Leishmania donovani*. *Antimicrobial agents and chemotherapy*, *56*(2), 1031-1041.

113. Pérez-Victoria, F. J., Castanys, S., & Gamarro, F. (2003). *Leishmania donovani* resistance to miltefosine involves a defective inward translocation of the drug. *Antimicrobial agents and chemotherapy*, *47*(8), 2397-2403.

114. Gebre-Hiwot, A., Tadesse, G., Croft, S. L., & Frommel, D. (1992). An in vitro model for screening antileishmanial drugs: the human leukaemia monocyte cell line, THP-1. *Acta tropica*, *51*(3-4), 237-245.

115. Peña, I., Manzano, M. P., Cantizani, J., Kessler, A., Alonso-Padilla, J., Bardera, A. I. & de Dios-Anton, F. (2015). New compound sets identified from high throughput

phenotypic screening against three kinetoplastid parasites: an open resource. *Scientific reports*, *5*. Article no. 8771

116. Khare, S., Nagle, A. S., Biggart, A., Lai, Y. H., Liang, F., Davis, L. C. & Gillespie, J. R. (2016). Proteasome inhibition for treatment of leishmaniasis, Chagas disease and sleeping sickness. *Nature*, *537*(7619), 229-233.

117. DiMasi, J. A., Grabowski, H. G., & Hansen, R. W. (2016). Innovation in the pharmaceutical industry: new estimates of R&D costs. *Journal of health economics*, *47*, 20-33.

118. Kola, I., & Landis, J. (2004). Opinion: Can the pharmaceutical industry reduce attrition rates?. *Nature reviews. Drug discovery*, *3*(8), 711-716.

119. Morris, Z. S., Wooding, S., & Grant, J. (2011). The answer is 17 years, what is the question: understanding time lags in translational research. *Journal of the Royal Society of Medicine*, *104*(12), 510-520.

120. Astashkina, A., Mann, B., & Grainger, D. W. (2012). A critical evaluation of in vitro cell culture models for high-throughput drug screening and toxicity. *Pharmacology & therapeutics*, *134*(1), 82-106.

121. Horvath, P., Aulner, N., Bickle, M., Davies, A. M., Del Nery, E., Ebner, D. & Shorte, S. L. (2016). Screening out irrelevant cell-based models of disease. *Nature Reviews Drug Discovery*, *15*(11), 751-769.

122. Campion, S., Aubrecht, J., Boekelheide, K., Brewster, D. W., Vaidya, V. S., Anderson, L. & Saikumar, J. (2013). The current status of biomarkers for predicting toxicity. *Expert opinion on drug metabolism & toxicology*, *9*(11), 1391-1408.

123. Masters, J. R., & Stacey, G. N. (2007). Changing medium and passaging cell lines. *Nature protocols*, *2*(9), 2276-2284.

124. Nestor, C. E., Ottaviano, R., Reinhardt, D., Cruickshanks, H. A., Mjoseng, H. K., McPherson, R. C. & Anderton, S. M. (2015). Rapid reprogramming of epigenetic and transcriptional profiles in mammalian culture systems. *Genome biology*, *16*(1), 11-16.

125. Shi, Y., Inoue, H., Wu, J. C., & Yamanaka, S. (2017). Induced pluripotent stem cell technology: a decade of progress. *Nature Reviews Drug Discovery*, *16*(2), 115-130.

126. Morris, C. C. (1962). Maintenance and loss in tissue culture of specific cell characteristics. *Advances in applied microbiology*, *4*, 117-212.

References

127. Carreau, A., Hafny-Rahbi, B. E., Matejuk, A., Grillon, C., & Kieda, C. (2011). Why is the partial oxygen pressure of human tissues a crucial parameter? Small molecules and hypoxia. *Journal of cellular and molecular medicine*, *15*(6), 1239-1253.

128. Newby, D., Marks, L., & Lyall, F. (2005). Dissolved oxygen concentration in culture medium: assumptions and pitfalls. *Placenta*, *26*(4), 353-357.

129. Sullivan, M., Galea, P., & Latif, S. (2006). What is the appropriate oxygen tension for in vitro culture?. *Molecular human reproduction*, *12*(11), 653-653.

130. Halliwell, B. (2014). Cell culture, oxidative stress, and antioxidants: avoiding pitfalls. *Biomedical journal*, *37*(3), 99–105.

131. Tiede, L. M., Cook, E. A., Morsey, B., & Fox, H. S. (2011). Oxygen matters: tissue culture oxygen levels affect mitochondrial function and structure as well as responses to HIV viroproteins. *Cell death & disease*, *2*(12), e246.

132. Redshaw, Z., & Loughna, P. T. (2012). Oxygen concentration modulates the differentiation of muscle stem cells toward myogenic and adipogenic fates. *Differentiation*, *84*(2), 193-202.

133. Bhatia, S. N., & Ingber, D. E. (2014). Microfluidic organs-on-chips. *Nature biotechnology*, *32*(8), 760-772.

134. Wells, R. G. (2008). The role of matrix stiffness in regulating cell behavior. *Hepatology*, *47*(4), 1394-1400.

135. Discher, D. E., Janmey, P., & Wang, Y. L. (2005). Tissue cells feel and respond to the stiffness of their substrate. *Science*, *310*(5751), 1139-1143.

136. Levental, I., Georges, P. C., & Janmey, P. A. (2007). Soft biological materials and their impact on cell function. *Soft Matter*, *3*(3), 299-306.

137. Floren, M., Bonani, W., Dharmarajan, A., Motta, A., Migliaresi, C., & Tan, W. (2016). Human mesenchymal stem cells cultured on silk hydrogels with variable stiffness and growth factor differentiate into mature smooth muscle cell phenotype. *Acta biomaterialia*, *31*, 156-166.

138. Lee, J., Abdeen, A. A., Zhang, D., & Kilian, K. A. (2013). Directing stem cell fate on hydrogel substrates by controlling cell geometry, matrix mechanics and adhesion ligand composition. *Biomaterials*, *34*(33), 8140-8148.

139. Wells, R. G. (2008). Cellular sources of extracellular matrix in hepatic fibrosis. *Clinics in liver disease*, *12*(4), 759-768.

References

140. Wolf, M. T., Daly, K. A., Brennan-Pierce, E. P., Johnson, S. A., Carruthers, C. A., D'Amore, A., … & Badylak, S. F. (2012). A hydrogel derived from decellularized dermal extracellular matrix. *Biomaterials*, *33*(29), 7028-7038.

141. Teranishi, Y., Matsubara, T., Krausz, K. W., Le, T. T., Gonzalez, F. J., Yoshizato, K. & Kawada, N. (2015). Involvement of hepatic stellate cell cytoglobin in acute hepatocyte damage through the regulation of CYP2E1-mediated xenobiotic metabolism. *Laboratory Investigation*, *95*(5), 515.

142. Roberts, R. A., Ganey, P. E., Ju, C., Kamendulis, L. M., Rusyn, I., & Klaunig, J. E. (2006). Role of the Kupffer cell in mediating hepatic toxicity and carcinogenesis. *Toxicological Sciences*, *96*(1), 2-15.

143. Baragaña, B., Hallyburton, I., Lee, M. C., Norcross, N. R., Grimaldi, R., Otto, T. D. & Ruecker, A. (2015). A novel multiple-stage antimalarial agent that inhibits protein synthesis. *Nature*, *522*(7556), 315-320.

144. Paul, S. M., Mytelka, D. S., Dunwiddie, C. T., Persinger, C. C., Munos, B. H., Lindborg, S. R., & Schacht, A. L. (2010). How to improve R&D productivity: the pharmaceutical industry's grand challenge. *Nature reviews. Drug discovery*, *9*(3), 203-214.

145. Sena, E. S., Van Der Worp, H. B., Bath, P. M., Howells, D. W., & Macleod, M. R. (2010). Publication bias in reports of animal stroke studies leads to major overstatement of efficacy. *PLoS biology*, *8*(3), e1000344.

146. Curry, S. H., & Whelpton, R. Extrapolation from Animals to Human Beings and Translational Science. *Drug Disposition and Pharmacokinetics: From Principles to Applications*, 269-278.

147. Soldatow, V. Y., LeCluyse, E. L., Griffith, L. G., & Rusyn, I. (2013). *In vitro* models for liver toxicity testing. *Toxicology Research*, *2*(1), 23–39.

148. Tuyttens, F. A. M., de Graaf, S., Heerkens, J. L., Jacobs, L., Nalon, E., Ott, S & Ampe, B. (2014). Observer bias in animal behaviour research: can we believe what we score, if we score what we believe? *Animal Behaviour*, *90*, 273-280.

149. Brehm, M. A., Shultz, L. D., & Greiner, D. L. (2010). Humanized mouse models to study human diseases. *Current opinion in endocrinology, diabetes, and obesity*, *17*(2), 120-125.

150. Denton, P. W., & Garcia, J. V. (2011). Humanized mouse models of HIV infection. *AIDS reviews*, *13*(3), 135–148.

151. Arnold, L., Tyagi, R. K., Mejia, P., Van Rooijen, N., Pérignon, J. L., & Druilhe, P. (2010). Analysis of innate defences against Plasmodium falciparum in immunodeficient mice. *Malaria journal*, *9*(1), 197.

References

152. Mercer, D. F., Schiller, D. E., Elliott, J. F., Douglas, D. N., Hao, C., Rinfret, A. & Tyrrell, D. L. (2001). Hepatitis C virus replication in mice with chimeric human livers. *Nature medicine*, *7*(8), 927–933.

153. Azuma, H., Paulk, N., Ranade, A., Dorrell, C., Al-Dhalimy, M., Ellis, E. & Grompe, M. (2007). Robust expansion of human hepatocytes in Fah−/−/Rag2−/−/Il2rg−/− mice. *Nature biotechnology*, *25*(8), 903–910.

154. Vinks, A. A., Derendorf, H., & Mouton, J. W. (Eds.). (2014). *Fundamentals of antimicrobial pharmacokinetics and pharmacodynamics*. Springer New York.

155. Mattock, N. M., & Peters, W. (1975). The experimental chemotherapy of leishmaniasis: II: The activity in tissue culture of some antiparasitic and antimicrobial compounds in clinical use. *Annals of Tropical Medicine & Parasitology*, *69*(3), 359-371.

156. Dermine, J. F., Goyette, G., Houde, M., Turco, S. J., & Desjardins, M. (2005). Leishmania donovani lipophosphoglycan disrupts phagosome microdomains in J774 macrophages. *Cellular microbiology*, *7*(9), 1263-1270.

157. Croft, S. L. (1986). In vitro screens in the experimental chemotherapy of leishmaniasis and trypanosomiasis. *Parasitology Today*, *2*(3), 64-69.

158. Roy, G., Kündig, C., Olivier, M., Papadopoulou, B., & Ouellette, M. (2001). Adaptation of *Leishmania* cells to in vitro culture results in a more efficient reduction and transport of biopterin. *Experimental parasitology*, *97*(3), 161-168.

159. Titus, R. G., Marchand, M., Boon, T., & Louis, J. A. (1985). A limiting dilution assay for quantifying *Leishmania major* in tissues of infected mice. *Parasite immunology*, *7*(5), 545-555.

160. Calvo-Álvarez, E., Álvarez-Velilla, R., Fernández-Prada, C., Balaña-Fouce, R., & Reguera, R. M. (2015). Trypanosomatids see the light: recent advances in bioimaging research. *Drug discovery today*, *20*(1), 114-121.

161. Calvo-Álvarez, E., Guerrero, N. A., Álvarez-Velilla, R., Prada, C. F., Requena, J. M., Punzón, C., ... & Pérez-Pertejo, Y. (2012). Appraisal of a *Leishmania major* strain stably expressing mCherry fluorescent protein for both in vitro and in vivo studies of potential drugs and vaccine against cutaneous leishmaniasis. *PLoS neglected tropical diseases*, *6*(11), e1927.

162. Roy, G., Dumas, C., Sereno, D., Wu, Y., Singh, A. K., Tremblay, M. J., ... & Papadopoulou, B. (2000). Episomal and stable expression of the luciferase reporter gene for quantifying *Leishmania spp.* infections in macrophages and in animal models. *Molecular and biochemical parasitology*, *110*(2), 195-206.

163. Mikus, J., & Steverding, D. (2000). A simple colorimetric method to screen drug cytotoxicity against *Leishmania* using the dye Alamar Blue®. *Parasitology international*, *48*(3), 265-269.

164. Kiderlen, A. F., & Kaye, P. M. (1990). A modified colorimetric assay of macrophage activation for intracellular cytotoxicity against *Leishmania* parasites. *Journal of immunological methods*, *127*(1), 11-18.

165. van den Bogaart, E., Schoone, G. J., England, P., Faber, D., Orrling, K. M., Dujardin, J. C., ... & Adams, E. R. (2014). Simple colorimetric trypanothione reductase-based assay for high-throughput screening of drugs against *Leishmania* intracellular amastigotes. *Antimicrobial agents and chemotherapy*, *58*(1), 527-535.

166. Roy, G., Dumas, C., Sereno, D., Wu, Y., Singh, A. K., Tremblay, M. J., ... & Papadopoulou, B. (2000). Episomal and stable expression of the luciferase reporter gene for quantifying *Leishmania spp.* infections in macrophages and in animal models. *Molecular and biochemical parasitology*, *110*(2), 195-206.

167. Sereno, D., Da Silva, A. C., Mathieu-Daude, F., & Ouaissi, A. (2007). Advances and perspectives in *Leishmania* cell based drug-screening procedures. *Parasitology international*, *56*(1), 3-7.

168. LeBowitz, J. H., Coburn, C. M., & Beverley, S. M. (1991). Simultaneous transient expression assays of the trypanosomatid parasite *Leishmania* using β-galactosidase and β-glucuronidase as reporter enzymes. *Gene*, *103*(1), 119-123.

169. van den Bogaart, E., Schoone, G. J., Adams, E. R., & Schallig, H. D. (2014). Duplex quantitative reverse-transcriptase PCR for simultaneous assessment of drug activity against *Leishmania* intracellular amastigotes and their host cells. *International Journal for Parasitology: Drugs and Drug Resistance*, *4*(1), 14-19.

170. van der Meide, W., Guerra, J., Schoone, G., Farenhorst, M., Coelho, L., Faber, W., & Schallig, H. (2008). Comparison between quantitative nucleic acid sequence-based amplification, real-time reverse transcriptase PCR, and real-time PCR for quantification of *Leishmania* parasites. *Journal of Clinical Microbiology*, *46*(1), 73-78.

171. Croft, S. L., & Olliaro, P. (2011). Leishmaniasis chemotherapy—challenges and opportunities. *Clinical Microbiology and Infection*, *17*(10), 1478-1483.

172. Siqueira-Neto, J. L., Moon, S., Jang, J., Yang, G., Lee, C., Moon, H. K. & Freitas-Junior, L. H. (2012). An image-based high-content screening assay for compounds targeting intracellular *Leishmania donovani* amastigotes in human macrophages. *PLoS neglected tropical diseases*, *6*(6), e1671.

References

173. De Rycker, M., Hallyburton, I., Thomas, J., Campbell, L., Wyllie, S., Joshi, D. & Fairlamb, A. H. (2013). Comparison of a high-throughput high-content intracellular *Leishmania donovani* assay with an axenic amastigote assay. *Antimicrobial agents and chemotherapy*, *57*(7), 2913-2922.

174. Singh, N., & Dube, A. (2004). Fluorescent Leishmania: application to anti-leishmanial drug testing. *The American journal of tropical medicine and hygiene*, *71*(4), 400-402.

175. Osorio, Y., Travi, B. L., Renslo, A. R., Peniche, A. G., & Melby, P. C. (2011). Identification of small molecule lead compounds for visceral leishmaniasis using a novel ex vivo splenic explant model system. *PLoS neglected tropical diseases*, *5*(2), e962.

176. Moreno, I., Domínguez, M., Cabañes, D., Aizpurua, C., & Toraño, A. (2010). Kinetic analysis of ex vivo human blood infection by Leishmania. *PLoS neglected tropical diseases*, *4*(7), e743.

177. Cos, P., Vlietinck, A. J., Berghe, D. V., & Maes, L. (2006). Anti-infective potential of natural products: how to develop a stronger in vitro 'proof-of-concept'. *Journal of ethnopharmacology*, *106*(3), 290-302.

178. McGonigle, P., & Ruggeri, B. (2014). Animal models of human disease: challenges in enabling translation. *Biochemical pharmacology*, *87*(1), 162-171.

179. Shanks, N., Greek, R., & Greek, J. (2009). Are animal models predictive for humans?. *Philosophy, ethics, and humanities in medicine*, *4*(1), 2.

180. Singh, H., Teoh, S. H., Low, H. T., & Hutmacher, D. W. (2005). Flow modelling within a scaffold under the influence of uni-axial and bi-axial bioreactor rotation. *Journal of biotechnology*, *119*(2), 181-196.

181. Vogel,Steven Life in moving fluids : the physical biology of flow (1994) SN - 0-691-03485-0

182. Martin, Y., & Vermette, P. (2005). Bioreactors for tissue mass culture: design, characterization, and recent advances. *Biomaterials*, *26*(35), 7481-7503.

183. Yeon, J. H., & Park, J. K. (2007). Microfluidic cell culture systems for cellular analysis. *Biochip J*, *1*(1), 17-27.

184. Simon, M. C., & Keith, B. (2008). The role of oxygen availability in embryonic development and stem cell function. *Nature reviews. Molecular cell biology*, *9*(4), 285.

185. Allen, J. W., & Bhatia, S. N. (2003). Formation of steady-state oxygen gradients in vitro: Application to liver zonation. *Biotechnology and bioengineering*, *82*(3), 253-262.

186. Haycock, J. W. (2011). 3D cell culture: a review of current approaches and techniques. *3D cell culture: methods and protocols*, 1-15.

187. Pampaloni, F., Reynaud, E. G., & Stelzer, E. H. (2007). The third dimension bridges the gap between cell culture and live tissue. *Nature reviews. Molecular cell biology*, *8*(10), 839.

188. Baker, B. M., & Chen, C. S. (2012). Deconstructing the third dimension–how 3D culture microenvironments alter cellular cues. *J Cell Sci*, *125*(13), 3015-3024.

189. Yu, M., Huang, S., Yu, K. J., & Clyne, A. M. (2012). Dextran and polymer polyethylene glycol (PEG) coating reduce both 5 and 30 nm iron oxide nanoparticle cytotoxicity in 2D and 3D cell culture. *International journal of molecular sciences*, *13*(5), 5554-5570.

190. Pan, C., Kumar, C., Bohl, S., Klingmueller, U., & Mann, M. (2009). Comparative proteomic phenotyping of cell lines and primary cells to assess preservation of cell type-specific functions. *Molecular & Cellular Proteomics*, *8*(3), 443-450.

191. Ellis, J., & Bhatia, M. (2011). iPSC technology: platform for drug discovery. *Clinical Pharmacology & Therapeutics*, *89*(5), 639-641.

192. Kim, C. (2014). Disease modeling and cell based therapy with iPSC: future therapeutic option with fast and safe application. *Blood research*, *49*(1), 7-14.

193. Miki, Y., Ono, K., Hata, S., Suzuki, T., Kumamoto, H., & Sasano, H. (2012). The advantages of co-culture over mono cell culture in simulating in vivo environment. *The Journal of steroid biochemistry and molecular biology*, *131*(3), 68-75.

194. Albrecht, D. R., Underhill, G. H., Wassermann, T. B., Sah, R. L., & Bhatia, S. N. (2006). Probing the role of multicellular organization in three-dimensional microenvironments. *Nature methods*, *3*(5), 369-375.

195. Hirt, C. *et al* (2014) "*In vitro*" 3D models of tumor-immune system interaction *Advanced Drug Delivery Reviews 79–80,* 145-154

196. Weiswald, L. B., Bellet, D., & Dangles-Marie, V. (2015). Spherical cancer models in tumor biology. *Neoplasia*, *17*(1), 1-15.

197. Mehta, G., Hsiao, A. Y., Ingram, M., Luker, G. D., & Takayama, S. (2012). Opportunities and challenges for use of tumor spheroids as models to test drug delivery and efficacy. *Journal of Controlled Release*, *164*(2), 192-204.

References

198. Däster, S., Amatruda, N., Calabrese, D., Ivanek, R., Turrini, E., Droeser, R. A. & Mele, V. (2017). Induction of hypoxia and necrosis in multicellular tumor spheroids is associated with resistance to chemotherapy treatment. *Oncotarget*, *8*(1), 1725.

199. Zanoni, M., Piccinini, F., Arienti, C., Zamagni, A., Santi, S., Polico, R. & Tesei, A. (2016). 3D tumor spheroid models for in vitro therapeutic screening: a systematic approach to enhance the biological relevance of data obtained. *Scientific reports*, *6*.

200. Costin, G. E., & Norman, K. G. (2014). Application of In Vitro Methods in Preclinical Safety Assessment of Skin Care Products. *Textbook of Aging Skin*, 1-19.

201. Epiderm™ https://www.mattek.com/products/epiderm/ Acessed 17/01/2017 MatTek corporation

202. Casas, J. W., Lewerenz, G. M., Rankin, E. A., Willoughby, J. A., Blakeman, L. C., McKim, J. M., & Coleman, K. P. (2013). In vitro human skin irritation test for evaluation of medical device extracts. *Toxicology in vitro*, *27*(8), 2175-2183.

203. Desprez, B., Barroso, J., Griesinger, C., Kandárová, H., Alépée, N., & Fuchs, H. W. (2015). Two novel prediction models improve predictions of skin corrosive sub-categories by test methods of OECD Test Guideline No. 431. *Toxicology in Vitro*, *29*(8), 2055-2080.

204. Pfuhler, S., Fautz, R., Ouedraogo, G., Latil, A., Kenny, J., Moore, C. & Barroso, J. (2014). The Cosmetics Europe strategy for animal-free genotoxicity testing: project status up-date. *Toxicology in Vitro*, *28*(1), 18-23.

205. Witting, M., Boreham, A., Brodwolf, R., Vavrova, K., Alexiev, U., Friess, W., & Hedtrich, S. (2015). Interactions of hyaluronic acid with the skin and implications for the dermal delivery of biomacromolecules. *Molecular pharmaceutics*, *12*(5), 1391-1401.

206. Danilenko, D. M., Phillips, G. D. L., & Diaz, D. (2016). In Vitro Skin Models and Their Predictability in Defining Normal and Disease Biology, Pharmacology, and Toxicity. *Toxicologic pathology*, *44*(4), 555-563.

207. Helm, C. L. E., Fleury, M. E., Zisch, A. H., Boschetti, F., & Swartz, M. A. (2005). Synergy between interstitial flow and VEGF directs capillary morphogenesis in vitro through a gradient amplification mechanism. *Proceedings of the National Academy of Sciences of the United States of America*, *102*(44), 15779-15784.

208. Helm, C. L. E., Zisch, A., & Swartz, M. A. (2007). Engineered blood and lymphatic capillaries in 3-D VEGF-fibrin-collagen matrices with interstitial flow. *Biotechnology and bioengineering*, *96*(1), 167-176.

209. Ng, C. P., Helm, C. L. E., & Swartz, M. A. (2004). Interstitial flow differentially stimulates blood and lymphatic endothelial cell morphogenesis in vitro. *Microvascular research*, *68*(3), 258-264.

210. Semino, C. E., Kamm, R. D., & Lauffenburger, D. A. (2006). Autocrine EGF receptor activation mediates endothelial cell migration and vascular morphogenesis induced by VEGF under interstitial flow. *Experimental cell research*, *312*(3), 289-298.

211. Buschmann, M. D., Gluzband, Y. A., Grodzinsky, A. J., & Hunziker, E. B. (1995). Mechanical compression modulates matrix biosynthesis in chondrocyte/agarose culture. *Journal of cell science*, *108*(4), 1497-1508.

212. Maroudas, A., & Bullough, P. (1968). Permeability of articular cartilage. *Nature*, *219*(5160), 1260-1261.

213. Mow, V. C., Holmes, M. H., & Lai, W. M. (1984). Fluid transport and mechanical properties of articular cartilage: a review. *Journal of biomechanics*, *17*(5), 377-394.

214. Grodzinsky, A. J., Levenston, M. E., Jin, M., & Frank, E. H. (2000). Cartilage tissue remodeling in response to mechanical forces. *Annual review of biomedical engineering*, *2*(1), 691-713.

215. Ng, C. P., & Swartz, M. A. (2003). Fibroblast alignment under interstitial fluid flow using a novel 3-D tissue culture model. *American Journal of Physiology-Heart and Circulatory Physiology*, *284*(5), H1771-H1777.

216. Ng, C. P., & Swartz, M. A. (2006). Mechanisms of interstitial flow-induced remodeling of fibroblast–collagen cultures. *Annals of biomedical engineering*, *34*(3), 446-454.

217. Wang, S., & Tarbell, J. M. (2000). Effect of fluid flow on smooth muscle cells in a 3-dimensional collagen gel model. *Arteriosclerosis, thrombosis, and vascular biology*, *20*(10), 2220-2225.

218. Halldorsson, S., Lucumi, E., Gómez-Sjöberg, R., & Fleming, R. M. (2015). Advantages and challenges of microfluidic cell culture in polydimethylsiloxane devices. *Biosensors and Bioelectronics*, *63*, 218-231.

219. Mazzei, D., Guzzardi, M. A., Giusti, S., & Ahluwalia, A. (2010). A low shear stress modular bioreactor for connected cell culture under high flow rates. *Biotechnology and bioengineering*, *106*(1), 127-137.

220. Kolnik, M., Tsimring, L. S., & Hasty, J. (2012). Vacuum-assisted cell loading enables shear-free mammalian microfluidic culture. *Lab on a chip*, *12*(22), 4732-4737.

References

221. Zheng, W., Wang, Z., Zhang, W., & Jiang, X. (2010). A simple PDMS-based microfluidic channel design that removes bubbles for long-term on-chip culture of mammalian cells. *Lab on a Chip*, *10*(21), 2906-2910.

222. Ayuso, J. M., Virumbrales-Muñoz, M., Lacueva, A., Lanuza, P. M., Checa-Chavarria, E., Botella, P. & Pardo, J. (2016). Development and characterization of a microfluidic model of the tumour microenvironment. *Scientific reports*, *6*, 36086.

223. Singh, A., Freeman, B. D., & Pinnau, I. (1998). Pure and mixed gas acetone/nitrogen permeation properties of polydimethylsiloxane [PDMS]. *Journal of Polymer Science Part B: Polymer Physics*, *36*(2), 289-301.

224. Ochs, C. J., Kasuya, J., Pavesi, A., & Kamm, R. D. (2014). Oxygen levels in thermoplastic microfluidic devices during cell culture. *Lab on a Chip*, *14*(3), 459-462.

225. Cuchiara, M. P., Allen, A. C., Chen, T. M., Miller, J. S., & West, J. L. (2010). Multilayer microfluidic PEGDA hydrogels. *Biomaterials*, *31*(21), 5491-5497.

226. Chen, Y. A., King, A. D., Shih, H. C., Peng, C. C., Wu, C. Y., Liao, W. H., & Tung, Y. C. (2011). Generation of oxygen gradients in microfluidic devices for cell culture using spatially confined chemical reactions. *Lab on a Chip*, *11*(21), 3626-3633.

227. Daniel, H., Morse, E. L., & Adibi, S. A. (1991). The high and low affinity transport systems for dipeptides in kidney brush border membrane respond differently to alterations in pH gradient and membrane potential. *Journal of Biological Chemistry*, *266*(30), 19917-19924.

228. Cabrera, C. R., Finlayson, B., & Yager, P. (2001). Formation of natural pH gradients in a microfluidic device under flow conditions: model and experimental validation. *Analytical Chemistry*, *73*(3), 658-666.

229. Tostoes, R. M., Leite, S. B., Serra, M., Jensen, J., Björquist, P., Carrondo, M. J. & Alves, P. M. (2012). Human liver cell spheroids in extended perfusion bioreactor culture for repeated-dose drug testing. *Hepatology*, *55*(4), 1227-1236.

230. Cuchiara, M. P., Allen, A. C., Chen, T. M., Miller, J. S., & West, J. L. (2010). Multilayer microfluidic PEGDA hydrogels. *Biomaterials*, *31*(21), 5491-5497.

231. Toh, Y. C., Lim, T. C., Tai, D., Xiao, G., van Noort, D., & Yu, H. (2009). A microfluidic 3D hepatocyte chip for drug toxicity testing. *Lab on a Chip*, *9*(14), 2026-2035.

232. Tzima, E., Del Pozo, M. A., Shattil, S. J., Chien, S., & Schwartz, M. A. (2001). Activation of integrins in endothelial cells by fluid shear stress mediates Rho-dependent cytoskeletal alignment. *The EMBO journal*, *20*(17), 4639-4647.

References

233. Swartz, M. A., & Fleury, M. E. (2007). Interstitial flow and its effects in soft tissues. *Annu. Rev. Biomed. Eng.*, *9*, 229-256.

234. Dafni, H., Israely, T., Bhujwalla, Z. M., Benjamin, L. E., & Neeman, M. (2002). Overexpression of vascular endothelial growth factor 165 drives peritumor interstitial convection and induces lymphatic drain. *Cancer research*, *62*(22), 6731-6739.

235. Haessler, U., Teo, J. C., Foretay, D., Renaud, P., & Swartz, M. A. (2012). Migration dynamics of breast cancer cells in a tunable 3D interstitial flow chamber. *Integrative Biology*, *4*(4), 401-409.

236. Cartmell, S. H., Porter, B. D., García, A. J., & Guldberg, R. E. (2003). Effects of medium perfusion rate on cell-seeded three-dimensional bone constructs in vitro. *Tissue engineering*, *9*(6), 1197-1203.

237. Bakshi, R. P., & Shapiro, T. A. (2016). Pharmacodynamics of Antimalarial Agents. *Antibiotic Pharmacodynamics*, 415-439.

238. Toh, Y. C., Lim, T. C., Tai, D., Xiao, G., van Noort, D., & Yu, H. (2009). A microfluidic 3D hepatocyte chip for drug toxicity testing. *Lab on a Chip*, *9*(14), 2026-2035.

239. Farokhzad, O. C., Khademhosseini, A., Jon, S., Hermmann, A., Cheng, J., Chin, C. & Langer, R. (2005). Microfluidic system for studying the interaction of nanoparticles and microparticles with cells. *Analytical chemistry*, *77*(17), 5453-5459.

240. Vinci, M., Gowan, S., Boxall, F., Patterson, L., Zimmermann, M., Lomas, C. & Eccles, S. A. (2012). Advances in establishment and analysis of three-dimensional tumor spheroid-based functional assays for target validation and drug evaluation. *BMC biology*, *10*(1), 29.

241. Ravi, M., Paramesh, V., Kaviya, S. R., Anuradha, E., & Solomon, F. D. (2015). 3D cell culture systems: advantages and applications. *Journal of cellular physiology*, *230*(1), 16-26.

242. Antoni, D., Burckel, H., Josset, E., & Noel, G. (2015). Three-dimensional cell culture: a breakthrough in vivo. *International journal of molecular sciences*, *16*(3), 5517-5527.

243. Pampaloni, F., Reynaud, E. G., & Stelzer, E. H. (2007). The third dimension bridges the gap between cell culture and live tissue. *Nature reviews. Molecular cell biology*, *8*(10), 839-845.

244. Hsiao, A. Y., Tung, Y. C., Qu, X., Patel, L. R., Pienta, K. J., & Takayama, S. (2012). 384 hanging drop arrays give excellent Z-factors and allow versatile formation of co-culture spheroids. *Biotechnology and bioengineering*, *109*(5), 1293-1304.

245. Ingram, M., Techy, G. B., Saroufeem, R., Yazan, O., Narayan, K. S., Goodwin, T. J., & Spaulding, G. F. (1997). Three-dimensional growth patterns of various human tumor cell lines in simulated microgravity of a NASA bioreactor. *In Vitro Cellular & Developmental Biology-Animal*, *33*(6), 459-466.

246. Hirschhaeuser, F., Menne, H., Dittfeld, C., West, J., Mueller-Klieser, W., & Kunz-Schughart, L. A. (2010). Multicellular tumor spheroids: an underestimated tool is catching up again. *Journal of biotechnology*, *148*(1), 3-15.

247. Sutherland, R. M., Sordat, B., Bamat, J., Gabbert, H., Bourrat, B., & Mueller-Klieser, W. (1986). Oxygenation and differentiation in multicellular spheroids of human colon carcinoma. *Cancer research*, *46*(10), 5320-5329.

248. Mehta, G., Hsiao, A. Y., Ingram, M., Luker, G. D., & Takayama, S. (2012). Opportunities and challenges for use of tumor spheroids as models to test drug delivery and efficacy. *Journal of Controlled Release*, *164*(2), 192-204.

249. Fatehullah, A., Tan, S. H., & Barker, N. (2016). Organoids as an in vitro model of human development and disease. *Nature cell biology*, *18*(3), 246-254.

250. Resau, J. H., Sakamoto, K., Cottrell, J. R., Hudson, E. A., & Meltzer, S. J. (1991). Explant organ culture: a review. *Cytotechnology*, *7*(3), 137-149.

251. Kang, H. W., Lee, S. J., Ko, I. K., Kengla, C., Yoo, J. J., & Atala, A. (2016). A 3D bioprinting system to produce human-scale tissue constructs with structural integrity. *Nature biotechnology*, *34*(3), 312-319.

252. Zhao, Y., Yao, R., Ouyang, L., Ding, H., Zhang, T., Zhang, K. & Sun, W. (2014). Three-dimensional printing of Hela cells for cervical tumor model in vitro. *Biofabrication*, *6*(3), e035001

253. Mouser, V. H., Levato, R., Bonassar, L. J., D'Lima, D. D., Grande, D. A., Klein, T. J., & Malda, J. (2016). Three-dimensional bioprinting and its potential in the field of articular cartilage regeneration. *Cartilage,* p1-14.

254. Evans, M. (2005). Ethical sourcing of human embryonic stem cells—rational solutions? *Nature Reviews Molecular Cell Biology*, *6*(8), 663-667.

255. Grieshaber, S. E., Jha, A. K., Farran, A. J., & Jia, X. (2011). Hydrogels in tissue engineering. In *Biomaterials for Tissue Engineering Applications* (pp. 9-46).

References

256. Liang, Y., Jeong, J., DeVolder, R. J., Cha, C., Wang, F., Tong, Y. W., & Kong, H. (2011). A cell-instructive hydrogel to regulate malignancy of 3D tumor spheroids with matrix rigidity. *Biomaterials*, *32*(35), 9308-9315.

257. Pires, M. M., Przybyla, D. E., & Chmielewski, J. (2009). A Metal–Collagen Peptide Framework for Three-Dimensional Cell Culture. *Angewandte Chemie International Edition*, *48*(42), 7813-7817.

258. Chen, Q. Z., Efthymiou, A., Salih, V., & Boccaccini, A. R. (2008). Bioglass®-derived glass–ceramic scaffolds: Study of cell proliferation and scaffold degradation in vitro. *Journal of biomedical materials research Part A*, *84*(4), 1049-1060.

259. Freed, L. E., Vunjak-Novakovic, G., Biron, R. J., Eagles, D. B., Lesnoy, D. C., Barlow, S. K., & Langer, R. (1994). Biodegradable polymer scaffolds for tissue engineering. *Nature Biotechnology*, *12*(7), 689-693.

260. Vozzi, G., Flaim, C., Ahluwalia, A., & Bhatia, S. (2003). Fabrication of PLGA scaffolds using soft lithography and microsyringe deposition. *Biomaterials*, *24*(14), 2533-2540.

261. Ji, Y., Ghosh, K., Shu, X. Z., Li, B., Sokolov, J. C., Prestwich, G. D., ... & Rafailovich, M. H. (2006). Electrospun three-dimensional hyaluronic acid nanofibrous scaffolds. *Biomaterials*, *27*(20), 3782-3792.

262. Kunze, A., Giugliano, M., Valero, A., & Renaud, P. (2011). Micropatterning neural cell cultures in 3D with a multi-layered scaffold. *Biomaterials*, *32*(8), 2088-2098.

263. Lam, C. X. F., Mo, X. M., Teoh, S. H., & Hutmacher, D. W. (2002). Scaffold development using 3D printing with a starch-based polymer. *Materials Science and Engineering: C*, *20*(1), 49-56.

264. Appel, A. A., Anastasio, M. A., Larson, J. C., & Brey, E. M. (2013). Imaging challenges in biomaterials and tissue engineering. *Biomaterials*, *34*(28), 6615-6630.

265. Zhang, J., Skardal, A., & Prestwich, G. D. (2008). Engineered extracellular matrices with cleavable crosslinkers for cell expansion and easy cell recovery. *Biomaterials*, *29*(34), 4521-4531.

266. Brotherton, J. D., & Chau, P. C. (1996). Modeling of Axial-Flow Hollow Fiber Cell Culture Bioreactors. *Biotechnology progress*, *12*(5), 575-590.

267. Ye, H., Das, D. B., Triffitt, J. T., & Cui, Z. (2006). Modelling nutrient transport in hollow fibre membrane bioreactors for growing three-dimensional bone tissue. *Journal of Membrane Science*, *272*(1), 169-178.

268. Neuhaus, W., Lauer, R., Oelzant, S., Fringeli, U. P., Ecker, G. F., & Noe, C. R. (2006). A novel flow based hollow-fiber blood–brain barrier in vitro model with immortalised cell line PBMEC/C1–2. *Journal of biotechnology*, *125*(1), 127-141.

References

269. X Deng, X., Zhang, G., Shen, C., Yin, J., & Meng, Q. (2013). Hollow fiber culture accelerates differentiation of Caco-2 cells. *Applied microbiology and biotechnology*, *97*(15), 6943-6955.

270. LaPlaca MC, Vernekar VN, Shoemaker JT, Cullen DK. (2010) Three-Dimensional Neuronal Cultures. *Methods in Bioengineering: 3D Tissue Engineering*, 187–204.

271. Matsusaki M, Hikimoto D, Nishiguchi A, et al. (2015) 3D-fibroblast tissues constructed by a cell-coat technology enhance tight-junction formation of human colon epithelial cells. Biochem Biophys Res Commun. Vol 457 Issue 3 p363–369.

272. Matsusaki, M., Hikimoto, D., Nishiguchi, A., Kadowaki, K., Ohura, K., Imai, T., & Akashi, M. (2015). 3D-fibroblast tissues constructed by a cell-coat technology enhance tight-junction formation of human colon epithelial cells. *Biochemical and biophysical research communications*, *457*(3), 363-369.

273. Edmondson, R., Adcock, A. F., & Yang, L. (2016). Influence of Matrices on 3D-Cultured Prostate Cancer Cells' Drug Response and Expression of Drug-Action Associated Proteins. *PloS one*, *11*(6), e0158116.

274. Shen, F. H., Werner, B. C., Liang, H., Shang, H., Yang, N., Li, X. & Katz, A. J. (2013). Implications of adipose-derived stromal cells in a 3D culture system for osteogenic differentiation: an in vitro and in vivo investigation. *The Spine Journal*, *13*(1), 32-43.

275. Tanimizu, N., Miyajima, A., & Mostov, K. E. (2007). Liver progenitor cells develop cholangiocyte-type epithelial polarity in three-dimensional culture. *Molecular biology of the cell*, *18*(4), 1472-1479.

276. Muguruma, K., Nishiyama, A., Kawakami, H., Hashimoto, K., & Sasai, Y. (2015). Self-organization of polarized cerebellar tissue in 3D culture of human pluripotent stem cells. *Cell reports*, *10*(4), 537-550.

277. Decaestecker, C., Debeir, O., Van Ham, P., & Kiss, R. (2007). Can anti-migratory drugs be screened in vitro? A review of 2D and 3D assays for the quantitative analysis of cell migration. *Medicinal research reviews*, *27*(2), 149-176.

278. Elliott, N. T., & Yuan, F. A. N. (2011). A review of three-dimensional in vitro tissue models for drug discovery and transport studies. *Journal of pharmaceutical sciences*, *100*(1), 59-74.

279. Tung, Y. C., Hsiao, A. Y., Allen, S. G., Torisawa, Y. S., Ho, M., & Takayama, S. (2011). High-throughput 3D spheroid culture and drug testing using a 384 hanging drop array. *Analyst*, *136*(3), 473-478.

References

280. MILLER, H. C., & TWOHY, D. W. (1967). Infection of macrophages in culture by leptomonads of *Leishmania donovani*. *Journal of Eukaryotic Microbiology*, *14*(4), 781-789.

281. Handayani, S., Chiu, D. T., Tjitra, E., Kuo, J. S., Lampah, D., Kenangalem, E. & Russell, B. (2009). High deformability of Plasmodium vivax-infected red blood cells under microfluidic conditions. *The Journal of infectious diseases*, *199*(3), 445-450.

282. Shelby, J. P., White, J., Ganesan, K., Rathod, P. K., & Chiu, D. T. (2003). A microfluidic model for single-cell capillary obstruction by Plasmodium falciparum-infected erythrocytes. *Proceedings of the National Academy of Sciences*, *100*(25), 14618-14622.

283. Li, Z. J., Mohamed, N., & Ross, J. M. (2000). Shear stress affects the kinetics of Staphylococcus aureus adhesion to collagen. *Biotechnology progress*, *16*(6), 1086-1090.

284. Kim, J., Hegde, M., & Jayaraman, A. (2010). Co-culture of epithelial cells and bacteria for investigating host–pathogen interactions. *Lab on a Chip*, *10*(1), 43-50.

285. Leclerc, E., Sakai, Y., & Fujii, T. (2004). Microfluidic PDMS (polydimethylsiloxane) bioreactor for large-scale culture of hepatocytes. *Biotechnology progress*, *20*(3), 750-755.

286. Sodunke, T. R., Bouchard, M. J., & Noh, H. M. (2008). Microfluidic platform for hepatitis B viral replication study. *Biomedical microdevices*, *10*(3), 393-402.

287. Walker, G. M., Ozers, M. S., & Beebe, D. J. (2004). Cell infection within a microfluidic device using virus gradients. *Sensors and Actuators B: Chemical*, *98*(2), 347-355.

288. Rennert, K., Steinborn, S., Gröger, M., Ungerböck, B., Jank, A. M., Ehgartner, J. & Peters, F. T. (2015). A microfluidically perfused three dimensional human liver model. *Biomaterials*, *71*, 119-131.

289. Raimondi, M. T., Boschetti, F., Falcone, L., Migliavacca, F., Remuzzi, A., & Dubini, G. (2004). The effect of media perfusion on three-dimensional cultures of human chondrocytes: Integration of experimental and computational approaches. *Biorheology*, *41*(3-4), 401-410.

290. Silanikove, N., & Shapiro, F. (2012). Combined assays for lactose and galactose by enzymatic reactions. *Dietary Sugars: Chemistry, Analysis, Function and Effects, Food and Nutritional Components in Focus*, *3*, 397-406.

291. Nibourg, G. A., Boer, J. D., van der Hoeven, T. V., Ackermans, M. T., van Gulik, T. M., Chamuleau, R. A., & Hoekstra, R. (2012). Perfusion flow rate substantially contributes

References

to the performance of the HepaRG-AMC-bioartificial liver. *Biotechnology and bioengineering*, *109*(12), 3182-3188.

292. Tilles, A. W., Baskaran, H., Roy, P., Yarmush, M. L., & Toner, M. (2001). Effects of oxygenation and flow on the viability and function of rat hepatocytes cocultured in a microchannel flat-plate bioreactor. *Biotechnology and bioengineering*, *73*(5), 379-389.

293. Rinkenauer A. C *et* al (2015) Comparison of the uptake of methacrylate-based nanoparticles in static and dynamic *in vitro* systems as well as *in vivo J Control Release*. Oct Vol 28 Issue 216 p158-68

294. Wyler, D. J., Sypek, J. P., & McDonald, J. A. (1985). *In vitro* parasite-monocyte interactions in human leishmaniasis: possible role of fibronectin in parasite attachment. Infection and Immunity, 49(2), 305–311.

295. Rashidi, H., Alhaque, S., Szkolnicka, D., Flint, O., & Hay, D. C. (2016). Fluid shear stress modulation of hepatocyte-like cell function. *Archives of toxicology*, *90*(7), 1757-1761.

296. Tegazzini, D., Díaz, R., Aguilar, F., Peña, I., Presa, J. L., Yardley, V. & Cantizani, J. (2016). A replicative in vitro assay for drug discovery against *Leishmania donovani*. *Antimicrobial agents and chemotherapy*, *60*(6), 3524-3532.

297. Zhao, C., Papadopoulou, B., & Tremblay, M. J. (2004). Leishmania infantum promotes replication of HIV type 1 in human lymphoid tissue cultured ex vivo by inducing secretion of the proinflammatory cytokines TNF-α and IL-1α. *The Journal of Immunology*, *172*(5), 3086-3093.

298. Petropolis, D. B., Rodrigues, J. C., Viana, N. B., Pontes, B., Pereira, C. F., & Silva-Filho, F. C. (2014). *Leishmania amazonensis* promastigotes in 3D Collagen I culture: an in vitro physiological environment for the study of extracellular matrix and host cell interactions. *PeerJ*, *2*, e317.

299. Michel, G., Ferrua, B., Lang, T., Maddugoda, M. P., Munro, P., Pomares, C. & Marty, P. (2011). Luciferase-expressing *Leishmania infantum* allows the monitoring of amastigote population size, in vivo, ex vivo and in vitro. *PLoS neglected tropical diseases*, *5*(9), e1323.

300. Straub, T. M., Zu Bentrup, K. H., Coghlan, P. O., Dohnalkova, A., Mayer, B. K., Bartholomew, R. A., ... & Nickerson, C. A. (2007). In vitro cell culture infectivity assay for human noroviruses. *Emerging infectious diseases*, *13*(3), 396–403.

301. Sainz, B., TenCate, V., & Uprichard, S. L. (2009). Three-dimensional Huh7 cell culture system for the study of Hepatitis C virus infection. *Virology journal*, *6*(1), 103.

References

302. Garcez, P. P., Loiola, E. C., da Costa, R. M., Higa, L. M., Trindade, P., Delvecchio, R., & Rehen, S. K. (2016). Zika virus impairs growth in human neurospheres and brain organoids. *Science*, *352*(6287), 816-818.

303. Kapoor, N., Pawar, S., Sirakova, T. D., Deb, C., Warren, W. L., & Kolattukudy, P. E. (2013). Human granuloma in vitro model, for TB dormancy and resuscitation. *PLoS One*, *8*(1), e53657..

304. Nickerson, C. A., Richter, E. G., & Ott, C. M. (2007). Studying host–pathogen interactions in 3-D: organotypic models for infectious disease and drug development. *Journal of Neuroimmune Pharmacology*, *2*(1), 26-31.

305. Carterson, A. J., Zu Bentrup, K. H., Ott, C. M., Clarke, M. S., Pierson, D. L., Vanderburg, C. R., ... & Schurr, M. J. (2005). A549 lung epithelial cells grown as three-dimensional aggregates: alternative tissue culture model for Pseudomonas aeruginosa pathogenesis. *Infection and immunity*, *73*(2), 1129-1140.

306. Nickerson, C. A., Ott, C. M., Wilson, J. W., Ramamurthy, R., & Pierson, D. L. (2004). Microbial responses to microgravity and other low-shear environments. *Microbiology and Molecular Biology Reviews*, *68*(2), 345-361.

307. zu Bentrup, K. H., Ramamurthy, R., Ott, C. M., Emami, K., Nelman-Gonzalez, M., Wilson, J. W., & Pellis, N. (2006). Three-dimensional organotypic models of human colonic epithelium to study the early stages of enteric salmonellosis. *Microbes and infection*, *8*(7), 1813-1825.

308. RePass, M. A. D., Chen, Y., Lin, Y., Zhou, W., Kaplan, D. L., & Ward, H. D. (2017). Novel Bioengineered Three-Dimensional Human Intestinal Model for Long-Term Infection of Cryptosporidium parvum. *Infection and immunity*, *85*(3), e00731-16.

309. Ng, S., March, S., Galstian, A., Gural, N., Stevens, K. R., Mota, M. M., & Bhatia, S. N. (2017). Towards a Humanized Mouse Model of Liver Stage Malaria Using Ectopic Artificial Livers. *Scientific Reports*, *7*, 45424.

310. Walochnik, J., Obwaller, A., Gruber, F., Mildner, M., Tschachler, E., Suchomel, M. & Auer, H. (2009). Anti-Acanthamoeba efficacy and toxicity of miltefosine in an organotypic skin equivalent. *Journal of antimicrobial chemotherapy*, *64*(3), 539-545.

311. Ise, H., Takashima, S., Nagaoka, M., Ferdous, A., & Akaike, T. (1999). Analysis of cell viability and differential activity of mouse hepatocytes under 3D and 2D culture in agarose gel. *Biotechnology letters*, *21*(3), 209-213.

References

312. Bonnier, F., Keating, M. E., Wrobel, T. P., Majzner, K., Baranska, M., Garcia-Munoz, A. & Byrne, H. J. (2015). Cell viability assessment using the Alamar blue assay: a comparison of 2D and 3D cell culture models. *Toxicology in vitro*, *29*(1), 124-131.

313. Lan, S. F., Safiejko-Mroczka, B., & Starly, B. (2010). Long-term cultivation of HepG2 liver cells encapsulated in alginate hydrogels: a study of cell viability, morphology and drug metabolism. *Toxicology in Vitro*, *24*(4), 1314-1323.

314. Kenny, P. A., Lee, G. Y., Myers, C. A., Neve, R. M., Semeiks, J. R., Spellman, P. T. & Gray, J. W. (2007). The morphologies of breast cancer cell lines in three-dimensional assays correlate with their profiles of gene expression. *Molecular oncology*, *1*(1), 84-96.

315. Miranda-Verastegui, C., Llanos-Cuentas, A., Arevalo, I., Ward, B. J., & Matlashewski, G. (2005). Randomized, double-blind clinical trial of topical imiquimod 5% with parenteral meglumine antimoniate in the treatment of cutaneous leishmaniasis in Peru. *Clinical Infectious Diseases*, *40*(10), 1395-1403.

316. Rocha, M. N., Corrêa, C. M., Melo, M. N., Beverley, S. M., Martins-Filho, O. A., Madureira, A. P., & Soares, R. P. (2013). An alternative in vitro drug screening test using *Leishmania amazonensis* transfected with red fluorescent protein. *Diagnostic microbiology and infectious disease*, *75*(3), 282-291.

317. Friedrich, J., Seidel, C., Ebner, R., & Kunz-Schughart, L. A. (2009). Spheroid-based drug screen: considerations and practical approach. *Nature protocols*, *4*(3), 309-324.

318. Kim, J. B. (2005, October). Three-dimensional tissue culture models in cancer biology. In *Seminars in cancer biology*, *15(*5), 365-377.

319. Stark, H. J., Boehnke, K., Mirancea, N., Willhauck, M. J., Pavesio, A., Fusenig, N. E., & Boukamp, P. (2006, September). Epidermal homeostasis in long-term scaffold-enforced skin equivalents. In *Journal of Investigative Dermatology Symposium Proceedings, 11*, (1), 93-105.

320. Takahashi, K., & Yamanaka, S. (2006). Induction of pluripotent stem cells from mouse embryonic and adult fibroblast cultures by defined factors. *cell*, *126*(4), 663-676.

321. Saha, K., & Jaenisch, R. (2009). Technical challenges in using human induced pluripotent stem cells to model disease. *Cell stem cell*, *5*(6), 584-595.

322. Yeung, A. T., Hale, C., Lee, A. H., Gill, E. E., Bushell, W., Parry-Smith, D. & Thomson, N. (2017). Exploiting induced pluripotent stem cell-derived macrophages to unravel host factors influencing Chlamydia trachomatis pathogenesis. *Nature communications*, *8*, 15013.

References

323. Forbester, J. L., Goulding, D., Vallier, L., Hannan, N., Hale, C., Pickard, D. & Dougan, G. (2015). Interaction of Salmonella enterica serovar Typhimurium with intestinal organoids derived from human induced pluripotent stem cells. *Infection and immunity*, *83*(7), 2926-2934.

324. Ye, L., Wang, J., Beyer, A. I., Teque, F., Cradick, T. J., Qi, Z. & Levy, J. A. (2014). Seamless modification of wild-type induced pluripotent stem cells to the natural CCR5Δ32 mutation confers resistance to HIV infection. *Proceedings of the National Academy of Sciences*, *111*(26), 9591-9596.

325. Sanderson, L., Yardley, V., & Croft, S. L. (2014). Activity of anti-cancer protein kinase inhibitors against *Leishmania spp. Journal of Antimicrobial Chemotherapy*, *69*(7), 1888-1891.

326. Zhuang, J. C., & Wogan, G. N. (1997). Growth and viability of macrophages continuously stimulated to produce nitric oxide. *Proceedings of the National Academy of Sciences*, *94*(22), 11875-11880.

327. Mattock, N. M., & Peters, W. (1975). The experimental chemotherapy of leishmaniasis: I: Techniques for the study of drug action in tissue culture. *Annals of Tropical Medicine & Parasitology*, *69*(3), 349-357.

328. Coelho, A. C., Trinconi, C. T., Costa, C. H., & Uliana, S. R. (2014). In vitro and in vivo miltefosine susceptibility of a *Leishmania amazonensis* isolate from a patient with diffuse cutaneous leishmaniasis. *PLoS neglected tropical diseases*, *8*(7), e2999.

329. Bielecka, M. K., Tezera, L. B., Zmijan, R., Drobniewski, F., Zhang, X., Jayasinghe, S., & Elkington, P. (2017). A bioengineered three-dimensional cell culture platform integrated with microfluidics to address antimicrobial resistance in tuberculosis. *MBio*, *8*(1), e02073-16.

330. Yardley, V., & Croft, S. L. (1997). Activity of liposomal amphotericin B against experimental cutaneous leishmaniasis. *Antimicrobial agents and chemotherapy*, *41*(4), 752-756.

331. Sindermann, H., Croft, S. L., Engel, K. R., Bommer, W., Eibl, H. J., Unger, C., & Engel, J. (2004). Miltefosine (Impavido): the first oral treatment against leishmaniasis. *Medical microbiology and immunology*, *193*(4), 173-180.

332. Neves, N. M. (2016). *Biomaterials from Nature for Advanced Devices and Therapies*. John Wiley & Sons.

333. Kirkstall Ltd QV500 information page http://www.kirkstall.com/qv500/ Accessed 31/08/17

References

334. Kirkstall Ltd QV900 information page http://www.kirkstall.com/qv900/ Accessed 31/08/17

335. Nugraha, B., Hong, X., Mo, X., Tan, L., Zhang, W., Chan, P. M. & Choudhury, D. (2011). Galactosylated cellulosic sponge for multi-well drug safety testing. *Biomaterials*, *32*(29), 6982-6994.

336. Kinnari, T. J., Esteban, J., Martin-de-Hijas, N. Z., Sanchez-Munoz, O., Sanchez-Salcedo, S., Colilla, M., ... & Gomez-Barrena, E. (2009). Influence of surface porosity and pH on bacterial adherence to hydroxyapatite and biphasic calcium phosphate bioceramics. *Journal of medical microbiology*, *58*(1), 132-137.

337. Ananthanarayanan, A., Nugraha, B., Triyatni, M., Hart, S., Sankuratri, S., & Yu, H. (2014). Scalable spheroid model of human hepatocytes for hepatitis C infection and replication. *Molecular pharmaceutics*, *11*(7), 2106-2114.

338. Gao, Y., Majumdar, D., Jovanovic, B., Shaifer, C., Lin, P. C., Zijlstra, A. & Li, D. (2011). A versatile valve-enabled microfluidic cell co-culture platform and demonstration of its applications to neurobiology and cancer biology. *Biomedical microdevices*, *13*(3), 539-548.

339. Hale, C., Yeung, A., Goulding, D., Pickard, D., Alasoo, K., Powrie, F. & Mukhopadhyay, S. (2015). Induced pluripotent stem cell derived macrophages as a cellular system to study salmonella and other pathogens. *PloS one*, *10*(5), e0124307.

340. Spiller, K. L., Wrona, E. A., Romero-Torres, S., Pallotta, I., Graney, P. L., Witherel, C. E. & Vunjak-Novakovic, G. (2016). Differential gene expression in human, murine, and cell line-derived macrophages upon polarization. *Experimental cell research*, *347*(1), 1-13.

341. Maia, C., Rolão, N., Nunes, M., Gonçalves, L., & Campino, L. (2007). Infectivity of five different types of macrophages by *Leishmania infantum. Acta tropica*, *103*(2), 150-155.

342. Koniordou, M., Patterson, S., Wyllie, S., & Seifert, K. (2017). Snapshot profiling of the antileishmanial potency of lead compounds and drug candidates against intracellular *Leishmania donovani* amastigotes, with a focus on human-derived host cells. *Antimicrobial agents and chemotherapy*, *61*(3), e01228-16.

343. Alvar, J., Croft, S., & Olliaro, P. (2006). Chemotherapy in the treatment and control of leishmaniasis. *Advances in parasitology*, *61*, 223-274.

344. Bosshart, H., & Heinzelmann, M. (2016). THP-1 cells as a model for human monocytes. *Annals of translational medicine*, *4*(21), 438-444.

References

345. Moffat, J. G., Vincent, F., Lee, J. A., Eder, J., & Prunotto, M. (2017). Opportunities and challenges in phenotypic drug discovery: an industry perspective. *Nature Reviews Drug Discovery*, *16*(8), 531-543.

346. Singh, N. (2006). Drug resistance mechanisms in clinical isolates of *Leishmania donovani*. *Indian Journal of Medical Research*, *123*(3), 411-422.

347. Williams, C. S., Watson, A. J., Sheng, H., Helou, R., Shao, J., & DuBois, R. N. (2000). Celecoxib prevents tumor growth in vivo without toxicity to normal gut: lack of correlation between in vitro and in vivo models. *Cancer research*, *60*(21), 6045-6051.

348. Swartz, M. A., & Lund, A. W. (2012). Lymphatic and interstitial flow in the tumour microenvironment: linking mechanobiology with immunity. *Nature reviews. Cancer*, *12*(3), 210.

349. Assreuy, J., Cunha, F. Q., Epperlein, M., Noronha-Dutra, A., O'Donnell, C. A., Liew, F. Y., & Moncada, S. (1994). Production of nitric oxide and superoxide by activated macrophages and killing of *Leishmania major*. *European journal of immunology*, *24*(3), 672-676.

350. Bryan, N. S., & Grisham, M. B. (2007). Methods to detect nitric oxide and its metabolites in biological samples. *Free Radical Biology and Medicine*, *43*(5), 645-657.

351. Zhang, X., & Morrison, D. C. (1993). Lipopolysaccharide-induced selective priming effects on tumor necrosis factor alpha and nitric oxide production in mouse peritoneal macrophages. *Journal of Experimental Medicine*, *177*(2), 511-516.

352. Zhuang, J. C., & Wogan, G. N. (1997). Growth and viability of macrophages continuously stimulated to produce nitric oxide. *Proceedings of the National Academy of Sciences*, *94*(22), 11875-11880.

353. Götz, C., Pfeiffer, R., Tigges, J., Blatz, V., Jäckh, C., Freytag, E. M. & Edwards, R. J. (2012). Xenobiotic metabolism capacities of human skin in comparison with a 3D epidermis model and keratinocyte-based cell culture as in vitro alternatives for chemical testing: activating enzymes (Phase I). *Experimental dermatology*, *21*(5), 358-363.

354. Groeber, F., Holeiter, M., Hampel, M., Hinderer, S., & Schenke-Layland, K. (2011). Skin tissue engineering—in vivo and in vitro applications. *Advanced drug delivery reviews*, *63*(4), 352-366.

References

355. Dieterich, C., Schandar, M., Noll, M., Johannes, F. J., Brunner, H., Graeve, T., & Rupp, S. (2002). In vitro reconstructed human epithelia reveal contributions of Candida albicans EFG1 and CPH1 to adhesion and invasion. *Microbiology*, *148*(2), 497-506.

356. Andrei, G., Duraffour, S., Van den Oord, J., & Snoeck, R. (2010). Epithelial raft cultures for investigations of virus growth, pathogenesis and efficacy of antiviral agents. *Antiviral research*, *85*(3), 431-449.

357. Andrei, G., Van Den Oord, J., Fiten, P., Opdenakker, G., De Wolf-Peeters, C., De Clercq, E., & Snoeck, R. (2005). Organotypic epithelial raft cultures as a model for evaluating compounds against alphaherpesviruses. *Antimicrobial agents and chemotherapy*, *49*(11), 4671-4680.

358. Ma, L., Barker, J., Zhou, C., Li, W., Zhang, J., Lin, B. & Honkakoski, P. (2012). Towards personalized medicine with a three-dimensional micro-scale perfusion-based two-chamber tissue model system. *Biomaterials*, *33*(17), 4353-4361.

359. Nithiananthan, S., Crawford, A., Knock, J. C., Lambert, D. W., & Whawell, S. A. (2017). Physiological Fluid Flow Moderates Fibroblast Responses to TGF-β1. *Journal of cellular biochemistry*, *118*(4), 878-890.

360. Mattei, G., Giusti, S., & Ahluwalia, A. (2014). Design criteria for generating physiologically relevant in vitro models in bioreactors. *Processes*, *2*(3), 548-569.

361. Allen, J. W., Khetani, S. R., & Bhatia, S. N. (2004). In vitro zonation and toxicity in a hepatocyte bioreactor. *Toxicological sciences*, *84*(1), 110-119.

362. dos Santos Ferreira, C., Martins, P. S., Demicheli, C., Brochu, C., Ouellette, M., & Frézard, F. (2003). Thiol-induced reduction of antimony (V) into antimony (III): a comparative study with trypanothione, cysteinyl-glycine, cysteine and glutathione. *Biometals*, *16*(3), 441-446.

363. Hutson, J. R., Garcia-Bournissen, F., Davis, A., & Koren, G. (2011). The human placental perfusion model: a systematic review and development of a model to predict in vivo transfer of therapeutic drugs. *Clinical Pharmacology & Therapeutics*, *90*(1), 67-76.

364. Bakshi, R. P., Nenortas, E., Tripathi, A. K., Sullivan, D. J., & Shapiro, T. A. (2013). Model system to define pharmacokinetic requirements for antimalarial drug efficacy. *Science translational medicine*, *5*(205), 205, ra135-205ra135.

365. Ojeh, N. O., & Navsaria, H. A. (2014). An in vitro skin model to study the effect of mesenchymal stem cells in wound healing and epidermal regeneration. *Journal of Biomedical Materials Research Part A*, *102*(8), 2785-2792.

References

366. Rajman, I. (2008). PK/PD modelling and simulations: utility in drug development. *Drug discovery today*, *13*(7), 341-346.